
SLOVAK GEOLOGICAL MAGAZINE

VOLUME 8 NO 1

ISSN 1335-096X

1 C 66 b

<i>Šarinová, K. & Maglay, J.:</i> Sedimentology and petrography of Lukáčovce Mb. in the Nitrianska pahorkatina Upland	3
<i>Vass, D., Elečko, M. & Fordinál, K.:</i> Závada – Bielice Rise – a buried elevation between Bánovce and Rišňovce Depressions in the Danube Basin	13
<i>Majzlan, J., Chovan, M. & Michálek, J.:</i> Mineral and chemical composition of the ores at the Dve Vody Sb-Au deposit, Western Carpathians	21
<i>Bakoš, F., Pršek, J. & Tuček, P.:</i> Variscan granitoid hosted hydrothermal gold deposit Pezinok-Staré Mesto (Malé Karpaty Mts., Western Carpathians): Mineralogy, paragenesis, fluid inclusions study	37
<i>Dyda, M.:</i> Cooling and uplift trajectories of the Malé Karpaty Variscan Basement (West Carpathians)	49
<i>Putiš, M., Korikovský, S. P., Unzog, W. & Olesen, N. Oe.:</i> HP rocks associated with mylonitoclastites: a result of polystage overprint of the Austro-Alpine basement (Kreuzeck Massif, Eastern Alps)	65
<i>Weber, L., Ebner, F. & Haysberger, G.:</i> The Interactive Raw Material Information System ("IRIS") of Austria - the computer based Metallogenetic Map of Austria	89
<i>Siblík, M.:</i> New genus (<i>Superbirhyncha</i> gen. n.) for a rhynchonellid (Brachiopoda) from the Alpine Upper Triassic	101



Geological Survey of Slovak Republic, Bratislava
Dionýz Štúr Publishers

1/2002

SLOVAK GEOLOGICAL MAGAZINE

Periodical journal of Geological Survey of Slovak Republic is a quarterly presenting the results of investigation and researches in a wide range of topics:

- regional geology and geological maps
- lithology and stratigraphy
- petrology and mineralogy
- paleontology
- geochemistry and isotope geology
- geophysics and deep structure
- geology of deposits and metallogeny
- tectonics and structural geology
- hydrogeology and geothermal energy
- environmental geochemistry
- engineering geology and geotechnology
- geological factors of the environment
- petroarcheology

The journal is focused on problems of the Alpine-Carpathian region.

Editor in Chief

JOZEF VOZÁR

Editorial Board

INTERNAL MEMBERS

Vladimír Bezák	Jaroslav Lexa
Miroslav Bielik	Karol Marsina
Dušan Bodiš	Ján Mello
Pavol Grecula	Jozef Michalík
Vladimír Hanzel	Milan Polák
Juraj Janočko	Michal Potfaj
Michal Kaličiak	Martin Radvanec
Michal Kováč	Dionýz Vass
Ján Král'	Anna Vozárová

EXTERNAL MEMBERS

Dimitros Papanikolaou	Athens
Franz Neubauer	Salzburg
Jan Veizer	Bochum
Franco Paolo Sassi	Padova
Niek Rengers	Enschede
Géza Császár	Budapest
Miloš Suk	Brno
Zdeněk Kukal	Praha
Vladica Cvetkovic	Beograd
Nestor Oszczypko	Kraków

Managing and technical Editor: Gabriela Šipošová

Address of the publishers: Geological Survey of Slovak Republic, Mlynská dolina 1, 817 04 Bratislava, Slovakia

Printed at: Gupress Bratislava

Price of single issue: USD 12

Ústredná geologická knižnica SR
ŠGÚDŠ

Annual subscrip

© Geological Survey of Slovak Repu

clude the postage

. 817 04 Bratislava, SLOVAKIA



3902001018506

SLOVAK GEOLOGICAL MAGAZINE

VOLUME 8 NO 1

ISSN 1335-096X



Geological Survey of Slovak Republic, Bratislava
Dionýz Štúr Publishers

1/2002

Sedimentology and petrography of Lukáčovce Mb. in the Nitrianska pahorkatina Upland

KATARÍNA ŠARINOVÁ¹ & JURAJ MAGLAY²

¹Faculty of Natural Sciences, Comenius University, Mlynská dolina, 845 15 Bratislava, Slovakia

²Geol. Survey of Slovak Republic, Mlynská dolina 1, 817 04 Bratislava, Slovakia

Abstract: Lukáčovce Mb. is comprised by coarse-grained and very coarse-grained sandy fluvial-limnic sediments having admixture of gravels with grain-size up to 30 mm. The sediments are characterized by conspicuous rusty, dark red and brownish red colour. They subhorizontally and horizontally overlie Neogene deposits of Volkovce Formation. Their contact is erosive. The gravel is mostly composed of sandstone, quartz, chert and limonite concretions. It often contains coatings of limonite and Mn. Sublithic and lithic sands are poorly sorted. Except clastic quartz and feldspar the clay fraction contains smectite (montmorillonite), illite, kaolinite and goethite. Based on preliminary results, the sediments of Lukáčovce Mb. are assigned to the Early Pleistocene (Biber).

Key words: Nitrianska pahorkatina upland, Lukáčovce Mb., Early Pleistocene, fluvial-limnic sediments

Introduction

Nitrianska pahorkatina upland and Nitra flood plain comprise areally the most widespread and the northernmost intermountain promotory of the Danube lowland. The promotory tapers into the Považský Inovec, Trábeň and Strážovské vrchy Mts. According to Mazúr and Lukniš (1978) from north toward south the area can be divided into Nitra table, Zálužie, Bojňany and Bánovce uplands (Fig. 1) respectively. The geographic division is geologically and tectonically identical with the northern promotory of the Danube basin consisting of Rišnovce and Bánovce depressions separated by Závada-Bielice ridge (Vass et al., 1988). The main part of the basin fills is comprised by Tertiary deposits capped by the youngest Pliocene Volkovce Formation (Elečko and Fordinál in Pristaš et al. 2000) and Quaternary cover mainly represented by eolic, fluvial and deluvial deposits ranging from the Early to Late Pleistocene and Holocene.

In order to elucidate geological structure and evolution of the area a detail regional geologic research and mapping was done in period from 1994 to 2000. The results are published in the latest works of Pristaš and co-workers (2000a, 2000b) where also a detail list of previous works is given. Based on the mentioned research Maglay (Maglay et al., 1997, 1998) drew attention to the repeating horizon of conspicuous redish-brown sandy-loamy gravel prevailingly occurring in summit parts of interdepressional ridges of the upland. The occurrence was mainly recorded from the middle part of the Nitrianska pahorkatina upland which is marked as Blatňany upland. The northern part of the upland trends to the neotectonically active Ripňany depression (Fig. 2). Sedi-

mentary-petrographic analysis of Quaternary deposits including gravels of the Lukáčovce Mb. was given in the framework of a wider draft work by Šarinová (2000). The limonitized sandy-loamy gravels were later described and based on the Lukáčovce locality defined as Lukáčovce Mb. (Maglay in Pristaš et al., 2000).

Brief characteristics of Lukáčovce Mb.

Lukáčovce Mb. forms specific, irregularly preserved phenomenon of the oldest Quaternary accumulation not only in the Nitra upland region but also, according to the latest knowledge, in the other uplands of the Danube lowland. According to the genesis, habitus, location, deposition, lithologic and sedimentary-petrographic characteristics the gravels are preliminary suggested to be an equivalent of Strekov Mb. (Biber) described by Harčár and Schmidt (1965) and Schmidt and Halouzka (1970) from the Hronska pahorkatina upland. In the Nitrianska pahorkatina upland they mainly occur in the area of the young Ripňany depression intervening into the Bojňany upland.

At localities without loess cover the occurrence of the Lukáčovce Mb. sediments is indicated by a striking change in colour and lithology of overlying slope deposits and exposures of colouring very conspicuous rusty, dark red, redish-brown and maroon sandy loams and fine-grained, limonitized gravels lithified by the loams. The gravels are either regularly scattered in the whole profile or they are concentrated at the base or eventually they form multiple repeating layers. In the basal parts of layers sporadically thin layers of coarser gravel with scattered boulders occur. At individual localities slight differences



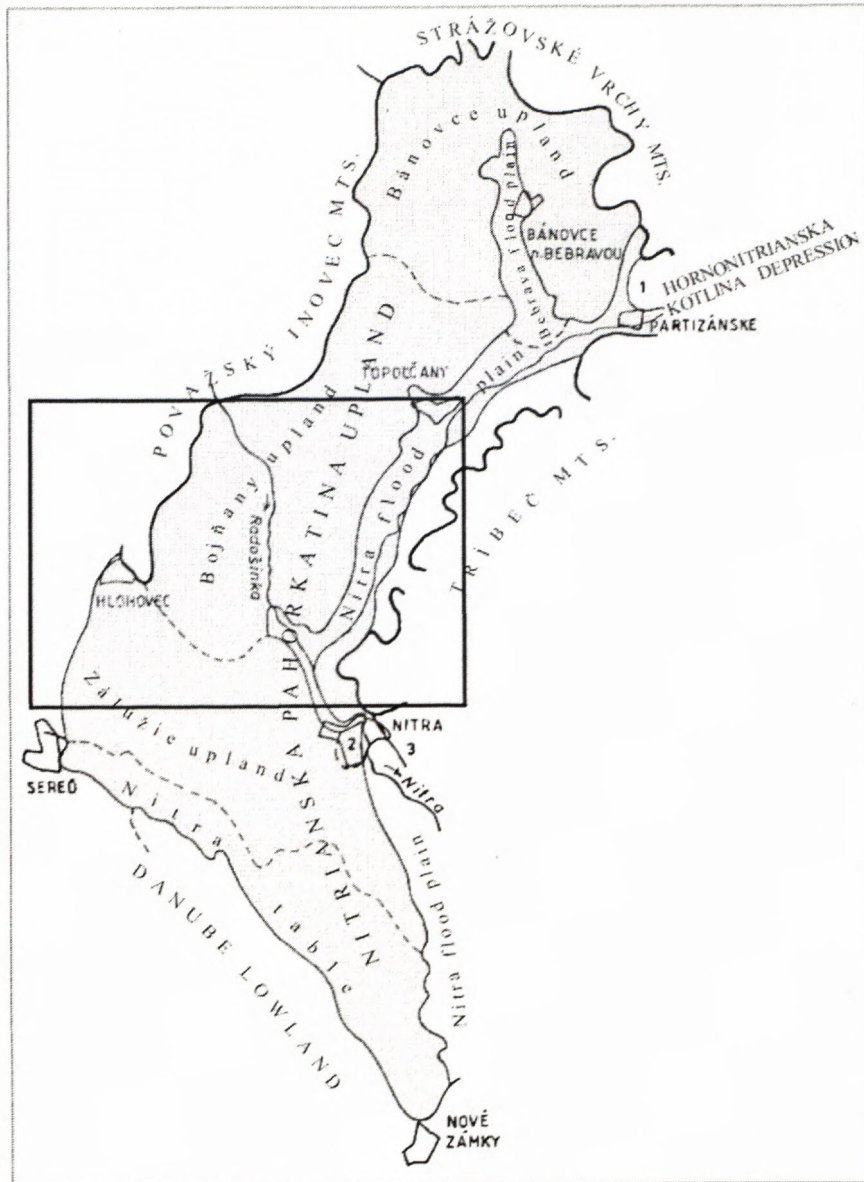


Fig. 1. Geomorphological units of the Nitrianska pahorkatina upland (according to Mazúr & Lukniš, 1978), adopted and partly modified from the work by Pristaš et al. (2000b). The thick – framed part designate the area of interest.

in lithology, sedimentology, sedimentary petrographic and other analysed parameters were recorded. The common and characteristic sign of the sediments is their sub-horizontal and horizontal position and exclusively erosive contact with sediments of the Volkovce Formation having a gravely-sandy lithology with clay intercalations (Locality Lukáčovce – point 1).

The most of recorded outcrops (Fig. 2) is located in the upper parts of small depression slopes at sites where the slopes pass into plain interdepression ridges covered by loess. This suggests their location immediately beneath or on the level of the older Late Pliocene river level (SSE of Tekold'any in the Rybníky part – point 7, in the village Merašice near cemetery - point 4, in the Veľké Ripňany - Piesočnica - point 3, in the Cerový creek valley near the water dam SW of Veľké Ripňany – point 8, W of Biskupová, in the part Surdok - point 6 and others). The originally unified base level of the Lukáčovce Mb. was during the Pleistocene tectonically vertically differentiated into more altitude levels having max. difference about 50 m today. Other occurrences probably form remnants of lito-

ral sections of an open lake or remnants of input of distributary channels with features of abrasive activity in the underlying deposits of the Volkovce Formation (Dolné Otrokovce - part Bučovské – point 9, sand pit between Horné and Dolné Otrokovce – point 2, Horné Trhovište - Farské – point 10 and others). Depositional characteristics suggest postgenetic redeposition into lower morphologic position at some localities during the Quaternary.

Vague, however, the most frequent outcrops are comprised by directly exposed coarse-grained and very coarse-grained loamy-sandy gravels having reddish brown and maroon colour. In deluvium they typically are developed as rusty and reddish-brown sandy gravels (W of Biskupová – point 6 and others). At base of field roads (SSE of Tekold'any – point 7 and near Merašice - point 4 and others) they only form 2 – 3 cm thick beds. The gravel and sand with Mn-Fe oxides coatings is almost exclusively composed of quartz and quartzose arenites (87,5%). Feldspar, mica and carbonate contents vary from 4 to 9%. In light fraction of minerals high amount of limonitized quartz and limonite grains occur.

sands, is deformed by microtectonics of NW-SE and W-E direction. The deformations dissect the sediment into a system of small, intermutually shifted blocks.

Based on the field data and new knowledge from other parts of marginal uplands of the Danube lowland we can state that the sediment extension has a global character and is depended on specific climatic conditions governing type of weathering. This also suggests sediment occurrence on higher blocks of marginal parts of the Ripňany depression beneath the loess cover at altitudes corresponding to the level or closely below the level of the Late Pliocene river plain. The individual deviation corresponds to the deposition mode in local open lakes. Stratigraphically we can assign them into the oldest part of the Early Pleistocene (Biber). From the lithological viewpoint they are identical to the Strekov Mb. which stratigraphy was proved by fauna of vertebrate (Harčár and Schmidt, 1965; Schmidt and Halouzka, 1970) in the Hronská pahorkatina upland.

The paper brings several new sedimentary-petrographic knowledge and opinions on environment and characteristics of sedimentation of the Lukáčovce Mb. Laboratory analyses were performed on larger amount of samples taken from selected localities by using newer methods.

For laboratory evaluations samples from following localities were used (Fig. 2):

- Lukáčovce sand pit, samples 1 = L+, L+A, L2, L3
- Dolné Otrokovce sand pit, samples 2 = O1, O2, O2A
- Veľké Ripňany sand pit Piesočnica, samples 3 = R1, R2
- Merašice road cut, 4 = sample M1
- Alekšince road cut 5 = sample A1

Petrography of Lukáčovce Mb.

Granulometry and petrography of gravel fraction

The most frequently occurred fraction of 7 – 15 mm was used for granulometric analysis. The fraction is sufficiently represented in all samples except the sample L2 from the locality Lukáčovce.

In the lithologic composition (Tab. 1) sandstone clasts predominate. In average they comprise 43% of the volume amount. They are represented by lithified sandstones having high degree of sphericity (0.8), marly sandstones and other sandstones without macroscopically conspicuous features. The coarse grained sandstones comprise about 1 vol.% of the whole amount of sandstones at every locality. The marly sandstones take about 2 vol.% and they are strikingly oblate. Cherts are represented by some 18 vol.% and their shape and sphericity vary depending on locality. A part of cherts has signs of eolic abrasion. Quartz is represented by some 26 volume percents and it prevalingly has disc-like shape with shape factor Fr (Sneed and Folk, 1958) close to 0. Limonite concretions are represented by some 9.5 % of the volume amount which is several times exceeded at locality Alekšince where concretions form about 42% of the volume amount. Granitoid rocks, glassy pyroclasts and calcareous concretions occur in small amount (0 – 3 vol.%). The mean clast composition is shown in the Fig. 3.

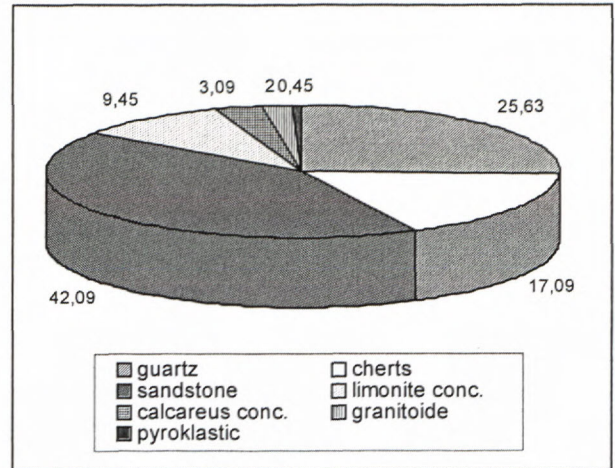


Fig. 3. Average composition gravels of the Lukáčovce Mb.

The values of maximum projection sphericity and shape factor (Fr) calculated for cherts and quartz pebbles and their comparison to values given by Sneed and Folk (1958) suggest a medium long transport of deposits. The only exception is made by sediments from the locality Otrokovce where sediments underwent a short and medium long transport. The relationship between the Fr and maximum projection sphericity is shown in the Fig. 4.

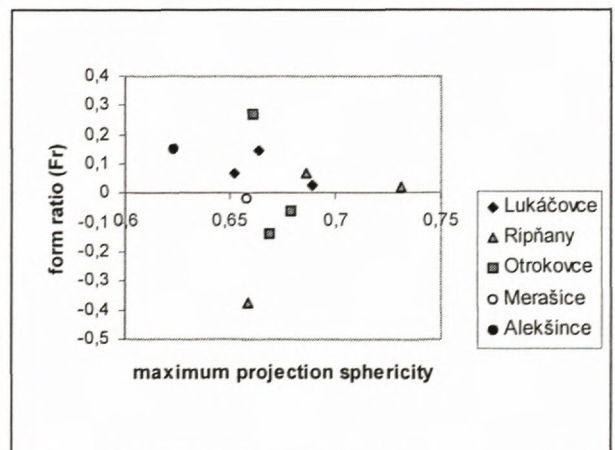


Fig. 4. Plot of form ratio and maximum projection sphericity gravels of the Lukáčovce Mb.

The sandstone clast occurrence decreases with the decreasing size of the gravel clasts. The granulometric analysis of the larger grain size fractions is not reliable due to small amount of clasts available. The gravels of larger clast size were used for analysis of lithologic composition.

Lithology of gravel fraction

Based on petrographic analysis we can divide several type of sandstones:

- Arcose metawackes of Permian age with recrystallized sericitic pseudomatrix and grains of undulatory quartz, twinned crystal of plagioclases, K-feldspars and in smaller amount also heavy minerals (zircon, rutile).

Tab. 1. Results granulometry and lithological analyse gravels of the Lukáčovce Mb.

Locality	Q u a r t z			C h e r t s			sandstone content %	limonite con. content %	calcareous con. content %	granitoides content %	pyro- klastics content %	t o g e t h e r		
	content %	Fr	sphericity	form	content %	Fr						sphericity	form	form ratio
15-7 mm	26	0,25	0,724	platy	22	0,1	0,634	platy	46	2	0	0,07	0,652	platy
L-1	31	0,142	0,685	platy	11	0,4	0,652	platy	48	2	2	0,144	0,664	platy
L-1A	35	0,125	0,641	platy	13	0,08	0,705	platy	40	8	0	0,03	0,689	platy-elong.
L-3	29	0,076	0,69	platy	11	0	0,698	blade	53	2	1	0,02	0,731	platy-elong.
R-1	14	0,07	0,692	platy	24	-0,3	0,642	elongated	61	1	0	-0,375	0,659	elongated
R-1A	22	0	0,715	blade	26	0,08	0,672	platy	40	2	0	0,07	0,686	platy
R-2	20	0,111	0,652	platy	8	0,125	0,612	platy	42	20	0	0,27	0,661	platy
O-1	20	0,05	0,643	compact	17	-0,875	0,681	elongated	48	15	0	-0,14	0,669	elongated
O-2	44	-0,07	0,72	blade-elong.	15	0,142	0,648	platy	30	6	1	-0,06	0,679	blade-elong.
O-2A	26	0,08	0,676	platy-blade	33	-0,2	0,626	elongated	35	4	1	-0,02	0,658	blade
M-1	15	0,42	0,71	platy	8	0,25	0,602	platy	20	42	0	0,15	0,623	platy
A-1	25,63				17,09				42,09	9,45	2			
average									42,09	9,45	2			

- Early Triassic subarcoses composed of quartz, less orthoclase, plagioclase, microcline, in smaller amount mica, heavy minerals and felsitic volcanic glass. The matrix is composed of sericite.
- Early Triassic quartzose arenites composed of quartz, orthoclase and microcline. Plagioclase is less common. Felzites and heavy minerals are rare. The matrix is mostly composed of recrystallized quartz which is locally of syntaxial character.
- Non-metamorphosed fine-grained sandstones having clayey matrix and composed of weakly rounded quartz and feldspar clasts. Less common are mica, felsites and heavy minerals.
- Marly lithic sandstones have clayey carbonate matrix containing quartz, feldspar and other rocks clasts. The rock clasts are represented by fine-grained sandstones, micritic limestones and radiolarites. They also contain organic remnants, probably bottom of algae.

After then silicites in a form of cryptocrystallized cherts with organogenic structure follow. Brown silicites predominate. They contain silicified radiolarites of Spumelaria type and spicule of sponge. Sometimes cherts only contain filaments. They have various colours ranging from brownish-red to green. The brown colours prevail. The only exceptions are black cherts which only occur in fraction below 15 mm. They have organogenic structure and cryptocrystalline matrix. They also contain silicified radiolarites of Spumelaria type with preferred orientation. The silicites are probably of Jurassic age and originate from the Tatric envelope unit or/and Křížna Nappe.

The limonites consist of pure limonite concretions or they form matrix among grains of sand size. The composition of sandy gravels corresponds to the neighbouring rocks. These type of concretions predominate and the amount of sandy grains in individual concretions varies.

Pyroclastics are represented by pumice and volcanic glass which contain nucleus of mafic minerals and plagioclases. Occasionally they contain magmatic corroded grains of monocrySTALLINE quartz.

Sands of Lukáčovce Mb.

Lukáčovce Mb. mainly consist of sandy sediment. Prevaillingly coarse-grained sands (Tab. 2) are poorly sorted (So from 0.87 fi to 3.77 fi) and contain admixture of gravel having maximum grain size rarely exceeding 30 mm. The exception is only made by channel fills at the Otrokovce locality where the gravel is medium to coarse-grained. Sk values varies from -0.43 fi to 0.78 fi and Kg values vary from 0.69 to 4.31 (the calculation was made by arithmetic method by the programm KORN).

According to the mineral composition of the light fraction the sands comprise boundary between subarcoses and sublithic arenites and they fall into field of lithic arenites (Fig. 5). The light fraction is composed of quartz (37 - 82%), feldspar (6 - 20%), mica and lithic clasts where carbonate grains and grains of dark colour were assigned. These grains are probably composed of silicites, limonite and grains coated by Fe and Mn oxides (together 6.3 - 44%). The precise content is given in Tab. 3.

Heavy minerals

Composition of heavy minerals is given in Tab. 4. The content of magnetic fraction is relatively small and only in few samples it exceeds 1 vol.%. In parafraction limonite (5-41 vol.%) and ilmenite (6-35 vol.%) predominates. Minor occurrence has garnet (1-8 vol.%), epidote (1-7 vol.%) and turmaline (0-2 vol.%). In diafraction zircon occurs in larger amount (3-11 vol.%), rutile (5-11 vol.%) and milky grains. Sillimanite, kyanite, apatite, staurolite, monazite (ceric) and gold only occurs as scattered grains with contents rarely higher than 0.1 vol.% (staurolite, monazite).

Rutiles indicating two different sources of heavy minerals are interesting. Rutiles with quartz inclusions indicate more acid source, rutiles with inclusions melting of basanite and foid composition indicate source formed by alkaline basalts. A part of rutiles contains niob.

The calculated ZTR and GAS indices suggest medium mature and mature degree of Lukáčovce Mb. sands. The weathering coefficients ($K_3 = 0.01-0.2$, $F = 0$, $KV = 8-56.7$) (Tab. 5) were compared to values calculated for limnofluvial sediments by Vaškovská (1992). They indicate Early Pleistocene age. The mean occurrence of heavy minerals is given in Fig. 6.

Composition of clay minerals in matrix

Clay minerals at locality Lukáčovce are represented by smectite, illite and minerals from the kaolinite group, most probably by halloyzite.

At locality Ripňany the clay contains illite, kaolinite and smectite. On X-ray graph specialized for Fe hydroxide low content of weakly crystalline goethite was found. The shape and thickness of the kaolinite peak (Ripňany) suggest non-structuralized, possibly redeposited kaolinite.

Tab. 2. Grain-size analyse of the Lukáčovce Mb. Results was obtained mathematical calculation. $T = \text{Trask (1930)}$, $I = \text{Inman (1952)}$, $F/W = \text{Folk and Ward (1957)}$.

sample	L-1	L-1A	L-2	L-3	O-1	O-2	O-2A	R-1	R-2	M-1	A-1
Md (mm)	0,685	0,923	0,571	0,49	0,691	35,565	42,660	0,900	0,652	0,960	0,58
Md	0,544	0,114	0,807		0,531	-5,152	-5,414	0,150	0,616	0,058	
Mz (T)	1,005	1,866	0,578	0,908	0,593	27,571	43,541	2,505	0,665	1,639	2,669
Mz (I)	1,514	1,160	0,965	1,481	0,241	-3,086	-5,415	-0,834	1,627	-0,730	0,252
Mz (F/W)	1,191	0,812	0,912	1,252	0,338	-3,775	-5,415	-0,506	1,290	-0,467	0,190
So (F/W)	3,774	3,461	0,878	3,023	1,726	2,454	1,132	2,274	2,754	1,724	3,426
Sk (F/W)	0,421	0,262	0,167	0,232	-0,214	0,789	0,414	-0,365	0,362	-0,437	0,030
Kg (F/W)	1,896	0,695	1,094	1,486	1,144	1,142	4,312	0,825	2,208	1,144	0,940
Typ of sediments	medi- umsand	coarse sand	coarse sand	medium sand	coarse sand	pebble	cobble	very coarse sand	medium sand	very coarse sand	coarse sand

Tab. 3. Association light minerals of the Lukáčovce Mb., fraction 0,25-0,10 mm.

sample	L-1	L-1A	L-2	L-3	O-1	O-2	O-2A	R-1	R-2	M-1	A-1
quartz %	60,80	45,84	72,40	71,50	82,09	82,73	79,06	68,08	37,08	87,50	63,49
feld spar %	20,16	19,50	15,06	15,27	8,20	7,77	7,98	19,04	18,82	6,16	11,11
mica %	6,47	8,25	5,26	4,77	5,24	2,88	5,39	9,85	23,52	2,51	3,10
other %	12,57	26,43	7,28	8,24	4,47	6,62	7,57	3,03	20,58	3,83	22,22

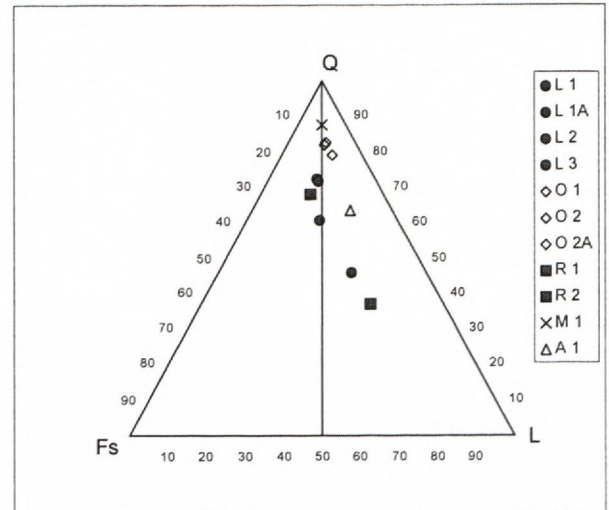


Fig. 5 Classification diagram for sands, Petijohn, Potter and Siever (1972)

In sample from locality Merašice smectite, kaolinite and illite are present. All these minerals are typical by low crystallinity. Hydroxide is represented by goethite.

Sedimentary source

The gravel lithology and composition of clay and heavy minerals suggest several sedimentary sources during deposition of Lukáčovce Mb.

Early Triassic sandstones and silicites as well as rare granitoid clasts suggest source area consisting of acid magmatic and crystalline rocks with their Mesozoic envelope of the Tatric Unit and Mesozoic rocks of higher nappes (mainly Fatric Nappe). Based on the absence of

Tab. 4. Association heavy minerals of the Lukáčovce Mb., fraction 0,25 – 0,10 mm.

Sample	HM %	magnetite	limonite	ilmenite	garnet	epidote	turmaline	staurolite	monazite	zircon	rutile	sill.	kyanite	apatite	amfib.	gold	milky grain	together %	ZTR	GAS
L-1	1,75	0,15	10,1	35,92	3,11	0,77	0	0	0	4,18	6,15	0		0			38,99	100	72,69	21,88
L-1A	1,59	0,16	5,67	34,03	7,69	2,49	0	0	0,17	2,08	3,56	0	0	0			43,3	100	35,27	48,09
L-2	0,5	0,36	7,89	28,93	8,23	3,68	1,06	0	0	4,26	8,29	0	0	0			36,68	100	52,1	33,8
L-3	0,85	0,15	7,13	27,48	8,21	5,69	0,53	0,17	0,7	2,81	4,92	0	0	0			42,21	100	35,85	36,37
O-1	0,94	0,47	9,61	31,36	5,85	0,84	2,09	0,17	0	6,59	10,65		0	0		0	32,02	100	73,8	22,98
O-2	1,68	1,69	20,64	23,97	3,59	0,26	0,67	0,16	0,16	11,89	8,97	0	0	0			27,77	100	83,77	14,59
O-2A	2,07	2	15,06	28,14	3,8	0,61	1,36	0,17	0	11,52	10,7	0	0	0		0	26,01	100	83,73	14,09
R-1	0,8	0,44	23,6	19,68	0,58	1,37	1,57	0,29	0,14	2,9	11,04		0	0			38,39	100	86,69	4,86
R-2	0,73	0,16	20,35	12,71	5,08	7,16	0,69	0,45	2,77	6,84	11,04	0	0	0	0		32,34	100	54,56	16,25
M-1	1,53	0,27	41,02	5,99	1,41	1,1	0,32	0,3	0	5,19	8,3		0	0			36,12	100	83,09	10,28
A-1	2,26	0,14	12,52	34,27	2,23	0,52	0,13	0,25		2,96	5,5		0	0			41,47	100	74,11	21,39

Tab. 5. Weathering coefficients of the Lukáčovce Mb. (calculation by Vašková (1992).

sample	K1	K2	K3	F	K-A	K-B	K-V
L-1	0	0	0,01	0	0	0	
L-1A	0	0	0,06	0	0	0	21,36
L-2	0	0	0,09	0	0	0	29,86
L-3	0	0	0,16	0	0	0	9,01
O-1	0	0	0,02	0	0	0	
O-2	0	0	0,005	0	0	0	
O-2A	0	0	0,01	0	0	0	
R-1	0	0	0,03	0	0	0	43,65
R-2	0	0	0,21	0	0	0	7,94
M-1	0	0	0,02	0	0	0	56,81
A-1	0	0	0,01	0	0	0	

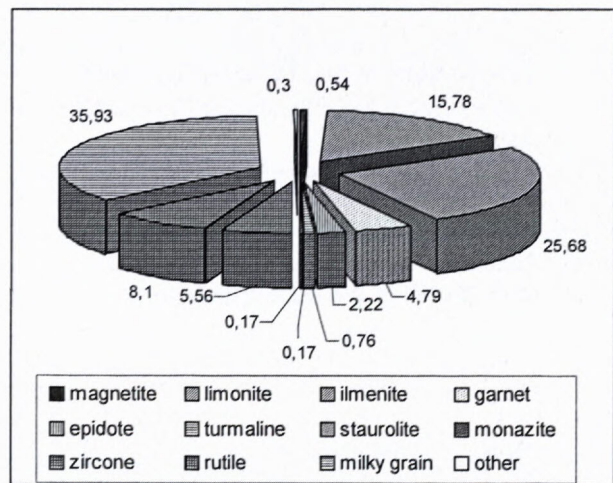


Fig.6. Average composition heavy minerals.

Cretaceous fossils (Boorová, pers. communication) it is possible to assume Jurassic silicites (partly structured black silicites) of Mesozoic envelope unit and Fatric Nappe as main source area of the sediments. The composition of source area is also confirmed by the composition of heavy minerals (turmaline, staurolite, sillimanite).

Pumice, volcanic glass having corroded quartz and glasses with plagioclases and nucleus of mafic minerals indicate volcanic source area. The source is confirmed by heavy minerals. Together they suggest neotectonic character of the source probably represented by the Vtáčnik Mts. Taking into account their small amount and flow direction, we assume that the volcanoclastics could be redeposited from the underlying Neogene sediments.

Clay minerals, Fe hydroxides and red colour of fine-grained fraction of Lukáčovce Mb. sediments has a character of redeposited subaerial weathering crusts and red paleosols. There are indications that the red paleosols are still preserved on the top of the Neogene sediments in the Nitrianska pahorkatina upland.

The genesis and source of limonite concretions is not clear. Theoretically, the source area could be represented by:

- ore deposits which, however, were not found in the area
- by limonite concretions originated in pedogenic process and after then rounded during a transport
- syngenetic lake environment

According a detail study and analysis of more data the most probable source area of limonite concretions seems to be lake environment (Kukal, 1964). The origin of limonite concretions in so called iron-ore lakes is supported by fact, that concretions lithified by limonite contain sand grains of identical composition as sediments of the Lukáčovce Mb. including lithic clasts of silicites having psamitic grain-size. From literature it is generally known that lacustrine limonite concretions originate in near-shore shallow waters and near tributaries. Maximum occurrence of limonite concretions in coarse-grained sediments corresponds to this knowledge. The medium-grained sands of the Lukáčovce locality were probably deposited in deeper part of lake. The theory is also confirmed by high content of limonite grains in heavy fraction and by absence of fossils suggesting lake rich in organic matter (acids) and barren of living organisms.

The idea that the source area is represented by humificate lakes without great organic production, located in the northern part of the temperate zone, is questioned by results of sediment pH analyses. According Kukal (1964) the recent sediments of the same type have pH 5.5 - 6.5. The samples of Lukáčovce Mb. have pH higher. At the locality Lukáčovce the value of pH was 7.29, in Merašice 7.92 and in Ripňany 8.25. This increasing may be a result of diagenetic change as well as postgenetic infiltration of carbonates from overlying loesses.

Alcalic pH (7.2 and 8.2) is typical for arid climate and acid pH connected with formation of limonite concretions is typical for humid climate. As far as the pH of Lukáčovce Mb. was not postsedimentary changed, the increased value confirms formation of limonite concretions (orzstein) in pedogenic process during existence of red paleosoils in humid climate and their redeposition after change of climatic conditions.

Climate

Because the redish-brown sediments can not originate subaqueously, it is possible to state that fine-grained material of the Lukáčovce Mb. was at some places postgenetically redeposited in a form of red paleosoils and weathering crusts into smaller local lakes from the neighbouring area of higher relief. The redeposition is evidenced by a thick peak of kaolinite.

The soils of such colour and mineral composition originate in subtropic and tropic conditions. Such conditions prevailed in our region until the Cromerian which corresponds in the Alpine paleoclimatic scale to interglacial G/M. After this stage, such paleosoils have not originated (cooler climate).

However, in the Lukáčovce Mb. also eolic material in smaller amount occurs. It is mainly represented by eolic

abraded cherts. Such type of material is also suggested by results of grain size analysis applied to a Fig. 7 after Friedman (1961). Alcaline pH also indicates arid climate. It suggests that during the formation of red soils, which characterize Lukáčovce Mb., tropic climate prevailed and redeposition process started after the transition of climate from tropic to arid.

Sedimentary environment

The grain-size analyses (Fig. 7 and 8) imply prevailing formation of the Lukáčovce Mb. sediments in fluvial-limnic environment with admixture of eolic material during the sedimentation. As long as we consider all red horizons as Lukáčovce Mb. we have to assign all primary occurrences of red soils into residual sediments - weathering crust.

If we apply this model, all analysed samples are entirely and partly redeposited into fluvial - limnic environment. The redeposition occurred after the change of climate from tropic to arid mode when also more intensive eolic activity existed.

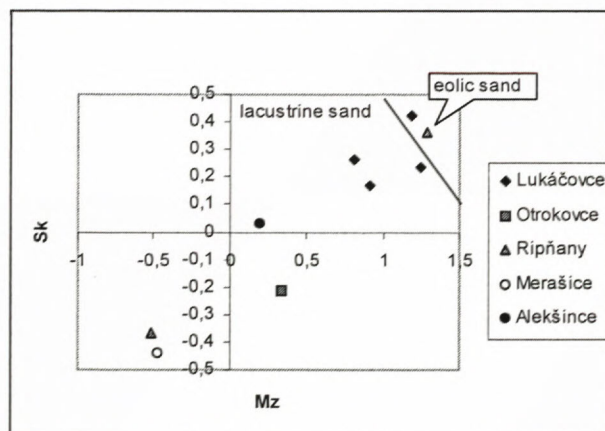


Fig.7. Plot of first moment (Mz) and third moment (Sk -skewnees) using phi scale, Friedman (1961).

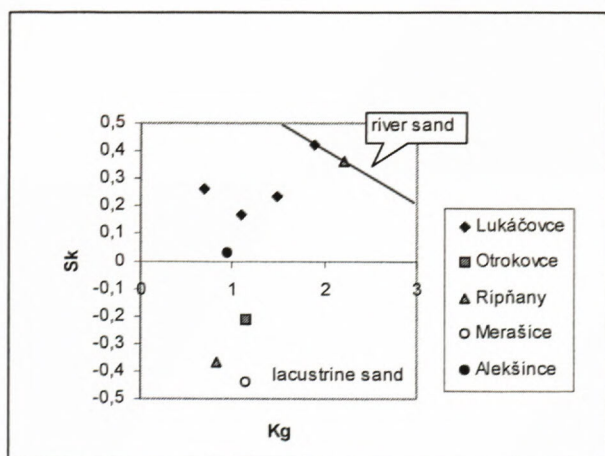


Fig.8. Plot of third moment (Sk -skewnees) and fourth moment (Kg -kurtosis) using phi scale, Friedman (1961).

Based on results of grain size analysis we may assume transport of the sediment in fluvial environment while a part of the material was before or during the transport and sedimentation redeposited by eolic processes. Gravel clasts floated in sandy matrix without preferred orientation suggests redeposition by torrential floods when mixing of paleosoils and coarser clasts from the Považský Inovec Mts. occurred.

Conclusion

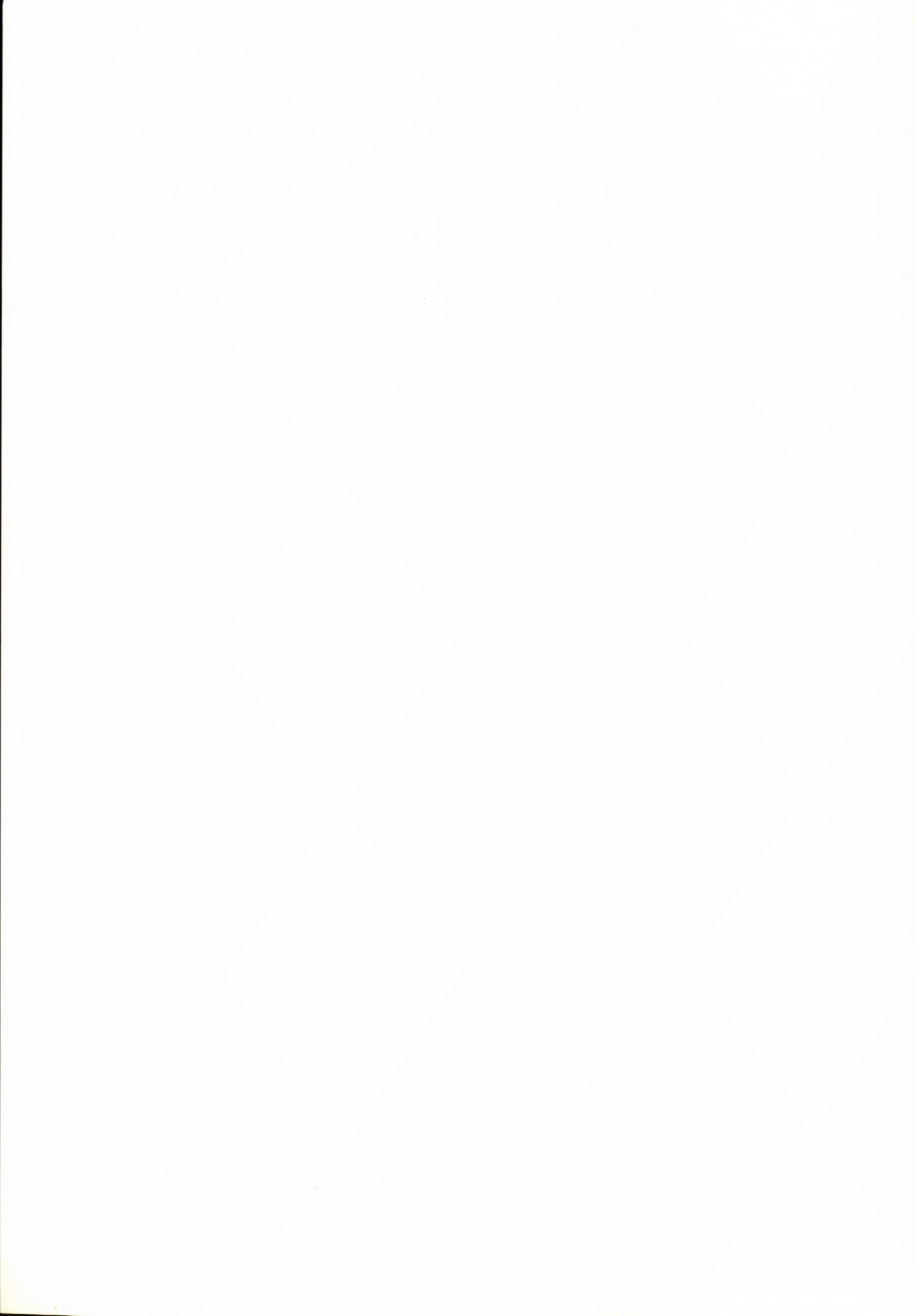
The results of complex sedimentary-petrographic analysis of sediments comprising the Lukáčovce Mb., which were analysed at several localities, suggest their depositional environment. They originated in a sporadically closed and open shallow lake and fluvial-lacustrine environments occurring in neotectonically young Ripňany depression. Characteristic feature of sediments is a striking input of alluvial fan sediments transported for a short distance from the Považský Inovec Mts. Occurrence of redeposited sands and gravels from the underlying Volkovce Formation (Dacian) is important.

The sediments comprising Lukáčovce Mb. originated in several sources, however, dominant direction is from the Považský Inovec Mts. The fine-grained part was formed by red paleosoils. Change of climatic conditions probably resulted in loss of vegetation and eolic sedimentation. Probably in this period local heavy rainfalls occurred driving redeposition of sediments and soils by floods on the level of the Late Pliocene river plain. From this level the sediments were redeposited into lower levels into a fluvial - lacustrine system.

The results of the sample analyses show Early Pleistocene age (Biber?, Günz) of primary sediments and Cromerian age of redeposited sediments. This corresponds to the age of similar deposits in the area of Starý Grunt yielded by paleomagnetism (Vaškovská and Vaškovský, 1989).

References

- Folk R. L. & Ward W., 1957: Brazos river bar. a study in the significance of grain size parameters. *J. of Sedimentary, Petrology*, vol. 27, No 1.
- Friedman G. M., 1961: Distinction dune, beach, and river sands from their textural characteristics. *Journal of Sedimentary, Petrology*, vol. 31, 514 – 529.
- Harčár J. & Schmidt Z., 1965: Kvartér v okolí Strekova na Hronskej pahorkatine. *Geol. Práce, Zprávy, Zoš.* 34, GÚDŠ Bratislava, 143 – 151 (in Slovak, Engl. Resume).
- Inman D. L., 1952: Sorting of sediments in the light of fluid mechanics. *Jour. of Sediment. Petrol.*, vol. 22, 125 – 145.
- Kukal Z., 1964: Geologie recentních sedimentů. ČSAV, Praha, p. 157 – 158 (in Czech).
- Maglay J., Pristaš J., Nagy A. & Kernátsová J., 1997: Vysvetlivky ku geologickým mapám 1: 25 000, listy: 35-343 Dvorníky, 35-344 Alekšince, 35-433 Lužianky-Nitra (časť). Manuskript – archív Št. Geol. Úst. D. Štúra, Bratislava, 17 – 18 (in Slovak).
- Maglay J., Fordinál K., Havrila M., Fejdiová O. & Kernátsová J., 1998: Vysvetlivky ku geologickým mapám 1: 25 000, listy: 35-342 Veľké Ripňany, 35-324 Piešťany (časť). Manuskript – archív Št. Geol. Úst. D. Štúra, Bratislava, 65 p. (in Slovak).
- Mazúr E. & Lukniš M., 1978: Regionálne geomorfologické členenie SSR. *Geogr. Čas.*, 30, 2, Bratislava, 101-122 (in Slovak, Engl. Resume).
- Pettijohn F. J., Potter P.E., & Siever, 1972: Sand and sandstone. Springer Verlag, Berlin – Heilderberg – New York, 618 p.
- Pristaš J., Elečko M., Maglay J., Fordinál K., Šimon L., Gross P., Polák M., Havrila M., Ivanička J., Határ J., Vozár J., Mello J & Nagy A., 2000a: Geologická mapa Podunajskej nížiny – Nitrianskej pahorkatiny 1: 50 000. Št. Geol. Úst. D. Štúra, Bratislava.
- Pristaš J., Elečko M., Maglay J., Fordinál K., Šimon L., Gross P., Polák M., Havrila M., Ivanička J., Határ J., Vozár J., Tkáčová H., Tkáč J., Liščák P., Jánová V., Švasta J., Remšík A., Žáková E. & Töröková I., 2000b: Vysvetlivky ku geologickej mape Podunajskej nížiny – Nitrianskej pahorkatiny 1:50 000, Št. Geol. Úst. D. Štúra, Bratislava, 250 p. (in Slovak, Engl. Resume).
- Schmidt Z. & Halouzka R., 1970: Nová fauna vertebrát villafranchienu zo Strekova na Hronskej pahorkatine. *Geol. práce, Správy*, 51, Bratislava, 173-183 (in Slovak, Engl. Resume).
- Sneed E. & Folk R., 1958: Pebbles in the lower Colorado River, Texas a study in particle morfogenesis. *J. Geology*, 66, Chicago, 114 – 150.
- Šarinová K., 2000: Sedimentárno-petrografická analýza kvartérnych sedimentov Ripňanskej priehlbiny. Diplomová práca – archív Kat. min. petr. PriF UK. Bratislava, 60 p. (in Slovak).
- Trask P.D., 1930: Mechanical analysis of sediments by centrifuge. *Econ. Geol.* 25, 581 – 599.
- Vass D., Began A., Gross P., Kahan Š., Krystek I., Köhler E., Lexa J., Nemčok J., Růžička M & Vaškovský I., 1988: Vysvetlivky k mape Regionálne geologické členenie Západných Karpát a severných výbežkov panónskej panvy na území ČSSR v mierke 1 : 500 000. *Geol. Úst. D. Štúra, Bratislava*, 31– 32 (in Slovak, Engl. Resume).
- Vaškovská E. & Vaškovský I., 1989, Niektoré novšie poznatky o kvartéri severnej časti Bratislavy a okolia. *Reg. geol. Záp. Karpát*, N 25, *Geol. Úst. D. Štúra, Bratislava*, 23 – 30 (in Slovak, Engl. Resume).
- Vaškovská E., 1992: Koeficienty zvetrávania a možnosti ich využitia pri stratigrafickom členení kvartérnych sedimentov a paleopód. *Geol. Práce, Správy* 96, *Geol. Úst. D. Štúra, Bratislava*, 75 – 83. (in Slovak, Engl. Resume).



Závada – Bielice Rise – a buried elevation between Bánovce and Rišňovce Depressions in the Danube Basin

DIONÝZ VASS¹, MICHAL ELEČKO² & KLEMENT FORDINÁL²

¹Faculty of Forestry, Technical University of Zvolen, Masarykova 24, 960 53 Zvolen, Slovakia

²Geological Survey of Slovak Republic, Mlynská dolina 1, 817 04 Bratislava, Slovakia

Abstract. Bánovská kotlina Depression (Bánovce Depression) and Rišňovská priehlbina Depression (Rišňovce Depression) are adjacent depressions at the northern margin of the Danube Basin. They had different tectonic and paleogeographic development. The Bánovce Depression started to open in the Eggenburgian and until the end of Early Miocene, sedimentation took place in marine environment there. Sea ingressions penetrated into basin still during the Early Badenian. The Rišňovce Depression started to open only in the Middle Badenian and until the end of Badenian, marine sedimentation survived there. Both depressions were divided by the Závada – Bielice Rise with axis in the ENE-WSW direction and with a combined faulted – folded structure. It originated in the Early Miocene paleostress field with a maximal compression in NW-SE and/or WSW- ENE (recent) directions. Already during the Early Miocene and in the beginning of Badenian, the Rise blocked southward directed ingressions from the Bánovce Depression. On the contrary during the Middle and Late Badenian, it prevented marine transgression from the south, from the Rišňovce Depression to the Bánovce Depression. The Rise preserved its paleogeographic function also during the Sarmatian, when it controlled fluvial deltaic sedimentation (the Ripňany Formation) in the Rišňovce depression, whereas in the Bánovce Depression, the volcano-clastic Ruskovce Member – a peripheral member of the Vtáčnik Andesite Formation, transported by the debris flow type mechanism – deposited. After the Early Pannonian, the Závada – Bielice Rise lost its paleogeographic function and was buried by younger Neogene sediments.

Key words: Danube Basin, Negene, paleogeography, Závada – Bielice Rise, Rišňovce Depression, Bánovce Depression.

Introduction

The Nitrianska pahorkatina Upland – more closely its part, which is surrounded from three sides by the Považský Inovec Mts., Stražovské vrchy Mts. and Trábeč Mts. – has been further divided by Mazúr & Lukniš (1978) into the Bojnianska pahorkatina and Bánovská pahorkatina Uplands (Fig. 1). This geomorphologic division broadly displays buried Neogene tectonics, hidden by the younger, loaded up geological and geomorphologic processes, and its expression in paleogeography. Geophysical research revealed that both uplands were built on two well detectable depressions in pre- Tertiary basement. The Bojnianska pahorkatina Upland were built on the Ripňany Depression and Bánovská pahorkatina Upland is underlain by the Svinná Depression (Fusán et al., 1971, 1987). In pre-Tertiary relief, the Ripňany Depression had an asymmetric form with the axis of NE-SW direction. The northwestern depression's margin is steeper than the southeastern one. The Svinná Depression has a symmetric, slightly elongated form. Both depressions are divided by a saddle between Prašice and Veľké Bielice (Fusán et al., 1971, 1987; Fig. 2). Brestenská and Vass (unpublished), Vass (in Keith 1989) attributed a paleogeographic importance to the saddle, announcing it as the Závada – Bielice Rise. Whereas

both depressions are filled with the Neogene sediments and their tectonic and paleogeographic development was essentially different, they were clearly divided in geological literature. Buday in Maheľ & Buday et al., (1968) described them as the Rišňovská priehlbina and Bánovská kotlina depressions. The same division was applied in regional and geological classification of the Danube Basin (Vass et al., 1988; Fig. 1).

New information about geology of the Bánovská kotlina Depression (Bánovce Depression) and an analysis and interpretation of geophysical measurements enabled to define the function of the Závada – Bielice Rise.

Brief characteristics of geology of the Bánovce and Rišňovce Depressions

Comparing with the Rišňovská priehlbina Depression (Rišňovce Depression), the Bánovce Depression is older. The lower part of the Bánovce Depression's fill is formed by the Early Miocene sediments, which indicate begin of depression's opening in the Eggenburgian. The opening took place in a paleostress field with maximal compression in the direction from NW-SE to NNW-SSE (recent co-ordinates; Kováč et al., 1989, 1993; Marko et al., 1995). Predominantly the normal faults of NW-SE direc-

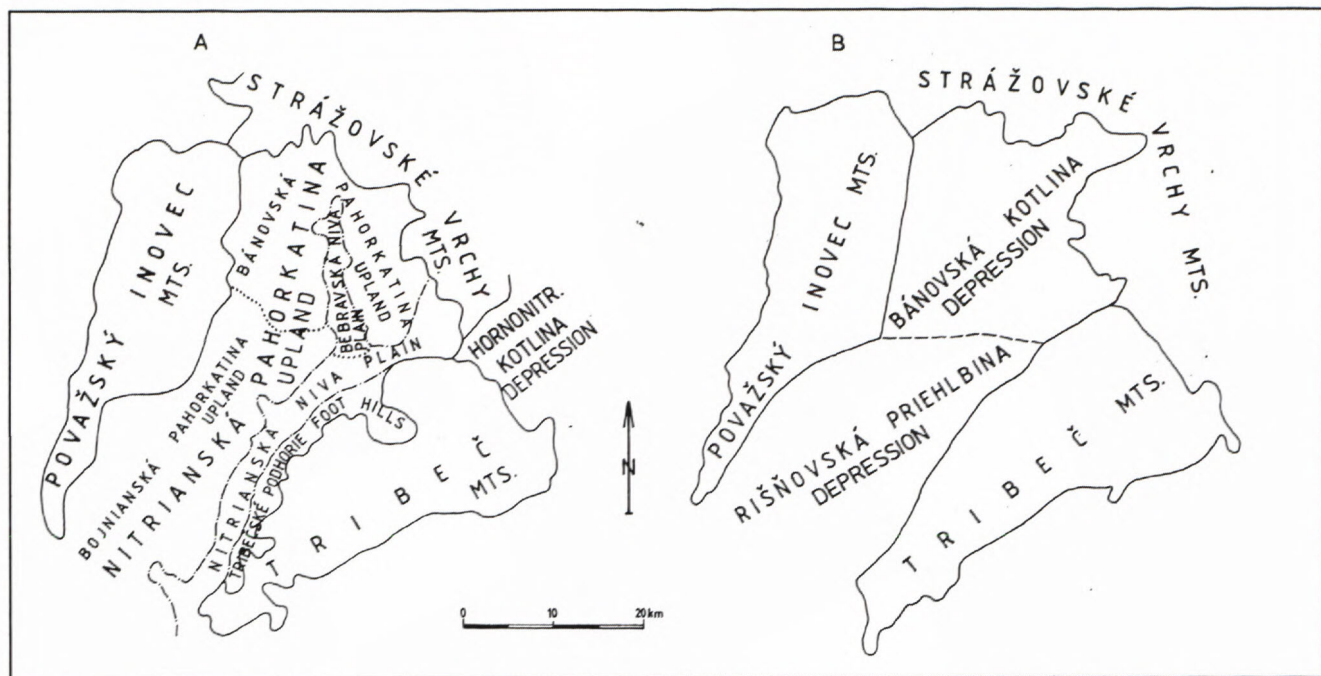


Fig. 1: Relief of pre-Tertiary basement in area between the Považský Inovec, Strážovské vrchy and Tribeč Mts. The Ripňany and Svinná Depressions divided by the Prašice – Veľké Bielice saddle (after Fusán et al., 1971, 1987)
 Explanation: 1 – basement relief isohypses (above sea level)

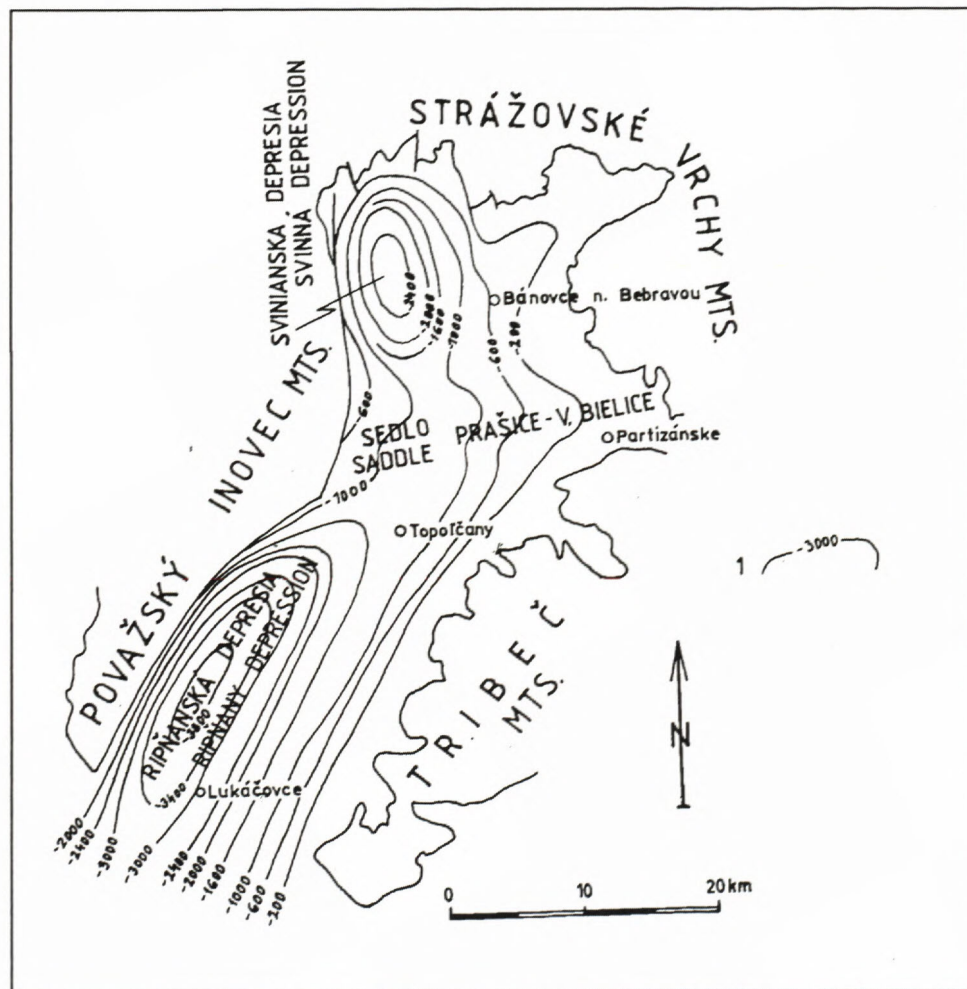


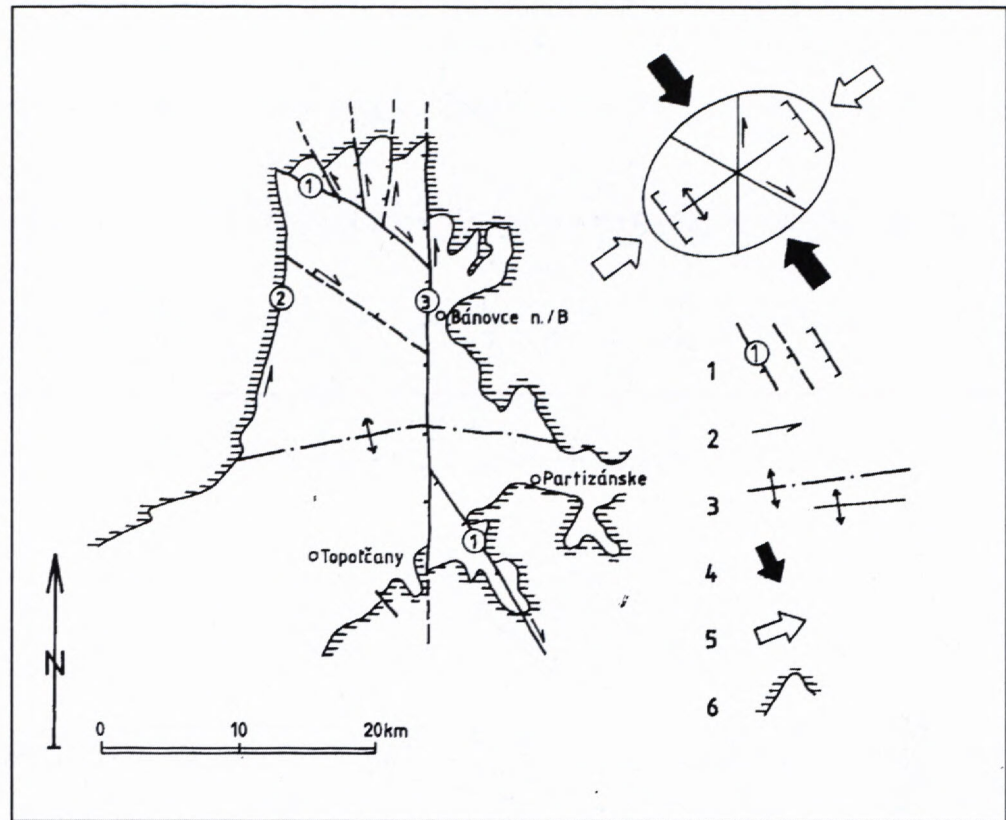
Fig. 2: A – Regional geomorphological division of the Nitrianska pahorkatina Upland (Mazúr & Lukniš 1978);
 B – Regional geological division of the Danube Basin's bay between the Považský Inovec, Strážovské vrchy and Tribeč Mts. (Vass et al., 1988)

Fig. 3: Main faults controlling opening and sedimentation in the Bánovce Depression during the Early Miocene. Coexisting stress field after Kováč et al., (1989, 1993) and Marko et al., (1995) in recent coordinates.

Explanation: 1 – normal faults, 2 – strike slip direction, 3 – fold structure axis, 4 – maximum compression direction, 5 – maximum extension direction, 6 – present margin of the Bánovce Depression

Significant faults:

1 – Jastrabie Fault; 2 – Dubodiel Fault; 3 – Bebrava (Timoradza) Fault



tion, with possible right slip component, were active during opening of the Bánovce Depression. The Jastrabie Fault (Maheľ 1969) was most significant dividing the depression's Early Miocene fill from the younger one (Fig. 3). The fault is deep seated, which has been documented by Blakely gravity gradients (Tkáč et al., 1997). Left slips on the N-S directed faults boosted depression's opening. However these faults manifested themselves during the later depression filling periods as the normal faults. So they are revealed also in actual patterns of the depression's geology. At the depression's eastern margin, the Bebrava Fault outlines the Neogene from the Paleogene and Mesozoic of the Stražovské vrchy Mts. in the depression's present pattern. The fault is of an inverse character, while the Paleogene sediments occur on its eastern side, they are missing on the western side. The Neogene sediments have a reverse distribution (Fordinál et al., in press.). The Bebrava Fault is deep seated, which is confirmed by Blakely gravity gradient. Spatial relations between the Jastrabie and Skýcov Faults (Maheľ 1969) and Bebrava Fault in Fig. 3, support an idea that the Jastrabie and Skýcov Faults are two fragments of the same fault, which has been obliquely disturbed by about 15 km long right slip of the Bebrava Fault. The segmentation had to take place before the Miocene, while right slip of this length has not been observed in other structure elements of the Bánovská kotlina Depression. For example, the Závada – Bielice Rise does not show any sign of the right slip segmentation. In actual pattern, horst of the Považský Inovec Mts. is outlined from the Bánovce Depression by the Dubodiel Fault (Závada F.; Maheľ 1969) at the depression's western margin. Northward of the

Dubodiel village, its activity during the Eggenburgian is indicated by conglomerates of the Eggenburgian age. In the Bánovce Depression, they represent a marginal facies of the Čausa Formation (Elečko & Fordinál in Pristaš et al., 2000). Also in this case, deep seating of the fault has been confirmed by Blakely gravity gradient (Fig. 4).

The Early Miocene stress field pressure conditions enabled formation of fold structures oriented straight to the direction of maximal compression. Already during this period, generation of the Závada-Bielice Rise were probably beginning, preventing the sea to break from the Bánovce Depression southward to recent area of the Danube basin. But optimal conditions of the elevation formation originated in paleostress field, which was deduced from the brittle deformation measurements for the Otnangian – Early Badenian period by Marko et al. (1995).

Sea encroached into the opening Bánovce Depression already during the Eggenburgian. In the Early Miocene (Eggenburgian to Karpatian) clastic sediments of the Čausa, Bánovce and Lakšársy Formations deposited (Brestenská et al., 1980; Brestenská in Samuel & Gašpariková 1983; Vass 1999; Elečko & Fordinál in Pristaš et al., 2000). In that time the Bánovce Depression was a part of – or at least in connection with – the west-Slovakian shear zone, where similar smaller depressions with a marine environment were opened out (Marko & Kováč 1996). These depressions ceased at the end of Early Miocene. The opening and filling of the Bánovce Depression went on also during the Middle Miocene, but connection with the sea was limited. Sea ingressions, indicated by the brackish fauna occurrence in the Svinná

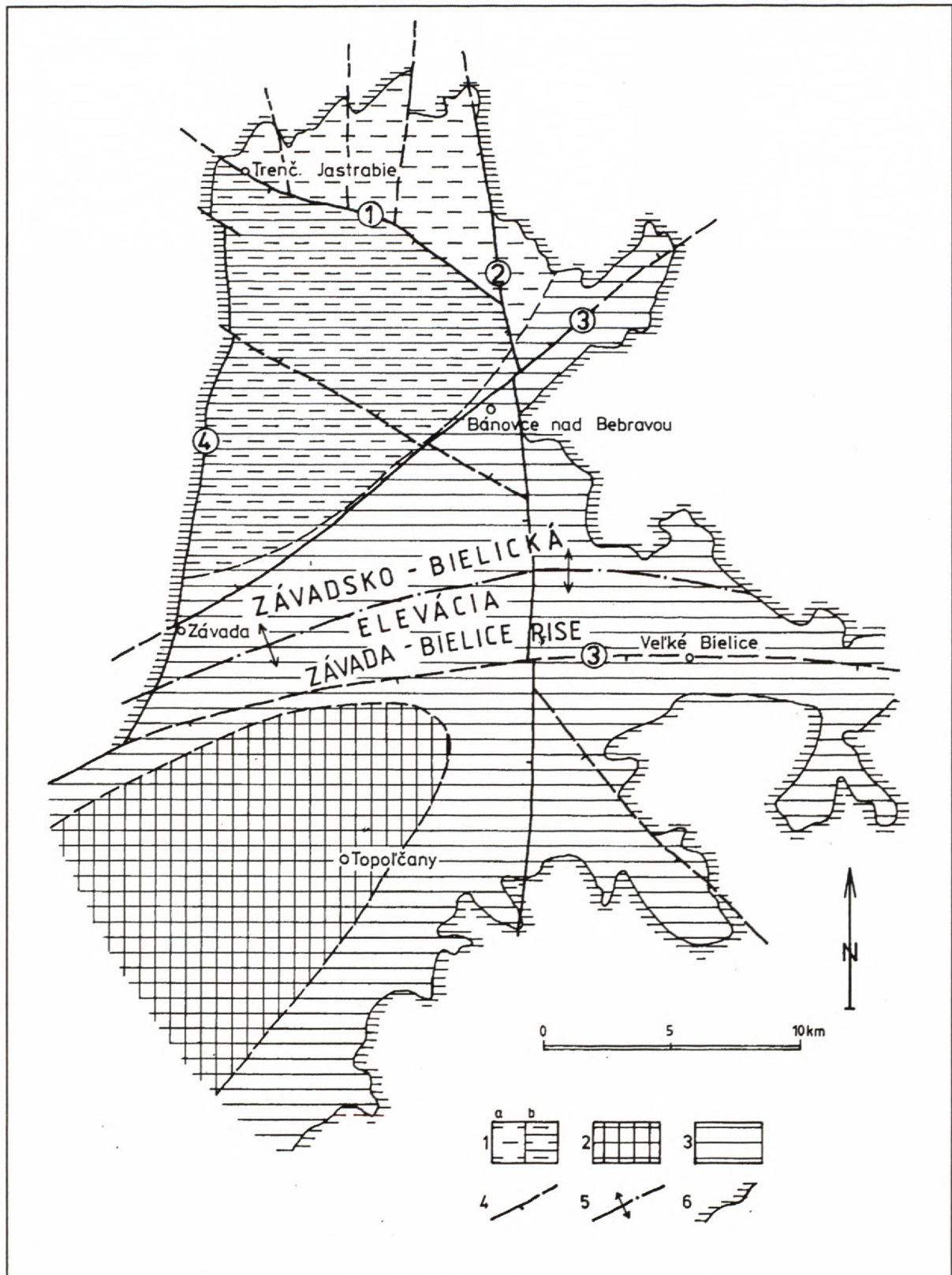


Fig. 4: Paleogeographic manifestations of the Závada – Bielice Rise.

Explanation: 1 – Early Miocene marine fill of the Bánovce Depression (Eggenburgian – Karpatian), a – at surface, b – hidden, 2 – marine sediments of the Middle Miocene (Middle and Late Badenian) in the Rišňovce Depression, 3 – brackish to freshwater sediments of the Middle Miocene to Pliocene, 4 – faults, 5 – elevation axis, 6 – margin of the basin

Significant Faults:

1 – Jastrabie Fault; 2 – Bebrava (Timoradza) Fault; 3 – faults outlining the Závada – Bielice Rise (in sense Fusán et al., 1987); 4 – Dubodiel Fault

Formation (Brestenská et al., 1980), reached the Bánovce Depression from the east, from the Hornonitrianska kotlina Depression and/or Handlovská kotlina Depression, where Elečko (in Šimon edit. 1997) assumes marine sedimentation during the Early Badenian. Marine sediments were reliably established in the Kordíky Formation in the borehole HV-9 (Gašpariková in Blaško et al., 1989) at the boundary of the Hornonitrianska kotlina and Žiar-ska kotlina Depressions. Connection to the open sea southward through the Rišňovce Depression was not possible, while this depression did not exist then. The younger Middle Miocene sediments that went on to fill the Bánovce Depression (Kamenec Formation, equivalent of the Handlová Formation and Ruskovce Member) have an affinity to the Middle Miocene development in the Hornonitrianska kotlina Depression (Šimon in Pristaš et al., 2000). Connection of both depressions took place in the area between raising Trábeč Mts. and Strážovské vrchy Mts. There is no evidence that during the Middle Miocene, even when the Rišňovce Depression was already being formed, a connection between the Rišňovce and Bánovce Depressions existed. The Bánovce Depression joined with the Rišňovce Depression only during the Late Miocene and Pliocene.

The Rišňovce Depression began to open during the Middle Miocene. Opening had been preceded by a long-term emergence and denudation. Erosion of the pre-Tertiary structures removed rocks of the Hronicum, most of the Veporicum rocks (Křížna nape) and outcropped the Tatricum (Fusán et al., 1987). The Rišňovce Depression were opening out in a stress field with maximum compression in the NE-SW (Vass et al., 1993, Hók et al., 1995), to NNE-SSW (Marko et al., 1995) directions, as showed by brittle deformation measurement results. In this stress field normal faults of the NE-SW to NNE-SSW directions controlling depression margins were active (Fig. 5). Western flank of the depression was controlled by the synsedimentary Majcichovo and Sládkovičovo Faults (Buday in Buday et al., 1967, in Maheľ & Buday et al., 1968). Smoother inclining eastern flank of the depression was controlled by the Veľké Zálužie Faults or fault complex (Pěničková & Dvořáková in Gaža et al., 1985; Fig. 6). The Majcichov Western Fault and eastern Veľké Zálužie Faults are manifested by horizontal Blakely gravity gradients (Fig. 5). Sea transgressed into the opening depression from the south-west, from central part of the Danube Basin, which already started to subside as an unit, with exception of the Kolárovo elevation. Throws on faults outlining the Rišňovce Depression were synsedimentary. From the Middle Badenian to the end of Sarmatian, they were contributing to accumulation of sediments more than 2000 m thick (without decompaction; Vass & Pereszlényi 1998). In relation to the thermal back-arc Danube Basin opening by a heterogeneous lithosphere stretching mechanism, the Rišňovce Depression was a part of the outer zone with an initial subsidence. Thermal effect of the lithosphere stretching, spreading from basin centre to the outer zone, was manifested by the upper crust faulting and stretching, which caused a synrift sedimentation (Lankreijer et al., 1995; Vass & Pereszlényi 1998).

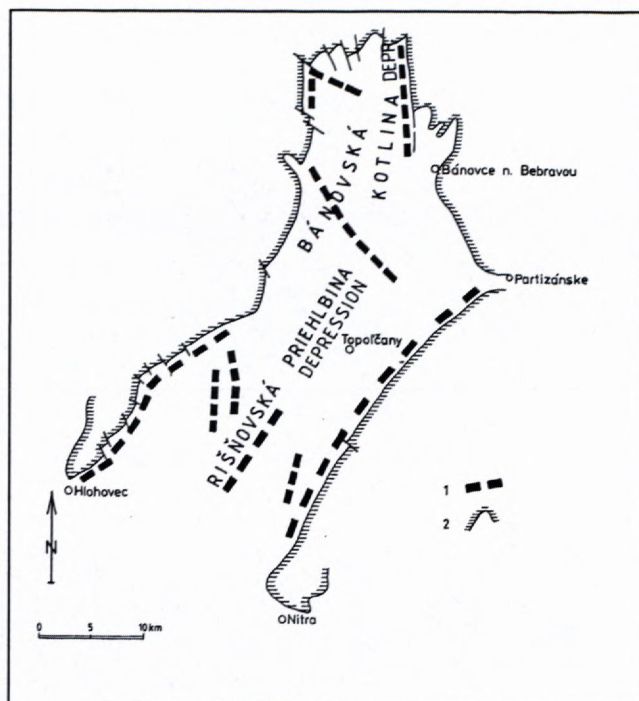


Fig. 5: Blakely horizontal gravity gradients indicating deep seating of some faults in the Bánovce and Rišňovce Depressions. Explanation: 1 – horizontal gravity gradients, 2 – margin of the Bánovce and Rišňovce Depressions.

In northern part of the Rišňovce Depression, marine sedimentation was replaced by deltaic one with a dominant river influence during the Sarmatian. From the north to the Hlohovec-Nitra horst, the depression was filled up by sediments of the Ripňany Formation. These sediments are without marine or brackish fauna and have no signs indicating a sea reworking of delta (Fordinál & Elečko 2000). According to their age, the deltaic sediments range from the Sarmatian to the Early Pannonian. A river forming the Ripňany delta was flowing from the Hornonitrianska kotlina Depression (Fig. 7). In the Hornonitrianska kotlina Depression, this river (paleostream of the Nitra river) deposited coarse detritic sediments of the Lehota Formation (Late Badenian – Early Sarmatian). Delta sediments of the Ripňany Formation could be deposited by smaller streams flowing into the Rišňovce Depression from the northwest and/or north i.e. from the Považský Inovec Mts., which had been risen then (F.T. apatite cooling age is 16 Ma, Král in Kováč et al., 1994).

The upper part of the Rišňovce Depression is formed by Caspian-type brackish and freshwater sediments of the Pannonian, Pontian and the Pliocene (the Ivánka, Beladice and Volkovce Formations). These sediments represent margins of the Danube Basin postrift development. Comparing with the basin's central part the sediments thickness is significantly reduced there (Vass & Pereszlényi 1998).

The different Miocene development in the Rišňovce and Bánovce Depressions points to paleogeographic function of the Závada – Bielice Rise. Fusán et al., (1987) outlined the elevation by faults. Its southern limitation is

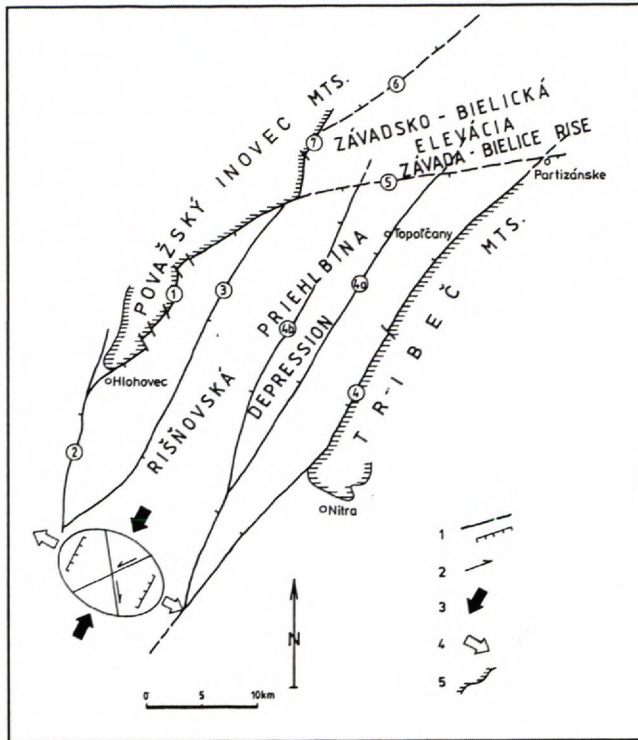


Fig. 6: Main faults of the Rišňovce Depression and diagram of a stress field enabling depression's opening in the Middle and Late Badenian.

Explanation: 1 – normal faults, 2 – strike slips direction, 3 – maximum compression direction, 4 – maximum extension direction, 5 – margin of the Rišňovce Depression

Significant faults: 1 – Majcichov Fault, 2 – Eastern Trnava (Váh) Fault, 3 – Sládkovičovo Fault, 4 – Eastern Veľké Zálužie Fault, 4a – Western Veľké Zálužie Fault, 4b – Middle Veľké Zálužie Fault, 5, 6 – marginal faults of the Závada – Bielice Rise (5 – continuation of the Majcichov Fault in sense Buday et al., 1967).

distinct on the Map of total Bouguer anomalies (Tkáč et al., 1997). The northern limitation of the elevation has been defined by the fault, which was syndimentary during the Early and Middle Miocene. This is indicated by 800 m thick Svinná Formation on the downthrow block, i.e. in the Bánovce Depression (Brestenská et al., 1980). Elevation's paleogeographic influence can be observed already in the Early Miocene, when the elevation was the southern limitation of the Bánovce Depression and the sea could not break from there further to the south. Though a fold character of this elevation may not be excluded. Direction orientation of the Závada – Bielice Rise was best matched with paleostress in the Oligocene and Early Badenian (Marko et al., 1995). Then during the maximum compression in the NNW-SSE direction, folds with axis oriented in the ENE-WSW direction, which is the axis direction of the Závada – Bielice Rise, could be formed (Fig. 4).

We know that the geological and especially facial development of the Middle Miocene was contrasting in the Bánovce and Rišňovce Depressions. The Svinná Formation representing the Early Badenian in the Bánovce Depression comprises along with freshwater organic

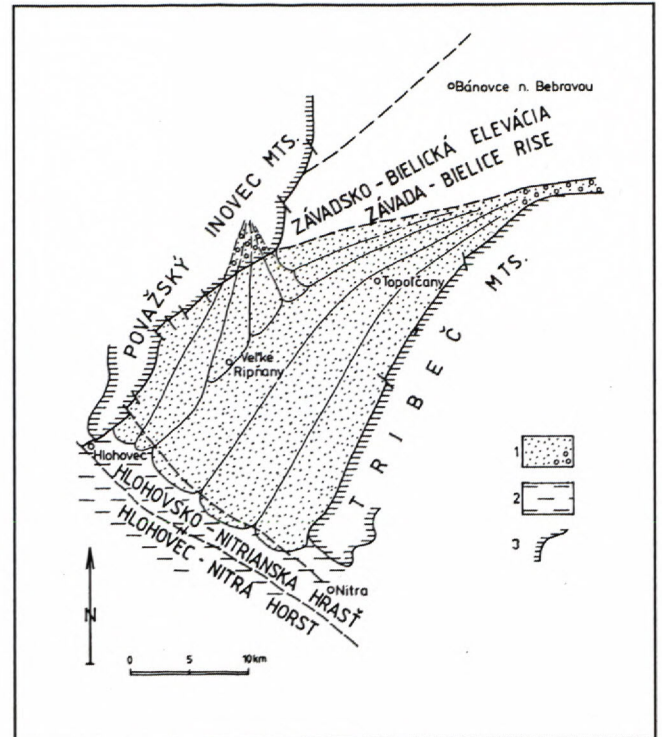


Fig. 7: Distribution of the Ripňany Formation (Sarmatian – Lower Pannonian) interpreted as a deltaic complex controlled in the north by the Závada – Bielice Rise and in the south by the perpendicularly directed Hlohovec – Nitra horst.

Explanation: 1 – Ripňany Formation (Sarmatian – Lower Pannonian), 2 – Vrable (Sarmatian) and Ivánka (Pannonian) Formations, 3 – margin of the Považský Inovec and Tribeč Mts.

remnants also brackish ostracodes and foraminifers of the species *Ammonia beccarii*. This points to sea ingressions most probably from the Hornonitrianska kotlina Depression (Elečko & Fordinál in Pristaš et al., 1999). In the Rišňovce Depression the Early Miocene sediments are missing, while the depression began to open and the sea intruded there only in the Middle Miocene. But this ingressions did not reach the Bánovce Depression, where the Middle and Upper Miocene development took place in a freshwater environment (Fig. 4). Sea ingressions into the Bánovce Depression was hindered by the Závada – Bielice Rise. It was so rigid that the faults opening the Rišňovce Depression did not break through this elevation, they have died away there (Fig. 6). The Ripňany delta during the Sarmatian and Early Pannonian in the Rišňovce Depression was fed by the paleo-Nitra river's clastic material. This was transported over a breakthrough in horst of the Tribeč Mts. Delta fan was formed south of the Závada – Bielice Rise (Fig. 7). The elevation also controlled southern margin of the Ruskovce Member (Middle Sarmatian) distribution.

The Ruskovce Member represents a complex of upward coarsening alluvial fans – Gilbert deltas. Coarse-grained clastic material was transported by streams of „debris flow“ type (Kováč et al., 1993). It had a genetic affinity to the Vtáčnik Formation, which participated in structure of the volcanic Vtáčnik Mts. and forms a mem-

ber of this formation (Šimon in Pristaš et al., 2000). Differently from the Ruskovce Member, the delta of the Ripňany Formation represents a delta built by a river mouth into the Danube Basin of that time.

After the Early Pannonian the Závada – Bielice Rise lost its paleogeographic function and waters of a lake occupying the Danube Basin transgressed also into the Bánovce Depression. The Bánovce Depression was unified with the Rišňovce Depression then and through this with the Gabčíkovo Depression.

Discussion

During the Early Miocene a large part of the present Danube Basin area was emerged and exposed to a denudation. The Paleogene sediments, which had been more likely distributed there, were removed during this denudation. In the Bánovce Depression and its surrounding, the Paleogene sediments have been spared thank to the fact that they were covered by the Early Miocene sediments. The Paleogene sediments were not even removed from the Závada – Bielice Rise, especially from its eastern part. They are cropping out there (in the area of Hradište and between towns Bánovce nad Bebravou and Partizánske). This fact points to a delayed formation of the elevation comparing to the Early Miocene uplift of the future Danube Basin area. It looks like the elevation originated in the Early Badenian. Presence of the Paleogene sediments points also to the fact that the elevation was not strongly exposed. But its uplift was sufficient to play role of a paleogeographic dividing line between the Rišňovce and Bánovce Depressions. But rising of the elevation did not caused its deep erosional destruction. Therefore the Paleogene has been preserved in the elevation area but its thickness should be smaller than in the basement of the Bánovce Depression.

Conclusion

Knowledge of geology of the Bánovská kotlina and Rišňovská priehlbina Depressions supported by numerous geophysical indications shows that both depression structures were evolving independently until the Upper Miocene and/or Pliocene. This happened thanks to the presently buried Závada – Bielice Rise. The elevation was of folded – faulted character. Its function can be observed from the Early Miocene and especially from the Badenian, when it divided both depression structures causing a diametrically different sedimentation type within them. The Bánovce Depression was reached by the sea during the Early Miocene, so in this depression the Lower Miocene is represented by marine facies. Sea incursions encroached into the depression also during the Early Badenian. In the Rišňovce Depression south of the Závada – Bielice Rise, the Lower Miocene and Lower Badenian sediments are missing. Later during the Middle and Late Badenian sedimentation took place in a non-marine environment in the Bánovce Depression. On the contrary southward of the Závada – Bielice Rise, the Rišňovce Depression was reached by the sea from the south, the Middle and Upper Badenian are represented by

marine facies there. The contrasting development went on also in the Sarmatian and Early Pannonian. The Rišňovce Depression was filled by delta sediments (the Ripňany Formation) then, while in the Bánovce Depression deposited peripheral volcano-clastic sediments of the Ftáčnik Formation (Ruskovce Member) representing upward coarsening alluvial fan sediment facies with the transport mechanism of „debris flow“ type.

References

- Blaško, D., Juriš, F., Tupý, P., Laffers, F., Hruškovičová, M., Malý, S. & Klubert, J., 1989: Handlová – východ – VP – uhlie. Závěrečná správa a výpočet zásob (Final report on Handlová - East brown coal – in Slovak). Manuscript, Geol. Survey of SR, Bratislava.
- Brestenská, E., Havrila, M., Kullmanová, A., Lehotský, I., Remšík, A., Vaškovský, I., Gross, P. & Maheľ M., 1980: Geologická mapa a vysvetlivky k regiónu Bánovskej kotliny M = 1 : 50 000 (Geological map and Explanatory Notes to the Bánovce Depression Region in the scale 1:50 000 – in Slovak). Manuscript, Geol. Survey of SR, Bratislava.
- Buday, T., Cicha, I., Hanzlíková, E., Chmelík, F., Koráb, T., Kuthan, M., Nemček, J., Pícha, F., Roth, Z., Seneš, J., Scheibner, E., Stráňík, Z., Vaškovský, I. & Žebera, K., 1967: Regionální geologie ČSSR, díl II. Západní Karpaty, zv. 2, (Regional Geology of Czechoslovakia, vol. II./2 – in Czech). Ústí. Úst. Geol., Academia, Praha, 7 – 651.
- Fordinál, K. & Elečko, M., 2000: Ripňanske súvrstvie – sladkovodné sedimenty sarmatu a spodného panónu rišňovskej priehlbiny (Ripňany Formation – a Sarmatian and Early Pannonian fresh water sedimentary assemblage of the Rišňovce Depression – in Slovak with English summary). Mineralia Slovaca 32, Bratislava, 55 – 60.
- Fordinál, K., Elečko, M., Šimon, L. & Holcová, K., (in press): Bánovská kotlina Depression (northern part of the Danube Basin); Neogene stratigraphy and geological development. Slovak Geol. Mag., Geol. Survey of Bratislava.
- Fusán, O., Biely, A., Ibrmajer, J., Plančár, J. & Rozložník, L., 1987: Podložie terciéru vnútorných Západných Karpát (Basement of the Tertiary of the Inner Carpathians – in Slovak with English summary). Geol. Úst. D. Štúra, Bratislava, 5 – 123.
- Fusán, O., Ibrmajer, J., Plančár, J., Slávik, J. & Smíšek, M., 1971: Geologická stavba podložia zakrytých oblastí južnej časti vnútorných Západných Karpát (Geological Structure of the Basement of the Covered Southern Part of the Inner West Carpathians – in Slovak with English summary). Západ. Karpaty 15, Bratislava, 1 – 173.
- Gaža, B., Pěničková, M., Dvořáková, V., Altanová, G., Jihlavec, F., Nemeček, V. & Uhmán, J., 1985: Závěrečná zpráva vyhledávacího průzkumu na živice v podunajské pánvi v letech 1973-1983 (Final report on the oil and gas exploration in the Danube Basin in the years 1973-1983 – in Czech). Manuscript, Geofyzika Brno. 1-131.
- Hók, J., Šimon, L., Kováč, P., Elečko, M., Vass, D., Halmo, J. & Verbich J., 1995: Tectonics of the Hornonitrianska kotlina Depression in the Neogene. Geol. Carpathica, 46, 4, Bratislava, 191–196.
- Keith, J.F., jr., Vass, D., Kanes, W.H., Pereszlényi, M., Kováč, M. & Král, M., 1989: Sedimentary basins of Slovakia, Part II. Final report on the hydrocarbon potential of Danube Lowland Basin, vol. 1, Manuscript Univ. South Carolina ESRI, Technical Report 89-0019, 1 – 143.
- Kováč, P., Baráth, I., Holický, I., Marko, F. & Túnyi I., 1989: Basin opening in the Lower Miocene strike-slip zone in the SW part of the Western Carpathians. Geol. Carpath. 40/1, Bratislava, 37 – 62.
- Kováč, M., Nagy, A. & Baráth, I., 1993: Ruskovské súvrstvie – sedimenty gravitačných tokov (sz. časť Bánovskej kotliny) [Ruskovce Formation - deposits of sediment gravity flows (NW part of the Bánovská kotlina depression) – in Slovak with English summary]. Miner. Slov. 25, 2, Bratislava, 117 – 124.
- Lankreijer, A., Kováč, M., Cloetingh, S., Pitoňák, P., Hlůška, M. & Biermann, C., 1995: Quantitative subsidence analysis and forward modelling of the Vienna and Danube Basins. Tectonophysics, 252, Amsterdam, 433 – 451.

- Kováč, M., Král, J., Márton, M., Plašienka, D. & Uher, P., 1994: Alpine Uplift History of the Central Western Carpathians: geochronological, paleomagnetic sedimentary and structural data. *Geol. Carpath.*, 45, 2, Bratislava, 83 – 96.
- Maheľ, M., 1969: Zlomy a ich úloha počas mezozoika vo vnútorných Karpatoch (Faults and their role in the Mesozoic of the Inner Carpathians – in Slovak with English summary). *Geol. Práce, Spr.* 47, Bratislava, 7 – 29.
- Maheľ, M., Buday, T., Čicha, I., Fusán, O., Hanzlíková, E., Chmelík, F., Kamenický, J., Koráb, T., Kuthan, M., Matějka, A., Nemček, J., Pícha, F., Roth, Z., Seneš, J., Schneibner, E., Stránfk, Z., Vaškovič, I. & Žebera, K., 1968: Regional Geology of Czechoslovakia, part II. West Carpathians. *Ústř. Úst. Geol. Praha*, 1 – 723.
- Marko, F. & Kováč, M., 1996: Rekonštrukcia miocénnej tektonickej evolúcie Vaďovskej kotliny na základe analýzy štruktúrneho a sedimentárneho záznamu [Reconstruction of the Miocene tectonic evolution of the Vaďovce Depression, based on the analysis of structural and sedimentary record (Western Carpathians) – in Slovak with English summary]. *Mineralia Slovaca* 28, Bratislava, 81 – 91.
- Marko, F., Plašienka, D. & Fodor, L., 1995: Meso-Cenozoic tectonic stress fields within the Alpine-Carpathian transition zone: a review. *Geol. Carpath.* 46/1, Bratislava, 19 – 27.
- Mazúr, E. & Lukniš, M., 1978: Regionálne geomorfologické členenie Slovenskej socialistickej republiky (Regional geomorphologic division of the Slovak Socialist Republic – in Slovak with Russian & German summary). *Geogr. Čas.*, 30, 2, Bratislava, 101–125.
- Pristaš, J., Elečko, M., Maglay, J., Fordinál, K., Šimon, L., Gross, P., Polák, M., Havrila, M., Ivanička, J., Határ, J., Vozár, J., Tkáčová, H., Tkáč, J., Liščák, P., Jánová, V., Švasta, J., Remšík, A. & Žáková, E., 2000: Vysvetlivky ku geologickej mape Podunajskej nížiny - Nitrianskej pahorkatiny 1 : 50 000 (Explanatory Notes to Geological map of Danube Lowland – Nitrianska pahorkatina Upland 1 : 50 000 – in Slovak with English summary). *Geol. Survey of SR, Bratislava*, 1 – 250.
- Pristaš, J., Elečko, M., Fordinál, K., Šimon, L., Polák, M., Ivanička, J., Vozár, J., Töröková, I., Žecová, K., Zlinská, A., Slamková, M., Boorová, D. & Kernátsová, J., 1999: Vysvetlivky ku geologickým mapám Bánovskej kotliny 1:25 000, listy: 35-231 (Trenčianská Turná, časť), 35-232 (Motešice, časť), 35-233 (Dubodiel, časť) a 35-233 (Uhrovec, časť) (Explanatory Notes to Geological maps of the Bánovce Depression in the scale 1: 25 000 – in Slovak). Manuscript, *Geol. Survey of SR, Bratislava*.
- Samuel, O. & Gašpariková, V., 1983: 18th European Colloquy on Micropaleontology. Excursion Guide. *Geol. Úst. D. Štúra, Bratislava*, 1 – 215.
- Šimon, L., Elečko, M., Lexa, J., Kohút, M., Halouzka, R., Gross, P., Pristaš, J., Konečný, V., Mello, J., Polák, M., Vozárová, A., Vozár, J., Havrila, M., Köhlerová, M., Stolár, M., Jánová, V., Marcin, D. & Szalaiová, V., 1997: Vysvetlivky ku geologickej mape Vtáčnika a Hornonitrianskej kotliny 1:50 000 (Explanatory Notes to Geological map of Vtáčnik Mts. and Hornonitrianska kotlina Depression 1:50 000 – in Slovak, with English summary). *Geol. Survey of SR, Bratislava*, 1 – 281.
- Tkáč, J., Šefara, J., Tkáčová, H., Šantavý, J., Kubeš, P. & Husák, L., 1997: Mapa geofyzikálnych indícií a interpretácií. Región Nitrianska pahorkatina [Map of geophysical indications and interpretations (MGII). Region Nitrianska pahorkatina Upland – in Slovak]. Manuscript, *Geofond, Bratislava*, 1 – 29.
- Vass, D., 1999: Litostratigrafia neogénu Západných Karpát (Lithostratigraphy of West Carpathian Neogene – in Slovak). Manuscript, *Geol. Survey of SR, Bratislava*.
- Vass, D., Began, A., Kahan, Š., Köhler, E., Krystek, I., Lexa, J. & Reptok, J., 1988: Regionálne geologické členenie Západných Karpát a sev. výbežkov Panónskej panvy na území ČSSR (Regional - Geological Division of West - Carpathians Mts. and N Promontories of Pannonian Basin on Czechoslovak Territory – in Slovak with English summary). *Geol. Ústav D. Štúra Bratislava, Geofond Bratislava, Vojenský kartografický ústav Harmanec*.
- Vass, D., Hók, J., Kováč, P., & Elečko, M., 1993: Sled paleogénnych a neogénnych tektonických udalostí v juhoslovenských kotlinách vo svetle napätových analýz (The Paleogene and Neogene Tectonic Events of the Southern Slovakia Depressions in the Light of the Stress-field Analyses – in Slovak with English summary). *Miner. Slovaca* 25, Bratislava, 79 – 92.
- Vass, D., & Pereszlényi, M., 1998: Assymmetric lithospheric stretching in Danube Basin. *Slovak Geol. Mag.* 4, Bratislava, 61 – 74.

Mineral and chemical composition of the ores at the Dve Vody Sb-Au deposit, Western Carpathians

JURAJ MAJZLAN¹, MARTIN CHOVAN² & JOZEF MICHÁLEK³

¹ Department of Geology, University of California at Davis, Davis, CA 95616, USA

² Department of Mineralogy and Petrology, Comenius University, Mlynská dolina G, 842 15 Bratislava, Slovakia

³ EnviGeo, Ltd., Kynceľová 10, 974 01 Banská Bystrica, Slovakia

Abstract. The Hercynian crystalline complex of the Nízke Tatry Mountains (Western Carpathians, Slovakia) hosts a number of hydrothermal ore deposits, variable in their mineral and chemical composition. The Dve Vody deposit is one of them, with several separate vein systems in gneisses and migmatites. The ore samples, collected at waste dumps of the adits, were investigated by the means of optical microscopy, electron microprobe analyses, X-ray diffraction, and bulk analyses for Ag, As, Au, Cu, Pb, Sb, and Zn by a combination of spectroscopic techniques. There are As-Au, Sb, base-metals, and siderite mineralizations developed in the deposit, listed in the order in which they were formed. The As-Au mineralization is represented by fine-grained pyrite-arsenopyrite ores hosted by gray quartz. These ores are the principal gold carrier in the deposit (up to 14 ppm Au). The Sb mineralization comprises three parageneses: carbonate, sulfosalts-sphalerite, and stibnite. Carbonates, varying in their composition from early siderite to late Fe-dolomite, with minor calcite and magnesite, are the earliest paragenesis. Sphalerite is always earlier than the sulfosalts. The most common sulfosalt in the Sb mineralization is zinckenite. Stibnite usually occurs in white quartz or as monomineral veinlets in strongly altered rocks. The principal ore minerals of the base-metals mineralization are galena and pyrite. Silver in these ores appears to be concentrated in infrequent tetrahedrite inclusions in galena. The most abundant minerals of the siderite mineralization are siderite, tetrahedrite, and bournonite. The rock-forming minerals of the wall-rocks, with the exception of quartz, were altered to illite. The investigation of the ore samples was complemented by panning of alluvial sediments. The streams draining the area of the deposit showed elevated concentration of gold flakes (up to 7 gold flakes).

Key words: Nízke Tatry Mts, hydrothermal mineralization, stibnite, gold

Introduction

Nízke Tatry Mts, a mountain ridge in the Western Carpathian arc, is a region with long history of mining of gold, antimony, iron, copper, and other metals (Chovan et al. 1996). Despite the amount of metals extracted, little is known about mineral and chemical composition of the ores. Detailed information on the ores and the rocks that host the ores is necessary to answer the questions of metallogenesis of the region. As a part of our systematic work on the ore deposits in the Nízke Tatry Mts (see also Chovan et al. 1995, Majzlan et al. 1998), we paid attention to one of the larger ore deposits in the region, the deposit Dve Vody. The goal of the presented work is to offer a detailed description of the ore samples from Dve Vody, with emphasis on their mineral and chemical composition. The Dve Vody deposit is compared to other ore deposits in the Nízke Tatry Mts.

Geologic settings

The deposit Dve Vody is located on southern slopes of the Nízke Tatry Mountains, in Stellerova dolina valley, appr. 7 km north from the village of Dolná Lehota. The

valley exposes crystalline rocks of the Tatric unit (Biely & Bezák, 1997), dominated by gneisses and migmatites with small amphibolite bodies (Fig. 1). Petrogenetic and regional geological problems of the metamorphosed crystalline rocks were addressed by Janák et al. (1993), Hovorka et al. (1994), Petřík et al. (1998) and others.

History of ore exploitation and research on the Dve Vody deposit is briefly summarized by Michálek (1999). Results of a detailed mineralogical study of the Dve Vody ores were reported by Hak (1966). In addition to the minerals detected in the present study, he found scarce antimony, chalcostibite, jamesonite, and unidentified gold tellurides. We have also not found cinnabar inclusions in stibnite reported by Cambel et al. (1976). Kantor (1948) gives an analysis of the ores of siderite-tetrahedrite veins as Sb 7.96 %, As 0.53 %, Pb 5.57 %, Au 1.4 ppm, Ag 471.6 ppm, Fe 9.26 %, and Cu 3.99 %. Michálek (1993) determined the average metal concentration of the Dve Vody ores from are 3.8 % Sb, 0.4 % As, 4.2 ppm Au, and 3.5 ppm Ag. Munde (1944 in Michálek, 1999) analyzed the Sb-Au ores of the Main vein in the adits 1 and 2 to find Sb 4.48 %, As 0.27 %, 9.08 ppm Au, 11.57 ppm Ag at average vein thickness of 0.70 m. Metalometric prospecting activities (Gubač, 1980) detected an antimony

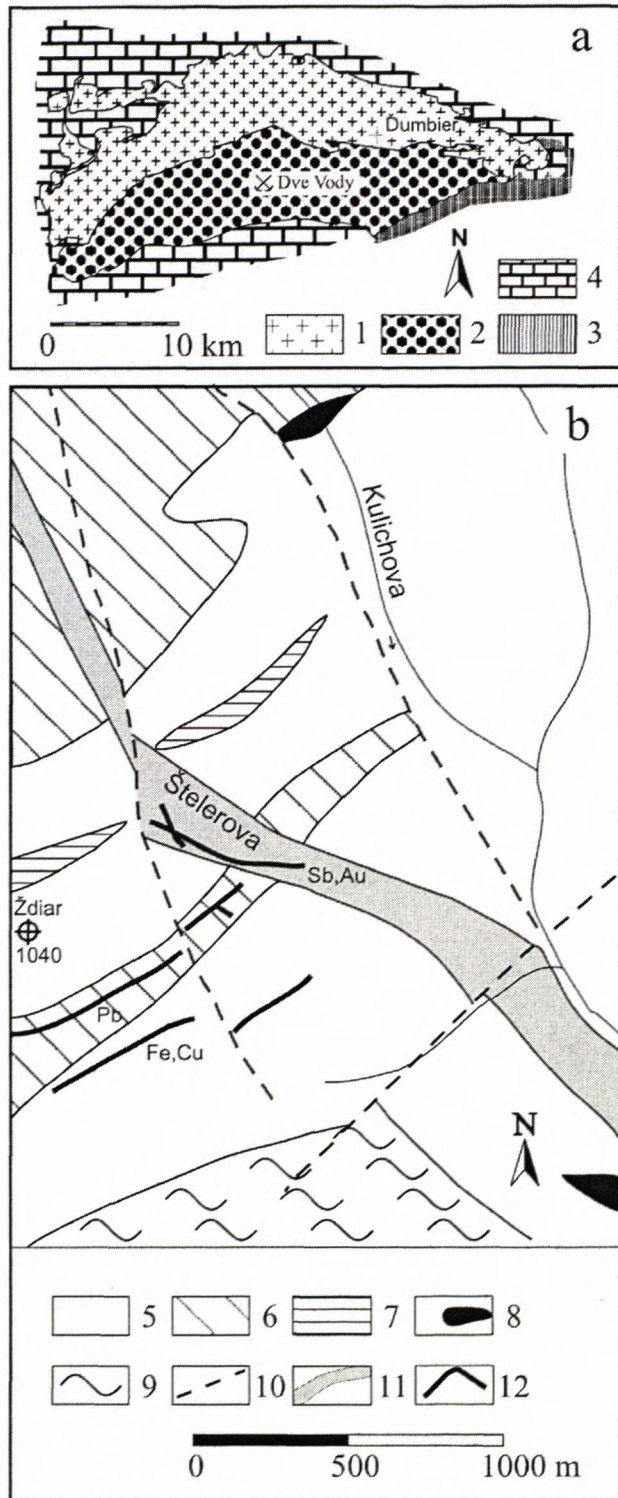


Fig. 1. a) a schematic geologic map of the Ďumbier part of the Nízke Tatry Mts with localization of the Dve Vody deposit, 1 – granitoid rocks of Tatric unit, 2 – high-grade metamorphic rocks of Tatric unit, 3 – Mesozoic sedimentary sequences of Tatric, Veporic, and Hronic unit, 4 – low-grade metamorphic rocks of Veporic unit, b) schematic geologic map of the Dve Vody deposit and vicinity, 5 – biotite – two-mica banded gneisses, 6 – biotite – two-mica ophthalmitic gneisses, 7 – metasediments and metavolcanoclastic rocks with subgraphitic admixture, 8 – amphibolites, 9 – orthogneisses of the Struhár type, 10 – faults, 11 – zones with As-Au and Sb ores, 12 – ore veins.

anomaly northward from the deposit, in the Kulichova dolina valley. Pulec et al. (1983) evaluated the composition of heavy mineral concentrates from the streams in the southern part of the Nízke Tatry Mountains, including the area of the Dve Vody deposit.

The paragenetic studies of the deposit are limited to the work of Kantor (1948) and Hak (1966). Figure 2 reproduces the unpublished paragenetic sequence of Kantor (1948). Hak (1966) distinguished the principal ore formation stages of ore deposits in the Nízke Tatry Mts. The general features of his work are re-iterated in the latest metallogenetic classification of the ores in the Nízke Tatry Mts (Chovan et al. 1996).

(Kantor 1948)

	1	2	3	4
quartz	—	—	—	—
arsenopyrite	—	—	—	—
pyrite	—	—	—	—
sphalerite	—	—	—	—
ankerite	—	—	—	—
stibnite	—	—	—	—
boulangerite	—	—	—	—
calcite	—	—	—	—

Fig. 2. Paragenetic sequence of the Dve Vody deposit after Kantor (1948).

Methods and material

The samples of ore minerals and altered rocks were collected at waste dumps and in the entrance portion of the accessible adits. Sampling of the dumps was accompanied by panning of the stream sediments and the material from selected dumps. The heavy minerals were concentrated from 10-15 kg of sandy (<3 mm) material. In the laboratory, the concentrates were dried and separated to fractions >0.5 mm, 0.2-0.5 mm, and <0.2 mm by sieving. The fraction >0.5 mm usually represented a negligible portion of the concentrate and was not evaluated further. The concentrates were checked for the presence of scheelite with a UV lamp. Cassiterite and wolframite were identified by coloring tests in hot dilute HCl (1:1) and hot aqua regia, respectively. The reported number of gold grains represents a sum for the fraction <0.2 mm and 0.2 – 0.5 mm. Cassiterite, scheelite, wolframite and cinnabar grains were counted only in fraction 0.2 – 0.5 mm.

Thin and polished sections were studied in reflected and transmitted light. All collected bulk samples were checked for the presence of scheelite with a UV lamp. Chemical analyses of the samples were carried out by a combination of atomic absorption spectroscopy techniques for Au (detection limit 0.02 ppm), Ag (0.4 ppm), Cu (0.001 wt.%), Zn (0.001 wt.%), Bi (0.0008 wt.%) in the laboratories of Geologický Prieskum (Geological Survey), Turčianske Teplice, Slovakia. The samples with gold concentration >5 ppm were re-analyzed for gold. The reproducibility of the analyses was inspected on selected samples in the laboratories of Westore Engineering

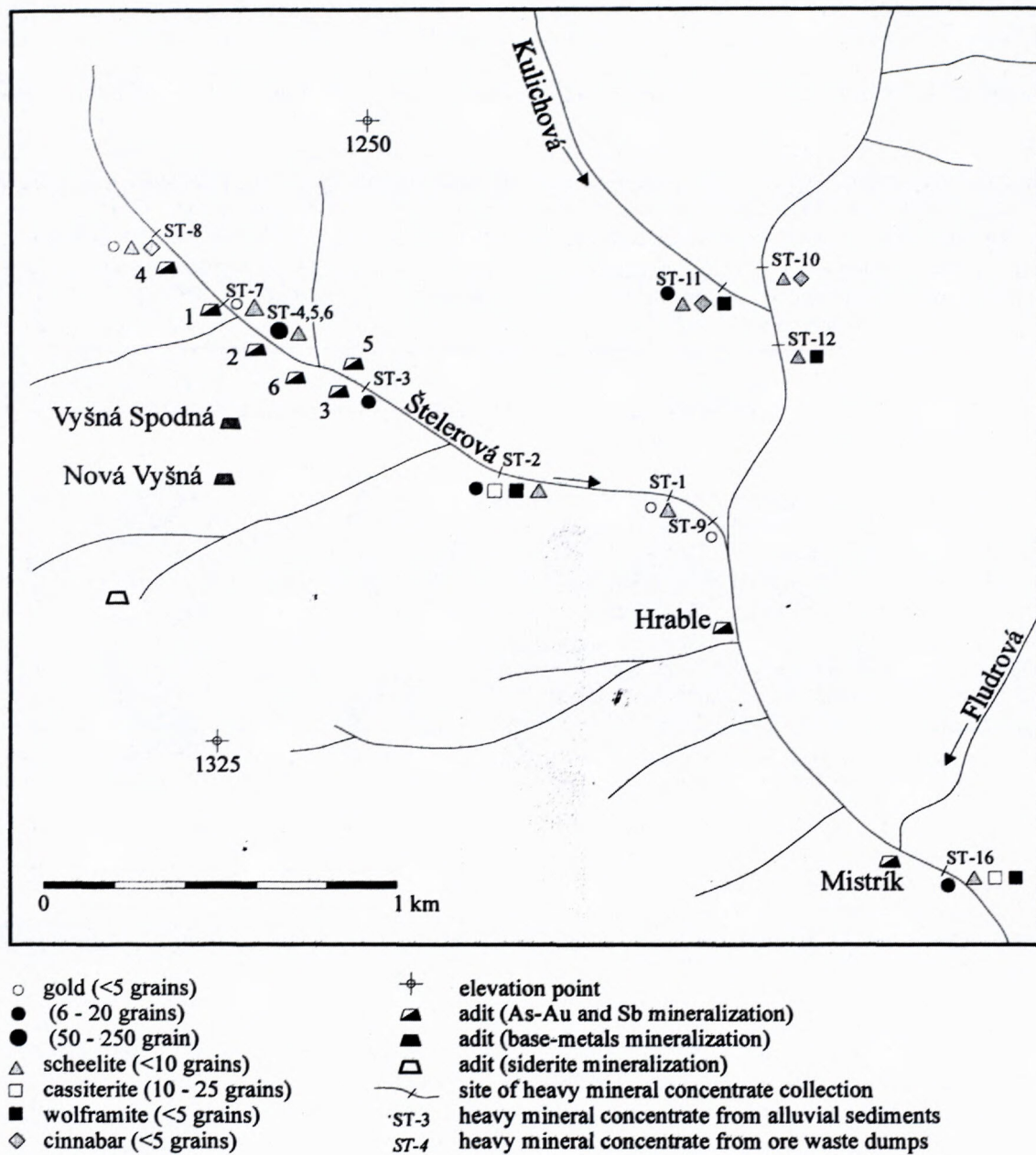


Fig. 3. Location of the adits of the Dve Vody deposit and results of panning.

Table 1. A comparison of chemical analyses of bulk ores as analyzed by Geologický Prieskum (Geological Survey), Turčianske Teplice, Slovakia (first entry) vs. Westore Engineering Ltd., Vancouver, Canada (second entry).

	Au	Ag	As	Pb	Sb	Zn	Cu
V-1	17.0/7.5	14.4/9.6	1367/600	4497/3700	3085/2440	59/50	447/300
V-7		15.0/5.2	5969/4300	3534/1270	3643/1300	173/50	67/20
V-10	5.51/7.2	1.1/0.4	759/2000	58/90	23212/10800	109/60	32/10
V-15		7.5/8.0	1901/1900	229/200	517/550	57/80	221/200
V-19	9.70/9.40	1.2/1.2	23116/20800	172/210	269/1040	36/30	25/10
V-20		6.9/2.4	638/500	2996/870	12060/3120	280/30	103/10
V-22A	1.82/2.06	0.3/2.0	2050/2100	31/1800	49/1700	10/530	29/50
V-22B		1.6/1.6	17405/26000	198/380	275/350	77/80	59/30
V-24	7.07/7.15	1.5/1.6	397/700	1041/1000	1336/1150	158/100	36/30
V-30		2.4/2.8	911/3200	151/880	22754/41000	15/tr	61/30

Ltd., Vancouver, Canada (Table 1). The reproducibility is satisfactory with the exception of zinc because the samples were selected on the base of their gold content and contained little zinc. The difference in gold concentration in the sample V-7 is caused by the presence of metallic gold which cannot be finely ground. It is homogeneously distributed in the powdered sample. We have observed metallic gold in this sample in the polished sections.

Oriented mounts of the <2 µm fraction of selected samples of altered rocks were prepared by fine-grinding, ultrasonic disintegration, gravitational sedimentation and coagulation of the fine-grained fraction of the rocks. X-ray diffraction patterns were collected with a Phillips 1710 diffractometer (Geological Institute of Slovak Academy of Science) with CuKα radiation and a Ni filter.

Electron microprobe analyses (EPMA) were performed on JEOL 733 Superprobe (Dionýz Štúr Geological Institute) with these conditions and standards: Pb-Sb sulfosalts: 20 kV, 15 nA, PbS (Pb), FeAsS (Fe, S), metallic Se, Ag, Sb, Bi, Cu, Fe; carbonates: 15 kV, 10 nA, wollastonite (Ca), hematite (Fe), MgO (Mg), rhodonite (Mn); pyrite and arsenopyrite: 20 kV, 20 nA, FeAsS (Fe, As, S), metallic Se, Ag, Sb, Cu, Au, Co, Ni. If possible, several electron microprobe analyses were averaged and the average is reported in tables along with two standard deviations of the mean.

Results

Similarly as most other ore deposits in the Nízke Tatry Mts, the Dve Vody deposit encompasses several types of ore mineralizations. These are the As-Au, Sb, base-metals, and siderite mineralizations, named according to the principal exploited metals or minerals, in agreement with the classification of the ore mineralizations in the Nízke Tatry Mts (Chovan et al. 1996). The samples of the As-Au and Sb mineralizations studied in this work came from the waste dumps of adits 1, 2, 4, and 6 (Fig. 3). The dumps and adits no. 3 and 5, also known to intersect the As-Au and Sb veins (Michálek, 1999), were not identified in the field. The samples of the base-metals mineralization were collected at the dumps of the adits Nová Vyšná and Vyšná Spodná, and the siderite mineralization was sampled from the heaps of four nameless adits in a ravine near elevation point Ždiar (Fig. 1). The three mineralizations occupy separate vein systems (Fig. 1). In the following text, the description of the ore minerals is divided into three parts, according to the distinguished mineralizations. The As-Au and Sb mineralizations are described together because of their close spatial relationship. The information on the distribution of heavy minerals in alluvial sediments and heap material and the chemical composition of the ore samples complements the mineralogical description.

Panning

Heavy mineral concentrates from the alluvial sediments frequently contained minerals that indicated the presence of ore mineralizations in the studied area. Gold

flakes were found in most samples of the alluvial sediments (Fig. 3). In the Štellerova dolina valley, gold (2-7 flakes) was found in every concentrate. Gold was also found in the end of the Kulichova dolina valley. The waste dumps of the adit 2 are rich in gold (up to 220 gold flakes per concentrate). Gold from the dumps has high fineness (Table 2). Most of the gold flakes are smaller than 0.2 mm, similarly as elsewhere in the Nízke Tatry Mts (Fig. 4). Alluvial sediments in the Štellerova dolina valley contain sporadic scheelite (up to 4 grains per concentrate), cassiterite (22), wolframite (1), and cinnabar (2). Common minerals of the concentrates are apatite, zircon, rutile, epidote, pyrite, and limonite. A group of rarer minerals comprises garnet, ilmenite, hematite, monazite, xenotime, and tourmaline.

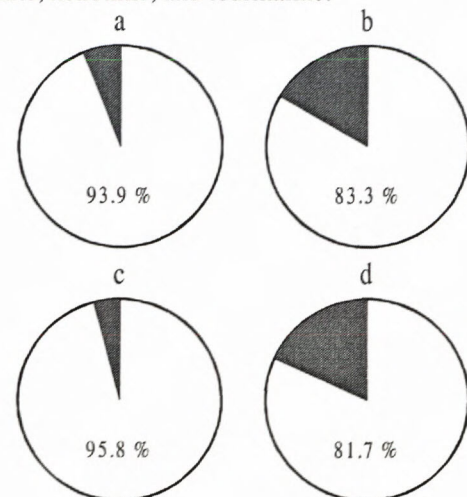


Fig. 4. Proportion of gold grains >0.2 mm (black) and <0.2 mm (gray) in a) alluvial sediments and sandy material of ore waste dumps from Dve Vody (445 gold grains), b) alluvial sediments in Mlynná dolina valley (84) (Majzlan, 1996), c) alluvial sediments in Magurka (3204) (Chovan et al. 1993), d) ore waste dumps from Magurka (465) (Chovan et al. 1993).

Mineral composition of the ore samples

As-Au and Sb mineralization

Arsenopyrite is one of the major minerals of the As-Au mineralization but rarely more abundant than pyrite. Arsenopyrite is found in fine-grained pyrite-arsenopyrite ores hosted by quartz or as impregnations of altered wall-rocks. It forms minute crystals in quartz, often skeletal with core filled by quartz, or inclusions in crystals and fine-grained aggregates of pyrite. Fine-grained arsenopyrite is rarely chemically zonal, as seen in back-scattered electron images (BSEI), and optically zonal with hourglass structure. Coarse-grained arsenopyrite crystals with minor pyrite were occasionally found in altered rock samples (Fig. 5a). Coarse-grained arsenopyrite often displays hourglass structure.

Beside the major elements, arsenopyrite contains only elevated concentrations of Sb (Table 3). Neither cobalt nor copper were detected by electron microprobe analyses

Table 2. Chemical composition (EPMA) of gold from the waste dumps (n.a. = not analyzed).

	Au	Bi	Hg	Cu	Pb	Ag	Te	Sb	total
DV1/1	93.65	0.80	1.15	0.18	0.21	3.66	0.10	n.a.	99.75
DV1/2	94.95	0.72	1.34	0.17	n.a.	3.61	0.19	0.11	101.09
DV2/1	96.86	n.a.	0.73	0.07	0.03	1.18	0.10	n.a.	98.97
DV2/2	97.37	0.16	0.18	0.07	n.a.	1.43	0.08	0.02	99.31
DV3 wt%	92.81	0.53	0.74	0.08	n.a.	5.94	n.a.	0.11	100.21
DV4/1	93.21	0.71	0.57	0.14	0.12	5.43	0.17	0.07	100.42
DV4/2	93.85	0.71	0.33	0.02	n.a.	5.40	0.17	0.11	100.59
DV1/1	90.81	0.73	1.09	0.54	0.19	6.48	0.15	n.a.	
DV1/2	90.83	0.65	1.26	0.50	n.a.	6.31	0.28	0.17	
DV2/1	96.73	n.a.	0.72	0.22	0.03	2.15	0.15	n.a.	
DV2/2	96.71	0.15	0.18	0.22	n.a.	2.59	0.12	0.03	
DV3 at%	88.13	0.47	0.69	0.24	n.a.	10.30	n.a.	0.17	
DV4/1	88.54	0.64	0.53	0.41	0.11	9.42	0.25	0.11	
DV4/2	89.21	0.64	0.31	0.06	n.a.	9.37	0.25	0.17	

Table 3. Chemical composition of arsenopyrite (EPMA) from As-Au mineralization.

	V-10	V-18	V-19
average of	2	6	5
S	21.87 (0.42)	21.40 (0.61)	21.60 (0.66)
Fe	34.96 (0.40)	35.12 (0.17)	35.12 (0.32)
As	40.77 (3.32)	43.12 (1.02)	42.72 (1.00)
Sb wt%	1.88 (3.35)	0.31 (0.20)	0.10 (0.17)
Au	0.17 (0.34)	0.06 (0.02)	0.01 (0.01)
Ni	0.00 (0.00)	0.01 (0.00)	0.01 (0.01)
Total	99.65	100.02	99.56
S	36.50 (0.06)	35.58 (0.81)	35.95 (0.85)
Fe	33.51 (0.31)	33.54 (0.11)	33.56 (0.15)
As	29.12 (1.77)	30.72 (0.86)	30.43 (0.90)
Sb at%	0.84 (1.49)	0.13 (0.08)	0.05 (0.07)
Au	0.05 (0.09)	0.02 (0.01)	0.00 (0.00)
Ni	0.00 (0.00)	0.01 (0.00)	0.01 (0.01)

Table 4.

	V-7	V-7	V-7	V-7	V-17A	V-20	V-20	V-20	V-28	V-28	V-43	V-43	V-43	V-43	
Au	95.4	94.26	89.15	90.81	97.44	98.16	96.97	96.94	94.44	94.29	77.01	76.81	66.75	67.84	65.55
Ag	2.92	3.55	3.89	3.71	0.38	0.86	0.66	0.87	0.45	0.17	22.44	22.63	28.05	28.09	30.79
Hg	1.76	0.93	0.99	0.83	0.93	1.33	1.3	1.62	0.55	0.89	0.68	0.8	0.77	0.98	0.92
Cu wt%	0.28	0.24	0.25	0.27	0.29	0.27	0.26	0.29	0.29	0.34	0.22	0.24	0.2	0.2	0.22
Fe	0.08	1.01	0.18	2.95	1.22	0.69	0.67	0.93	-	-	-	-	0.03	0.09	0.09
Total	100.44	99.99	94.46	98.57	100.26	101.31	99.86	100.65	95.88	95.69	100.35	100.48	95.8	97.2	97.57
Au	92.08	88.96	90.38	82.83	93.47	94.11	94.49	92.94	97.66	97.68	64.53	64.19	55.88	56.05	53.00
Ag	5.15	6.12	7.20	6.18	0.67	1.51	1.17	1.52	0.85	0.32	34.34	34.53	42.88	42.38	45.46
Hg at%	1.67	0.86	0.99	0.74	0.88	1.25	1.24	1.53	0.56	0.91	0.56	0.66	0.63	0.80	0.73
Cu	0.84	0.70	0.79	0.76	0.86	0.80	0.79	0.86	0.93	1.09	0.57	0.62	0.52	0.51	0.55
Fe	0.27	3.36	0.64	9.49	4.13	2.33	2.30	3.14	-	-	-	-	0.09	0.26	0.26



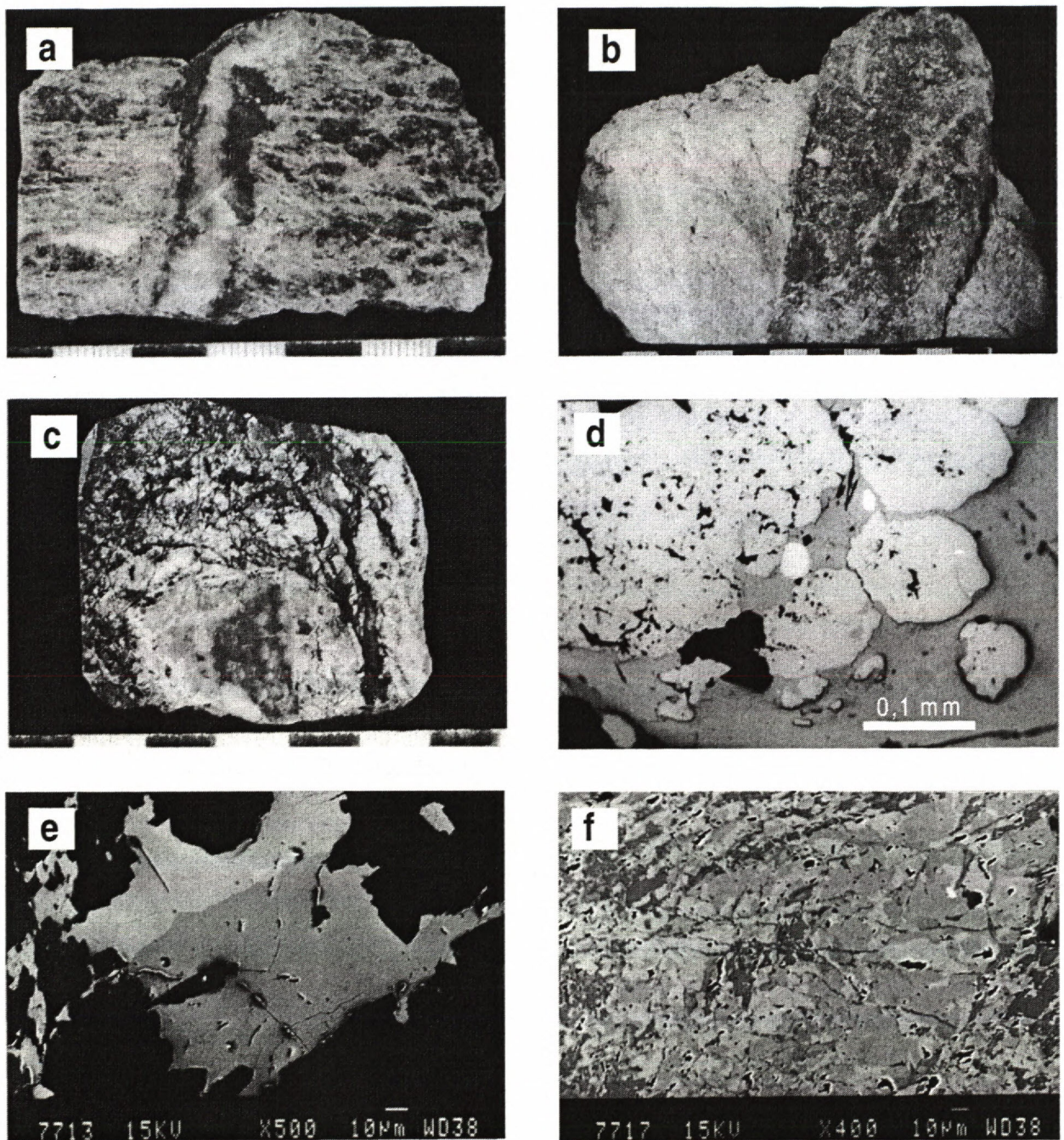


Fig. 5. a) altered rock impregnated by coarse-grained gold-bearing arsenopyrite, with a quartz veinlet with arsenopyrite mineralization (sample V-18); scale in cm; b) the contact of white quartz (cf. V-22A, Table 12) with no gold and gray quartz (V-22B, Table 12) with fine-grained pyrite and arsenopyrite, rich in gold; scale in cm; c) fragment of quartz with As-Au mineralization (pyrite, arsenopyrite) with a rim of sphalerite enclosed in carbonate-sulphosalt-stibnite matrix (V-26A), scale in cm; d) electrum inclusions (bright) in galena (gray) with pyrite crystals (V-43); (reflected light); e) intergrowths of zinckenite (darker gray) and robinsonite (brighter) in carbonate (black) (cf. EPMA analyses of sample V-26A, Table 5, Fig. 6) (SEM), f) intergrowth of carbonate species in V-26A (cf. Table 10a, Fig. 7a). Brighter gray are siderite I and II, replaced by calcite (darker gray). Quartz is black, sulfosalt inclusion is bright (SEM).

(EMPA). Low concentrations of gold and nickel (EMPA) are questionable without confirmation by a more sensitive analytical technique.

Stibnite hosts minute euhedral arsenopyrite crystals that were probably formed during the initial stages of Sb-sulfides precipitation.

Berthierite is encountered rarely, intimately intergrown with stibnite. Pink tint in parallel nicols and reflectivity slightly lower than that of stibnite distinguish berthierite from stibnite in reflected light.

Bournonite is rare, intergrown with Pb-Sb sulfosalts, stibnite, and tetrahedrite. It corrodes and replaces tetra-

hedrite and pyrite. In reflected light, bournonite has grayish color, moderately low reflectivity (lower than Pb-Sb sulfosalts), orange and blue anisotropy effect and typical polysynthetic twinning.

Gold is relatively frequent on microscopic scale. No macroscopic gold was observed in hand specimens from the dumps. Gold is associated with fine-grained pyrite and arsenopyrite, occasionally replacing pyrite. Stibnite impregnating fine-grained pyrite and arsenopyrite encloses gold grains. Minute gold grains and dendritic aggregates accompany Pb-Sb sulfosalts. High fineness is characteristic for both gold associated with Fe-As sulfides (90.1 at.% Au) and Sb sulfides (96.2 at.% Au) (Table 4). Small size of some gold grains is responsible for low totals of some microprobe analyses.

Pb-Sb sulfosalts are found commonly, with or without stibnite. The aggregates of Pb-Sb sulfosalts, up to several cm large, are composed of millimetre-sized needle-like crystals. The sulfosalts usually penetrate along grain boundaries of carbonates or forms rims of the quartz veinlets in carbonates. They can also be seen on quartz veinlets that penetrate into the fine-grained pyrite-arsenopyrite ores. We have occasionally found minute needles of Pb-Sb sulfosalts uniformly dispersed in Fedolomite, suggesting their contemporaneous crystallization. The optical properties of Pb-Sb sulfosalts are almost identical for the species encountered in this study. In reflected light, they have white color, inconspicuous birefringence, lower reflectivity than stibnite and weaker anisotropy than stibnite. Needles of zinckenite can be distinguished by their parallel extinction, as opposed to oblique extinction of the other sulfosalt species.

EMPA analyses (Table 5) have identified a variety of sulfosalt species. The most common sulfosalt is zinckenite. Robinsonite is intergrown with zinckenite (Fig. 5b) or forms minute needles and grains with inclusions of boulangerite. Heteromorfitite is found as small tabular crystals with boulangerite inclusions. The lead to copper ratio in the Pb-Sb sulfosalts is plotted in Fig. 6 versus the copper content. In agreement with crystal-chemical studies of sulfosalts (Mořlo, 1982), the tolerance of Pb-Sb sulfosalts for copper is low, with the exception of Cu-zinckenite. Co-existing zinckenite and robinsonite (Fig. 5b) display significantly different copper content (composition of the co-existing phases is indicated by a tie line in Fig. 6).

Pyrite is one of the most abundant minerals in the deposit. The oldest pyrite generation is represented by fine-grained pyrite aggregates, almost always with some arsenopyrite. Fine-grained pyrite and arsenopyrite impregnate vein quartz or altered wallrocks (Fig. 5c). This type of pyrite is characteristic by hexahedral habitus, chemical homogeneity (BSEI) with generally low arsenic content (Table 6), and crystal size averaging 10-20 μm , rarely exceeding 50 μm . Uncommon chemical zonation is caused by variable arsenic concentration (0 to 2.55 at.% As) (Table 7).

Pyrite is also abundant in stibnite and Pb-Sb sulfosalt ores. In contrast to the older fine-grained pyrite, here it forms larger (up to 1 mm) subhedral to euhedral pentago-

nal dodecahedral crystals. Pyrite crystals are often constituted of a core separated from the rim by a zone of quartz inclusions (photo). These pyrite crystals are homogeneous, with low arsenic content (Table 6). Electron microprobe detected no Se, Co, Sb, and Cu. Most of the measured nickel and gold concentrations are below the EPMA detection limit.

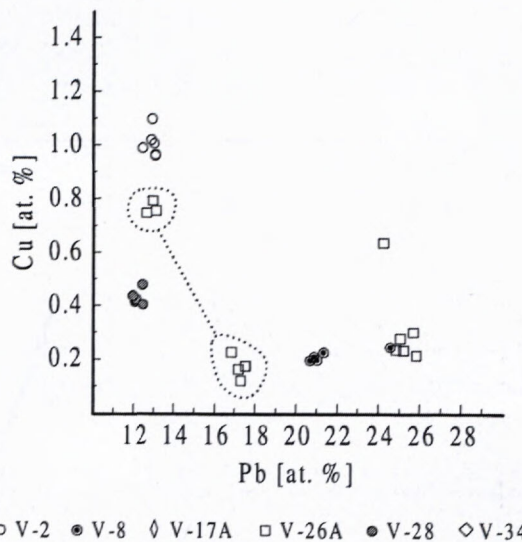


Fig. 6. Chemical composition of the sulfosalts from Dve Vody, in terms of their Pb vs. Cu content. Two marked fields, connected by a line represent the composition of co-existing of robinsonite and zinckenite (see Fig. 5e).

Sphalerite is found with Pb-Sb sulfosalts or separately in the gangue minerals. It forms grains of honey-yellow to brown color, up to 5 mm large. Beside the major elements, electron microprobe detected up to 0.24 at.% Fe, 0.10 at.% Cd, 0.10 at.% Mn, 0.07 at.% Sn and no Hg (Table 8). Sphalerite crystallized earlier than Pb-Sb sulfosalts (Fig. 5d).

Stibnite is the principal mineral of the Sb mineralization, forming aggregates of cm size in white quartz. It also forms monomineral veinlets in altered rocks, preferentially developed in porphyroblasts of the rock-forming quartz, only rarely emplaced in muscovite along the cleavage planes. Stibnite penetrates into the older fine-grained pyrite and arsenopyrite. There are infrequent stibnite relics in aggregates of Pb-Sb sulfosalts. The characteristic mosaic aggregates of stibnite carry few signs of tectonic deformation such undulose extinction or pressure-induced recrystallization.

Tetrahedrite is a scarce mineral in the Sb mineralization, intimately intergrown with bournonite.

Carbonates are common but not as abundant as quartz. The color of the polycrystalline carbonate aggregates varies from white to deep brown. Veinlets of fine-grained carbonates crosscutting older, coarser carbonates witness episodic remobilization and tectonization of the mineralization. Later stages of carbonate remobilization were accompanied by minor amount of quartz and Pb-Sb sulfosalts.

Table 5. Chemical composition (EPMA) of sulfosalts from Sb (V-2, V-26A, V-28, V-8) and base-metals (V-34) mineralization.

	Pb	Sb	Cu	Fe	S	Se	Total	Pb	Sb	Cu	Fe	S	Se
	wt%						at%						
V-28	31.39	45.58	0.33	0.04	22.89	0.01	100.24	12.16	30.05	0.42	0.06	57.30	0.01
V-28	32.21	44.78	0.38	0.05	22.81	0.00	100.23	12.52	29.62	0.48	0.07	57.30	0.00
V-2	32.00	43.99	0.78	0.06	22.50	0.11	99.44	12.53	29.32	1.00	0.09	56.95	0.11
V-2	32.92	42.09	0.78	0.07	22.24	0.00	98.10	13.11	28.53	1.01	0.10	57.24	0.00
V-2	32.94	42.87	0.80	0.04	22.46	0.07	99.18	12.97	28.72	1.03	0.06	57.14	0.08
V-2	33.18	43.18	0.75	0.03	22.00	0.08	99.22	13.19	29.21	0.97	0.04	56.50	0.08
V-26A	32.58	43.77	0.59	0.27	22.51	0.05	99.77	12.75	29.14	0.75	0.39	56.91	0.05
V-26A	33.60	43.97	0.63	0.06	22.72	0.00	100.98	13.05	29.06	0.80	0.09	57.01	0.00
V-26A	33.95	43.74	0.60	0.05	22.65	0.02	101.01	13.21	28.97	0.76	0.07	56.96	0.02
V-26A	41.18	36.78	0.17	0.27	21.15	0.12	99.67	16.99	25.83	0.23	0.41	56.40	0.13
V-26A	41.46	36.45	0.12	0.07	20.80	0.08	98.98	17.37	25.98	0.16	0.11	56.30	0.08
V-26A	42.23	36.82	0.09	0.28	21.00	0.00	100.42	17.46	25.90	0.12	0.43	56.09	0.00
V-26A	42.40	35.85	0.13	0.21	20.88	0.00	99.47	17.70	25.47	0.18	0.33	56.33	0.00
V-8	48.57	31.09	0.14	0.06	19.59	0.00	99.45	21.23	23.13	0.20	0.10	55.34	0.00
V-8	48.74	31.00	0.15	0.07	19.95	0.00	99.91	21.09	22.82	0.21	0.11	55.77	0.00
V-8	55.52	25.82	0.17	0.09	19.05	0.00	100.65	24.85	19.66	0.25	0.15	55.09	0.00
V-34	54.95	25.22	0.16	0.08	18.52	0.00	98.93	25.16	19.66	0.24	0.14	54.81	0.00
V-34	55.84	25.45	0.19	0.05	18.60	0.00	100.13	25.37	19.67	0.28	0.08	54.60	0.00
V-34	56.17	25.10	0.16	0.07	18.64	0.00	100.14	25.52	19.41	0.24	0.12	54.72	0.00
V-34	86.42	0.00	0.20	0.10	13.49	0.05	100.26	49.46	0.00	0.37	0.21	49.89	0.07

Table 6. Chemical composition of pyrite (EPMA) from As-Au (V-6, V-7, V-10), Sb (V-31), and base-metals (V-36) mineralization.

	V-6	V-7	V-10	V-19	V-31	V-36
average of	4	3	2	1	4	3
S	54.67 (0.97)	54.07 (0.16)	55.04 (0.60)	55.35	53.66 (1.98)	54.07 (0.37)
Fe	44.90 (0.51)	44.95 (0.23)	45.04 (0.99)	46.11	45.30 (0.50)	44.95 (0.50)
As	0.00 (0.00)	1.74 (0.68)	0.17 (0.09)	0.28	0.73 (1.46)	0.06 (0.13)
Sb	n.a.	n.a.	n.a.	n.a.	n.a.	n.a.
Au	0.12 (0.12)	0.08 (0.17)	0.03 (0.05)	0.00	0.04 (0.05)	0.00 (0.00)
Ni	0.00 (0.01)	0.00 (0.00)	0.03 (0.02)	0.00	0.01 (0.01)	0.01 (0.02)
Total	99.69	100.85	100.29	101.74	99.75	99.10
S	67.94 (0.42)	67.06 (0.23)	67.96 (0.68)	67.55	67.07 (1.16)	67.67 (0.14)
Fe	32.04 (0.43)	32.00 (0.18)	31.93 (0.73)	32.30	32.52 (0.37)	32.29 (0.14)
As	0.00 (0.00)	0.92 (0.36)	0.09 (0.04)	0.14	0.40 (0.81)	0.03 (0.07)
Sb	n.a.	n.a.	n.a.	n.a.	n.a.	n.a.
Au	0.03 (0.02)	0.02 (0.03)	0.01 (0.01)	0.00	0.01 (0.01)	0.00 (0.00)
Ni	0.00 (0.01)	0.00 (0.00)	0.02 (0.01)	0.00	0.01 (0.01)	0.01 (0.01)

Table 7. Chemical composition (EPMA) of zonal pyrite (sample V-15, Sb mineralization) arranged from the darkest (as seen in BSEI) to the lightest zone from left to right.

	darkest				lightest	
S	55.17	54.97	55.11	53.29	51.45	51.55
Fe	45.52	45.80	46.16	45.68	44.18	45.30
As	0.00	0.00	0.00	1.51	4.69	4.20
Au	0.00	0.15	0.00	0.00	0.01	0.10
Ni	0.00	0.03	0.00	0.00	0.00	0.00
Total	100.69	100.94	101.27	100.49	100.32	101.15
S	67.86	67.61	67.53	66.48	65.27	64.95
Fe	32.14	32.34	32.47	32.71	32.18	32.77
As	0.00	0.00	0.00	0.81	2.55	2.27
Au	0.00	0.03	0.00	0.00	0.00	0.02
Ni	0.00	0.02	0.00	0.00	0.00	0.00

Manometric analyses (Table 9) distinguished siderite and ankerite. A more detailed study with electron microprobe showed presence of two Fe-rich carbonates, siderite I and siderite II (Table 10a, Fig. 5e). Siderite appears to be the earliest carbonate in the deposit. Deposition of siderite is followed by precipitation of Fe-dolomite or calcite (Table 10b). Calcite encloses rare inclusions of magnesite. The magnesite inclusions were too small to obtain a reliable EPMA analysis, but an approximate composition can be read from Fig. 7a. Compositional differences and paragenetic relationships between these carbonates were observable only in back-scattered electron images.

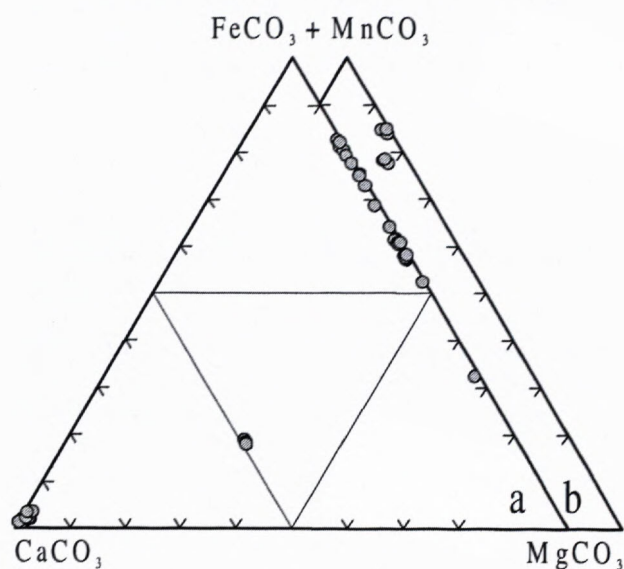


Fig. 7. Chemical composition of carbonates from Dve Vody. a) Sb mineralization, b) siderite mineralization.

A fine-grained mineral ubiquitous in the altered wall-rocks has been identified by X-ray diffraction analyses as **illite**. The mica-like aggregates partially or completely replace porphyroblasts of feldspars. Strongly altered rocks are composed only of quartz and illite with impregnations of sulfides. Less intensively altered rocks contain also large flakes of **muscovite**. It is not clear whether muscovite was formed during hydrothermal alteration of the wall-rocks or was an original component of the metamorphic rocks. Minute mica-like crystals were commonly found in vein quartz with Pb-Sb sulfosalts.

Quartz is the most abundant mineral of the ore veins. It accompanies almost all sulfidic minerals, with the exceptions of the monomineral stibnite veinlets. Grayish color of some quartz specimens is caused by impregnations of sulfides, predominantly fine-grained pyrite and arsenopyrite. Grayish quartz, with the associated sulfides, is the principal gold carrier in the deposit. According to our petrographic observations and chemical analyses, white quartz with no sulfide minerals contains virtually no gold.

Minute grains of Ti-minerals are frequent in strongly altered wall-rocks. Optical properties of these grains correspond to the optical properties of **rutile** and **ilmenite**.

Base-metals mineralization

Two oval inclusions of **electrum** were found in an aggregate of galena and pyrite (Fig. 5f). Electrum contains 58.7 at.% Au (Table 4).

Galena is one of the major sulfidic mineral of the mineralization. It forms large (up to several cm) aggregates, accompanied by abundant pyrite and quartz. Concentration of silver as determined by EPMA is low (Table 5).

Pb-Sb sulfosalts are a common component of the base-metals mineralization. Needle-like crystals and crystalline aggregates of the sulfosalts are locally more abundant than galena. Galena often encloses small inclusions of sulfosalts. The sulfosalts were identified by electron microprobe analyses (Table 5, Fig. 6) as **boulangerite**.

Pyrite and **galena** are the principal ore minerals. Subhedral, rarely euhedral pyrite crystals are often replaced by galena, sphalerite, and Pb-Sb sulfosalts. Massive monomineralic pyrite aggregates are common. Pyrite crystals are frequently composed of a core separated from the rim by a number of minute quartz inclusions. Some of the pyrite crystals display unusually strong anomalous anisotropy.

Sphalerite is common, invariably earlier than the sulfosalts. Beside the major elements, it contains only traces of Mn and Sn (Table 8).

Tetrahedrite is found seldomly as small oval inclusions in galena. According to the EPMA analyses (Table 11), tetrahedrite is the only silver-bearing mineral of the base-metals mineralization.

Carbonates are infrequent, often replaced by earthy mass of hydrated iron oxides.

Quartz is abundant, massive, usually grayish in color owing to the sulfide inclusions.

Siderite mineralization

Bournonite is one of the dominating sulfidic minerals of the siderite mineralization. Bournonite or intergrowths of bournonite and tetrahedrite form grains up to several cm large.

Small anhedral grains of **chalcopyrite** are infrequently found with other Cu sulfides, galena, and pyrite.

Isolated minute grains (< 0.5 mm) or veinlets of **galena** in quartz are rare. Galena is also found as inclusions in bournonite or along the contact of bournonite and tetrahedrite grains.

Massive aggregates of **tetrahedrite** in quartz or intergrowths of tetrahedrite and bournonite are common. According to the EPMA analyses (Table 11), the Ag content of tetrahedrite is low (< 1 wt.%), the tetrahedral M1 site is occupied dominantly by zinc, and the tennantite component fraction is low (< 6 mol.%).

Siderite forms mostly fine-grained massive aggregates, commonly cross-cut by veinlets of coarser carbonate. Electron microprobe (Fig. 7b, Table 10b) and manometric analyses (Table 9) identified only carbonate compositions classifiable as siderite.

Quartz is significantly less abundant than siderite, white in color, forming grains in siderite.

Table 8. Chemical composition (EPMA) of sphalerite from Sb (V-25, V-26A) and base-metals (V-41) mineralization.

Sample	V-25	V-26A	V-41
average of	4	4	4
S	32.65(0.40)	32.67(0.38)	32.78(0.37)
Zn	66.82(0.55)	67.05(0.24)	67.52(0.27)
Cu	-	-	-
Fe wt%	0.24(0.02)	0.17(0.09)	-
Cd	0.18(0.07)	0.17(0.04)	-
Sn	0.15(0.03)	0.14(0.02)	0.13(0.02)
Hg	-	-	-
Mn	0.05(0.02)	0.04(0.04)	0.08(0.05)
Total	100.06(0.68)	100.16(0.20)	100.47(0.67)
S	49.72(0.37)	49.71(0.36)	49.71(0.19)
Zn	49.91(0.37)	50.04(0.40)	50.21(0.20)
Cu	-	-	-
Fe at%	0.21(0.02)	0.15(0.08)	-
Cd	0.07(0.03)	0.08(0.02)	-
Sn	0.06(0.01)	0.06(0.01)	0.05(0.01)
Hg	-	-	-
Mn	0.05(0.01)	0.04(0.04)	0.07(0.04)

Table 9. Chemical composition (manometric analyses) of carbonates from Sb (V-8, V-17A, V-23D) and siderite (V-48) mineralization.

	S ^a	D ^b	IR ^c	CaO	MgO	FeO
V-8	79.24	3.26	24.30	0.99	11.63	30.76
V-17A	-	92.33	0.76	29.28	17.33	6.66
V-23D	-	91.29	2.65	28.61	16.37	7.47
V-48	96.41	-	7.63	-	6.60	48.71

^a per cent of the siderite component

^b per cent of the dolomite component

^c per cent of insoluble residuum

Chemical composition of the ore samples

The results of chemical analyses of the ore sample from the Dve Vody deposit can be correlated with the mineral composition as determined by optical microscopy (Table 12). The relationships between elemental concentrations in the analyzed samples are shown in Fig. 8. A correlation matrix of the metal concentrations is shown in Table 13.

Elevated gold concentrations were recorded in samples of the fine-grained pyrite-arsenopyrite ores (V-18, V-19, V-22B), more rarely in samples with Pb-Sb sulfosalts (samples V-20, V-28) and stibnite (V-30). Fig. 5c shows a typical example of white quartz with no sulfidic mineralization that contains little gold and gray quartz impregnated with pyrite and arsenopyrite rich in gold (cf. Au analyses for V-22A (white quartz) and V-22B (gray quartz), Table 12). This relationship documents the importance of fine-grained pyrite-arsenopyrite as the gold ore. Furthermore, no metallic gold was found in several arsenopyrite-rich samples with elevated gold content (V-18, V-19), suggesting that gold in these samples is chemi-

cally bound in arsenopyrite. On the other hand, a significant portion of gold occurs as metallic gold. The highest gold concentration was recorded in samples with low Sb content (Fig. 8a), stressing a relatively insignificant role of the Sb sulfides as gold carriers. We found gold grains enclosed in stibnite, however, they seem to have existed, together with pyrite and arsenopyrite, before the stibnite was emplaced. A comparison of gold and arsenic content (Table 12) in bulk samples suggests that arsenopyrite should contain 200-300 ppm Au (Fig. 8b), assuming that arsenopyrite is the only arsenic- and gold-bearing phase in those samples. The assumption may be incorrect where pyrite is present in larger amounts as it can contain both As and Au. Despite the neglect of pyrite presence in our samples, the estimated gold concentration of 200-300 ppm (Fig. 8b) compares well to the range of gold content in arsenopyrite from other deposits (Cabri, 1992). Arsenopyrite crystals from the sample V-18 were analyzed for gold by atomic absorption spectroscopy. The crystals were briefly leached, and the leachate was believed to represent the chemical composition of the outer portion of the crystals, giving 170 ppm of Au for this part of the crystals. A complete dissolution and correction for the outer portion gave a concentration of 99 ppm for the inner portion of the arsenopyrite crystals.

Lead and antimony are found either separately in galena (samples V-36, V-45) and stibnite (V-10, V-29, V-30) or combined in Pb-Sb sulfosalts (V-25, V-26, V-26A), as indicated by Fig. 8c. The principal carrier of Pb and Sb in the samples V-49 and V-50 is bournonite.

The observation of common occurrence of sphalerite and Pb-Sb sulfosalts is corroborated also by the chemical relationship between Pb and Zn (Fig. 8d). The association of sphalerite and Pb-Sb sulfosalts was observed both in the Sb and base-metals mineralization.

As-Au, Sb and base-metals mineralizations have only insignificant copper content. The dominant role of bournonite in the siderite mineralization (samples V-49 and V-50) is conspicuous from elevated concentration of Pb and Cu in these samples (Fig. 8e).

Higher silver content was observed in some samples of the Sb mineralization (V-25, V-26, and V-26A), correlating with their Pb content (Fig. 8f, Table 13). The mineral composition of these samples (pyrite, arsenopyrite, sphalerite, stibnite, Pb-Sb sulfosalts) indicates that most silver should be found in the sulfosalts. Calculation from bulk-rock analyses (Table 12) shows that the sulfosalts should contain 200-800 ppm of silver to account fully for all silver in the samples. However, electron microprobe analyses record no silver in the sulfosalts. Another possibility is accumulation of silver in submicroscopic Ag phases or Ag-rich domains in the sulfosalts. Abundance of galena and high silver content in the samples of the base-metals mineralization hint that silver is found dominantly in this mineral but microprobe analyses show no silver in galena. According to EPMA, the only mineral of the base-metals mineralization with significant Ag content is scarce tetrahedrite. The principal carrier of silver in the siderite mineralization (V-49, V-50) is tetrahedrite.

Table 10a. Chemical composition (EPMA) of carbonates from Sb mineralization.

	V-8	V-8	V-8	V-8	V-26A. sid I	V-26A. cc	V-26A. sid II	V-26A. mez
average of	1	2	2	3	4	4	2	1
FeO	45.06	40.73 (0.12)	36.85 (1.36)	0.54 (0.46)	48.73 (1.10)	1.69 (0.43)	40.09 (2.24)	24.02
MgO	11.61	14.17 (1.36)	17.26 (1.92)	0.18 (0.21)	8.71 (1.24)	0.39 (0.17)	15.49 (1.54)	28.88
CaO wt%	0.48	0.35 (0.11)	0.45 (0.22)	54.77 (0.60)	0.30 (0.07)	53.30 (0.88)	0.54 (0.05)	0.61
MnO	1.32	2.37 (0.37)	2.61 (0.23)	0.59 (0.14)	1.83 (0.05)	0.61 (0.32)	1.23 (0.27)	1.00
SrO	0.00	0.00 (0.00)	0.00 (0.00)	0.88 (0.29)	0.00 (0.00)	0.00 (0.00)	0.00 (0.00)	0.00
Total	58.47	57.61	57.16	56.96	59.56	55.99	57.34	54.51
FeCO ₃	72.66	65.68 (0.20)	59.42 (2.20)	0.87 (0.74)	78.58 (1.77)	2.73 (0.70)	64.65 (3.61)	38.73
MgCO ₃	24.29	29.65 (2.85)	36.10 (4.01)	0.37 (0.43)	18.21 (2.61)	0.81 (0.34)	32.40 (3.22)	60.42
CaCO ₃ wt%	0.86	0.62 (0.19)	0.80 (0.39)	97.75 (1.08)	0.53 (0.12)	95.14 (1.57)	0.96 (0.09)	1.09
MnCO ₃	2.14	3.83 (0.60)	4.22 (0.36)	0.96 (0.23)	2.97 (0.08)	0.99 (0.53)	1.99 (0.43)	1.62
SrCO ₃	0.00	0.00 (0.00)	0.00 (0.00)	1.25 (0.42)	0.00 (0.00)	0.00 (0.00)	0.00 (0.00)	0.00
Total	99.95	99.77	100.54	101.20	100.29	99.66	99.99	101.86

Table 10b. Chemical composition (EPMA) of carbonates from Sb (V-2, V-6, V-17A, V-23D) and siderite (V-47) mineralization.

	V-2	V-6	V-17A. ank	V-17A. sid	V-23D	V-47
average of	4	5	3	4	2	6
FeO	0.84 (0.05)	49.43 (1.61)	12.94 (0.33)	41.00 (0.99)	9.59 (0.09)	50.93 (1.38)
MgO	0.61 (0.07)	6.96 (1.06)	13.26 (0.20)	15.49 (0.50)	14.04 (0.13)	5.96 (0.60)
CaO wt%	54.10 (1.05)	0.29 (0.11)	27.80 (0.09)	0.31 (0.14)	27.10 (0.02)	1.31 (0.74)
MnO	0.63 (0.05)	2.32 (0.28)	0.36 (0.03)	0.88 (0.11)	0.78 (0.21)	2.14 (0.33)
SrO	0.00 (0.00)	0.00 (0.00)	0.00 (0.00)	0.00 (0.00)	0.00 (0.00)	0.00 (0.00)
Total	56.18	59.00	54.37	57.67	51.50	60.34
FeCO ₃	1.35 (0.07)	79.71 (2.60)	20.87 (0.52)	66.11 (1.59)	15.46 (0.15)	82.13 (2.23)
MgCO ₃	1.28 (0.14)	14.55 (2.21)	27.74 (0.41)	32.40 (1.03)	29.36 (0.28)	12.47 (1.26)
CaCO ₃ wt%	96.56 (1.87)	0.52 (0.20)	49.62 (0.16)	0.55 (0.26)	48.37 (0.03)	2.34 (1.32)
MnCO ₃	1.02 (0.09)	3.76 (0.46)	0.59 (0.05)	1.43 (0.18)	1.26 (0.34)	3.47 (0.53)
SrCO ₃	0.00 (0.00)	0.00 (0.00)	0.00 (0.00)	0.00 (0.00)	0.00 (0.00)	0.00 (0.00)
Total	100.21	98.55	98.82	100.48	94.44	100.40

Table 11. Chemical composition (EPMA) of tetrahedrite (Se, Hg, Bi not detected) from Sb (V-17), base-metals (V-43), and siderite (V-49) mineralization.

Sample	V-49	V-49	V-49	V-49	V-49	V-49	V-48	V-43	V-17	V-17	V-17
Cu	37.34	37.51	37.58	37.6	37.38	37.61	37.57	36.18	34.42	34.43	34.26
Ag	0.84	0.57	0.98	0.55	0.97	0.86	0.92	2.44	5.02	5.3	4.85
Zn	6.34	6.54	6.38	6.21	6.33	6.34	4.97	6.32	1.48	1.55	2.01
Fe wt%	1.04	0.98	0.95	0.93	1.01	0.98	2.05	1.06	4.83	4.6	4.34
Sb	28.6	28.56	28.63	28.96	28.07	28.48	26.99	28.37	25.88	25.81	26.06
As	0.27	0.4	0.15	0.27	0.25	0.37	0.92	0.64	0.82	0.84	1.1
S	23.61	23.77	24.01	24.22	24.21	24.01	24.74	23.51	23.8	23.93	23.88
Total	98.03	98.31	98.68	98.72	98.22	98.65	98.15	98.51	96.25	96.44	96.51
Cu	34.86	34.84	34.77	34.70	34.58	34.77	34.41	33.84	32.57	32.51	32.36
Ag	0.46	0.31	0.53	0.30	0.53	0.47	0.50	1.34	2.80	2.95	2.70
Zn	5.75	5.90	5.74	5.57	5.69	5.70	4.42	5.74	1.36	1.42	1.85
Fe at%	1.10	1.04	1.00	0.98	1.06	1.03	2.14	1.13	5.20	4.94	4.66
Sb	13.93	13.84	13.82	13.95	13.55	13.74	12.90	13.85	12.78	12.72	12.85
As	0.21	0.32	0.12	0.21	0.20	0.29	0.71	0.51	0.66	0.67	0.88
S	43.68	43.75	44.02	44.30	44.39	44.00	44.91	43.58	44.63	44.78	44.70

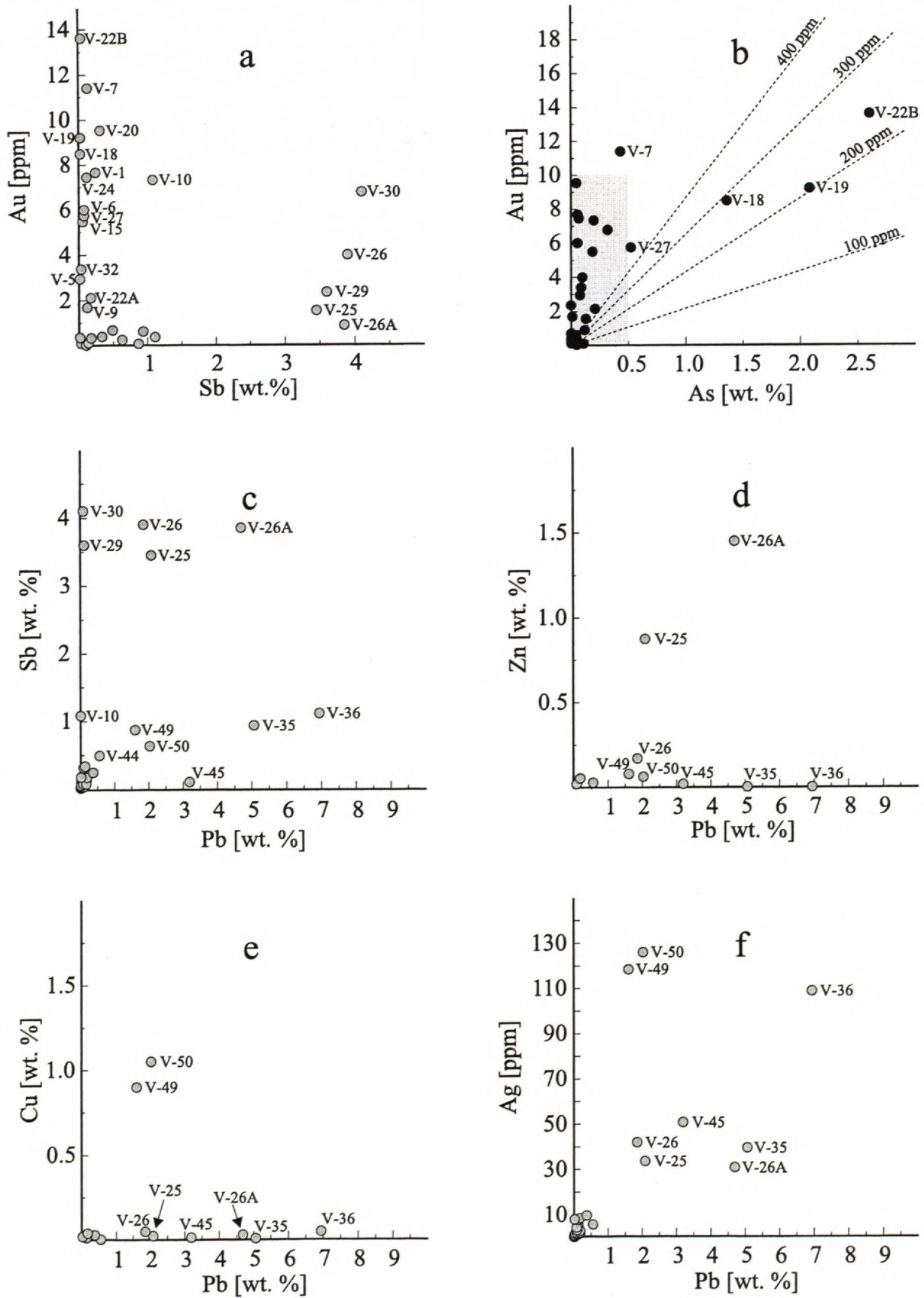


Fig. 8. Graphical representation of the chemical composition of ore samples from Dve Vody.

mineralizations parageneses	hydrothermal alteration	As-Au	Sb			base-metals	siderite
			carbonate	sphalerite- sulfosalt	stibnite		
illite	————						
muscovite	————						
Ti-oxides							
quartz		————		———		————	
arsenopyrite		————					
pyrite		————		———		————	
gold		———					
Fe-dolomite			————	———			
sphalerite				———		———	
zinckenite				————			
stibnite					————		
berthierite					———		
galena					————		
boulangerite						————	
siderite							————
tetrahedrite			———				————
bournonite							————
chalcopyrite							————

Fig. 9. Paragenetic sequence of the Dve Vody deposit.

Discussion and conclusions

The mineralizations distinguished in the Dve Vody deposit correspond, in terms of their mineralogical and chemical composition, to the mineralizations elsewhere in Nízke Tatry Mts as classified by Chovan et al. (1996). These are the As-Au, Sb, base-metals, and siderite mineralizations, listed in the order in which they were formed. The paragenetic sequence for the deposit, based on the observations made in this study and previous work (Kantor, 1948, Hak, 1966) is shown in Fig. 9. Penetration of quartz veinlets with Sb sulfides into brecciated As-Au mineralization documents the temporal relationship between the As-Au and Sb mineralization. An intersection of a stibnite vein (Sb mineralization) by a galena vein (base-metals mineralization) in Nová Vyšná adit (Kantor & Rybár, 1964) proves later deposition of the base-metals mineralization. According to Michálek (1999), the ores of As-Au, Sb, and base-metals mineralization occupy tectonic structures opened during the first deformation stage. The latest siderite mineralization fills structures created during the second deformation stage (Michálek, 1999).

The early As-Au mineralization, represented by fine-grained pyrite-arsenopyrite ores, is a typical feature of many ore deposits in the Nízke Tatry Mts. At the Dve Vody deposit, these ores are the most important gold carrier, either in chemical form in arsenopyrite and pyrite or as metallic gold. In contrast with the deposit Magurka (Chovan et al. 1995), the gold concentration at Dve Vody is low in white quartz devoid of sulfides, as opposed to

high gold content of gray quartz impregnated by fine-grained Fe-As sulfides (Fig. 5c). The abundance of metallic gold in the fine-grained pyrite-arsenopyrite ores is exceptional compared to other ore deposits in the Nízke Tatry Mts.

Rare brecciated textures (Fig. 5d), consisting of fragments of As-Au mineralization enclosed by the Sb mineralization document the temporal relationship among the two mineralizations. The Sb mineralization can be divided into three parageneses. The first one is rich in carbonates that are surprisingly variable in their chemical composition (Fig. 5e), especially in comparison with other deposits in the Nízke Tatry Mts. The second paragenesis comprises sphalerite and sulfosalts, usually associated with carbonates. On the other hand, stibnite, the most abundant sulfide of the third paragenesis, is found mostly in quartz or in monomineralic veins in altered rocks. The paragenetic sequence of the three parageneses within the Sb mineralization is not completely clear. There is satisfactory textural evidence that the major portion of the carbonates is earlier than sphalerite and sulfosalts, sphalerite being always earlier than sulfosalts. On the other hand, little information was gathered about the relationship between sulfosalts and stibnite. Rare irregular relics of stibnite in sulfosalts or zinckenite veinlets cutting through stibnite aggregates suggest that the sulfosalts were emplaced after the deposition of stibnite. Similar observations were recently documented from ore samples from Klačianka (Bakos et al. 2000). These infrequent occurrences are, in our opinion, an insufficient proof of

Table 12. Chemical and mineralogical composition of the samples from Dve Vody. Mineral abbreviations: asp – arsenopyrite, py – pyrite, Au – gold, sbt – stibnite, sfs – sulfosalts, ga – galena, sph – sphalerite, bour – bournonite, ttd – tetrahedrite, qtz – quartz, carb – carbonates, rt – rutile, ber – berthierite, ccp – chalcopyrite. Explanations: □ – abundant mineral, ◻ – uncommon minerals, * - other uncommon minerals (abbreviation given in the appropriate row).

Locality/sample	py	asp	Au	sbt	sfs	ga	sph	bour	ttd	*	qtz	carb	rt	As	Cu	Pb	Sb	Zn	Ag	Au	Au*	sample
dumps of adit 6																						
V-2	■	■		■	■			◻			■	■	◻									V/2
V-3	■	■	◻		◻						■	◻	◻									V/3
V-4	■	■			◻						■	◻	◻									V/4
V-5	■	◻	◻								■			0,08	0,001	0,008	0,0014	tr	0,8	2,94	2,97	V-5
dumps of adit 2, left bank of the creek																						
V-1	■	◻			◻						■	■	◻	0,06	0,030	0,370	0,244	0,005	9,6	7,66	7,50	V-1
V-6	■				◻						■	■	◻	0,06	0,040	0,167	0,076	0,006	8,4	6,00	6,02	V-6
V-7	■	◻	◻		◻						■	■	◻	0,43	0,002	0,127	0,130	0,005	5,2	11,40	11,78	V-7
V-8	■				■		◻				■	■										V-8
V-9	■				■						■	■		0,01	0,003	0,091	0,120	0,007	3,2	1,68	1,60	V-9
dumps of adit 4																						
V-10	■	■	◻	◻	◻						■	◻	■	0,20	0,001	0,009	1,080	0,006	0,4	7,32	7,20	V-10
V-11	■	■	◻	■	◻						■		◻									V-11
V-12	■				◻						■											V-12
V-13					◻						■			tr	0,002	0,018	0,028	0,009	tr	0,10		V-13
V-15	■				◻						■		◻	0,19	0,020	0,020	0,055	0,008	8,0	5,48	5,25	V-15
V-16	◻	◻		■							■	◻										V-16
dumps of adit 6																						
V-17	■	■			◻			◻	◻		■	■	◻									V-17
V-17A	◻	■	◻		■						■	■	◻									V-17A
V-17B	■	■			◻						■	■										V-17B
V-17C	■	◻			◻						■	■										V-17C
V-18	◻	◻			◻						■	■	◻	1,36	tr	0,001	0,020	0,002	tr	8,48	8,42	V-18
V-19	◻	■			◻						■	◻		2,08	0,001	0,021	0,104	0,003	1,2	9,2	9,40	V-19
V-20	■		◻		■						■	■		0,05	0,001	0,087	0,312	0,003	2,4	9,52	9,96	V-20
V-21											■	■		tr	tr	0,005	0,014	0,001	tr	0,36		V-21
V-22	■				◻			◻	◻		■	■										V-22
V-22A	■				◻			◻	◻		■	■		0,21	0,005	0,180	0,170	0,053	2,0	2,12	2,06	V-22A
V-22B	■	■	◻								■	◻		2,60	0,003	0,038	0,035	0,008	1,6	13,60	14,38	V-22B
dumps of adit 2, right bank of the creek																						
V-23	◻		◻		◻						■	■	◻									V-23
V-23A	■				■						■	◻	◻									V-23A
V-23D	■				■						■	◻	◻									V-23D
V-23E	◻	■		■	◻						■	◻										V-23E
V-24	■				◻						■	■		0,07	0,003	0,100	0,115	0,010	1,6	7,44	7,15	V24
V-25		◻		◻	■		◻				■	■		0,13	0,023	2,080	3,450	0,875	33,6	1,54	1,56	V-25
V-26	◻			■	◻		◻				■	■		0,10	0,048	1,850	3,900	0,170	42,0	3,98	3,91	V-26
V-26A	◻	◻			■		◻				■	■		0,12	0,030	4,690	3,850	1,450	30,8	0,88		V-26A
V-26B	◻		◻		■						■	■	◻									V/26B
V-27	■										■	■	◻	0,52	0,005	0,078	0,075	0,020	4,4	5,74	5,49	V-27

Locality/sample	py	asp	Au	sbt	sfs	ga	sph	bour	ttd	*	qtz	carb	rt	As	Cu	Pb	Sb	Zn	Ag	Au	Au*	sample
dumps of adit I																						
V-28	□		□	■	■						■	■										V-28
V-29	□	□		■							■	□		tr	0,003	0,118	3,600	0,005	1,2	2,34	2,45	V-29
V-30	■	□		■							■	□		0,32	0,003	0,088	4,100	tr	2,8	6,76	6,54	V-30
V-31	□	□		■						ber	■	■	□	tr	0,001	0,015	0,176	0,003	0,4	0,34		V-31
V-32	■				□						■		□	0,09	0,001	0,089	0,032	tr	2,0	3,38	3,32	V-32
dumps of adit Vyšná Spodná																						
V-34	■				■	□					■											
V-34A	■				□	■					■											
V-35	■					■					■			0,04	0,008	5,060	0,935	tr	39,6	0,62		V-35
V-36	■				□	■					■			0,04	0,048	6,940	1,110	tr	108,8	0,38		V-36
V-37	□				□						■	□		tr	0,001	0,174	0,134	0,001	2,8	0,12		V-37
dumps of adit Nová Vyšná																						
V-38	□			■	□						■											V-38
V-39	□			■	□		□				■		□									V-39
V-40	■				■		□				■	□	□									V-40
V-41	■				■		■				■											V-41
V-42	■			■	□						■											V-42
V-43	■		□		□	■	■		□		■											V-43
V-44	■				□	□	□				■			tr	0,003	0,555	0,490	0,028	5,6	0,68		V-44
V-45	■				□	□	□				■			0,05	0,013	3,190	0,100	0,018	50,8	0,02		V-45
dumps of adits with Fe-Cu mineralization																						
V-46	■					■					■	□										V-46
V-47	□							□	□		□	■										V-47
V-48	□							■	□		■	■										V-48
V-48A														0,05	0,014	0,132	0,336	0,006	7,6	0,40		V-48A
V-49	□							■	■		■			0,11	0,900	1,600	0,870	0,078	118,4	0,08		V-49
V-50	□							■	□	ccp	■	□		0,10	1,050	2,025	0,630	0,063	126,0	0,26		V-50
sample	py	asp	Au	sbt	sfs	ga	sph	bour	ttd	*	qtz	carb	rt	As	Cu	Pb	Sb	Yn	Ag	Au	Au*	sample

Table 13. Correlation matrix of element concentration in bulk samples from Dve Vody.

	As	Cu	Pb	Sb	Zn	Ag	Au
As	1.00						
Cu	-0.23	1.00					
Pb	-0.15	0.58	1.00				
Sb	-0.21	0.42	0.65	1.00			
Zn	-0.12	0.43	0.96	0.58	1.00		
Ag	-0.19	0.81	0.82	0.67	0.71	1.00	
Au	0.66	-0.13	-0.31	-0.25	-0.33	-0.23	1.00

temporal relationship between stibnite and sulfosalts. They may represent a product of local action of circulating fluids rather than a general picture of the deposit evolution. A tentative paragenetic relationship of the sphalerite-sulfosalt and stibnite parageneses is indicated in Fig. 9. However, a further detailed study is needed to resolve the question of temporal relationship between stibnite and sulfosalts.

The base-metals mineralization is simple in its mineral composition and was probably formed during a single hydrothermal event. The massive galena-pyrite ores strongly resemble the ores from the deposit Jasenie-Soviasko, situated about 5 km W from the Dve Vody deposit. Luptáková et al. (2000) investigated the ores of the Jasenie-Soviasko deposit and found that a) the silver concentration in galena (analyzed by EMPA) is lower than previously reported, and b) elevated silver concentration could be recorded only in tetrahedrite inclusions. These results are identical as the results for the base-metals mineralization in the Dve Vody deposit and may lead to rethinking of the role of galena in the deposits of the Nízke Tatry Mts as a major silver carrier.

Mineralizations rich in copper sulfides and variable amount of siderite are known from many localities in the Nízke Tatry Mts (Ozdín & Chovan, 1999, Ozdín & Pršek, 2000). At the Dve Vody deposit, the abundance of siderite along with copper sulfides links this mineralization unambiguously to the siderite mineralization in the Nízke Tatry Mts.

In summary, the presented work brings new information on mineral and chemical composition of the ores in the Dve Vody deposit. Many minerals, known from the deposit from previous work (mainly Hak, 1966), were analyzed and identified by electron microprobe for the first time here. The information about chemical composition of carbonates and sulfosalts and their successive relations is especially considered interesting. We attempted to identify the principal carriers of gold and silver in the deposit. In terms of mineral and chemical composition, and the sequence of ore deposition, the deposit Dve Vody is similar to other Sb-Au deposits in the Nízke Tatry Mts.

Acknowledgements

We are thankful to D. Ozdín, P. Konečný and P. Siman for assistance with electron microprobe analyses and M. Gregorová for help with laboratory treatment of the heavy mineral concentrates. We are also grateful to P. Andráš for the AAS analyses of arsenopyrite. P. Jancsy, P. Uhlík and L. Ludhová kept company to one of us (J.M.) during the field trips to the deposit. V. Szabadová prepared all thin and polished sections used in this study. The photographs in optical microscope were taken by L. Osvald. Chemical composition of the samples was determined by M. Tkáčzyková. We are grateful to L. Puškelová for help with XRD patterns and to M. Hacurová and J. Turan for the manometric analyses of carbonates and Š. Méres and K. Dubíková for technical assistance. The work was financially supported from Envigeo s.r.o., Banská Bystrica and from VEGA grant agency No. 1/5218/98 and 1/8318/01.

References

- Bakos F. & Chovan M., 1999: Genetical types of gold from Magurka deposit (Nízke Tatry Mts). *Min. Slov.*, 31, 217-224. (in Slovak)
- Bakos F., Chovan M. & Michálek J., 2000: Mineralogy of hydrothermal Sb, Cu, Pb, Zn, As mineralization in NE of the Magurka deposit, Nízke Tatry Mts. *Min. Slov.*, 32, 497-506. (in Slovak)
- Biely A. & Bezák V., 1997: Explanations to the geological map of Nízke Tatry Mts. Dionýz Štúr Geol. Inst. (Bratislava). (in Slovak)
- Cabri L.J., 1992: The distribution of trace precious metals in minerals and mineral products. *Miner. Mag.*, 56, 289-308.
- Cambel B., Jarkovský J., Gerthoferová H., Krištín J. & Streško V., 1976: Contribution to geochemistry of iron and mercury in antimonites of the West Carpathians. *Geol. Sborn.*, 27, 319-329.
- Chovan M., (ed.), 1993: Mineralogy of the ore waste dumps on the Au-Sb deposit Magurka. Manuscript, PRIFUK Bratislava, 72. (in Slovak)
- Chovan M., Póč I., Jancsy P., Majzlan J. & Krištín J., 1995: Sb-Au (As,Pb) ore mineralization at the Magurka deposit, Nízke Tatry Mts. *Min. Slov.*, 27, 397-406. (in Slovak)
- Chovan M., Slavkay M. & Michálek J., 1996: Ore mineralizations of the Ďumbierske Tatry (Western Carpathians, Slovakia). *Geol. Carp.*, 47, 371-382.
- Gubač J., 1980: On geochemical prospection for Sb in the Ďumbier zone of the Nízke Tatry Mts. In: J. Ilavský (ed.), *Antimony ore mineralizations of Czechoslovakia*, Dionýz Štúr Geological Institute (Bratislava), 89-102. (in Slovak)
- Hak J., 1966: Mineralogy and geochemistry of the stibnite deposit in the Nízke Tatry Mts. *Sbor. Geol. Věd, Ser. TG*, 7, 71-131. (in Czech)
- Hovorka D., Méres S. & Ivan P., 1994: Pre Alpine Western Carpathians basement complexes: lithology and geodynamic setting. *Mitt. Österr. Geol. Gesell.*, 86, 33-44.
- Janák M., Pitoňák P. & Spišiak J., 1993: Banded amphibolic rocks from the Low and Western Tatra Mts.: Evidence of the lower crustal components in the pre-Alpine basement of the Western Carpathians. *Geol. Carp.*, 44, 260.
- Kantor J., 1948: Stibnite at the Dve Vody deposit. Manuscript, Dionýz Štúr Geological Institute (Bratislava). (in Czech)
- Kantor J. & Rybár M., 1964: Isotopes of lead from several deposits of West Carpathian crystalline. *Geol. Sbor. Slov. Akad. Vied*, 15, 285-297.
- Luptáková J., Chovan M. & Huraiová M., 2000: Pb, Zn, Cu, Sb hydrothermal mineralization at the locality Jasenie-Soviasko (Nízke Tatry Mts). In: Uher et al. (eds.): *Mineralogical – petrological symposium Magurka '2000*, August 2000, p. 24. (in Slovak)
- Majzlan J., 1996: Ore mineralizations in the Mlynná dolina valley. Unpublished B.Sc. thesis, Comenius University (Bratislava). (in Slovak)
- Majzlan J., Chovan M. & Michálek J., 1998: Ore bodies at Rišianka and Malé Železné: Mineral composition and parageneses. *Min. Slov.*, 30, 52-59. (in Slovak)
- Michálek J., 1993: Metallogenesis and perspectives of Sb mineralizations in the crystalline complex of Ďumbierske Tatry Mts. *Min. Slov.*, 25, 5, 359-361. (in Slovak)
- Michálek J., 1999: Geological and metallogenetic characterization of the Au-polysulphidic mineralization of the Dve Vody-Karol deposit in the Ďumbierske Tatry Mountains. *Min. Slov.*, 31, 225-232. (in Slovak)
- Moëlo Y., 1982: Contribution à l'étude des conditions naturelles de formation des sulfures complexes d'antimoine et plomb (sulfosels de Sb/Pb); signification métallogénique. *Mem. Sci. Terre Univ. Curie*, (Paris), 82 pp.
- Ozdín D. & Chovan M., 1999: New mineralogical and paragenetic knowledge about siderite veins in the vicinity of Vyšná Boca, Nízke Tatry Mts. *Slovak Geol. Mag.*, 5, 255-271.
- Ozdín D. & Pršek J., 2000: Siderite mineralization in the Nízke Tatry Mts., Western Carpathians, Slovakia. *Acta Min.-Petrol., Supplementum* 2000, 82.
- Petrík I., Siman P. & Bezák V., 1998: Granitoid protolith of the othogneisses of the Ďumbier part of the Nízke Tatry Mts, distribution of barium in K-feldspar megacrysts. *Min. Slov.*, 30, 265-274. (in Slovak)
- Pulec M., Klíneč A. & Bezák V., 1983: Geology and prospection of the scheelite-gold mineralization in the area of Kyslá nearby Jasenie (delimitation of the perspective zone). In: J. Pecho (ed.), *Scheelite-gold mineralization in the Nízke Tatry Mts*. Dionýz Štúr Geological Institute (Bratislava), 11-38. (in Slovak)

Variscan granitoid hosted hydrothermal gold deposit Pezinok-Staré Mesto (Malé Karpaty Mts., Western Carpathians): Mineralogy, paragenesis, fluid inclusions study

FRANTIŠEK BAKOŠ, JAROSLAV PRŠEK & PETER TUČEK

Dept. of mineralogy and petrology, Fac. of nat. sciences, Comenius University, 842 15 Bratislava
e-mail: fbakoss@yahoo.com

Abstract: Pezinok-Staré Mesto gold deposit is hosted by a small massif of Variscan granodiorites, leucocratic granites and pegmatites. It is formed by several parallel NW-SE and transversal E-W veins, veinlets and impregnation bodies bounded on mylonitized granitoids. According to the area of old mining works, the length of mineralization can reach more than 1 km, vertical extent is unknown. The thickness of veins varied from 0.0X to 0.X m, max. 1 m. Quartz dominates from gangue minerals, carbonates are very rare. The content of gold varied from 0.X to X0 ppm Au, locally with bonanza accumulations. Au/Ag ratio is 5, the content of sulphides in vein filling is less than 1 %. Mineralization originated in several stages. The oldest one is characterized by arsenopyrite, pyrite and visible gold. Fineness of gold reaches values from 792 to 909. Minerals of later mineral stage (Cu, Pb, Sb, Ag sulphides and sulphosalts) are rare at the deposit. They fill thin cracks and form small grains and inclusions in quartz. This stage is characterised by remobilization of gold (684 - 753). In the quartz of the first mineral stage 3 types of fluid inclusions (1. $\text{CO}_2 \pm \text{CH}_4(?)$, 2. $\text{H}_2\text{O}-\text{CO}_2 \pm \text{NaCl}$, 3. $\text{H}_2\text{O}-\text{NaCl} \pm \text{KCl}$, $\text{CaCl}_2(?)$) have been. The mineralization originated from fluids with high salinity (17 - 25 wt. % NaCl eq.). Homogenization temperatures vary from 100 to 350 °C.

There is an anomalous content of gold grains in the alluvial sands and gravels in the vicinity of occurrences of Au-Ag mineralization. Gold placers were mined in Middle Ages. Nowadays content of gold in alluvial placers of Limbašský potok brook is max. 0.221 g/m³. Gold occurs mostly in the form of nuggets, less in the form of flakes up to 1 mm in size.

Key words: quartz veins, gold, sulphosalts, Slovakia

Introduction

Sb-As-Fe-Au mineralization in the Pezinok area is the most important type of mineralization in Malé Karpaty Mts. mined until the beginning of 1990's. The largest is the Pezinok - Kolársky vrch deposit. In the vicinity of the deposit, in a distance less than 2 km, several occurrences of Au-mineralization are hosted by a small massif of Variscan granitoids (fig. 1). The largest occurrence, the Pezinok-Staré mesto deposit, used to be mined with alternating successes. It has been abandoned several times. The first written note about the mining activity comes from the year 1339. Archive information about the deposit was used by Cotta & Fellenberg (1862) and Döll (1899) in Bergfest (1952), Dubovský (1990), Michal & Uher (1999) and Wittgrüber et al., (2001). In the 19th century the mining profit per one year was about 5-10 kg Au. The highest profit – 21 kg Au was achieved in 1826-1827. Small amounts of silver were mined, too. The site was abandoned in 1872 for the last time. Information from the 20th century about the mineralization in the studied area can be found in Cambel (1959), Polák & Rak (1979) and Chovan et. al. (1992). One of two archive samples was mineralogically investigated by Andráš et.

al. (1990). Despite of this fact, mineralogical and paragenetical relations of the deposit have up been unclear till now and there have been just guesses about its characteristics. This paper brings new results about the Au-mineralization from the Pezinok-Staré Mesto location.

Geological setting and deposit structure

The Pezinok-Staré Mesto deposit is situated on the southeastern slope of Malé Karpaty Mts., between Hrubá dolina and Slnčné údolie valleys, 380 to 500 m above the sea level (fig. 2). The gold deposit is hosted by a small massif (fig. 1) of variscan Bratislava granitoides (S-type) represented by two mica granodiorites, leucocratic granites and pegmatites. Geological structure of Malé Karpaty Mts. is characterized by several superimposed nappes – Prealpine crystalline Tatric basement, Mesozoic cover and upper nappes (Plašienka et. al. (1991). Tatric fundament is divided into the Harmónia series and Pezinok – Pernek series (Cambel, 1954). Plašienka et. al. (1991) distinguishes these units: Pezinok Sequence (metamorphic cover of the Bratislava granitoid massif), Pernek and Harmónia Sequence (metamorphic cover of the Modra granitoid massif) and Doľany Se-

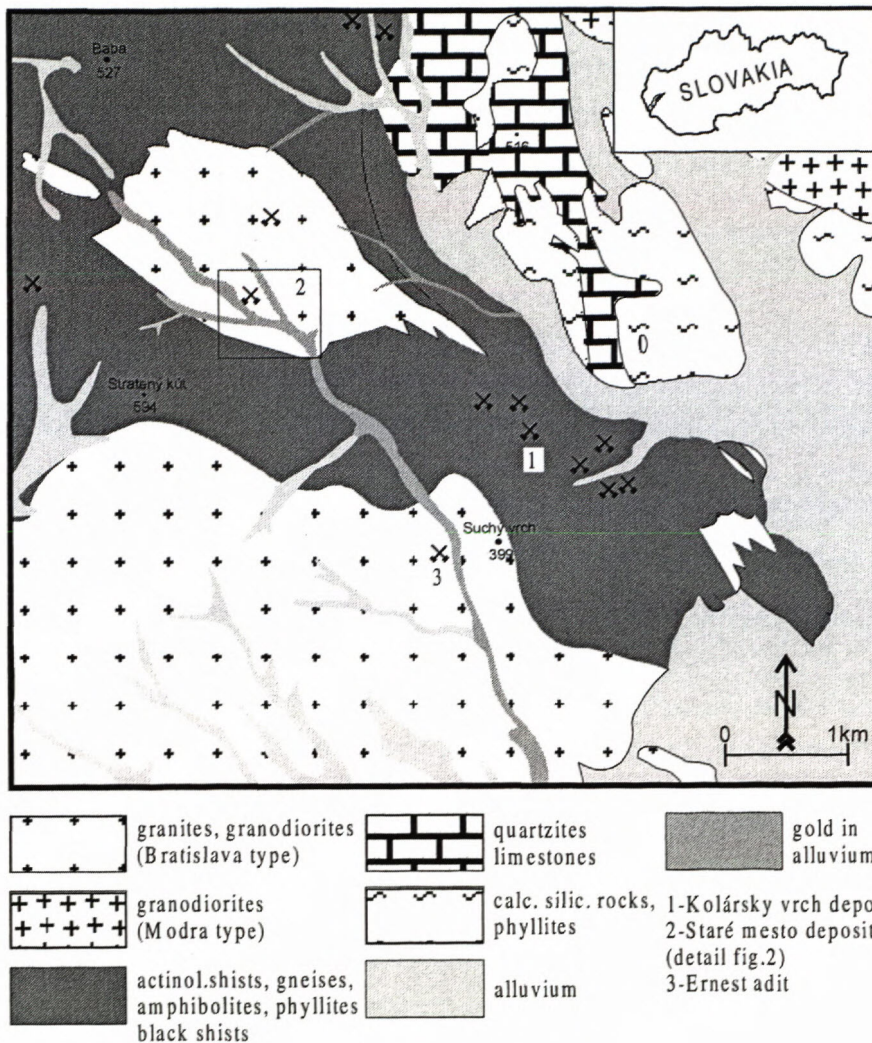


Fig. 1 Geological map of the vicinity of Pezinok – Staré Mesto deposit (according to Mahel' & Cambel eds., 1972)

g/t), 0.3-0.45 m (3 g/t), 0.01-0.15 m (32-50 g/t), 0.3 m (63-78 g/t). The highest content of gold, were in intersections of veins (Polák, 1970).

Three large and several small occurrences of Sb mineralizations are known in the Malé Karpaty Mts. More than 10 000 tons of Sb have been produced from the Pezinok - Kolársky vrch deposit in period until 1990. It is situated about 2 km SE from Pezinok-Staré Mesto deposit. The deposit is hosted by volcano-sedimentary Pezinok – Pernek crystalline formation. Stratabound type mineralization, represented mainly by stibnite, arsenopyrite with „refractory gold“ and other Sb, Fe-sulphides and sulphosalts, is associated with a large tectonic zone and located in the so-called productive zones in black shists and phyllites (Chovan et al., 1994).

Small occurrence of Sb-mineralization (Ernest adit) is situated cca 3 km SSE from Pezinok – Staré Mesto deposit in Slnčné údolie valley (fig.1). Mineralization is hosted by granitoides of Bratislava type (Andráš et al., 1999).

quence (Lower Silurian to Lower Devonian – of flysch character) and upper volcano – sedimentary formations (lower to middle Devonian).

The vein system is formed by the main Terézia vein of the general NW-SE direction steeply dipping to W and by several small combed veins (Plochá, Strmá, Pavol) of small thickness and length (Cambel, 1959). Veins are formed in mylonite zones. They often fork and thin out. The Terézia vein is an ore structure with the maximum thickness of 0.9 m with short productive areas. The Plochá vein is of E-W direction with the inclination 20° - 45° to S and the thickness 0.1– 0.2 m. The length of the productive area is about 100 m. The Pavol vein is approximately parallel to the Plochá vein. According to the location of the old mining sites the total length of the ore zone is even 1 km. The depth of the ore zone is not known. According to the archive information the the number of „unknown Fe-sulphides“ increases with depth. In the NE part of small Staré Mesto granitoid massif there are some unclear trails of a small old mining work. Vein filling is formed by quartz and mylonite, rarely pyrite, markacite and visible gold. In an archive sample of quartz veinstone electrum, galena, sphalerite, chalcopyrite, Ag-tetrahedrite and polybasite was found (Andráš et. al., 1990). The content of Au in the ore was very variable: thickness 0.3 – 0.45 m (2.5– 8

Methods

Concentrates of heavy minerals (28 samples) and the samples of large volume (5 samples of 0,1 m³) from the alluvium and the elluvium were taken by standard method (obtaining heavy minerals concentrates in a pan, using a sieve with 3 mm mash) and processed in the laboratory of Comenius University Bratislava. Heavy minerals concentrates were evaluated using binocular magnifying. 0.653 g of the alluvial gold and 0.487 g of the elluvial gold were mineralogically evaluated. The weight of gold was set by weighting of separated gold flakes and of gold obtained by amalgamation of samples of large volume.

The majority of tested samples (more than 150 samples of visible gold and other minerals) were picked up from old dumps material and from a shallow prospect pit (down to 0.5 m) in the area of the old mining activities. Polished samples were studied using the Jenapol and Amplival (Zeiss) microscopes. Ore minerals were analyzed by wave-dispersion (WDS) and energy-dispersion electron microprobe at Geological Survey of the Slovak Republic Bratislava, at CLEOM – Comenius University Bratislava and at Geology Institute University of Copen-

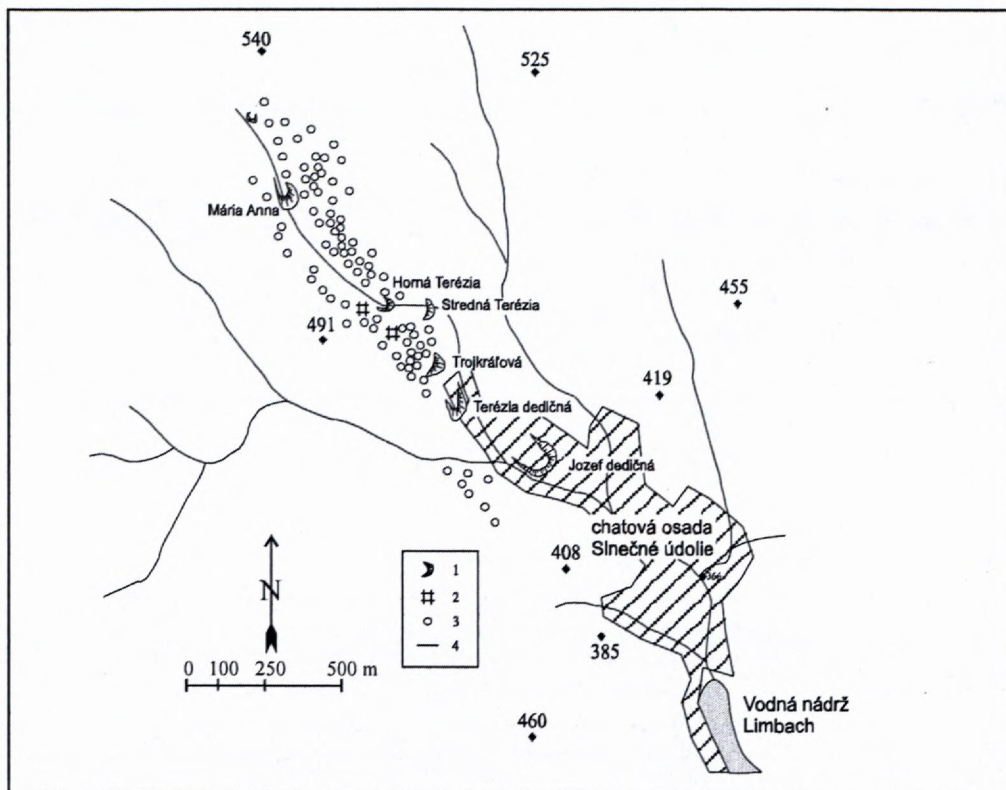


Fig. 2 Old miner works in the Pezinok - Staré Mesto deposit (modified by Cambel, 1959).
1 - mine dumps, 2 - shafts, 3 - slumps, 4 - brooks

hagen, Denmark (JEOL Superprobe 733). The operating conditions were 20kV and 20 nA. Natural (n) and synthetic (s) standards for unnamed mineral: Ag (AgL α) s, Sb (SbL α) s, PbS (PbL α) s, Bi₂S₃ (BiL α) s, CuFeS₂ (CuK α , FeK α , SK α) n and for tetrahedrite: Ag (Ag) s, Pb (PbS) s, Bi (Bi₂S₃) s, Cd (CdS) s, As (Cu₃AsS₄) s, Hg (HgS) s, Zn (ZnS) s, Sb (Sb) s, Cu, S (CuFeS₂) n. Operating conditions of Jeol Superprobe 733 and JXA 840A device (Geological Survey of the Slovak Republic Bratislava, CLEOM - Comenius University Bratislava): 20 kV, 15 - 20 nA, beam diameter 3 - 5 μ m. Standards: n FeS₂, FeAsS, HgS, PbS, Te, Sb, Ag, Bi, Cu, Au. SEM images were taken by JXA 840A device (Comenius University Bratislava). Fluid inclusions were analyzed by LINKAM THMS 600 heating-freezing stage (Comenius University Bratislava). Salinity was calculated according to the equation of Bodnar (1992).

Ore mineralization

Mineralization in the Pezinok-Staré Mesto deposit originated during several stages. The origin of wallrock alteration along tectonic zones preceded formation of Au-mineralization. Leucocrate granitoides forming near surroundings of exploited veins were striked by extensive silicification. The silicification zones gradually replace quartz veins and veinlets. They are characterised by the predominance of quartz and the presence of new-formed white mica. Feldspars were almost entirely replaced by fine-grained white mica and quartz. The presence of chlorite, as a desintegration product of biotite, is characteristi-

cal in more basic varieties of granitoids striked by alterations. It can also appear in areas of foliation of mylonitized rocks and it is abundant in hydrothermal quartz. Wallrock alteration out of tectonic zones did not appear in the vicinity of thin veins and veinlets. Carbonates were not found in altered zones. It is not possible to comment the zoning and the extent of altered zones associated with Au-mineralization are to the fact that there is no access to the old mines.

The main mass of the ore originated in the **oldest stage**. It is represented by quartz veins, veinlets and silicified zones with of pyrite, arsenopyrite and visible gold impregnations. However, usually there are no ore minerals in quartz veins. According to the archive information the maximum thickness of veins was 0,9 m (Cambel, 1959). However, usually the mineralization was formed by a group of several veins from 0,5 to 5 cm, or maximum 15 cm thick, located mostly in altered zones in mylonite granitoids. The content of Au in hydrothermal quartz (5 kg of quartz from the mine dump material samples) is 31.5 ppm. Even 204 ppm Au were found in one of the samples. The Au/Ag ratio in ores is 5. The deposit is strongly faulted according to findings of the cataclastic textures of vein filling (fig. 3). Quartz veins often join and thin out. It is often possible to see continuous changes of veins into quartz zones. The vein margins are closely associated with Fe-oxides and hydroxides (often even tectonically) of the thickness of several tenths of millimeter. Vein and veinlets type of mineralization is accompanied by impregnations of pyrite and arsenopyrite in altered zones. Extensively silicified zones are characterized also by the presence of gold.

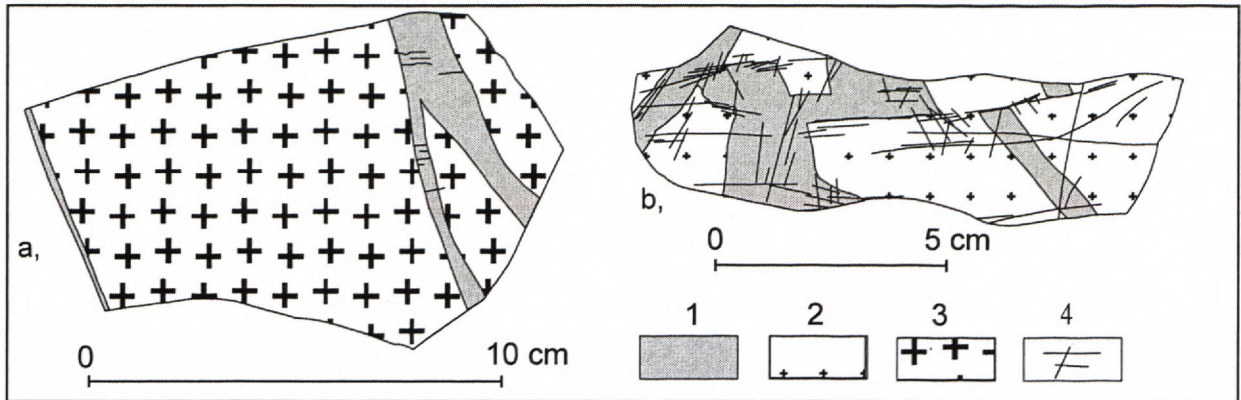


Fig. 3 Examples of auriferous quartz vein morphology (1 – quartz, 2 – silicified granite, 3 – unaltered granite, 4 – meso - micro faults). a: the veinlets of auriferous quartz in unaltered granite, b: strongly faulted auriferous quartz veinlets in silicified granite with impregnations of arsenopyrite and high finess gold.

Tab. 1 Selected electron microprobe analyses of gold

	1	2	3	4	5	6	7	8	9	10	11
Au	91,67	89,93	88,74	82,63	78,64	74,20	68,76	57,16	80,95	87,84	87,91
Ag	9,18	9,48	10,79	17,21	20,02	24,25	29,35	40,71	17,70	11,15	11,97
Hg	0,00	0,00	0,00	0,00	1,14	0,84	1,04	1,45	0,00	0,00	0,00
Cu	0,02	0,02	0,00	0,00	0,64	0,06	0,00	0,43	0,00	0,00	0,00
Sb	0,03	0,09	0,00	0,00	0,10	0,01	1,00	0,11	0,16	0,02	0,07
Bi	0,03	0,00	0,01	0,01	n.a.	n.a.	n.a.	n.a.	0,00	0,00	0,00
Fe	0,00	0,03	0,00	0,00	0,15	0,12	0,71	0,15	0,01	0,00	0,00
Σ	100,94	99,55	99,54	99,84	100,68	99,49	100,85	100,01	98,82	99,01	99,95

anal. 1, 2, 3, 4, 5, 6, 7, 8 – prim. Gold; anal. 9, 10, 11 – alluv. Gold; n.a. – not analysed; anal. 1, 2, 3, 4, 9, 10, 11 – ŠGUDŠ Bratislava; anal. 5, 6, 7, 8 – CLEOM Comenius University, Bratislava

Gold occurs most often as isometric grains, dendrites and flakes in quartz. Crystals of gold are rare. Sometimes two crystals, octahedral and hexahedral joined together, 0.1 mm in size were found (fig. 4f). Gold is relatively coarse-grained, more than 40 wt. % occurs in the fraction 0.5 – 2 mm (fig. 5a). More than 50 % of gold grains in polished samples are concentrated in fraction – 0.16 mm (fig. 5b). It fills the spaces among the quartz grains in the form of isolated grains of the size 0.0X – 5 mm. Locally it forms rich impregnations that often change continuously into veinlets of the maximum width 1 mm. There are several tens of 0.05 – 0.2 mm flakes in a 15 cm² area. The most of flakes are found on the margins of quartz veins on the contact zone with altered granitoid rock. There are clusters of small flakes on the margins of quartz veins and tectonically smoothed surfaces. They form almost continuous surface (a gold film) of up to 40 mm² in size. Gold along with pyrite and arsenopyrite is concentrated also in quartz from altered silicified granitoids (fig. 3). It is dominated mostly at the margins, less in the cracks (fig. 4a). It is often joined together by Fe-secondary minerals (pyrite relicts), rarely with micas. According to the chemical composition and paragenetic relations it is possible to assign two generations of gold on the deposit (fig. 6, tab. 1). The older gold I, with the fineness of 792 – 909 associate with pyrite and arsenopyrite (fig. 4a). The younger gold II is accompanied by Cu, Sb, Pb, Ag sulfides and sulphosalts (fig. 4b) with lower fineness (684 – 753). Gold II with a high content of Ag

(fineness 584) was found as thin veins and margins penetrating and dominating over flakes of gold I (fig. 4c).

Pyrite and arsenopyrite are the most common minerals at the deposit. Despite of this fact, their volume in vein-stones is relatively low and it usually does not exceed 1%. Most often they form 0.2 – 2 mm, often cataclased, well-terminated and subhedral grains in quartz and silicified granitoid rock. Rarely they form 5 mm big nests in quartz. Pyrite and arsenopyrite very often occur along with gold, which dominates and encloses them in cracks and in direction from margins. 0.0X flakes are often enclosed by pyrite and arsenopyrite. The content of As (tab. 2) varies from 26.29 to 31.99 at. %. The content of other elements (Sb, Au, Cu, Ni, Co) in arsenopyrite is lower than 0.5 at. %. Higher content of Au was found in arsenopyrite aggregates. These enclose visible gold or penetrate it.

Based on the presence of arsenopyrite - pyrite assemblage, arsenopyrite geothermometer (Kretschmar & Scott, 1976) was applied to determine the formation temperature of the first mineral stage. Considerable variation of As content in arsenopyrite resulted in large-scale crystallization temperature. The determination of the lower limit of the crystallization temperature was not possible because the arsenopyrite geothermometer is not calibrated for such low temperature values. According to the geothermometer, arsenopyrite have crystallized at 340 – 360 °C, upper limit for crystallization temperature is 445 °C.

In the younger stage of the mineralization origin, after ore tectonic event, the new structures were filled

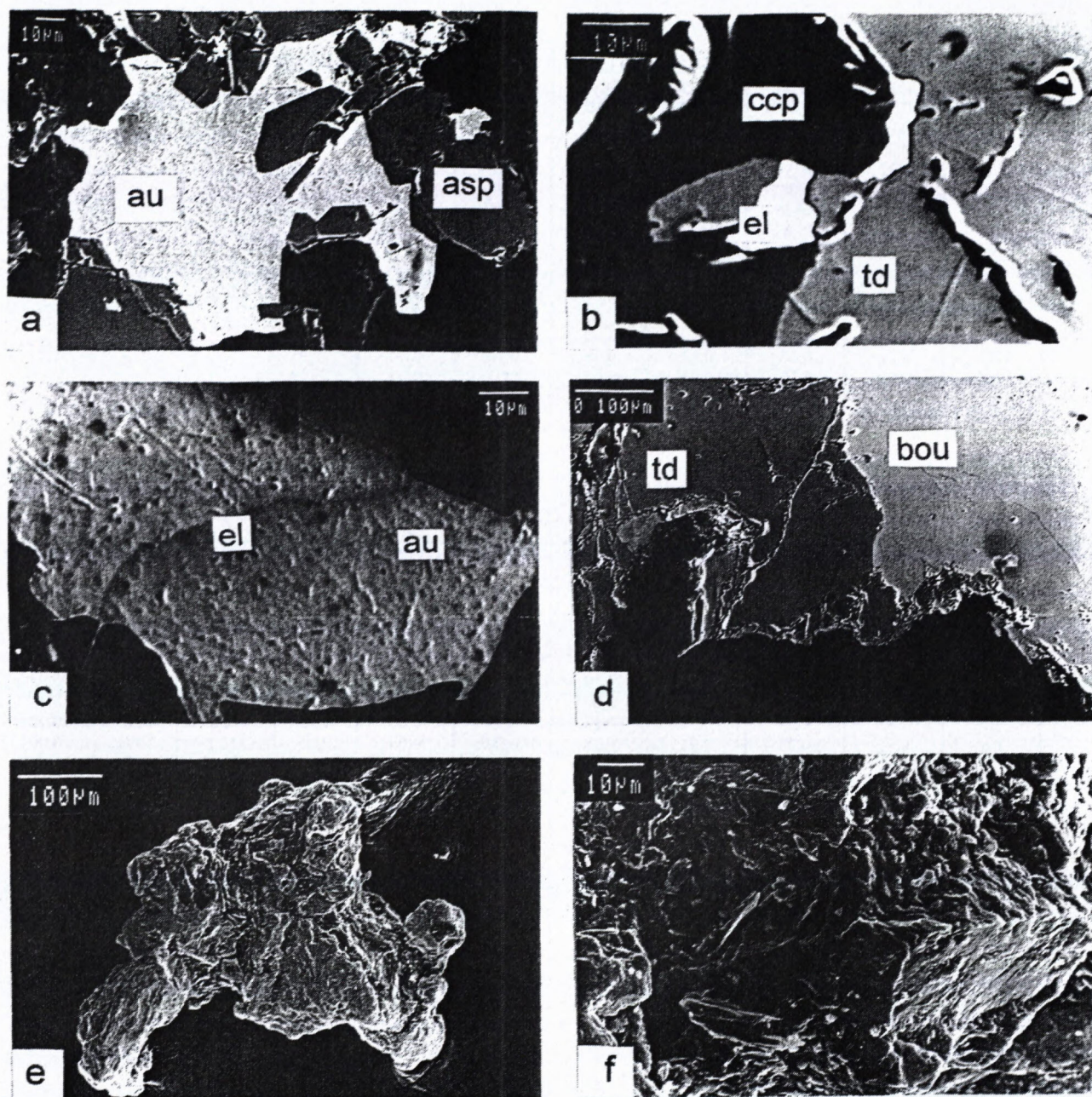
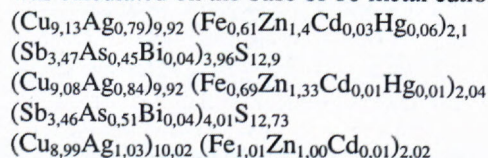


Fig. 4a: high finess gold (au) replacing arsenopyrite (asp), b: an intergrowth of low finess gold (el) with tetrahedrite (td) and chalcopyrite (ccp), c: the veinlet of low finess gold (el) in high finess gold (au), d: tetrahedrite (td) is affected by bournonite (bou), e: typical alluvial gold particle from Limbašský potok brook, f: crystal of gold isolated from the eluvial sediments on the deposit Pezinok – Staré Mesto.

with younger generation of quartz II, which is the bearer of the Cu, Sb, Pb, Ag mineralization. This mineralization is not evolved much at the deposit and its extent is only local. From ore minerals, pyrite II, tetrahedrite and chalcopyrite, occasionally also bournonite and unnamed Pb-Sb-Cu sulphosalt are present. Tetrahedrite and chalcopyrite occur in grains 0,0X – 5 mm and veinlets along with quartz II in quartz I. They penetrate each other, enclose crystals of pyrite II and grains of gold II (fig. 4b). Gold II has higher content of Ag instead of gold I. They were mostly found as inclusions in pyrite I and arsenopyrite. Locally chalcopyrite dominates over tetrahedrite. Chalcopyrite also forms 0,02 mm inclusions and veinlets in

tetrahedrite. We distinguished tetrahedrite in two paragenetic associations. Association with chalcopyrite and gold II is the most wide-spread. Rarely, tetrahedrite occurs together with bournonite, galena and unnamed sulphosalt. Tetrahedrite in association with Pb-Sb minerals has higher content of Ag (up to 7 wt. %) and Zn (more than 8 wt. %), (tab. 3). Crystallochemical formula of tetrahedrite was calculated on the base of 16 metal cations:



Tab. 2 Selected electron microprobe analyses of arsenopyrite

		1	2	3	4	5	6
wt. %	Fe	35,04	35,91	35,13	34,44	34,66	35,61
	Sb	0,34	0,46	0,12	0,15	0,16	0,15
	Co	0,00	0,00	0,00	0,00	0,00	0,29
	Ni	0,00	0,00	0,00	0,00	0,00	0,00
	Cu	0,32	0,08	0,16	0,21	0,20	0,05
	Au	0,00	0,00	0,18	0,25	0,27	0,00
	As	38,50	39,88	41,61	41,99	45,42	42,31
	S	25,82	23,88	21,74	21,52	21,24	20,95
	Σ	100,02	100,21	98,95	98,56	101,94	99,36
at. %	Fe	32,10	33,40	33,70	33,26	32,75	34,23
	Sb	0,14	0,20	0,05	0,07	0,07	0,06
	Co	0,00	0,00	0,00	0,00	0,00	0,26
	Ni	0,00	0,00	0,00	0,00	0,00	0,00
	Cu	0,26	0,06	0,13	0,18	0,16	0,04
	Au	0,00	0,00	0,05	0,07	0,07	0,00
	As	26,29	27,65	29,75	30,23	31,99	30,32
	S	41,21	38,69	36,32	36,20	34,95	35,07

anal. – CLEOM Comenius University, Bratislava

Tab. 3 Selected electron microprobe analyses of tetrahedrite

		1	2	3	4	5	6	7	8	9	10	
wt. %	Cu	35,11	35,06	34,06	33,78	34,76	34,55	32,79	34,67	33,32	35,23	
	Sb	25,59	25,62	25,54	26,25	24,16	24,68	25,85	24,90	25,32	24,39	
	S	25,02	24,79	24,46	24,38	24,44	24,42	25,36	25,82	24,03	23,93	
	As	2,06	2,33	1,84	1,55	2,05	1,96	0,38	0,37	2,07	1,94	
	Cd	0,19	0,07	0,07	0,13	n.a.	n.a.	n.a.	n.a.	n.a.	n.a.	
	Ag	5,17	5,53	6,62	7,12	6,67	6,72	5,61	5,51	6,21	6,35	
	Zn	5,57	5,29	3,91	4,14	5,27	4,53	7,43	8,35	4,89	5,93	
	Fe	2,06	2,35	3,37	3,09	3,33	3,32	1,60	1,57	3,42	3,23	
	Bi	0,53	0,57	0,39	0,63	0,25	0,00	0,25	0,22	0,02	0,00	
	Hg	0,75	0,20	0,01	0,18	0,00	0,08	0,00	0,00	0,00	0,00	
		Σ	102,05	101,89	100,47	100,25	100,93	100,26	99,26	101,41	99,28	100,99
	at. %	Cu	31,60	31,62	31,32	30,30	31,47	31,51	30,00	30,86	30,79	31,97
Sb		12,02	12,06	12,22	12,67	11,41	11,74	12,34	11,57	12,21	11,55	
S		44,63	44,31	44,33	44,67	43,85	44,13	45,99	45,53	44,00	43,03	
As		1,57	1,78	1,43	1,22	1,57	1,52	0,29	0,28	1,62	1,49	
Cd		0,01	0,04	0,04	0,07	n.a.	n.a.	n.a.	n.a.	n.a.	n.a.	
Ag		2,74	2,94	3,57	3,88	3,56	3,61	3,03	2,89	3,38	3,39	
Zn		4,87	4,64	3,48	3,72	4,63	4,02	6,61	7,23	4,39	5,23	
Fe		2,11	2,41	3,51	3,25	3,43	3,45	1,67	1,59	3,59	3,34	
Bi		0,15	0,16	0,11	0,18	0,07	0,00	0,07	0,06	0,01	0,00	
Hg		0,21	0,06	0,00	0,05	0,00	0,02	0,00	0,00	0,00	0,00	

anal. 1, 2, 3, 4 – Copenhagen, Denmark; anal. 5, 6, 7, 8, 9, 10 – CLEOM Comenius University, Bratislava; n.a. – not analysed

Tab. 4 Selected electron microprobe analyses of Pb-Sb-Cu sulphosalts

		1	2	3	4	5	6	7	8
wt. %	Pb	39,66	40,04	42,84	42,92	43,09	46,18	44,26	45,95
	Sb	23,64	24,68	26,30	23,97	24,23	27,67	26,70	26,75
	Cu	13,83	13,99	11,62	13,54	13,48	1,96	2,76	2,23
	Bi	0,00	0,00	0,00	0,01	0,34	0,00	0,00	0,00
	Ag	0,09	0,06	0,02	0,01	0,01	0,00	0,00	0,00
	Fe	0,25	0,14	0,18	0,02	0,01	0,14	0,21	0,21
	Zn	0,00	0,00	0,08	n.a.	n.a.	0,01	0,01	0,01
	S	21,51	20,47	20,52	19,85	19,72	23,93	24,00	23,32
	As	0,39	0,35	0,38	n.a.	n.a.	0,50	0,49	0,47
		Σ	99,37	99,74	101,95	100,31	100,88	100,40	98,43
at. %	Pb	14,90	15,31	16,47	16,75	16,82	18,02	17,29	18,27
	Sb	15,12	16,06	17,21	15,92	16,10	18,38	17,75	18,07
	Cu	16,94	17,44	14,57	17,23	17,16	2,05	3,51	2,90
	Bi	0,00	0,00	0,00	0,01	0,13	0,00	0,00	0,00
	Ag	0,06	0,05	0,01	0,01	0,01	0,00	0,00	0,00
	Fe	0,35	0,20	0,25	0,03	0,01	0,20	0,30	0,31
	Zn	0,00	0,00	0,09	n.a.	n.a.	0,01	0,02	0,01
	S	52,22	50,57	50,99	50,06	49,76	60,35	60,60	59,92
	As	0,40	0,37	0,40	n.a.	n.a.	0,54	0,53	0,52

anal.: 1, 2, 3, 4, 5 – bounonite; anal.: 6, 7, 8 – unnamed mineral; n.a. – not analysed; anal. 1, 2, 3, 6, 7, 8 – CLEOM Comenius University, Bratislava; anal. 4, 5 – Copenhagen, Denmark

$(Sb_{3,52}As_{0,41}Bi_{0,03})_{3,96}S_{12,79}$
 $(Cu_{8,88}Ag_{1,1})_{9,98} (Fe_{0,92}Zn_{1,06}Cd_{0,02}Hg_{0,01})_{2,01}$
 $(Sb_{3,6}As_{0,35}Bi_{0,05})_{4,00}S_{12,71}$
 $(Cu_{8,97}Ag_{1,01})_{9,98} (Fe_{0,98}Zn_{1,32})_{2,3} (Sb_{3,25}As_{0,45}Bi_{0,02})_{3,72}S_{12,5}$
 $(Cu_{9,02}Ag_{1,03})_{10,05} (Fe_{0,99}Zn_{1,15})_{2,14} (Sb_{3,36}As_{0,43})_{3,79}S_{12,64}$
 $Cu_{8,89}Ag_{0,89})_{9,78} (Fe_{0,49}Zn_{1,96})_{2,45} (Sb_{3,66}As_{0,09}Bi_{0,02})_{3,77}S_{13,63}$
 $(Cu_{9,07}Ag_{0,85})_{9,92} (Fe_{0,47}Zn_{2,12})_{2,59} (Sb_{3,4}As_{0,08}Bi_{0,02})_{3,5}S_{13,38}$
 $(Cu_{8,8}Ag_{0,97})_{9,77} (Fe_{1,03}Zn_{1,25})_{2,28} (Sb_{3,49}As_{0,46})_{3,95}S_{12,58}$
 $(Cu_{8,98}Ag_{0,95})_{9,93} (Fe_{0,94}Zn_{1,47})_{2,41} (Sb_{3,24}As_{0,42})_{3,66}S_{12,09}$

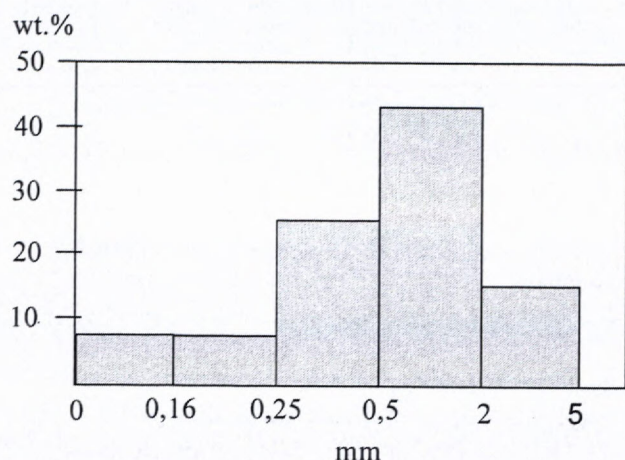


Fig. 5a Histogram of primary gold grain size from Pezinok - Staré Mesto deposit

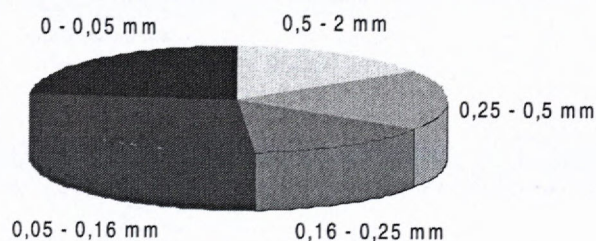


Fig. 5b Histogram of gold grain size measured in polished samples

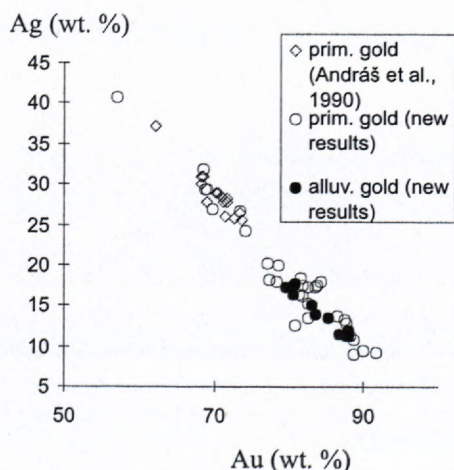


Fig. 6 Plot of Au vs. Ag content (wt. %) in gold from the Pezinok - Staré Mesto deposit

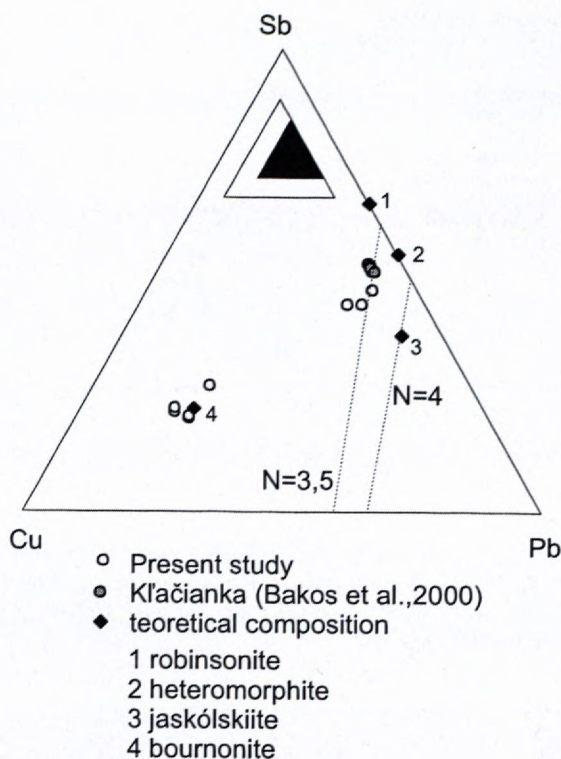


Fig. 7 Triangular diagram of Pb-Sb-Cu tetrahedrite (at.%)

Tetrahedrite accompanied by chalcopyrite is strongly replaced by secondary minerals. We can see two groups of points from microprobe analyses (fig.7). Bournonite, galena and unnamed Pb-Sb-Cu sulphosalt (tab. 4) were found in one sample, where quartz II, tetrahedrite and chalcopyrite form an aggregate approximately 5 mm in size. They replace tetrahedrite from the margins (fig. 4d). Unnamed Pb-Sb-Cu sulphosalt (fig. 8) has the reflectance very similar to that of bournonite, it is greyish-white and strong anisotropic. Bireflectance and internal reflects were not observed. Unnamed mineral from Pezinok-Staré Mesto deposit contains 2-3,5 at. % Cu and no Ag, Bi (tab. 4). The Fe content is ~ 0,2 - 0,3 at. % and As content ~ 0,5 at. %.

The latest stage is characterized by nests and veinlets of calcite. They cement cataclased vein filling. This type of mineralization is very rare and evolved only locally.

Fluid inclusions

Fluid inclusions appropriate for the microthermometry were found in quartz of first generation. Fluid inclusions were not found in darker varieties of quartz. Measurements were performed in 3 different quartz samples with pyrite-arsenopyrite mineralization with visible gold. The size of inclusions was 1 - 10 μm, in the mostly 5 μm. Three types of inclusions were found. The most of the inclusions had of one phase at the room temperature, lower amount had two phases and contained liquid and gaseous CO₂. We expect presence of another compounds (CH₄?) in the inclusions based on the shift of the melting point of CO₂ rich inclusions (fig. 10) towards lower temperatures. The second type of inclusions was found only rarely and the microthermometry was not possible due to

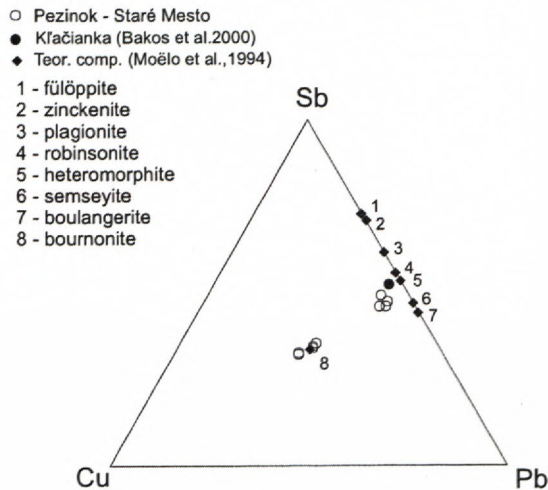


Fig. 8 Triangular diagram of X-ray electron microanalyses of Pb-Sb-Cu sulphosalts (at. %). Theoretical composition of sulphosalts are after Makovický (1989) for 1,2,4 and after Makovický & Nørrestam (1985) for 3.

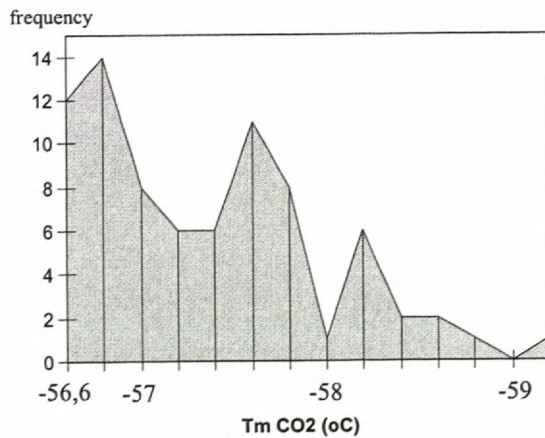


Fig. 10 Histogram of melting temperatures for the CO_2 - rich fluid inclusions from quartz

their small dimensions. They had of two and three phases and contained liquid – gaseous CO_2 and a small amount of aqueous phase (H_2O - electrolytes). The third type of inclusions had two phases, rarely three phases and contained aqueous phase, small amount of vapour. There were also cubes of halite in the three-phased inclusions. Except for the primary inclusions several secondary inclusions were found (fig. 11). According to the melting point shift of the last solid H_2O rich inclusions towards lower temperatures (down to $-24,9^\circ\text{C}$) we deem that except for NaCl, there is also CaCl_2 or KCl. It was not possible to measure the eutectic temperatures due to the small dimensions of inclusions. The salinity of H_2O - NaCl \pm KCl(?), CaCl_2 (?) inclusions was from 17 to 25 wt. % NaCl eq. and salinity of the secondary inclusions was from 5 to 10 wt. % NaCl eq. (fig. 11). Homogenization temperatures of these inclusions were between 100 and 350°C with the maximum at around 225°C (fig. 12). Temperatures of homogenization of some of the secondary inclusions were around 210°C .

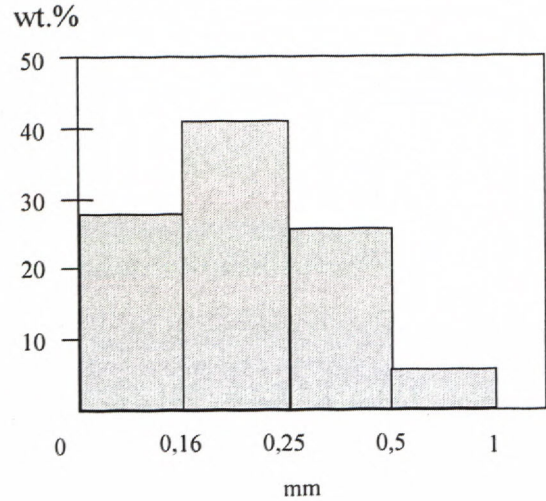


Fig. 9 Histogram of alluvial gold grain size from Limbašský potok brook

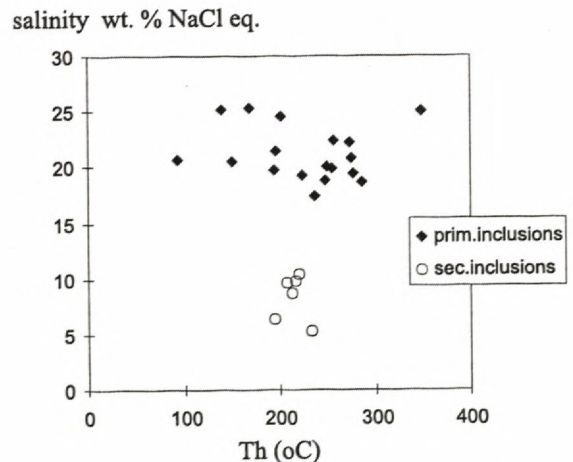


Fig. 11 Plot of homogenization temperature vs. salinity for fluid inclusions from quartz

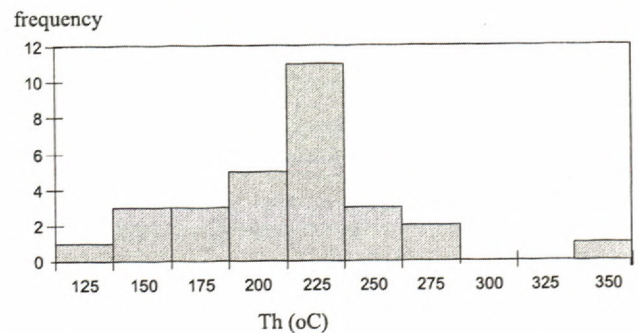


Fig. 12 Histogram of homogenization temperatures for fluid inclusions from quartz

Alluvial sediments

In heavy minerals concentrates of alluvial sediments, mostly garnets, ilmenite, magnetite, zircon, apatite, micas, monazite, xenotime and gold, less pyrite, epidote and rutile are present. We investigated mostly the distri-

bution, size, shape and the chemical composition of gold. The majority of gold from the alluvium occurs as small bunches and thick flakes (fig. 4e). It is modified to a relatively small extent, just sharp edges are-shaped deformed. Even in the distance of more than 4 km from the source, there are relatively abundant flakes with the shape similar to that of gold grains on the primary mineralization. Only about 50 % of grains are deformed. Grains deformed into thin plates by a mechanic pressure are rare. The most abundant are bunch grains with smooth surface. Dendritic grains are rare. More than 30 % of grains are penetrated with quartz or they enclose small grains of quartz. They form almost 100 % of the fraction exceeding 0,5 mm. Occasionally they are penetrate by Fe-oxides. Alluvial gold is relatively small-grained. There are more than 40% of flakes in the fraction from 0,16 to 0,25 mm. Almost 95 % of flakes are smaller than 0,5 mm (fig. 9). As for heavy minerals concentrates, gold exceeding 1 mm occur only rarely (the maximum is 4 mm).

The Au content of alluvial sediments in the lower part of Slnéčné údolie valley (in the depth of 0-0,4 m) is from 0,094 g.m⁻³ to 0,221 g.m⁻³. We found the biggest number of flakes in heavy minerals concentrates from this area (138 grains per heavy minerals concentrate at the most). Either upstream or downstream, the amount of gold is small in the area (up to ten grains per heavy minerals concentrate).

Interestingly there is a large amount of monazite in the vicinity of the primary location of the Au-mineralization (maximum 70 % in the heavy minerals concentrate). Monazite can be found as clear honey-yellow, yellow-and-brown and brown crystals and subhedral and xenomorphic grains up to 3 mm in size.

Discussion

Au mineralization at the Pezinok-Staré Mesto deposit is related to tectonic zones in Staré Mesto granitoid massif. According to the heavy minerals concentrates (Polák and Hanas, 1981, present study) the mineralization is spread in the whole massif. The mineralization is represented mostly by arsenopyrite, pyrite and visible gold and is related to the quartz veins, veinlets and impregnation zones in altered granitoides. Gold bearing „pyrites“ described by Döll (1899) and gold bearing pyrite described by Andráš et. al. (1990) are probably arsenopyrite and pyrite with 0,0X gold inclusions. Higher amounts of gold in arsenopyrite were found in grains in which free gold occurred. The occurrence of the secondary gold that originates from weathering of sulfides was not found, although Döll (1899) supposed so. Archive information about the occurrence of „gold bearing stibnite“ (Cotta & Fellenberg, 1862) at the deposit was not proved.

Younger base metal mineralization at the deposit is rare and occurs only locally. typical is higher amount of Ag in the hydrothermal solutions because of which more Ag minerals and Ag-rich tetrahedrite (Andráš et. al., 1990) originated. Higher amount of Ag in the younger stage of mineralization caused also the transport of gold of high fineness. It also caused the origin of the Ag - rich rims and veinlets and also the origin of gold of low fine-

ness. Newly found sulphosalts (bournonite and unnamed Pb-Sb-Cu sulphosalt) contribute to the paragenetic association of minerals of younger base metal period described by Andráš et. al. (1990). Microprobe analyses of tetrahedrites form three distinct group of points. Intergrowths of polybasite with Ag-rich tetrahedrite explain higher content of Ag in tetrahedrites described by Andráš et al. (1990). Two another groups of analyses vary in Zn and As contents while Ag content is nearly constant. We suppose that zonal tetrahedrite has two different phases. Older tetrahedrite with lower content of Zn originated together with chalcopyrite. Association of Pb-Sb minerals caused partial remobilization of tetrahedrite, which can be demonstrated by a phase with higher content of Zn. Higher content of Zn is typical for tetrahedrites from Sb mineralizations (Chovan, 1990). This paragenetic association of minerals conspicuously resembles the mineralization described from Ernest adit in Slnéčné údolie valley (Andráš et. al., 1999). Mineralizations at Ernest adit and Pezinok-Staré Mesto deposit differ by the absent stibnite mineralization with gudmundite, berthierite and other Pb-Sb sulphosalts at Pezinok-Staré Mesto deposit. Association of Pb-Sb minerals can be considered as an example of stibnite mineralization at the Pezinok-Staré Mesto deposit. Tetrahedrites from Ernest adit are not known to have higher Cu content and Ag content (Andráš et al., 1999). Furthermore, tenantite with As content 10 wt. % and Fe 6 wt.% was also described. Fe-As rich tetrahedrites are typical for siderite mineralization (Cambel & Jarkovský 1985). Quartz veins with stibnite at the deposit were not present in granitoid massive Staré mesto, described by Polák and Rak (1980).

Very rare is the occurrence of the unnamed Pb-Sb-Cu sulphosalt that probably belongs to the meneghinite homologue series. Its first finding in Western Carpathians was described from Kľačanka NE of Magurka (Nízke Tatry Mts.). Several occurrences of Sb-Au mineralization are known from this area there with a rich sulphosalt paragenetic association (Bakos et. al., 2000). Unnamed sulphosalt occurs here together with bournonite, heteromorphite, robinsonite and galena in younger period of the base metal mineralization. Compared to the theoretical composition of heteromorphite it contains about 1.8 at. % Cu and 0.2 at. % Ag. Cu and Ag can be introduce into the structure by the following possible substitutions: $Ag + Sb = 2 Pb$, $Cu + Pb = Sb + vac.$, which is a typical form of substitution in sulphosalts. The order number N is ~ 3.5 which corresponds to the hypothetical new member of meneghinite homologue series. Unnamed Pb-Sb-Cu sulphosalt from the Pezinok-Staré Mesto deposit contains 2 - 3.5 at. % Cu and no Ag and the order number N is ~ 3.5. Balance charge valence of analyses is wrong. Analyses points on the line for the hypothetical N ~ 3,5 rather than jaskolskiite which is N = 4. It seems to be a similar sulphosalt like the one from the Kľačianka occurrence.

Fluid inclusion study showed that the quartz from the arsenopyrite-pyrite-gold mineralization originated from CO₂ - rich (CO₂ - H₂O - NaCl ± KCl, CaCl₂(?) - CH₄(?)), fluids with salinity 17 - 25 wt. % NaCl eq. The fluid separation could be one of the reasons for the gold deposition. This can be proved by a presence of CO₂-CH₄(?)

rich inclusions and by the presence of high salinity H₂O inclusions. In the mineralized bodies gold is located at the margins of the quartz veins. The fluid - rock interaction is considered to be the most important mechanism of gold deposition at deposits of this type (Pirajno, 1992, McCuaig & Kerrich, 1998). In the first stages of fluid penetration through rocks there sulphidic reactions occur. Here the altered zones with Fe-sulphidic impregnations originate. Under favourable conditions a chemical absorption occurs resulting in the origin of sulfides and „refractory gold“ (Pezinok-Kolársky vrch deposit - Andráš et al., 1995). Due to a high occurrence of free gold it is not possible to exactly find the presence of „refractory gold“ in arsenopyrites and pyrites from the Pezinok-Staré mesto deposit. Homogenization temperatures of fluid inclusions in studied samples are from 100 °C to 350 °C. Th around 225 °C had most of the inclusions. As for the adjacent Pezinok deposit, homogenization temperatures of the first stage of mineralization (pyrite – arsenopyrite with „refractory gold“) are from 300 °C to 320 °C (Chovan et al., 1992). Arsenopyrite mineralization (\pm visible and refractory gold) in Ďumbierske Nízke Tatry Mts. originated at temperatures from 315 °C to 355 °C (Dúbrava deposit - Chovan et al., 1995) or from 280 °C to 360 °C (Mlynná dolina deposit - Majzlan et al., 2001). Temperature of origin of the orogenic type Au mineralization ranges from 150 °C to 700 °C, but most often from 250 °C to 400 °C (Kerrich & Cassidy, 1994, Groves et al., 1998 and others). Conditions of origin of the younger base metal mineralization were not determined from the studied samples. Homogenization temperatures (180 °C to 255 °C) of inclusions from younger stages from Pezinok-Kolársky vrch deposit mineralization (Chovan et al., 1992) are very similar to that secondary aqueous inclusions of Pezinok-Staré mesto deposit (Th 210 °C, salinity 5-10 wt. % NaCl eq.). CO₂ - rich fluid inclusions were found in arsenopyrite – pyrite mineralizations at Dúbrava (Chovan et al., 1995), Mlynná dolina (Majzlan et al., 2001) and Kriváň (Bakos, 2000) deposits too.

It was not possible to find out the power limit of the formation temperature of arsenopyrite using the arsenopyrite geothermometer (Kretschmar & Scott, 1976). The formation temperature is 340 – 360 °C, max. 445 °C. Such values fully correspond to temperature values determined from other localities of arsenopyrite mineralization in Western Carpathians. Temperature values at Dúbrava deposit vary from 395 to 430 °C (Sachan & Chovan, 1991), 320 – 380 °C at Mlynná dolina valley (Majzlan et al., 2001), 445 °C at Nižná Boca (Smirnov, 2000) and 350 - 410 °C at Pezinok - Kolársky vrch deposit (Andraš, et al., 1998).

Very high amounts of monazite in dry heavy minerals concentrates from the vicinity of Au-Ag mineralization do not correlate with accessory amounts of monazite in granitoids of Bratislava massif. This refers to a likelihood that the origin of a part of monazite is joined with the origin of the Au mineralization.

Au mineralization at the Pezinok-Staré Mesto deposit represents typical Au deposits of orogenic type (depth of formation 2 – 5 km, compressional/transpressional

environments), described in Groves et. al. (1998). The deposit is a part of Sb-Au formation, that is developed in crystalline basements of Tatric unit and it is abundant mainly in Nízke Tatry and Malé Karpaty Mts. Three sub-groups of Sb-Au mineralizations it are possible to assign in Western Carpathians: 1. Sb-As-Au (\pm Pb,Cu, Zn), 2. Sb-Au (\pm Pb,Cu,Zn) and 3. Au (Ag \pm Sb,Cu,Pb) mineralization. Dúbrava and Pezinok-Kolársky vrch deposits are typical representants of the first type mineralizations, which are characteristic by the presence of „refractory gold“ fixed mainly in the arsenopyrite. Magurka, Nižná Boca, Mlynná dolina, Dve Vody and Chvojníca deposits belong to the second sub-group, where mainly „visible gold“ and Sb-sulphide/sulphosalt mineralization is present. Third sub-group is characterised by „visible gold“ with a very low content of sulphides (less than 1 % in ores) and the presence of Ag-minerals. This sub group was distinguished according to the similarity of mineral assemblages, paragenesis and the character of mineralization on the Pezinok - Staré Mesto and Kriváň deposits. These deposits are so similar, that it is possible to assign an Au mineralization sub-group on the basis of similarity/dissimilarity compared to other Sb-Au deposits described in Western Carpathians. Noteworthy at Pezinok - Staré Mesto deposit compared to other „visible gold“ deposits in Western Carpathians is the absence of stibnite mineralization in ore bodies and presence of Ag-minerals. Cambel & Khun (1979) and Chovan et al. (1992) showed evidence about genetic relationship of Au and Sb mineralizations at Kolársky vrch and Pezinok - Staré Mesto deposits located at the structural continuation of the Kolársky vrch deposit. Based on the knowledge about other similar deposits (Kriváň deposit, Bakos (2000)) it is very probable that Sb-As-Au ore-like mineralization at Pezinok-Kolársky vrch deposit, mineralization in Ernest adit and gold mineralization at Pezinok-Staré Mesto deposit are genetically related. Some differences can occur due to the different rock composition and other conditions of mineral deposition which have a considerable influence to the deposition of minerals. Various mineralization stages at adjacent deposits did not have to occur at all, or only to a small extent.

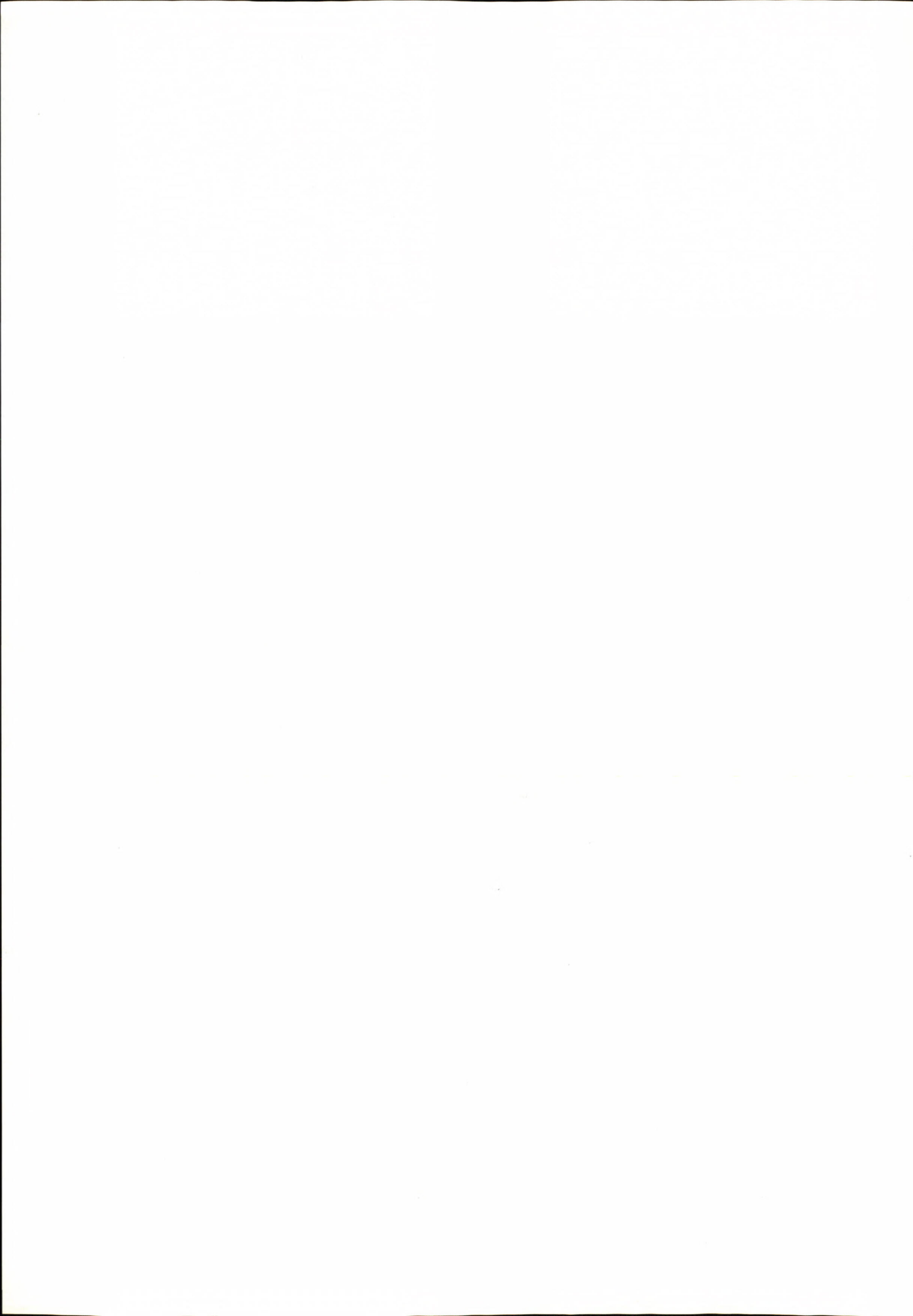
Acknowledgements

We would like to thank doc. RNDr. Martin Chovan, CSc. for the stimulating comments and Dr. Monika Huraiová for help in study of fluid inclusions. The research was financially supported by a grant VEGA 1/8318/01 and the grant project PRIFUK 17/1999.

References

- Andraš, P., Caño, F., Nagy, G. & Ďurža, O., 1988a : Gold-bearing arsenopyrite of the Pezinok antimonite deposit. Geol. Zbor. Geol. Carpath., 39, 87 - 98.
- Andraš, P., Caño, F. & Nagy, G., 1988b : Contribution to the characteristics of gold-bearing pyrite on the Pezinok-Kolársky vrch, Vinohrady deposit. Mineralia Slovaca 20, 463 - 471. (in Slovak).
- Andraš, P., Jeleň, S. & Caño, F., 1990: Paragenetic relations between gold-quartz ore mineralization and antimonite ores of the Pezinok deposit, Western Slovakia. Mineralia Slovaca 22, 429 - 435. (in Slovak).
- Andraš, P. & Ragan, M., 1995: Sulphide ores with invisible gold in Slovakia. Mineralia Slovaca 27, 57 - 63. (in Slovak).

- András, P., Dubaj, D. & Kotulová, J., 1998: Application of arsenopyrite geothermometer from Pezinok deposit (Western Carpathians, Slovakia). *Mineralia Slovaca* 30, 147 - 156.
- András, P., Uher, P., Stankovič, J. & Kotulová, J., 1999: Mineralogical and geochemical characteristics of mineralization in Ernest adit (Limbach, Malé Karpaty Mts., SW Slovakia). *Mineralia Slov.* 31, 238 - 290. (in Slovak).
- Bakos, F., Chovan, M. & Michálek, J., 2000: Mineralogy of hydrothermal Sb, Cu, Pb, Zn, As mineralization in NE of the Magurka deposit (Nízke Tatry Mts.). *Mineralia Slovaca* 32, 497 - 506. (in Slovak).
- Bakos, F., 2000: Mineralogy, paragenesis and fluid inclusion study at Kriváň Au-Sb deposit (Tatra Mts.). Abstract, ŠVK, PriF UK, Bratislava, 156. (in Slovak).
- Bergfest, A., 1952: Mining activity in Pezinok and in the vicinity. Manuscript, Geofond, Bratislava, 50. (in Slovak).
- Bodnar, R. J., 1992: Experimental determination of the liquidus and isochores of a 40 wt. % NaCl - H₂O solution using synthetic fluid inclusions. PACROFI IV, Program and abstracts, California, USA, 14 p.
- Cambel, B., 1954: Geological - petrographical problems in the north - eastern part of the Malé Karpaty Mts. crystalline complex. *Geol. Práce, Zoš.* 36, 3 - 74. (in Slovak).
- Cambel, B., 1959: Hydrothermal deposits in the Malé Karpaty Mts., mineralogy and geochemistry of their ores. *Acta geol. geogr. Univ. Comen.* 3, 538. (in Slovak).
- Cambel, B. & Jarkovský J., eds., 1985: The Rudňany ore field - geochemical-metagenetic characteristics. Veda, SAV, Bratislava 363 p. (in Slovak).
- Cotta, B. & Fellenberg, E., 1862: Die Erzlagerstätten Ungars und Siebenbürgen, Gangstudien, IV, Freiberg, 236 p.
- Döll, E., 1899: Das Gold von Bösing. *Vehr. Vereins für Natur und Heikunde zu Pressburg (Bratislava)*, 43 p.
- Dubovský, J., 1990: Gold mining at Pezinok in 14. - 19. cent. In: Old mining towns in Slovakia. *Osveta, Martin*, 182 - 187. (in Slovak).
- Groves, D. I., Goldfarb, R. J., Gebre-Mariam, M., Hagemann, S.G. & Robert, F., 1998: Orogenic gold deposits: A prodused classification in the context of their crustal distribution and relationship to other gold deposit types. *Ore Geol. Reviews*, 13, 7 - 27.
- Chovan, M., 1990: Mineralogical-paragenetical relationships on the Dúbrava Sb deposit and their significance for metalogenesis of the Nízke Tatry Mts. *Acta Geol. Geogr. Univ. Comen.* 45, 89-101.
- Chovan, M., Rojkovič, I., András, P. & Hanas, P., 1992: Ore mineralization of the Malé Karpaty Mts. (Western Carpathians). *Geol. Carpath.*, 43, 5, 275 - 286.
- Chovan, M., Hurai, V., Sachan, H. K. a Kantor, J., 1995b: Origin of the fluids asociated with granodiorite hosted, Sb-As-Au-W mineralization at Dúbrava (Nízke Tatry Mts., Western Carpathians). *Mineral. Deposita*, 30, 48 - 54.
- Kerrick, R. and Cassidy, K. F., 1994: Temporal relationships of lode gold mineralization to accretion, magmatism, metamorphism and deformation - Archean to present: A review. *Ore Geol. Reviews*, 9, 263 - 310.
- Kretchsmar, U. & Scott, S. D., 1976: Phase relations involving arsenopyrite in the system Fe-As-S and their application. *Canad. Mineralogist*, 14, 364 - 386.
- Majzlan, J., Hurai, V. & Chovan, M., 2001: Fluid inclusion study on hydrothermal As-Au-Sb-Cu-Pb-Zn veins in the Mlynná dolina valley (Western Carpathians, Slovakia). *Geologica Carpathica*, 52, 5, 277 - 286.
- Maheľ, M. & Cambel, B., eds., 1972: Geological map of Malé Karpaty Mts. GÚDŠ Bratislava, (in Slovak).
- Makovický E., 1989: Modular classification of sulphosalts - current status. Definition and application of homologous series N Jb. *Miner. Abh* 160 3 269-297.
- Makovický E & Nørrestam R., 1985: The crystal structure of jaskolskiite, Cu_xPb_{2+x}(Sb,Bi)_{2-x}S₂ (x~0,2), a member of the meneghinite homologous series. *Zeitsch. fur Kristall.* 171 179-194.
- McCuaig, C. T. and Kerrich, R., 1998: P - T - t deformation - fluid characteristics of lode gold deposits: evidence from alteration systematics. *Ore Geol. Reviews*, 12, 381 - 453.
- Michal, S. & Uher, P., 1999: Gold in the Malé Karpaty Mts. (SW Slovakia) - a historical review. *Mineralia Slov.* 31, 319 - 320, (in Slovak).
- Pirajno, F., 1992: Hydrothermal mineral deposits. Principles and fundamental concepts for the exploration geologist. Springer Verlag, Berlin Heidelberg, 709 p.
- Polák, S. & Rak, D., 1979: Gold in the antimonite deposit at Pezinok - Malé Karpaty Mts., SW Slovakia. *Mineralia Slov.* 11, 553 - 554. (in Slovak).
- Polák, S. & Rak, D., 1980: Prognostic probleme of antimony metalogeny in the Malé Karpaty Mts. In: *Antimony ores of Czechoslovakia*. GÚDŠ, Bratislava, 69 - 89, (in Slovak).
- Polák, S. & Hanas, P., 1981: On the alluvial gold aureole around the Pezinok - Kolársky vrch hill antimony mineralization (Malé Karpaty Mts., Western Slovakia). *Mineralia Slov.*, 13, 451 - 456, (in Slovak).
- Polák, S., 1986: Au and Au-Sb mineralization in the region of Pezinok. *Mineralia Slov.* 18, 517 - 524, (in Slovak).
- Plašienka, D., Michalík, J., Kováč, M., Gross, P. & Putiš, M., 1991: Paleotectonic evolution of Malé Karpaty Mts. - an overview. *Geol. Carpath.*, 42, 195 - 208.
- Sachan, K. H. & Chovan, M., 1991: Thermometry of arsenopyrite-pyrite mineralization in the Dúbrava antimony deposit (Western Carpathians). *Geol. Carpathica*, 42, 265 - 269.
- Smirnov, A., 2000: Sb-Au mineralization in the vicinity of Nižná Boca. Dipl. work, Dept. of min. and petrol., Fac. of Nat. Scs., Comenius University, Bratislava, 131 p.
- Wittgrüber, P., Tuček, P. a Vitáloš, J., 2001: History of mining at Malé Karpaty Mts. Road Bratislava, 48 p. (in Slovak).



Cooling and uplift trajectories of the Malé Karpaty Variscan Basement (West Carpathians)

MARIAN DYDA

Department of Mineralogy and Petrology, Comenius University, Mlynská dolina, SK-84215 Bratislava.
e-mail: dyda@fns.uniba.sk

Abstract. In the Malé Karpaty the Variscan regional metamorphic recrystallisation temperatures (570-620 °C) and pressures (4.7-6.1 Kbar) in Bratislava massive differ significantly from contact periplutonic processes in Modra massive. The approximative P-T trajectories express the first order tectonic motion and specific uplift conditions of the particular basement blocks. The culmination whole rock reaction paths have steep slopes ($dP/dT \approx 89-121$ bar/K) and later compositional changes modified dominantly by diffusion processes run during decompression cooling ($dP/dT \approx 62-68$ bar/K). These trajectories are consistent with regional metamorphic environment and the metamorphic culmination was associated with granitoidic polyphase magmatism. The post culmination multiple heating events are absent and mineral assemblages reflect the one thermal culmination event. The annealing estimates indicate that ca. 0.10-0.53 garnet mass fraction was transferred during cooling. These estimates are good cooling rate indicators and the values testify about the regional metamorphic processes. The calculated depth and heating rate data ($4 \cdot 10^{-5}$ °C/y) may provide corresponding burial rate of 1-2 km/Ma. Cooling rate data calculated from garnet diffusional zonality ($\sim 4.7-94$ °C/Ma) assess the approximate exhumation rate at 0.2-3.8 km/Ma. The data confirm different cooling scenarios for tectonically controlled rapid uplift end erosion. The orogenic block transport, stacking and restructuring occurred in the Variscan era and the tectonic complexity in the region was also shaded by complicated tectono deformation development in the Alpine period.

Key words: geothermobarometry, reaction slope, cooling rate, metamorphic trajectories, West Carpathians.

Introduction

The complicated nappe structure of the Western Carpathian mountain range was recognized as early as 1898 and 1903 by Viktor Uhlig and later in 1903 by M. Lugeon. Since works of Andrusov (1936, 1968), Andrusov et al., (1973) it has been accepted that two upper Mesozoic sedimentary sequences form groups of nappes, lower the Křížna nappe and the upper the Choč nappe. The lowermost Mesozoic sequences create the Cover formation underlying nappe formations and overlying the crystalline basement complexes. Recently, the crystalline basement complexes and their sedimentary cover rocks are considered to be allochthonous (Leško et al., 1980, Maheľ, 1983, Maheľ, 1986, Bezák et al., 1998, Vozárová, 1998).

The „core mountains“ are situated in the outer zone of the Western Carpathians segment. They crop out within the unfolded Paleogene and Neogene rocks and exhibit dome structure with the crystalline core, tectonical overprinting by Mesozoic events and a distinct style of Paleogene sedimentation. There are some deviations from more central „core mountains“ that, in some cases, suggest facies and tectonic similarities with the Eastern Alpine segment.

The largest tectonic superunit of the Central Western Carpathian is the Tatricum. It forms the lowermost basement substratum of the „core mountains“, laying between the Klippen Belt in north and other basement superunits further south, the Veporicum and the Gemicum (Putiš, 1991, Plašienka et al., 1991).

The Malé Karpaty have a prominent position in the crystalline basement studies. The basement rocks are represented by paragneisses, orthogneisses, amphibolites and other high grade metamorphic rock complexes later intruded by Variscan granitoidic rocks.

Geological Setting

The Malé Karpaty (M.K.) play a specific and important role in the Eastern Alpine and Western Carpathian relationship and correlation as they bear some typical geological features of both mountain systems, but they have a prevailing Carpathian influence (Maheľ, 1983).

The Variscan postkinematic granitoidic rocks are the predominant constituent of the M.K. crystalline complex. They form two separate massifs, the Bratislava and Modra massifs, separated by a 4-8 km wide zone of schists. According to the genetic I/S classification, the M.K. granitoid rocks are transitional. Their geochemical fea-

tures are suggestive of being I-Caledonian type. The Bratislava granitoid massif clearly shows a tendency towards S-type granitoids (Cambel & Vilišovič, 1987).

The age of contact metamorphism dated on contact metamorphic biotites, is within the range of age determination of Bratislava granitoidic massif intrusion, 298 - 354 m.y. (Bagdasarjan et al., 1983). The biotite pairs Rb/Sr isochron gives age of 344 ± 3 m.y. (Cambel et al., 1990b). This age determination is considered to be the age of Bratislava granitoid massif intrusion.

The sedimentary overburden was regionally metamorphosed before granitoid rocks intruded and periplutonic processes became dominant in some areas. The metamorphic process took place during the late Variscan era (Cambel & Valach, 1956; Cambel et al., 1990a,b). The spatial relationship and metamorphic zonation exists in some areas only as rudimentary remnants. In other places the complete metamorphic zonation was preserved (Broška & Janák, 1985; Dyda & Mikláš, 1993).

Disturbances of the Variscan metamorphic structures caused by Alpidic tectonic movements destroyed the original metamorphic zonation. This is evident from appearance of index minerals, irregularity of dehydration reaction progress and reaction volume changes in metapelites and paragneisses of the periplutonic zones (Dyda and Mikláš 1993). These processes do not progress continually in the profiles and at some places have no relation to the distance from granitoidic contact. This serves as a petrological argument for distinguishing between paraautochthonous and allochthonous metamorphic zones in the area and support the concept of tectonic destruction of the Variscan periplutonic zones and the basement as a whole (Dyda, 1997).

Earlier tectonic concepts (Cambel, 1952,1954) were not in favour of any Alpidic orogenic activity in the crystalline basement complexes, and only development of Alpidic fault retrograde processes were considered. However, recent tectonometamorphic and petrological research indicates complex tectonic and structural development of this core mountain mass (Dyda, 1977, 1980a, 1980b, 1994, 1999, 2000; Cambel et al., 1981; Korikovskij et al., 1984; Mikláš, 1986, 1987). This requires the assumption of several superimposed nappe units consisting of pre-Alpine crystalline basement with its Mesozoic cover (Putiš, 1987, 1991; Plašienka et al., 1991; Marko et al., 1991).

Complex structures of the mountains reflect their complicated development, which started hundreds of kilometers southwards, and the remnants of Variscan mountains were overridden by Paleo-Alpine nappe piles. Their structures were modified by back-thrusts and transpressional tectonics (Plašienka, 1989; Plašienka et al., 1991).

The reconstruction of the Hercynian orogenic cycle in Western Carpathians is complicated because of the presence of the Alpine tectonic overprinting. Fragments of Hercynian structure were incorporated into new paleoalpine units. To reconstruct their original tectonic position, the elimination of younger tectonic effects is needed as

well as the analysis of their development (Bezák, 1993). Thus, due to the tectonic disturbances of the Variscan orogen, it is still unclear whether the crystalline complexes in some „core mountains“ are in an autochthonous position.

The present petrologic study is focused on metamorphic reaction extent, geothermobarometry, whole rock reaction paths, cooling estimates and metapelitic rocks uplift trajectories with the aim to describe and approximate specific petrological processes that bring new aspects of metamorphic development of this important geological area. The contribution of this paper is to place a larger amount of information relevant to the determination of uplift trajectories on a more accessible format than was previously available.

Methods and data

The initial mineral constituents of the studied metapelites have been approximated by protolith calculations (Dyda & Mikláš, 1993) that determines protolithic presence of quartz, plagioclase, K-feldspar, chlorite, illite, montmorillonite, calcite, ankerite, rodochrosite and rutile in the protolithic sediments. The present modal composition of studied paragneisses is given in Tab.1.

Table 1. Chemical * and modal composition of the representative Tatric basement paragneisses from the Malé Karpaty.

Sample	KB-2.	KB-3.	KB-5.	17.
SiO ₂	62.77	65.26	56.05	62.16
TiO ₂	0.82	0.69	1.03	0.81
Al ₂ O ₃	17.27	16.55	19.59	17.04
Fe ₂ O ₃	4.24	3.58	4.72	3.82
FeO	3.60	2.67	5.01	4.10
MnO	0.18	0.13	0.28	0.15
MgO	2.35	1.46	2.58	2.18
CaO	1.77	2.48	2.04	1.49
Na ₂ O	2.88	3.84	3.10	2.46
K ₂ O	2.38	1.85	2.82	2.60
H ₂ O ⁺	1.18	0.65	1.47	1.79
Σ	99.45	99.16	98.69	98.60
Number of ions in rock on 160 hydrous oxygen basis				
Fe ³⁺	2.853	2.406	3.270	2.578
Fe ²⁺	2.692	1.994	3.857	3.075
Mn	0.136	0.098	0.218	0.113
Mg	3.132	1.943	3.540	2.913
X _{Fe} **	0.629	0.683	0.654	0.651
Modal composition				
Quartz	34.1	31.1	24.3	38.0
Plagioclase	32.5	39.1	35.1	26.1
Biotite	27.5	27.6	33.8	29.9
Muscovite	0.6	0.5	2.1	2.5
Garnet	3.5	1.2	1.8	1.6
Staurolite	0.7	-	0.4	1.3
Sillimanite	0.9	0.2	2.3	0.4
Opaque ***	0.2	0.3	0.2	0.2

*Wet chemical analyses. Analyst: E.Waltzel; **X_{Fe}= ΣFe/(Fe³⁺+Fe²⁺+Mn+Mg) *** dominantly ilmenite.

With increasing metamorphic grade the rock experienced transformations via unspecified progressive reaction. It is to notice that no reaction rests from earlier metamorphic stages indicating pre-culmination trajectory have been observed as e.g. inclusions in garnets. Thus, the major whole rock reactions encountered in the rocks represent terminal stability of staurolite which occurs at culmination temperature and pressure in sillimanite stability field. Staurolite remove from the assemblages is accompanied with progressive growth of garnet and sillimanite in the assemblage $St+Ms+Bt+Grt+Sil+Pl+Qtz$, where important kyanite rests are consumed and eventually disappear. During decompression stages kyanite \rightarrow sillimanite reaction boundary is crossed and kyanite presence is replaced by fibrolitic sillimanite. Kyanite is almost completely resorbed and significant unresorbed kyanite rests remain only in some assemblages (Fig.1.). Existing homogenous garnet porphyroblasts possess no kyanite inclusions (Fig.2.).



Fig. 1. Higher pressure kyanite relics in the Tatric basement paragneisses from Malé Karpaty, first described by Dyda (1999), prove the higher pre culmination metamorphic pressures and are consistent with the steep whole rock reaction path during decompression. (Scale bar = 0.5 mm).

The evaluation of metamorphic trajectories primarily relies on geothermobarometric data based on chemical composition of equilibrium mineral assemblages. However, the portion of the trajectory may be eradicated by later higher temperature processes. Thermodynamic modelling of the zoned minerals e.g. garnet (Spear & Selverstone, 1983) provides reliable P-T trajectory reconstruction in fulfilling the fundamental assumption that the zoning observed in the garnet is the product of growth of continuous equilibrium reaction and that zoning has not been later modified by thermal diffusional processes. Simultaneously the assemblage present during garnet growth must be known. This imperative requirement can not always be fulfilled and in addition, mineral dise-

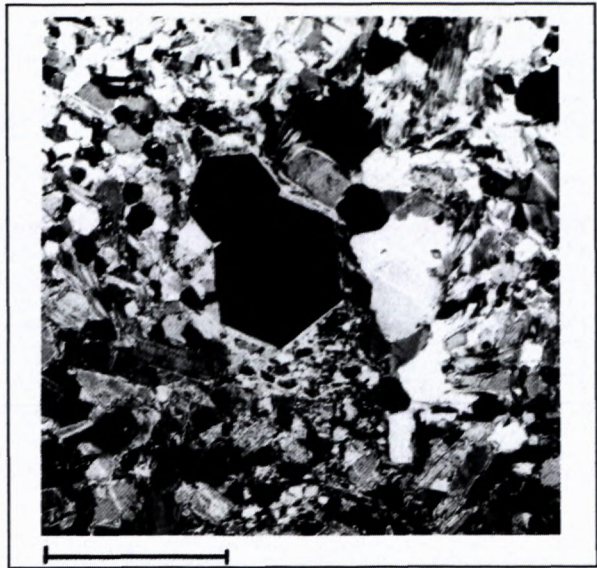


Fig. 2. Idioblastic garnet morphology and its progressive growth in sillimanite stability field is consistent with calculated staurolite decomposition reaction (A1) and with no microscopic decomposition features clearly indicates a quenched assemblage and a rapid decompression uplift process. (Sample 17., Scale bar = 0.5 mm).

disequilibrium features form, during the P-T changes. Thus the inherited mineral disequilibrium features from previous metamorphic stages coexist as the consequence of slow mineral reactions rate.

JEOL Superprobe 733 and JEOL 840 microprobe served for mineral analyses. The operating conditions were 20 kV accelerating voltage, specimen current of 15-20 μA and beam diameter 1-2 μm . For sodic plagioclase and muscovite the beam diameter was increased to 5-7 μm to avoid sodium loss. In order to obtain the representative chemical analyses of the centre of zoned minerals (garnet, plagioclase), only the largest grains assumed to be in equilibrium contact with surrounding minerals were selected and analysed from polished thin section.

In each sample 3-6 grains of each mineral have been analysed in two to three locations to test the homogeneity of the grain. Total iron has been calculated as ferrous. Fe^{3+} in garnets and biotites was not calculated as the accuracy depends highly on all of the elements analysed, H_2O , Al^{IV} , Al^{VI} content, compositional limits and on the structural balance. Anyhow, the numerical approach of Shumacher (1991, 1997) may be useful in this respect. The chemical compositions of the coexisting garnets, biotites, muscovites, plagioclases and staurolites of the equilibrium mineral assemblages are given in Tab. 2.

In the thermobarometrical approach some differences occurred stemming from different calibrations of the particular mineral reactions. Uncertainties and their estimates that have appeared in the literature usually adopt values of $\sigma T = 50 \text{ }^\circ C$ and $\sigma P = 1 \text{ Kbar}$. Many samples from single location reflect this general consensus (e.g. Ferry, 1980; Ghent & Stout, 1981) based on the reproducibility of the P-T data (Hodges & Crowley, 1985).

Table 2. Chemical composition of coexisting minerals in Tatric basement paragneisses.

Garnet analyses								
M.K.	17c	17r	KB2c	KB2r	KB3c	KB3r	KB5c	KB5r
SiO ₂	37.36	35.90	37.46	36.35	37.03	36.67	37.12	37.35
TiO ₂	0.04	0.00	0.03	0.03	0.02	0.01	0.08	0.01
Al ₂ O ₃	21.43	21.17	21.68	21.26	20.98	20.75	21.25	20.73
FeO	29.15	30.87	30.12	31.35	30.15	30.14	27.68	31.22
MnO	8.71	7.25	5.55	6.39	7.36	8.09	9.03	6.41
MgO	2.59	2.65	3.41	3.08	2.66	2.36	2.81	2.53
CaO	1.30	1.29	1.70	1.42	1.83	1.94	1.97	1.48
Σ	100.58	99.13	99.95	99.88	100.03	99.96	99.94	99.73
Cations / 12 oxygens								
Si	2.995	2.940	2.994	2.945	2.991	2.978	2.988	3.022
Ti	0.002	0.000	0.001	0.002	0.001	0.001	0.004	0.000
Al	2.025	2.043	2.043	2.031	1.997	1.987	2.017	1.977
Fe	1.954	2.114	2.013	2.124	2.036	2.047	1.863	2.113
Mn	0.591	0.502	0.375	0.438	0.503	0.556	0.616	0.439
Mg	0.309	0.323	0.406	0.372	0.320	0.285	0.337	0.305
Ca	0.111	0.113	0.145	0.123	0.158	0.168	0.170	0.128
Plagioclase analyses								
M.K.	17c	17r	KB2c	KB2r	KB3c	KB3r	KB5c	KB5r
SiO ₂	59.80	59.03	61.35	61.39	61.14	60.91	61.45	61.52
Al ₂ O ₃	23.82	24.40	24.53	25.10	24.54	24.30	23.56	24.03
FeO	0.05	0.15	0.15	0.01	0.10	0.08	0.10	0.10
CaO	5.25	5.91	5.80	6.41	5.50	5.80	5.12	5.41
Na ₂ O	10.98	10.62	8.49	7.96	8.54	8.80	8.85	8.66
K ₂ O	0.05	0.05	0.08	0.07	0.14	0.05	0.06	0.05
Σ	99.95	100.16	100.40	100.94	99.96	99.94	99.14	99.77
Cations / 8 oxygens								
Si	2.686	2.653	2.716	2.701	2.716	2.712	2.750	2.736
Al	1.261	1.292	1.280	1.302	1.285	1.275	1.243	1.260
Fe ²⁺	0.001	0.005	0.005	0.000	0.003	0.002	0.003	0.003
Ca	0.252	0.284	0.275	0.302	0.261	0.276	0.245	0.257
Na	0.956	0.925	0.728	0.679	0.735	0.759	0.768	0.746
K	0.002	0.002	0.004	0.003	0.007	0.002	0.003	0.002
Biotite analyses								
M.K.	17c	17r	KB2c	KB2r	KB3c	KB3r	KB5c	KB5r
SiO ₂	35.18	34.97	36.28	36.03	35.44	35.69	36.73	36.20
TiO ₂	1.60	1.38	2.06	2.08	1.89	2.10	1.91	1.80
Al ₂ O ₃	19.39	20.14	19.68	20.16	19.55	20.05	19.79	19.71
FeO	19.83	19.97	18.17	18.62	19.98	18.60	17.71	19.81
MnO	0.14	0.14	0.02	0.18	0.27	0.14	0.21	0.11
MgO	9.66	10.34	9.17	9.29	8.82	8.96	9.65	9.41
Na ₂ O	0.48	0.52	0.46	0.21	0.14	0.24	0.44	0.32
K ₂ O	8.37	7.43	8.91	8.52	9.14	9.70	8.96	8.09
Σ	94.68	94.89	94.75	95.08	95.23	95.46	95.40	95.45
Cations / 22 anhydrous oxygens								
Si	5.374	5.301	5.486	5.427	5.401	5.395	5.502	5.450
Ti	0.183	0.157	0.234	0.235	0.216	0.239	0.215	0.203
Al	3.493	3.599	3.508	3.580	3.512	3.577	3.495	3.498
Fe	2.534	2.532	2.298	2.345	2.546	2.354	2.219	2.494
Mn	0.018	0.017	0.002	0.022	0.034	0.020	0.026	0.014
Mg	2.199	2.336	2.066	2.085	2.003	2.020	2.154	2.111
Na	0.144	0.152	0.134	0.061	0.041	0.070	0.129	0.093
K	1.632	1.437	1.719	1.637	1.777	1.872	1.712	1.553

Table 2. (continued)

Muscovite analyses.					Staurolite analyses.				
M.K	17c	17r	KB5c	KB5r		17c	17r	KB5c	KB5r
SiO ₂	46.49	46.36	47.06	46.98	SiO ₂	27.41	27.42	27.27	27.33
TiO ₂	0.14	0.12	0.47	0.53	TiO ₂	0.69	0.60	0.56	0.60
Al ₂ O ₃	36.35	36.34	35.79	35.44	Al ₂ O ₃	52.89	53.25	54.49	52.98
FeO	1.05	1.08	1.35	1.65	FeO	12.67	12.99	12.25	12.66
MgO	0.54	0.57	0.50	0.51	MnO	0.08	0.04	0.03	0.07
CaO	0.00	0.02	0.02	0.03	MgO	1.86	1.64	1.81	1.78
Na ₂ O	1.52	1.53	1.38	1.24	ZnO	0.58	0.58	0.73	0.74
K ₂ O	8.85	8.85	8.60	8.97					
Σ	94.94	94.87	95.17	95.35	Σ	96.18	96.52	97.14	96.16
Cations / 22 anhydrous oxygens					Cations / 46 anhydrous oxygens				
Si	6.151	6.141	6.205	6.206	Si	7.672	7.706	7.591	7.708
Ti	0.013	0.011	0.046	0.052	Ti	0.146	0.126	0.117	0.127
Al	5.670	5.675	5.563	5.519	Al	17.627	17.642	17.882	17.616
Fe	0.116	0.119	0.148	0.182	Fe	2.995	3.053	2.851	2.986
Mg	0.106	0.112	0.098	0.100	Mn	0.019	0.009	0.007	0.016
Ca	0.000	0.002	0.002	0.004	Mg	0.783	0.686	0.750	0.748
Na	0.389	0.393	0.352	0.317	Zn	0.121	0.121	0.150	0.154
K	1.493	1.495	1.446	1.511					

Table 3. Metamorphic recrystallisation temperatures of representative Malé Karpaty Tatric basement paragneisses.*

Sample			ln K _D	T	F&S	N&H	G&S
KB-	17	c	1.701	570	587	602	610
		r	1.797	545	551	566	568
KB-	02	c	1.491	628	666	687	648
		r	1.626	589	610	626	610
KB-	03	c	1.610	594	619	641	639
		r	1.813	541	546	568	587
KB-	05	c	1.675	577	596	619	614
		r	1.764	553	562	579	580

* Using equilibrium calibrations of: T - Thompson (1976); F & S - Ferry a Spear (1978); N & H - Newton a Haselton (1981); G & S - Ganguly a Saxena (1984).

c - culmination temperatures of metamorphic recrystallization.
r - retrograde closure temperatures.

Geothermometric data based on the garnet rims and adjacent coexisting biotite at multiple mutual junctions approximate the retrograde closure temperature. Garnet cores and matrix biotites yielded an higher temperature related to a metamorphic thermal culmination. In metapelitic rocks with high biotite/garnet modal ratio the post culmination Fe-Mg mass balance reactions slightly change the biotite peak composition (Crowley, 1991).

Different sets of calibrated mineral equilibria were used to infer the P-T data of metamorphic thermal culmination and retrograde closing conditions to determine the position of the rock sample in the P-T coordinates (Tab. 3., 4., 5.). The accurate position of the sample in the P-T space may be uncertain, still within the limits of 2σ, but this is of lesser importance if regional metamorphic and tectonic interpretation of the obtained data are taken into consideration.

The lowest variance mineral assemblages of the studied paragneisses include St, Bt, Grt, Ms, Pl, Ilm, Sil, Qtz. The metamorphic whole rock reaction among these min-

erals is represented formally by a system of linear equations for components chosen. This algebraic approach may include all components and simultaneously exclude degenerative composition relations among minerals in the assemblage. Each composition balance for given component in the assemblage is defined as

$$A_i = v_1 X_{1i} + v_2 X_{2i} + v_3 X_{3i} + \dots + v_n X_{ni} \quad (1)$$

where v - is the stoichiometric coefficient, X_i - element concentration in the mineral and A_i - is the concentration of the same element in the reference mineral. The linear equation e.g. for Si and Al in the simplified metapelitic KMFASH system in the assemblage Chl+Ms+Grt+Bt+Qtz is then expressed:

$$0 = v_{\text{Chl}} \text{Si}_{\text{Chl}} + v_{\text{Ms}} \text{Si}_{\text{Ms}} + v_{\text{Qtz}} \text{Si}_{\text{Qtz}} + v_{\text{Grt}} \text{Si}_{\text{Grt}} + v_{\text{Bt}} \text{Si}_{\text{Bt}} \quad (2)$$

$$0 = v_{\text{Chl}} \text{Al}_{\text{Chl}} + v_{\text{Ms}} \text{Al}_{\text{Ms}} + v_{\text{Qtz}} \text{Al}_{\text{Qtz}} + v_{\text{Grt}} \text{Al}_{\text{Grt}} + v_{\text{Bt}} \text{Al}_{\text{Bt}} \quad (3)$$

The formulated set of chemical composition of minerals participating in particular metamorphic reaction thus divides and quantifies the minerals of the assemblage on the reaction reactants and products. Critical importance still has the appearance of equilibrium rock structure.

The mineral abundance in paragneisses (Tab.1.) and their compositions (Tab.2.) can thus be arranged in numerical form to express the whole rock metamorphic reactions. Reaction stoichiometry gives consequently a P-T vector determining the slope $dP/dT = \Delta S/\Delta V$ of the culmination reaction paths A1, B1 and specifies the reaction slopes of closing retrograde exchange processes as the reactions A2, B2 in the studied samples (Tab. 6.).

KB-5. Core

$$1 \text{ St} + 0.263 \text{ Ms} + 0.970 \text{ Pl} + 1.730 \text{ Qtz} = 8.135 \text{ Sil} + 1.398 \text{ Grt} + 0.223 \text{ Bt} + 0.156 \text{ Ilm} + 1.765 \text{ H}_2\text{O}$$

reaction path - slope $dP/dT = 121.7 \text{ bar/K}$. (A1)

Table 4. Metamorphic recrystallisation pressures of representative Malé Karpaty basement paragneisses.*

Sample		aAn	aGr	G	G&S	H&C	N&H	P&H	P&H ^P
KB -	17c	0.3298	0.0412	4.8	4.1	4.7	4.4	5.3	4.8
	r	0.4107	0.0411	3.6	3.6	3.8	3.1	4.1	4.0
KB -	2c	0.4083	0.0557	6.0			5.9	5.9	5.9
	r	0.5053	0.0449	3.8			3.3	4.2	3.7
KB -	3c	0.4142	0.0574	5.7			5.3	6.1	5.7
	r	0.4806	0.0604	4.6			3.8	4.9	4.4
KB -	5c	0.3920	0.0625	5.9	5.1	5.7	5.5	6.4	5.2
	r	0.4458	0.0476	4.0	4.0	4.2	3.4	4.4	4.1

* Using equilibrium pressure calibrations of: G - Ghent et al. (1979), G&S - Ghent & Stout (1981), H&C - Hodges & Crowley (1985), N&H - Newton & Haselton (1981), P&H - Powell & Holland (1988), P&H^P - THERMOCALC, Powell & Holland (1988, 1998). Activity of anorthite (aAn) and grossular (aGr) is based on formulation of Newton & Haselton (1981).

c - pressures of metamorphic recrystallisation at thermal maximum, r - pressures at retrograde temperature minimum.

Table 5. Composition and pressure characteristics of representative paragneisses in the Bratislava granitoidic massif area based on the calibration of Hoisch (1990, 1991).*

Composition characteristics:									
Sample			lnK _{D1}	lnK _{D2}	lnK _{D3}	lnK _{D4}	lnK _{D5}	lnK _{D6}	ΔV(J/bar)
KB	17	c	5.3558	3.6983	4.1446	0.8392	9.9161	4.9437	-0.2790
		r	5.7870	4.0361	4.6026	1.0438	10.676	5.4237	-0.2812
KB	05	c	4.5859	2.9750	3.4652	0.5296	8.8068	3.9774	-0.1696
		r	5.5383	3.8270	4.4224	0.9816	10.322	5.1887	-0.2569
Pressure characteristics P(bar):									
Sample			P1	P2	P3	P4	P5	P6	K&N**
KB-	17	c	4784	4754	4519	4830	4724	4631	4917
		r	3800	3762	3633	3988	3687	3601	3621
KB-	05	c	5821	5725	5653	5659	6044	5831	6164

R₁ 1/3 Pyrope + 2/3 Grossular + Eastonite + 2 Quartz = 2 Anorthite + Phlogopite

R₂ 1/3 Almandine + 2/3 Grossular + Siderophyllite + 2 Quartz = 2 Anorthite + Annite

R₃ 1/3 Pyrope + 2/3 Grossular + Muscovite + 2 Quartz = 2 Anorthite + MgAlCeladonite

R₄ 1/3 Phlogopite + 1/3 Grossular + 2/3 Muscovite + 2 Quartz = Anorthite + MgAlCeladonite

R₅ Pyrope + Grossular + Muscovite = 3 Anorthite + Phlogopite

R₆ Almandine + Grossular + Muscovite = 3 Anorthite + Annite

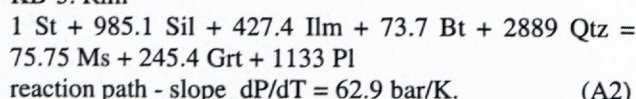
K&N** comparison calibration according to Koziol & Newton (1988).

Table 6. Entropies S_T ($J K^{-1} mol^{-1}$) and volumes V_M ($cm^3 mol^{-1}$) of coexisting phases at metamorphic peak culmination and closing retrograde temperatures and pressures used for metamorphic reaction P-T slopes calculations*.

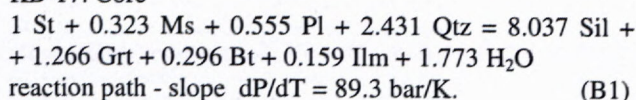
Sample	KB - 5.				KB - 17.			
	S_{601}	S_{568}	V_M^C	V_M^R	S_{592}	S_{557}	V_M^C	V_M^R
Plagioclase	489.07	482.88	100.23	100.24	492.21	478.53	101.21	100.23
Biotite	877.69	862.84	151.86	152.17	875.94	816.03	152.86	151.91
Muscovite	740.38	722.60	138.98	139.31	740.26	715.87	138.88	137.95
Staurolite	2816.46	2745.51	447.17	447.74	2796.13	2719.98	447.19	447.74
Garnet	816.32	797.07	115.92	115.65	813.98	786.20	115.85	114.98
Ilmenite	228.13	223.03	31.68	31.69	226.75	221.27	31.68	31.69
Sillimanite	269.09	261.89	49.86	49.86	267.12	259.44	49.86	49.86
Quartz	106.09	103.23	22.68	22.69	105.33	102.26	22.69	22.69
H ₂ O	227.41	-	21.45		227.01	-	22.66	

*Entropy and volume of the particular phase has been calculated according to Spear & Rumble (1986). Molar volume of the solid solution phase is given by the expression $V_M = \sum x_i V_i$, where x_i is the mole fraction of the i-th component and V_i is its molar volume. Entropy of mineral solid solution at given temperature is expressed as $S_M^T = \sum x_i S_i - n R \sum x_i \ln x_i$, where n is the site multiplicity. For plagioclase series albite and anorthite have been considered as the solid solution end members, for biotites - phlogopite and annite, muscovites - muscovite and paragonite, staurolite - MgStaurolite and FeStaurolite, garnets - almandine, spessartine, pyrope and grossular. The internally consistent thermodynamic database of Holland - Powell (1998) has been used

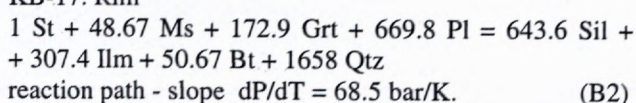
KB-5. Rim



KB-17. Core



KB-17. Rim



Generally considered, rock decompression accompanied with heating gives a stoichiometric reaction with negative reaction slope and decompression during cooling is characterised by a positive one. The changes in modal abundance and textural features of mineral growth or reactant consumption along this P-T vector determine the reaction extent as well (Fig.3.). Different reaction rock stoichiometry thus permits numerical solution for rock cooling along different reaction path on the post culmination metamorphic trajectories. The calculated reaction stoichiometry compared with microscopic study of the samples thus assures the resemblance to the calculated whole rock reaction that actually run in the rock. Both petrological approaches are consistent in the studied assemblages and the constraints are placed on the calculated P-T path (Fig.4.).

Processes that effect modal changes and element distribution among minerals are strictly path dependent and reflect P-T conditions along the reaction path. The dehydration maximum of rock thus coincides with temperature culmination of rock P-T trajectory and the equilibrium forming peak metamorphic assemblage (Fig.5.).

However, different bulk rock composition of the studied rocks (Tab.1.) attributes different reaction extent of these changes during each rock reaction P-T history and thus the changes in the modal proportions of minerals with respect to growth or consumption specify each rock trajectory.

The studied garnets are the products of growth during metamorphic culmination whole rock reaction and existing zoning is the product of diffusional processes after progressive metamorphic reactions ceased. Thus, the present garnet rim composition is assumed to reflect diffusional equilibrium adjustment during postculmination retrograde cooling of a particular metamorphic rock.

The calculated steep slopes of the whole rock reactions are consistent with their dehydration nature and water quantity released. The difference in entropy between structurally bound H_2O and H_2O in fluid phase is considerably large and thus the the reaction paths A1 and B1 are quasi vertical ($dP / dT = 121 \text{ bar/K}$ and 89 bar/K respectively).

These staurolite decomposition reactions and the rock mikrostructure confirm the progressive growth of Grt, Sil in the assemblages (Fig. 2.) and thus form the important

feature in the interpretation of the post culmination trajectory. Careful examination of garnet did not prove any important inclusions as they have been homogenised during culmination metamorphic process and existing chemical zonation is clearly related to diffusional processes that have occurred during retrogression. Thus the phase relations of the assemblages examined give reliable constraints on the culmination conditions and retrograde P-T path (Fig. 4.).

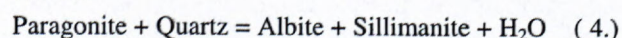
Calculated approximative P-T trajectories, in the range of 570-650 °C and 3.5-6.1 Kbar, express the first order tectonic motion and represent specific uplift conditions of the particular tectonic blocks. Some of the samples express uplift trajectories determined dominantly by decompression during cooling while the others may present more isothermal, probably rapid decompression during tectonically driven uplift period. The P-T data and the reaction paths are in accordance with index mineral appearances and mineral equilibrium domains. No occurrence of significant retrograde mineral domains and the microscopic appearance of garnets all confirm the individuality of these basement tectonic blocks.

Data for retrograde uplift trajectories (Tab. 3., 4., 5.) indicate an culmination period of higher temperature and medium pressure metamorphic conditions culminating in garnet sillimanite bearing assemblages. These trajectories are consistent with regional metamorphic environment and it is to note that the rock assemblages show differences in P-T conditions attained.

The maximum pressure experienced by the rocks implies that the overburden immediately following the metamorphic culmination stage was of the order of 16 - 20 km. Intrusion of the granodioritic rocks during metamorphic culmination and later might have heated the rocks to different temperatures because of their different ambient geological positions.

It is worth emphasising that not all rock samples collected in the terrane reveal the same P-T histories and confirm exceedingly complex geological development of the area. It is clear from differences in maximum pressures experienced by the rocks that they could not all have been adjacent throughout their metamorphic histories.

Trajectories form loops (Fig.4.) in which the early pressure increase is followed by decrease in pressure at slightly decreasing temperature. Calculated petrogenetic grids (Fig. 6.) determine the sequence of mineral reactions that occurred in the studied bulk rock compositions along the assessed P-T path. The calculations in the simplified KMFASH metapelitic system was based on the fluid composition $X_{\text{H}_2\text{O}} = 1$. For calculation of metamorphic culmination fluid composition ($X_{\text{H}_2\text{O}}$) the equilibrium reaction



with thermodynamic data of Ferry (1980) and paragonite activity formulation from Eugster et al., (1972) has been used. Thus the composition of metamorphic fluid produced by the reactions A1 and B1 during culmination conditions approaches $X_{\text{H}_2\text{O}} \approx 1$ (see Tab. 7.).

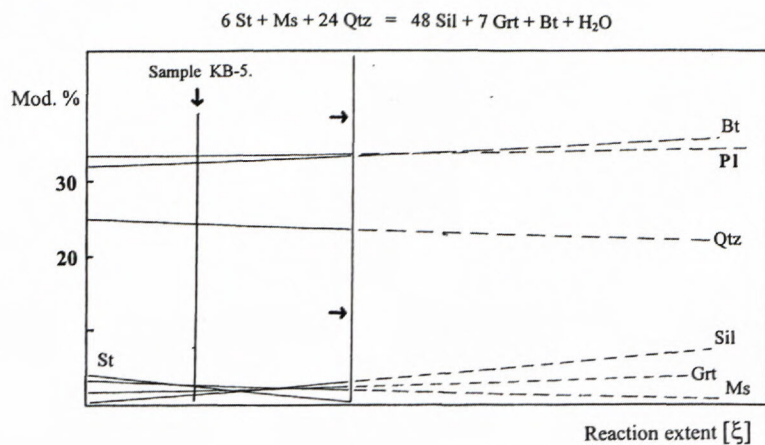


Fig. 3. The calculated changes in the modal proportions of phases with progressive metamorphic reaction path in the low variance assemblage $\text{St} + \text{Grt} + \text{Sil} + \text{Bt} + \text{Ms} + \text{Qtz}$ (sample KB-5). With the reaction progress the proportion of garnet and sillimanite increase at the expense of $\text{St} + \text{Ms} + \text{Qtz}$. The reaction A1 as presented has not been completed as the consumed reactants (St, Ms) remain present in the assemblage during the expected linear decrease in abundance in sample. As the reaction A1 has the steep slope it is more determined by temperature than by pressure and the implication is that St consumption in observed assemblage has not been completed as the consequence of temperature decrease during cooling and uplift. Later, the proportion of reactants and products remain practically constant and mineral rim compositions have been modified by diffusional processes.

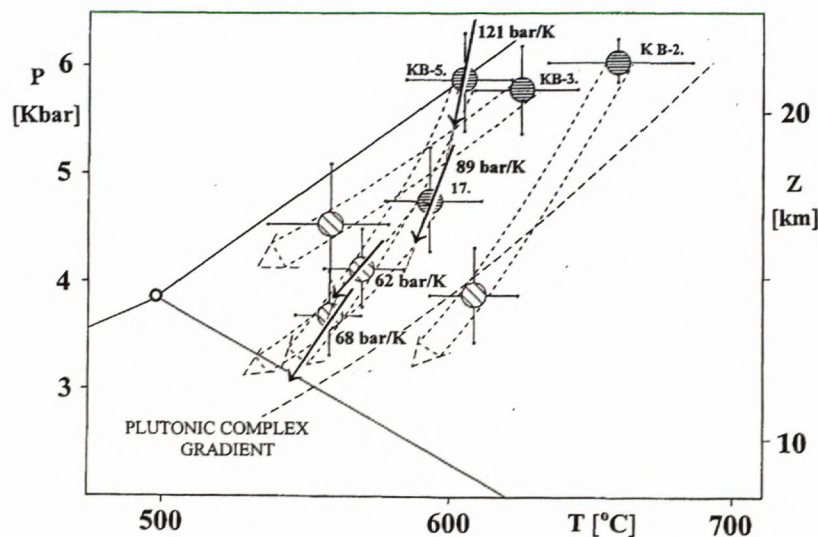


Fig. 4. The calculated metamorphic culmination and closing retrograde P-T characteristics of metamorphic recrystallization calculated from Grt-Bt-Ms-Plg-Sil-Qtz mineral equilibria. The whole rock culmination reaction paths are steep with high dP/dT values (121 bar/K and 89 bar/K for samples KB-5. and 17. Respectively). The post culmination exchange processes near the closing retrograde temperatures have the slopes determined by decompression cooling (see the reactions A2, B2). Temperature data were obtained on the basis of Grt-Bt calibrated equilibria (Ferry & Spear, 1978; Thompson, 1976; Newton & Haselton, 1981; Ganguly & Saxena, 1984; Hodges & Crowley, 1985). Pressure was calculated from calibrated equilibria Grt-Plg-Sil-Qtz (Ghent et al., 1979; Powell & Holland, 1988; Newton & Haselton, 1981) and equilibria including Grt-Bt-Ms-Plg-Qtz (Hoisch, 1990).

The calculated culmination temperatures are considered to produce the equilibrium mineral assemblage with uniform Fe-Mg distribution among the coexisting phases.

The compositional change in the profile of garnet at the biotite-garnet couple interface served as a primary source of data for petrological cooling rate estimates. As the post culmination cooling starts, the equilibrium conditions change with decreasing temperature and drives the diffusion exchange of mobile components at the grain interface boundaries. The diffusion process continue till the retrograde closure temperature froze in the compositional changes in garnet realised during cooling. The diffusion garnet profiles were then normalised for Mg concentrations as a function of normalised distance from the Bt-Grt edge to obtain the shape of the garnet compositional profile. Diffusion formalism and equations of Lasaga et al., (1977) and Lasaga (1983) served as the methodical tool and computation basis for petrological cooling rates estimates (Tab. 8.). However, for reliable and consisting cooling rate approximation more than 3-5 garnet compositional profiles have to be studied in a sample and more accuratete acti-

vation energy (ΔE^*) data are needed for calculation of accurate petrological cooling rate data for the paragneisses of the studied geological area.

Discussion

Most of the mountain belts of the world are believed to be the result of continental collision (Bird & Dewey, 1970). The first thermal model of continental collision was published by Oxburgh & Turcotte (1974) with respect to the Tauern Window in the Eastern Alps. Its metamorphic P-T evolution inferred from thermobarometry and fluid inclusions has been calculated by Selverstone et al., (1984), Selverstone (1985), Selverstone & Spear (1985), Spear & Franz (1986).

The retrograde P-T path is easier to obtain than the prograde path and thus most is known about the cooling histories of concrete terranes. However, in order to distinguish between different tectonic scenarios more information on the prograde portion of the path is required. Then the P-T path can place constraints on the depth and thermal conditions during fault movement or may even provide clues as to the existence of a fault where field evidence is ambiguous.

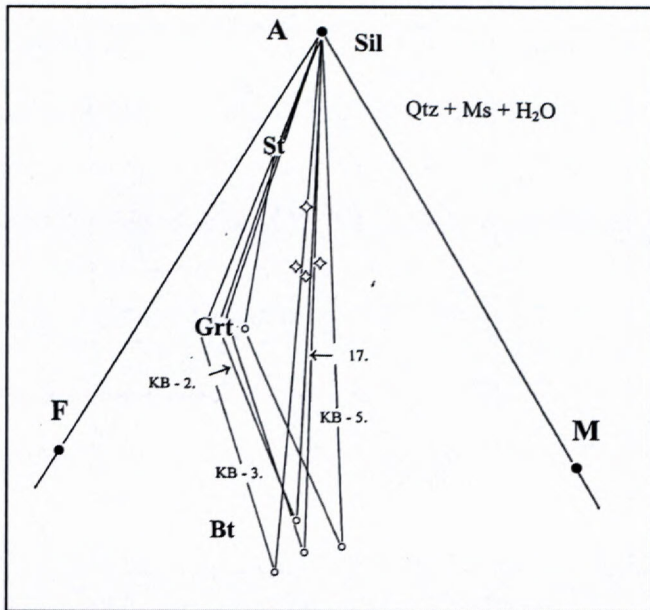


Fig. 5. Schematic AFM diagram representing studied mineral compositions and compatibility of phase relations. The bulk rock compositions (\diamond) are also presented. The sequence of the mineral assemblages depends on P-T trajectory and chemical composition of rock. Staurolite decomposition $St \rightarrow Sil + Grt + Bt$ in the studied assemblages (including $Qtz + Ms + H_2O$) is consistent with the whole rock reaction path and the mass balance of coexisting AFM minerals in rocks (see reaction A1, B1). Thus sillimanite appears, staurolite is consumed, and kyanite may eventually disappear during the reaction changes. The stability field of cordierite at calculated P-T conditions has been ignored. Formulas of Thompson (1957) have been used for the calculating and plotting the positions of minerals on the diagram: $A=Al_2O_3-3K_2O$, $F=FeO$, $M=MgO$.

The Alpine type P-T path is characterized by nearly isothermal decompression, which can only be caused by rapid exhumation and is generally thought to be caused by either tectonic unroofing such as occurs in the extensional terranes or by very rapid erosion (Ernst, 1973, 1988). Ernst cit. attributes the cause of rapid exhumation to the shift from the subduction of crust to the collision. Tectonic changes caused by continental collision result in rapid uplift of the higher pressure rocks and denudation by erosion or tectonically. The thermal relaxation may cause only minor heating that is frequently followed by rock cooling. The extension dynamics allows the underplated rocks to rise eventually to the earth surface where they are currently exposed. The time scale for the exhumation of higher graded metamorphic rocks is on the order of 10 - 15 Ma (Ernst, 1988).

Isothermal decompression paths are most likely produced by tectonic thickening of the crust followed by exhumation dominated by either erosion or tectonic denudation (England & Richardson, 1977; England & Thompson, 1984). Tectonic denudation will produce a steeper decompression path than erosion alone and Anovitz & Chase (1990) argue that some type of tectonic denudation is required to explain the shapes of isothermal decompression P-T paths.

Isobaric cooling paths (IBC) are more difficult to interpret unless some portion of the prograde P-T path can be deduced. IBC paths may arise from counterclockwise P-T loops as has been suggested by Bohlen (1987). In this interpretation the heat source for the early low pressure, high temperature part of the path is assumed to be magma accretion beneath existing crust.

Magma accretion at the base of the crust will produce an elevated geotherm and subsequent thermal relaxation will cause a long period of isobaric cooling. Continual thickening and rapid exhumation may give rise to isothermal decompression paths for rocks of the upper crustal block.

P-T characteristics of culmination recrystallisation of the M.K. basement paragneisses have been determined earlier (Dyda, 1977, 1980a,b; Pertchuk et al., 1984; Dyda and Miklós, 1993).

Korikovskii et al., 1984 present for the whole M.K. metamorphic region the pre culmination trend as isobaric heating recrystallisation process characterized by pressures ca. 3.3 Kbar and temperatures extent of ca. 350-550 °C. These trends are fully accepted by Krist et al., (1992). Thus the isobaric heating presupposed by these authors runs in progressive pre culmination metamorphic stages in the And stability field and the P-T trends would be typical of contact metamorphic terrane where crust has had considerable heat added by the addition of magmas. Isobaric heating might have been confirmed by garnet zonality development, reaction sequences and reaction slopes in equilibrium assemblages. Anyhow, the crucial contact metamorphic assemblages with And + Crd are missing in the Bratislava massive area studied by the author. Thus, the paths might have started out at similar conditions and end at nearly the same temperature, but followed different trajectories in essentially different metamorphic thermal regime.

The metamorphic trajectories, presented here, represent "clockwise" post culmination decompression cooling (Fig. 4.), that is typical of regions that have undergone crustal thickening followed by thermal relaxation and are principally different from isobaric heating trajectories. The early part of the trajectory is a heating phase through the kyanite stability field and is interpreted to result from regional metamorphism. The pressure peak was followed by slightly heating period and decompression cooling. As there is no reheating or significant retrogression signs the major Variscan orogeny is believed to have been caused by collision of the continental fragments. The differences in peak temperatures, pressures and cooling might show approximate position of the units along P-T at various stages of convergence followed by thermal relaxation and are not considered to represent some major fundamental differences in the tectonic setting.

A significant difference between low pressure paragneisses and studied intermediate pressure parageneses is that at low pressures, the composition of minerals are closer to the Fe-end members in the KMFASH system and increasing temperature results in the assemblage with andalusite + cordierite. If the sillimanite precursor in low pressure

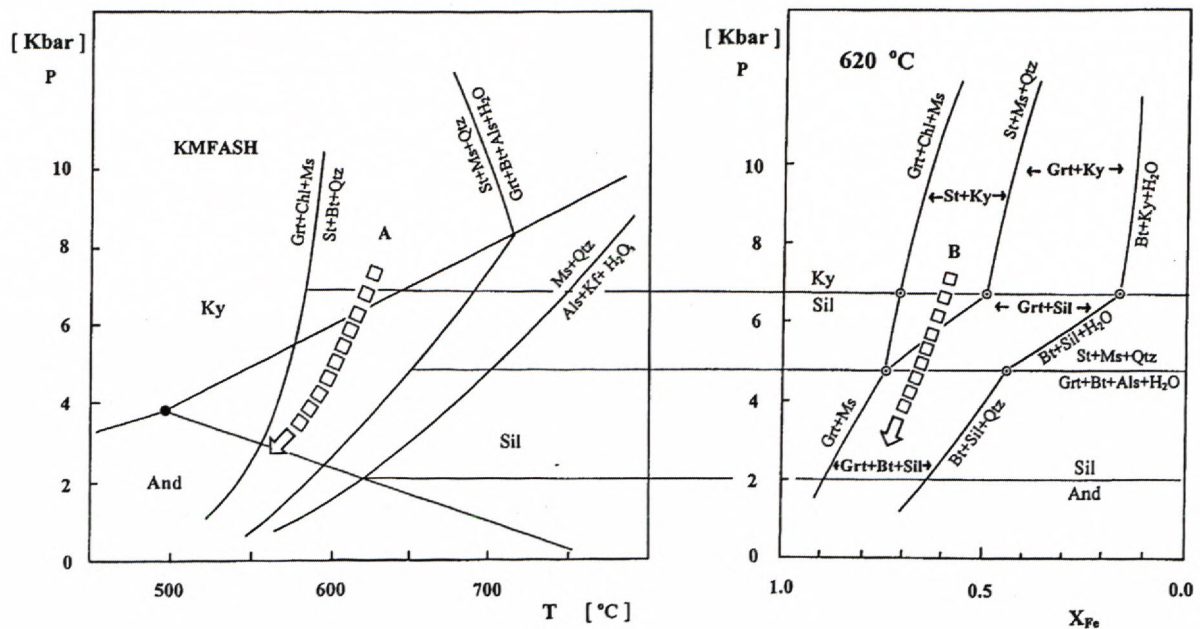


Fig. 6. Isothermal pseudobinary P - X_{Fe} section at culmination temperatures (~ 620 °C) presenting divariant reaction fields and phase relations among St - $Grts$ - Sil - Bt - Ms - Qtz - H_2O in the simplified matapelitic KMFASH model system. X_{Fe} for the studied rocks is taken from the Tab. 1., X_{H_2O} is taken to be 1 (see Tab. 7.). Path A is the generalised decompression trajectory during cooling of the crystalline complex obtained on the basis of the geothermobarometric data and the higher pressure kyanite rests present. Path B expresses decompression intersection of the reaction boundary $St+Ms+Qtz = Sil+Grt+Bt+H_2O$ consistent with the microscopic texture and the whole rock reaction path based on the thermal culmination mass balance.

Table 7. Fugacity (f , bars) and the mole fraction of water (X_{H_2O}) in metamorphic fluid at the culmination conditions calculated from the equilibrium $Par + Qtz = Ab + Sil + H_2O^*$.

Sample	X_{Ab}	X_{Pa}	γ_{Pa}	f_{H_2O}	X_{H_2O}
17.	0.787	0.286	3.797	2309	0.96
KB-5.	0.755	0.196	4.789	3734	0.98

*Thermodynamic formulation of the reaction is according to Ferry (1980): $\Delta H_R^\circ = 91190$ J, $\Delta S_R^\circ = 169.12$ J K $^{-1}$, $\Delta V_S = -0.447$ J bar $^{-1}$. X_{Ab} - mole fraction of albite in plagioclase; γ_{Pa} - activity coefficient for paragonite.

mineral assemblages was andalusite \pm cordierite, the recrystallisation obviously produces crystals of sillimanite and corresponding mineral changes over ca. 550 °C lead to stable, final peak low pressure contact matapelitic assemblage $Sil+Crd+Bt+Ms\pm Grt+Qtz$. Sillimanite present in the studied samples has, however, the appearance of fibrolitic form that is frequently, typically encountered on the regional metamorphic trajectories where mineral transformations kyanite \rightarrow sillimanite occur.

Although there is some scatter in the studied P - T paths, most of the paths show simultaneous decompression and cooling, consistent with the P - T data, whole rock reaction paths their slopes and the reaction sequence.

The regional cooling and exhumation processes depend on the trajectory shape expressing the tectonometamorphic evolution recorded by reaction paths and geothermobarometry. The regional metamorphism in the area has been documented (Dyda, 1997) by slow rate of nucleation $2.9 \cdot 10^{-8}$ cm 3 /s - $1.0 \cdot 10^{-7}$ cm 3 /s, the reaction

Table 8. Petrological cooling rate estimates for Malé Karpaty Tatric basement paragneisses.

Sample	17.	KB-2.	KB-3.	KB-5.
T [°C]	592 \pm 17	657 \pm 25	623 \pm 21	601 \pm 19
P [Kbar]	4.66 \pm 0.45	5.90 \pm 0.05	5.70 \pm 0.41	5.82 \pm 0.41
r [mm]	0.604	0.366	0.384	0.359
Diffusion coefficient [cm 2 /s] *				
$D_T(Ch\&G)$	$9.99 \cdot 10^{-21}$	$1.48 \cdot 10^{-19}$	$3.87 \cdot 10^{-20}$	$1.55 \cdot 10^{-20}$
$D_T(F)$	$1.00 \cdot 10^{-20}$	$2.84 \cdot 10^{-19}$	$5.24 \cdot 10^{-20}$	$1.64 \cdot 10^{-20}$
$D_T(E)$	$2.30 \cdot 10^{-19}$	$2.04 \cdot 10^{-18}$	$6.78 \cdot 10^{-19}$	$3.18 \cdot 10^{-19}$
$D_T(L)$	$5.49 \cdot 10^{-20}$	$9.48 \cdot 10^{-19}$	$2.55 \cdot 10^{-19}$	$8.35 \cdot 10^{-20}$
γ'	279	24	33	26
Cooling rate [°C/Ma]				
S (Ch&G)**	4.07	1.86	2.66	0.22
S (F)	4.01	3.56	3.61	0.24
S (E)	94.03	25.62	46.71	4.69
S (L)	22.39	11.89	15.48	1.23

* calculated for metamorphic culmination P - T conditions using pre-exponential factor D_0 and activation energy for diffusion ΔE^* according to **Ch&G - Chakraborty & Ganguly (1992), F - Freer (1981), E - Elphic et al., (1985), L - Lasaga (1977). Cooling rate [S] has been calculated according to formula of Lasaga (1983), $S = RT^2 \gamma' / \Delta E^* a^2$. γ' is given by the shape of the measured composition profile and a is the garnet size.

temperature overstep of ca. 0.15 °C/y and the modeled progressive heating rate trends of $4 \cdot 10^{-5}$ °C/y, they are in good agreement with the characteristics of the regional metamorphic thermal regime (see e.g. Thompson & England, 1984 for comparison).

Fig. 7. The calculated cooling rate (S , $^{\circ}\text{C}/\text{Ma}$) and the extent of garnet mass transfer ("X") in the mineral assemblages of basement paragneisses express the mutual relation between these petrological characteristics when rapid cooling enables only limited mass transfer and lasted residence of rock at higher postculmination temperatures favours assemblage ripening and diffusion adjustment processes.

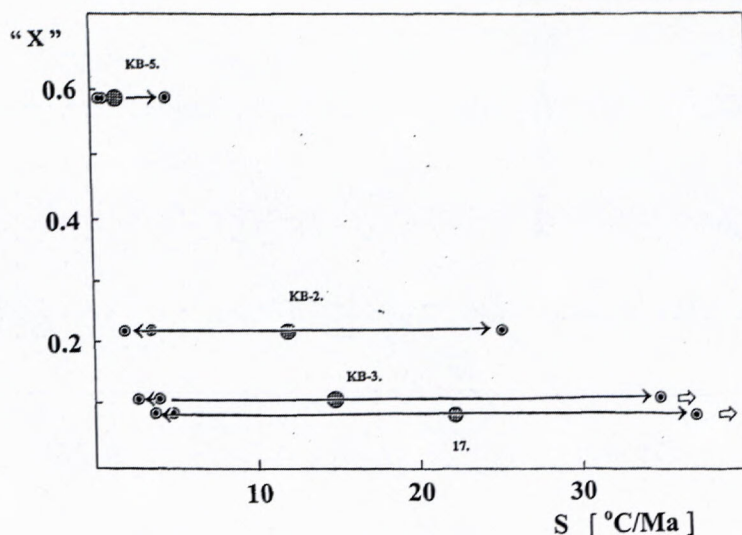
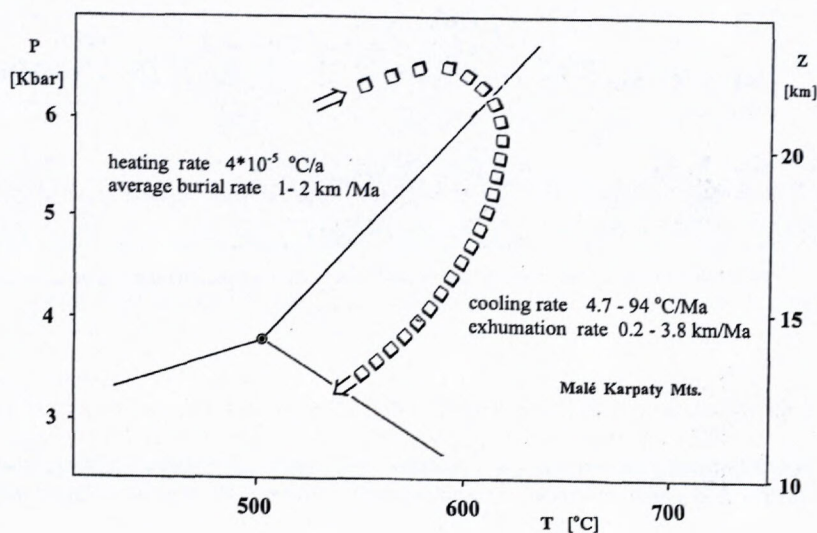


Fig. 8. Approximative time characteristics for Bratislava massive Tatric basement metamorphic trajectories inferred from petrological data. Average heating rate of the regional metamorphic complex ($4 \cdot 10^{-5} \text{ }^{\circ}\text{C}/\text{a}$) was determined on the basis of garnet crystal size distribution and is consistent muscovite dehydration time (unpublished data). In linear approximation, after anchimetamorphic zone crossing (ca. $150\text{-}200 \text{ }^{\circ}\text{C}$) time of ca. 11 Ma is needed for metamorphic complex to reach thermal culmination $\sim 600 \text{ }^{\circ}\text{C}$ in depth of $\sim 24 \text{ km}$. In this numerical approximation, average burial rate $\sim 1\text{-}2 \text{ km}/\text{Ma}$ may be considered. The cooling rates calculated on the basis of diffusional zoning in garnets and Elphic et al., (1985) experimental data are in the range of $4.7\text{-}94 \text{ }^{\circ}\text{C}/\text{Ma}$. The exhumation rate of the Tatric basement complex is then consequently ca. $0.2\text{-}3.8 \text{ km}/\text{Ma}$.



The regional recrystallisation products are usually subjected to prolonged cooling after thermal culmination ceased and processes of the assemblage ripening and diffusion adjustment operate. The diffusion processes and the annealing mass transfer are temperature and time dependent mineral changes. The calculated values of the post culmination garnet mass transfer ($X = 0.10\text{-}0.53$) are in particular samples significantly different documenting different annealing processes that lasted after the thermal culmination was attained and completed (Dyda, 1997).

Morphological appearance of idioblastic garnets with steep, narrow retrograde diffusion rims clearly testify rapid cooling during uplift. The apparently quenched mineral assemblages of particular tectonic blocks differ from the other assemblages which exhibit significantly higher garnet mass transfer estimates and different cooling history.

The tectonic reconstruction may partially use the estimates of crustal overburden that is inferred from computed changes in pressure. When these P-T data are combined with other petrological inferences including

post culmination garnet mass transfer and approximated petrological cooling rates (Fig. 7.), the observed P-T paths can then be useful for constraining tectonic differences in transport rates as well as of exhumation.

The duration of metamorphic event may be considerably long, estimates are well in excess of 100 Ma inferred on the basis of cooling rates of $1 \text{ }^{\circ}\text{C}/\text{Ma}$. As many minerals crystallize at prograde, others at culmination temperature and some at retrograde stages, the determination of equilibrium in particular thin sections may be complicated. Certain minerals have refractory nature and do not equilibrate easily during cooling (Sharp and Ulmer, 1993) and peak conditions may be assessed in carefully selected rocks.

In first numerical approximation, the petrological subduction estimates have been based on calculated peak temperature, depth and heating rate data ($4 \cdot 10^{-5} \text{ }^{\circ}\text{C}/\text{a}$) that provide corresponding average burial rate value of $1\text{-}2 \text{ km}/\text{Ma}$ for the studied basement paragneisses (Fig. 8.). The petrological cooling rate data obtained on the basis of evaluation of the diffusional zonality development in gar-

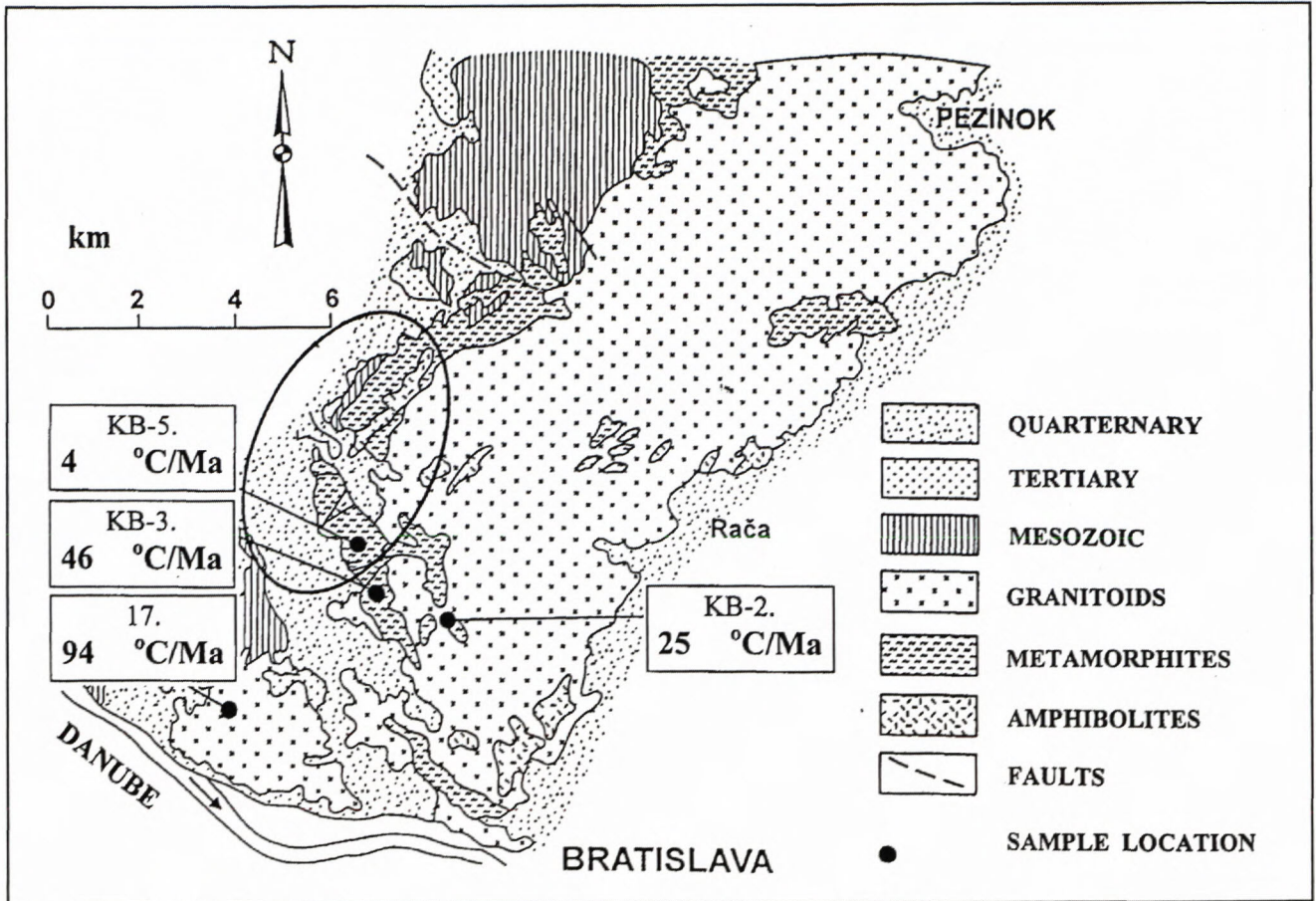


Fig. 9. Petrological cooling rate estimates S ($^{\circ}\text{C}/\text{Ma}$) for the Tatric basement paragneisses present considerable differences. This scattering is petrologically confirmed by differences in post culmination garnet mass transfer when quenched metamorphic assemblages exhibit minimum transfer changes. The S data are considered to represent the individuality of post culmination cooling development and fragmentation of the Tatric basement into Variscan tectonic blocks. For cooling rate calculation the diffusional parameter D_0 and activation energy for garnet diffusion ΔE^* have the crucial importance. However, more unifying, reliable diffusional characteristics are still missing and thus for cooling rates comparison the calculated S values of Elphic et al., (1985) are shown as they probably represent the most realistic cooling rate scenario in the Malé Karpaty Variscan basement. The geological area circled has been earlier subjected to the detailed periplutonic author's studies.

nets (Tab. 8.) may assess the approximate exhumation rate at 0.2 - 3.8 km/Ma for the Tatric metapelitic basement rocks.

Different diffusion zonality development and calculated post culmination cooling rates clearly document that the basement rocks stayed different period of time under thermal culmination conditions. The data presented (Tab. 8, Fig. 8, Fig. 9) form thus the first comparison basis for petrological heating and cooling rates in the Western Carpatian region.

The scattering of " S " data is partly caused by accepting cited D_0 and ΔE^* of different authors. This lead after computation consequently to scattered diffusion coefficients and cooling rates estimates.

From Spanish Betic metamorphic terranes minimum cooling rates of 200 $^{\circ}\text{C}/\text{Ma}$ are reported and uplift rates of 2 - 5 km/Ma have been given (Zeck et al., 1989). For the same geological area Monié et al., (1994) report cooling rates of 150-350 $^{\circ}\text{C}/\text{Ma}$ and corresponding exhumation rates of 5-10 km/Ma. For Tauern Window the exhumation rate varied from >5 km/Ma to <1 km/Ma (Clif et al., 1985). Exhumation and cooling rate of Dora Maira ter-

rane are 22 km/Ma and ca. 90 $^{\circ}\text{C}/\text{Ma}$ respectively (Gebauer, 1996).

Detailed cooling rate data for Buckskin-Rawhide metamorphic core complex (Scott et al., 1998) however reveal non-linear cooling process, as cooling rate of these rocks increased progressively, peaking at 280 $^{\circ}\text{C}/\text{Ma}$ documenting tectonically driven abrupt increase in cooling rates. This implies that cooling did not keep pace with denudation at upper crustal levels where high cooling rates primarily reflect the development of thermal discontinuity across the detachment fault.

The above methodical approach illustrates the types of different petrologic information that may be utilized in deciphering the evaluation of complex metamorphic terranes and their tectonic development.

Conclusions

The Variscan regional metamorphic processes in Malé Karpaty Tatric basement rocks attained conditions of amphibolite facies with temperatures of ~ 570 - 620 $^{\circ}\text{C}$

(Tab.3.) and pressure span ~ 4.5-6.1 Kbar (Tab. 4.5.). The culmination conditions in particular tectonic blocks represent different P-T data, metamorphic reaction extent and postculmination uplift characteristics expressed by mass transfer, diffusion zonality development and different cooling rates of particular rock blocks.

The culmination mineral assemblages (Tab.1.), index mineral appearance, sequence and extent of discontinuous metamorphic reactions (Fig.3.) and metamorphic fluid composition (Tab.7.) are consistent with the metapelitic KMFASH model system (Fig. 5, Fig. 6.) and the calculated geothermobarometric data.

The culmination temperatures, pressures, whole rock reaction paths and uplift trajectories of particular crystalline blocks (Fig. 4.) represent complex differences of Variscan tectonothermal activity in the Variscan basement. The crustal level conditions of intrusive magmatism may be approximated by 16 - 20 km for most granitoidic intrusions of Bratislava massive. The peak metamorphism is probably associated with the polyphase granitoid intrusions and thus some sillimanite bearing assemblages may be synchronous with plutonism in the area. However, to built an reliable detailed orogenic model, more data controlling the crustal heat distribution, tectonics and post-culmination cooling are needed.

The whole rock metamorphic culmination reactions (Tab.6.) have steep, quasi vertical slopes ($dP/dT \approx 89-121$ bar/K) determining almost isothermal decompression as a consequence of rapid tectonic uplift and erosion. Post culmination cooling processes associated with diffusional equilibrium adjustment was characterized by decompression cooling with the slopes $dP/dT \approx 62-68$ bar/K. Cooling rates of the rock blocks were different ($S \approx 4.7-94$ °C/Ma, Tab. 8, Fig. 9) and express first order tectonic fragmentation of Tatric basement rocks during Variscan crustal collision and shortening. Although there is some scatter in the P-T paths they show simultaneous decompression and cooling. Orogenic specific exhumation conditions and cooling rates data characterize rapid tectonic processes in the basement rocks at the collisional Variscan orogenic wedge.

However, the determined regional 'clockwise' metamorphic trajectories for particular paragneisses in the Bratislava granitoidic massive area, based on thermobarometry, reaction extent, reaction slopes and kyanite appearance, differ substantially from Crd+Sil assemblages in periplutonic zones of Modra massive described by Korikovkij et al., (1984) as a result of periplutonic isobaric heating.

The multiple heating events are absent and the studied metamorphic rocks display the mineral assemblage and mineral chemical composition reflecting the culmination metamorphic temperatures and later diffusional equilibrium mineral adjustment. Metamorphic grade increased to the peak metamorphic assemblages post-dating and eradicating earlier metamorphic assemblages and fabrics and thus the culmination mineral assemblage document single Variscan metamorphic event with different intensity of post culmination retrograde changes on the scale of

metamorphic crystalline core. The Alpine tectono deformation processes destroyed and displaced the crystalline basement units and emplaced previously assembled complexes into new tectonic structural positions.

The differences in peak temperatures, pressures and cooling rates predict discontinuities in P and T in crustal depths and are considered to form an additional evidence that the post metamorphic faulting juxtaposed the rock blocks of different P-T characteristics and the fragmented basement area was a locus of major tectonic fault.

Acknowledgements

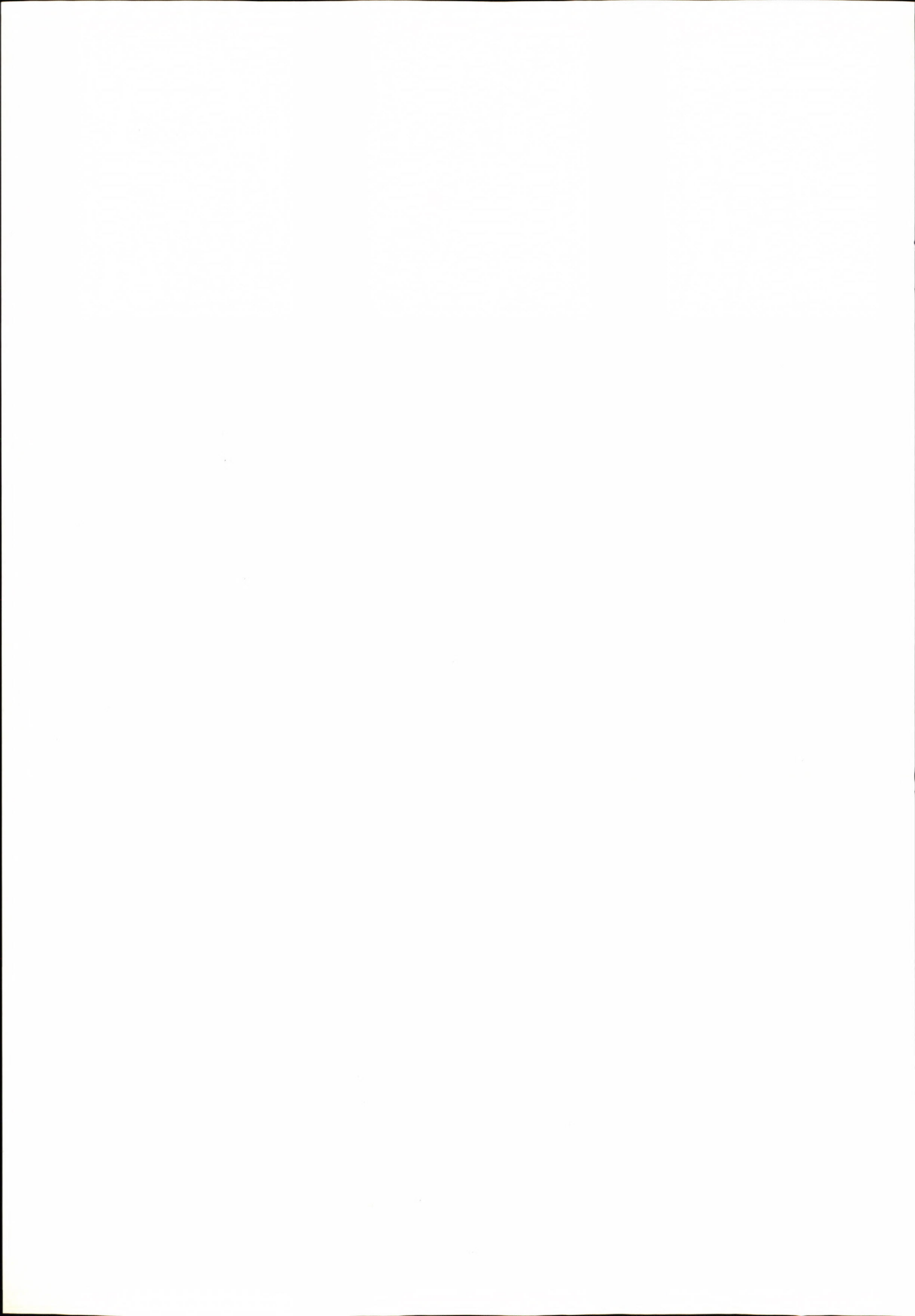
Thanks are expressed to Dr.F.Caňo, Doc.Dr.J.Krištín from Faculty of Science, Comenius University, for microprobe analytical work. Special thanks are due to W. Edwards (Kingston University, England) for kindly realized garnet analyses.

References

- Andrusov, D. 1936: Subtratic nappes in Western Carpathians. *Carpathica*, Praha, 1, 5-50.
- Andrusov, D. 1968: *Grundriss der Tektonik der Nördlichen Karpaten*. Veda SAV, Bratislava, 188 p.
- Andrusov, D., Bystrický, J. & Fusán, O. 1973: *Outline of the Structure of the West carpathian*. Guidebook for Geological Excursions. GÚDŠ, Bratislava.
- Anovitz, L. M. & Chase, C. G. 1990: Implications of post-thrusting extension and underplating for P-T-t paths in granulite terranes. A Grenville example. *Geology*, 18, 466 - 469.
- Bird, J. M. & Dewey, J. F. 1970: Lithospheric plate - continental margin tectonics and the evolution of the Appalachian orogen. *Geol. Soc. Amer. Bull.*, 81, 1031 - 1060.
- Bagdasarjan, G.P., Gukasjan, R.Ch., Cambel, B. & Veselský, J. 1983: *Resultaty Sb-Sr opredeleniji vozrasta metamorfičeskich porod kristaličeskogo kompleksa Malých Karpat*. *Geol.Zborn.Geol. Carpath.*, 34, 4, 387-397. (in Russian).
- Bezák, V. 1993: Herýnska a alpinska tektogenéza západnej časti Slovenského rudohoria: základné štádiá vývoja. In *Geodynamický model a hlbinná stavba Západných Karpát*. Rakús, M. & Vozár, J. Eds., Geologický ústav Dionýza Štúra, Bratislava 1993., 243 - 247. (in Slovak, Engl. summary).
- Bezák, V., Jacko, S., Ledru, P. & Siman, P. 1998: Hercynian development of the Western Carpathians. p.27-34. 45. In: Rakús, M. ed., 1998: *Geodynamic development of the Western Carpathians*. Dionýz Štúr Publishers, Bratislava, 290 p.
- Bohler, S. R. 1987: Pressure - temperature - time path and a tectonic model for the evolution of granulites. *J. Geology*, 95, 617 - 632.
- Broska, I. & Janák, M. 1985: Akcesorické minerály metapelitov a ich vzťah k metamorfóze v oblasti Záhorkej Bystrice (Malé Karpaty). In: *Akcesorické Minerály ich Petrogenetický a Metalogenetický Význam*. GÚDŠ Bratislava, 101-106. (in Slovak, Engl. summary)
- Cambel, B. 1952: Amfibolické horniny v Malých Karpatoch. *Geol. Práce, Zoš.*, 29, 70 (in Slovak).
- Cambel, B. 1954: K otázke kryštalických bridlic medzi Cajlou a Hornými Orešanmi v Malých Karpatoch. *Geol. Práce, Spr.*, 1, 16-20. (in Slovak).
- Cambel, B. & Valach, J. 1956: Granitoidné horniny v Malých Karpatoch, ich geológia, petrografia a petrochémiá. *Geol. Práce, Zoš.*, 42, 113-268. (in Slovak, Engl. summary).
- Cambel, B. & Vilinovič, V. 1987: *Geochémia a petrológia grantoidných hornín Malých Karpát*. Veda, Vyd. SAV, Bratislava, 183 p. (in Slovak, Engl. summary).
- Cambel, B., Dyda, M. & Spišiak, J. 1981: Thermodynamic measurement of origin of minerals in the area of crystalline of Malé Karpaty Mts., *Geol. Zbor. Geol. Carpath.*, 32, 745 - 768.
- Cambel, B., Mikláš, J., Khun, M. & Veselský, J. 1990a: Geochémia a petrológia flovito-kremítých metamorfovaných hornín kryštalínika Malých Karpát. *ŠVK, Banská Bystrica*, 267 p. (in Slovak, Engl. summary).

- Cambel, B., Kráľ, J. & Burchart, J. 1990b: Izotopová geochronológia kryštalinika Západných Karpát. *Veda, Vyd. SAV*, Bratislava, 183 p. (In Slovak, Engl. summary).
- Cliff, R.A., Droop, G.T.R. & Rex, D.C. 1985: Alpine metamorphism in the south-east Tauern Window, Austria. 2. Rates of heating, cooling and uplift. *J. Metamorphic Geol.*, 3, 403-415.
- Crowley, P. D. 1991: Thermal and kinetic constraints on the tectonic applications of thermometry. *Mineral. Mag.*, 55, 57 - 69.
- Dyda, M. 1977: Indexové minerály pararúl v oblasti bratislavského granitoidného masívu. *Disertation. Manuscript - GÚ SAV*, Bratislava, 136 p. (in Slovak).
- Dyda, M. 1980a: Physical properties and temperatures of crystallization of coexisting garnets and biotites from paragneisses of the Little Carpathians. *Geol. Zborn. Geol. Carpath.*, 31, 201- 213.
- Dyda, M. 1980b: Metamorphic grade and packing index in garnets. *Geol. Zborn. Geol. Carpath.*, 31, 359 - 374.
- Dyda, M. 1994: Geothermobarometric characteristics of some Tatric crystalline basement units (Western Carpathians). *Mitt. Österr. Geol. Ges.*, 86, 45 - 59.
- Dyda, M. 1997: Disturbance of the Variscan metamorphic complex indicated by mineral reactions, P-T data and crystal size of garnets (Malé Karpaty Mts.). In: Grecula, P. Hovorka, D. & Putiš, M. eds. 1997: *The Geological Development of the Western Carpathians*, Mineralia Slovaca Monographs, Bratislava.
- Dyda, M. 1999: Fragmentácia metamorfného obalu bratislavského masívu indikovaná vlastnosťami granátov. *Mineralia Slov.*, 31, 39 - 48. (in Slovak, Engl. summary).
- Dyda, M. 2000: Exhumation and cooling rates of the Variscan basement metamorphic complex inferred from petrological data (Malé Karpaty Mts.). *Slovak Geol. Mag.*, 6, 2-3, 293 - 297.
- Dyda, M. & Mikláš, J., 1993: Periplutonické zóny bratislavského granitoidného masívu (Malé Karpaty): rekryštalizácia, dehydratačné a objemové zmeny. *Mineralia Slov.*, 25, 93 - 103. (in Slovak, Engl. summary).
- Elphick, S.C., Ganguly, J. & Loomis, T.P. 1985: Experimental determination of cation diffusivities in aluminosilicate garnets. I. Experimental methods and interdiffusion data. *Contrib. Miner. Petrol.*, 90, 36-44.
- England, P. C. & Richardson, S. W. 1977: The influence of erosion upon the mineral facies of rocks from different metamorphic environments. *J. Geol. Soc. London*, 134, 201 - 213.
- England, P.C. & Thompson, A.B. 1984: Pressure-temperature-time paths of regional metamorphism. I.-Heat transfer during the evolution of regions of thickened continental crust. *J. Petrology*, 25, 894-928.
- Ernst, W.G. 1973: Interpretive synthesis of metamorphism in the Alps. *Geol. Soc. Am. Bull.*, 84, 2053-2078.
- Ernst, W.G. 1988: Tectonic history of subduction zones inferred from retrograde blueschist P-T paths. *Geology*, 16, 1081-1084.
- Eugster, H.P., Albee, A.A., Bence, A.E. & Thompson, J.B.Jr. 1972: The two-phase region and excess mixing properties of paragonite-muscovite crystalline solutions. *J. Petrology*, 13, 147-179.
- Ferry, J.M. 1980: A comparative study of geothermometers and geobarometers in pelitic schist from south-central Maine. *Amer. Mineralogist*, 64, 720-732.
- Ferry, J.M. & Spear, F.S. 197: Experimental calibration of the partitioning of Mg and Fe between biotite and garnet. *Contrib. Mineral. Petrology*, 66, 113 - 117.
- Ganguly, J. & Saxena, S.K. 1984: Mixing properties of aluminosilicate garnets: constrains from natural and experimental data and applications to geothermobarometry. *Amer. Mineralogist*, 69, 88 - 97.
- Gebauer, D. 1996: A P-T-t path for (ultra?) high-pressure ultramafic/mafic rock associations and their felsic country rocks based on SHRIMP dating of magmatic and metamorphic zircon domains: example: Alpe Arami (Central Swiss Alps). In: Basu, A., Hart, S., eds. *Earth Processes: reading the isotopic code. Geophys Monograph Series*, 95, 307-329.
- Ghent, E. D., Robbins, D. B. & Stout, Z.M. 197: Geothermometry, geobarometry and fluid composition of metamorphosed calc-silicates and pelites, Mica Creek, British Columbia. *Amer. Mineralogist*, 64, 874 - 885.
- Ghent, E. D. & Stout, Z.M. 1981: Geobarometry and geothermometry of plagioclase-biotite-garnet-muscovite assemblages. *Contrib. Miner. Petrol.*, 76, 92-97.
- Hodges, K. V. & Crowley, P. D. 1985: Error estimation in empirical geothermobarometry for pelitic systems. *Amer. Mineralogist*, 70, 702 - 709.
- Hoisch, T. D. 1990: Empirical calibration of six geobarometers for the mineral assemblage quartz + biotite + plagioclase + garnet. *Contrib. Mineral. Petrology*, 104, 225 - 234.
- Holland, T.J.B. & Powell, R., 1998: An internally consistent thermodynamic data set for phases of petrological interest. *J. Metamorphic Geol.*, 16, 309 - 343.
- Korikovskij, S.P., Cambel, B., Mikláš, J. & Janák, M. 1984: Metamorphism kristallinikuma Malých Karpát. Zonalnosť, etapy, sviaz s granitoidami. *Geol. Zborn. Geol. Carpath.*, 35, 437 - 462.
- Kozioł, A. M. & Newton, R. C. 1988: Redetermination of the anorthite breakdown reaction and improvement of the plagioclase-garnet-Al₂SiO₅-quartz geobarometer. *Amer. Mineralogist*, 73, 216-223.
- Krist, E., Korikovskij, S.P., Putiš, M., Janák, M. & Faryad, S.W. 1992: *Geology and Petrology of Metamorphic Rocks of the Western Carpathian Crystalline Complexes*. Comenius University Press, Bratislava 1992, 324 s.
- Lasaga, A.C. 1983: Geospeedometry: an extension of geothermobarometry. In: Saxena, S. K., (ed.) *Kinetics and Equilibrium in Mineral Reactions*. Advances in Physical Geochemistry 3., 81-114.
- Lasaga, A.C., Richardson, S.M. & Holland, H.D. 1977: The mathematics of cation diffusion and exchange between silicate minerals during retrograde metamorphism. In: *Energetics of Geological Processes* (ed. Saxena, S.K. & Battachanji, S.), s. 353-388. Springer Verlag, New York.
- Leško, B., Beránek, B. & Varga, I. 1980: Cisaillements horizontaux profonds sous les Karpates occidentales a la lumiere des connaissances géophysiques. *Rev. Géol. dyn. Géogr. phys.*, 22, 255-266.
- Lugeon, M. 1903: Les nappes de recouvrement de la Tatra et l'origine des Klippes des Carpathes. *Bull. Lab. geol. Univ., Lausanne*, 4.
- Mahel', M. 1983: Beziehung Westenkarpäten-Ostalpen, Position des Übergangs - Abschnittes, Deviner Karpäten. *Geol. Zborn. Geol. Carpath.*, 34, 131 - 149.
- Mahel', M. 1986: Geological Structure of the Czechoslovak Carpathians. *Paleoalpine Units I. Veda SAV*, Bratislava.
- Marko, F., Fodor, L. & Kováč, M. 1991: Miocene strike-slip faulting and block rotation in Brezové Karpaty Mts. (Western Carpathians). *Mineralia Slov.*, 23, 189 - 200.
- Mikláš, J. 1986: *Petrologia kryštalických bridlic metamorfnych zón Malých Karpát*. *Mineralia Slov.*, 18, 179 - 180.
- Mikláš, J. 1987: Príspevok k štúdiu protolitu kryštalických metamorfnych zón Malých Karpát. In: *Sborník príspevku z II. Celostátné konferencie mineralogů a petrologů*. Brno-Blansko, 93 - 95.
- Monié, P., Torres-Roldan, R.L. & Garcia-Casco, A. 1994: Cooling and exhumation of the Western Betic Cordilleras, 40Ar/39Ar thermochronological constraints on a collapsed terrane. *Tectonophysics*, 238, 353-379.
- Newton, R. C. & Haselton, H. T.: Thermodynamics of the garnet - plagioclase - Al₂SiO₅ - quartz geobarometer. In: Newton, R.C., Navrotsky, A., & Wood, B.J. (Eds.): *Thermodynamics of minerals and melts*, 131 - 147, Springer Verlag, New York.
- Oxburgh, E. R. & Turcotte, D. L. 1974: Thermal gradients and regional metamorphism in overthrust terrains with special reference to the eastern Alps. *Schweiz. Mineral. Ptol. Mitt.*, 54, 641 - 662.
- Pertchuk, L. L., Lavrentieva, I. V., Kotelnikov, A.R. & Petrik, I. 1984: Comparison characteristics of thermodynamic regimes of the Maine Caucasus chain and West Carpathians (in Russian), *Geol. Zborn. Geol. Carpath.*, 35, 105-156.
- Plašienka, D. 1989: Štruktúrny vývoj tatrika Malých Karpát. *Mineralia Slov.*, 21, 538.
- Plašienka, D., Michalík, J., Kováč, M., Gross, P. & Putiš, M. 1991: Paleotectonic evolution of the Malé Karpaty Mts. - An overview. *Geol. Carpath.*, 42, 195 - 208.
- Powell, R. & Holland, T.J.B. 1988: An internally consistent dataset with uncertainties and correlations: 3. Application to geobarometry, worked examples and computer program. *J. Metamorphic Geol.*, 6, 173 - 204.
- Putiš, M. 1987: *Geológia a tektonika juhozápadnej a severnej časti kryštalinika Malých Karpát*. *Mineralia Slov.*, 19, 135-157. (in Slovak, Engl. summary).

- Putiš, M. 1991: Tectonic styles and Late Variscan-Alpine evolution of the Tatric - Veporic crystalline basement in the Western Carpathians. *Zbl. Geol. Paleont. Teil.1, H.1*, 181 - 204.
- Scott, R. J., Foster, D. A. & Lister, G. 1998: Tectonic implications of rapid cooling of lower plate rocks from the Buckskin-Rawhide metamorphic core complex, west-central Arizona. *Geol. Soc. Amer. Bull.*, 110, 588 - 614.
- Selverstone, J. 1985: Petrologic constraints on imbrication, metamorphism and uplift in the SW Tauern Window, Eastern Alps. *Tectonics*, 4, 687-704.
- Selverstone, J. & Spear, F. S. 1985: Metamorphic P-T paths from pelitic schists and greenstones in the southwest Tauern Window, Eastern Alps. *J. Metamorphic Geol.*, 3, 439-465.
- Selverstone, J., Spear, F. S., Franz, G., & Morteani, G. 1984: High pressure metamorphism in the SW Tauern Window, Austria: P-T paths from hornblende-kyanite-staurolite schists. *J. Petrology*, 25, 501-531.
- Spear, F. S. & Selverstone, J. 1983: Quantitative P-T paths from zoned minerals: Theory and tectonic applications. *Contrib. Mineral. Petrol.*, 83, 348-357.
- Sharp, Z. D. & Ulmer, P. 1993: Stable isotope geochemistry of the aluminosilicates. *Geol. Soc. Amer. Annual meeting, Boston Ma*, Oct. 25-28., 100 p.
- Shumacher, J. C. 1991: Empirical ferric iron corrections necessity, assumptions, and effects on selected geothermobarometers. *Mineral. Mag.*, 55, 3 -18.
- Shumacher, J. C. 1997: Appendix 2. The estimation of the proportion of ferric iron in the electron - microprobe analysis of amphiboles. *Canad. Mineralogist*, 35, 238 - 246.
- Spear, F.S. & Franz, G. 1986: P-T evolution of metasediments from the Eclogite Zone, south central Tauern Window, Austria. *Lithos*, 19, 219-234.
- Spear, F. S. & Rumble, D. 1986: Pressure, temperature and structural evolution of the Orfordville Belt, west-central New Hampshire. *J. Petrology*, 27, 1071-1093.
- Thompson, J. B. Jr. 1957: The graphical analysis of mineral assemblages in pelitic schists. *Amer. Mineralogist*, 42, 842 - 858.
- Thompson, A.B. 1976: Mineral reactions in pelitic rocks: I. Prediction of P-T-X (Fe-Mg) phase relations. *Amer. J. Sci.*, 276, 401-424.
- Thompson, A.B. & England, P.C. 1984 : Pressure-temperature-time paths of regional metamorphism II: Their inference and interpretation using mineral assemblages in metamorphic rocks. *J. Petrology*, 25, 894 - 928.
- Uhlig, V. 1898: *Geologie des Tatragebirges I*. Denkschr. Ak. Wiss. Math., 64, 643-684.
- Uhlig, V. 1903: *Bau und Bild der Karpaten*. F. Tempsky Verlag, Wien, 911 p.
- Vozárová, A. 1998: Late Hercynian development in the Central Western Carpathians. p.41-45. In: Rakús, M. ed., 1998 : *Geodynamic development of the Western Carpathians*. Dionýz Štúr Publishers, Bratislava, 290 p.
- Zeck, H.P., Monié, P., Villa, I.M. & Hansen, B.T. 1992: High rates of cooling and uplift in the Betic Cordilleras, S. Spain. Alpine lithospheric slab detachment, mantle diapirism and extensional tectonics. *Geology*, 20, 79-82.



HP rocks associated with mylonitoclastites: a result of polystage overprint of the Austro-Alpine basement (Kreuzeck Massif, Eastern Alps)

MARIÁN PUTIŠ¹, SERGUEI P. KORIKOVSKY², WOLFGANG UNZOG³ & NIELS OE. OLESEN

¹J.A. Comenius University of Bratislava, Faculty of Natural Sciences, Dept. of Mineralogy and Petrology, Mlynská dolina, SK-84215 Bratislava, Slovak Republic, *Corresponding author. Fax: +421-2-60296293, E-mail address: putis@fns.uniba.sk

²Russian Academy of Sciences, Institute of Geology of Ore Deposits, Petrography, Mineralogy and Geochemistry, Staromonety per. 35, 109017 Moscow, Russian Federation.

³K.F. University of Graz, Institute of Geology and Paleontology, Heinrichstr. 26, A-8010 Graz, Austria.

⁴University of Aarhus, Faculty of Science, Dept. of Earth Sciences, Nordre Ringgade 1, DK-8000 Aarhus, Denmark.

Abstract. The studied region of the Kreuzeck Massif southeast of the Tauern Window in the Austrian Eastern Alps reveals contrasting early-Cretaceous overprint of the Austro-Alpine (AA) basement complexes from (sub-)greenschist- to HP amphibolite/eclogite facies. An unusual association of HP rocks with mylonitoclastites have been found along early-Tertiary lateral strike slip-fault shear zone within the Kreuzeck Massif.

Petrofabrics of strongly overprinted (reactivated) rocks from the pre-Alpine basement were used for identification of micromechanisms of brittle-ductile deformation and reconstruction of P-T conditions related to subductional burial and exhumation of HP and MP fragments recently located within the Tertiary dextral strike slip shear zone. The HP amphibolites to eclogites (?) and the host kyanite-garnet paragneisses and granitic orthogneisses form tectonic lenses of the AA Polinik structural complex along this shear zone. The rocks often show ductile deformation and dynamic recrystallization of plagioclase and quartz, while amphibole and pyroxene were subjected to reaction recrystallization. Ductile (plagioclase-quartz) fabrics in barroisite- and clinopyroxene (high-Na augite)-bearing HP amphibolites to eclogites (?) postdate metamorphic HP/MT fabrics. Calculated temperature of (Cretaceous) collisional metamorphism is ca. 530 °C at minimum pressure of 11 kbar. No relics of pre-Alpine fabrics have been preserved in the Polinik structural complex.

Variscan metamorphic assemblage of the AA Strieden structural complex (staurolite, garnet, andalusite, sillimanite, plagioclase, formed at T_{max} around 600 °C and 4-5 kbar of P) is discernible outside the strike slip shear zone. Approaching this zone, the degree of Alpine overprint is increasing according to newly-formed assemblage of chloritoid, margarite, albite, garnet-outer zone, which represents (Cretaceous) T_{max} of ca. 500 °C and 6-7 kbar of P. Structurally rebuilt northern part of the AA Strieden complex, adjoining the (early-Tertiary) shear zone, shows simultaneous micromechanisms of mylonitic (ductile) flow in quartz and mylonitic-cataclastic flow in feldspars of ortho- and paragneisses. Similarly, marbles show mechanical differences in alternating mylonitic calcite and mylonitic-cataclastic dolomite layers. This seems to be typical of frictional-viscous flow producing mylonitoclastites. The measured (plagioclase, quartz, calcite, dolomite) mineral textural patterns are related to dextral strike slip or top-to-WNW shifting of steeply south-dipping AA basement fragment.

Reactivated HP/MP AA basement fragments, finally exhumed in the early-Tertiary dextral strike slip fault shear zone, might be the fragments coming from Cretaceous continental subduction zone. The exhumed overprinted rocks were intruded by volcanic dykes ca. 32 Ma old, the latter being cut by (Miocene) ultracataclastites.

Keywords: HP rocks; mylonitoclastite; P-T path; polystage overprint; Eastern Alps

1. Introduction

The reviews of exhumation mechanisms of high-pressure (HP) rocks have been provided by Droop et al. (1990), Ring (1992), Platt (1993), Gebauer et al. (1993), Dal Piaz et al. (1993), Froitzheim et al. (1996), Spalla et al. (1996), Kurz and Neubauer (1998), Dal Piaz (1999), Putiš et al. (2000, 2002) mainly on the examples from the Alps using mineral and microstructural changes.

A few principal micromechanisms enhance a crustal volume to be exhumed in form of a tectonic fragment along a shear zone. The deeper horizons are characteristic of higher temperatures, lower strain rates and thus lower lithosphere strengths (rigidity) in deformation. There, a micromechanism of grain-size insensitive creep (e.g. Barber, 1990) is characteristic with lower values of shear strength or flow stress. Mylonitic rocks in the shear zones, therefore coincide with a crustal strength minimum and

enhance development of a detachment fault. The shallower horizons can accommodate a transitional frictional-viscous flow (Handy et al., 1999) producing clastomylonites or mylonitoclastites depending on a volume share of mylonitic vs. cataclastic matrix. Mylonitoclastites indicate lowering temperatures at increasing deformation rates. At the same time, the lithosphere strength is increasing towards dominated frictional flow in the upper crust.

Solution of exhumation mechanisms in the Kreuzeck Massif of central Eastern Alps was initiated by findings of eclogitic metabasites (Hoke, 1990) within the Austro-Alpine (AA) basement complexes in close association with mylonites, mylonitoclastites to ultracataclastites. Such unusual rock association indicates a polystage evolution of strongly deformed (overprinted) basement rocks. The local situation can be explained by predominated Cretaceous internal structure of the AA basement that is overprinted by superposed Tertiary tectonic structures, especially steeply

south dipping dextral (top-to-WNW) strike slip fault zones (Ratschbacher et al., 1991; Frisch et al., 1999; Mancktelow et al., 1999) truncating the studied Kreuzeck Massif area (Fig. 1).

The Austro-Alpine (AA) basement structural complexes represent an orogenic wedge (Platt, 1993) of continental crust that formed during the Early Cretaceous collision (Neubauer, 1994; Dallmeyer et al., 1998) fol-

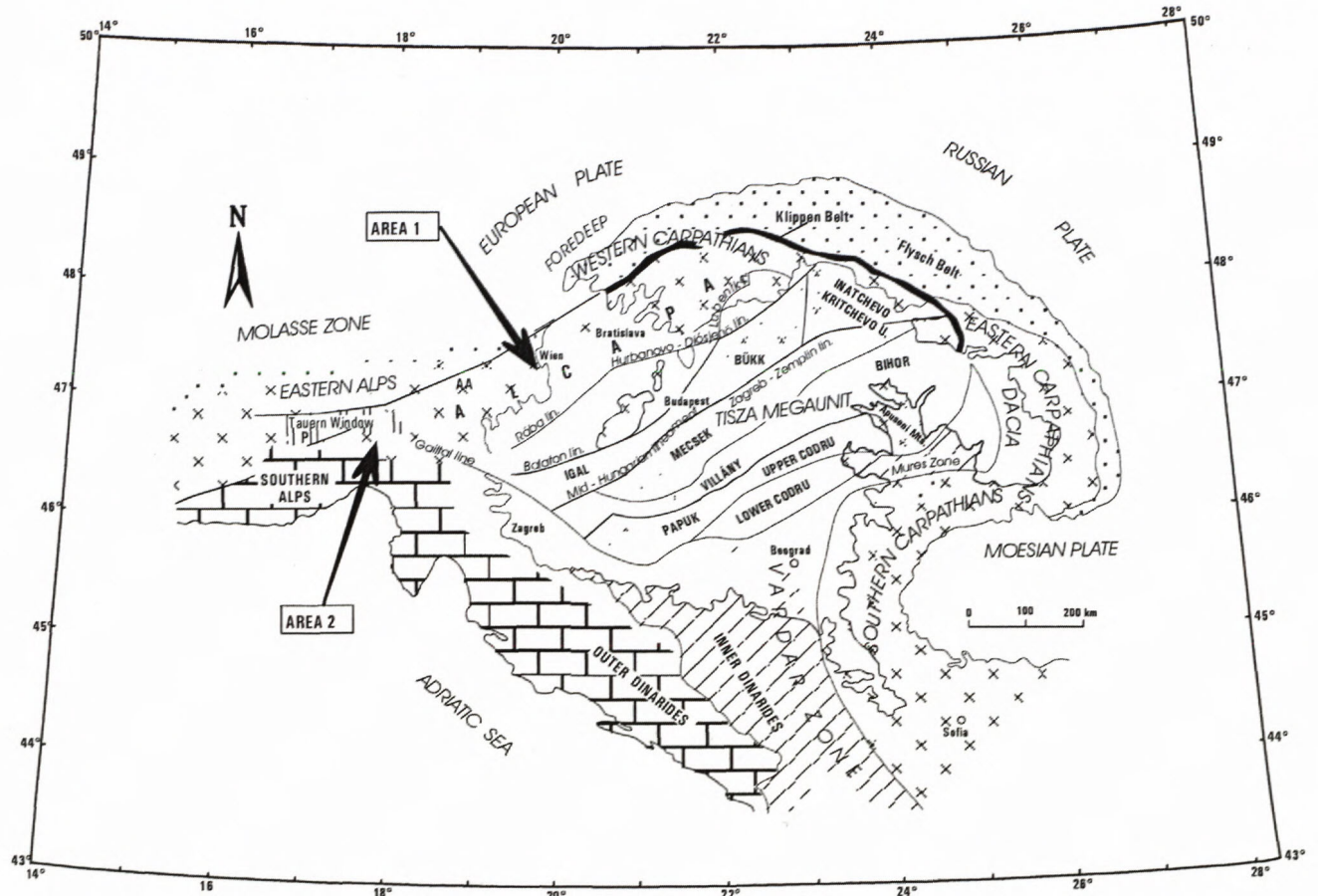


Fig. 1. Tectonic sketch map of the East Alpine-Carpathian-Pannonia (ALCAPA) orogen with position of the Austro-Alpine (AA) unit (after Plašienka et al., 1997). Area 1: documents subhorizontally stacked AA structural complexes due to Early Cretaceous collision (include the Middle AA structural complex with Cretaceous eclogites,). Area 2: The Kreuzeck Massif AA structural complexes piled up S of the Tauern Window undergone to Late Cretaceous-Tertiary transpression and normal faulting.

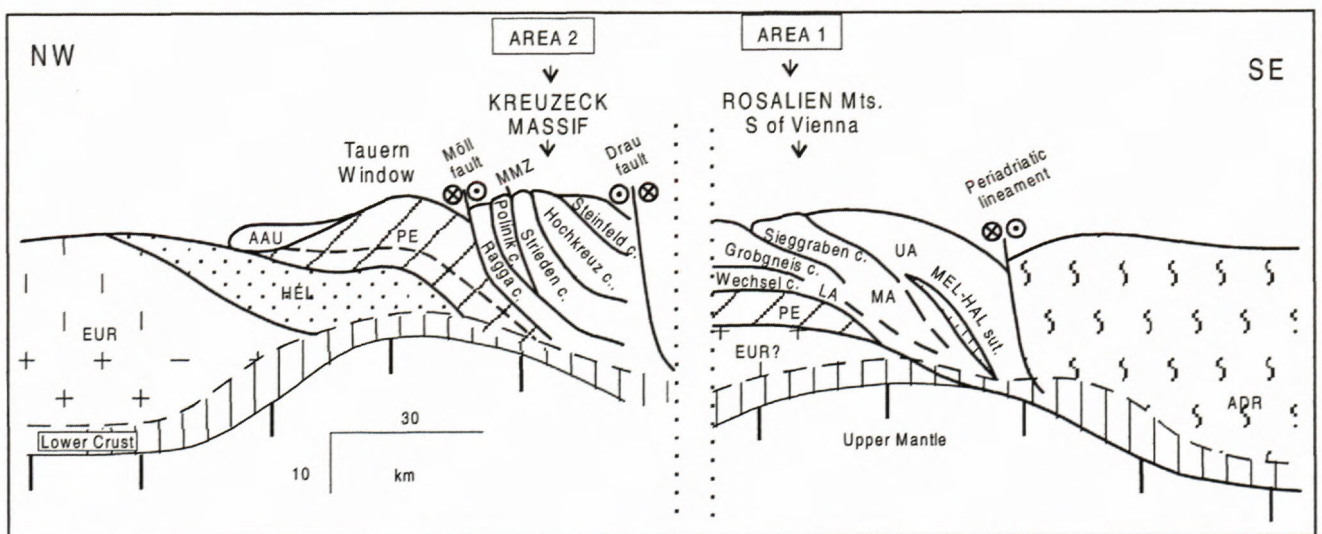


Fig. 2. Schematic tectonic cross-section of the Austro-Alpine unit (modified fig. 2 from Putiš et al., 2002). EUR=European plate, HEL=Helvetic zone, PE=Pennine zone, AAU=Austro-Alpine unit, LA=Lower AA, MA= Middle AA, UA=Upper AA, MEL-HAL sut.=Meliata-Hallstatt ocean suture zone, ADR = Adria (or Apulia) microplate.

lowing the closure of the Meliata-Halstatt ocean in the Late Jurassic. This event caused an extreme shortening of the AA unit and juxtaposed different structural complexes metamorphosed in eclogite to (sub)greenschist facies cropping out in the Kreuzeck Massif at the distance of a few kilometres (Fig. 2, 3).

The AA complexes (Tollmann, 1977) occupied a lower plate position during the Late Jurassic-Early Cretaceous collision, but the upper plate position during the Late Cretaceous-Tertiary collision. In the former case, they participated in shortened early Tethyan Meliata-Halstatt passive continental margin. In the latter case, following the closure of the Pennine ocean, the AA unit became frontal part of the Apulia (Adria) indenter, which collided with the European passive continental margin (Kozur, 1991; Neubauer, 1994; Stampfli, 1996; Froitzheim et al., 1996; von Blanckenburg and Davies, 1996; Dallmeyer et al., 1996; Stampfli and Mosar, 1999; Dal Piaz, 1999; Putiš et al., 2000, 2002). The studied regional tectonic structure developed by subhorizontal nappe thrusting that transformed to subvertical dextral (transpression?) strike slip and steepening the nappe slices. Some of the basement fragments, usually rich in metabasics, metaultrabasics, marbles along with metapelites, less granite gneisses, underwent even continental subduction in HP amphibolite- or eclogite facies P-T conditions (reviewed by Putiš et al., 2002).

The purpose of this paper is to document the function of a brittle-ductile shear zone that enhanced final exhumation of early-Alpine HP to MP rocks during earlier stages of Tertiary strike slip-fault tectonics following the collision between the AA and Pennine units in the Eastern Alps. We revealed principal characteristics and evolution steps of strain-accommodating minerals, including their textural patterns from the Kreuzeck Massif strike slip shear zone, and compared them to those from the normal-fault shear zone (dated 20-15 Ma, Cliff et al., 1985; Selverstone, 1988) at the eastern edge of the Pennine Tauern Window. While the reconstructed petrological P-T path is related to early-Alpine exhumation stage of HP/MP AA basement fragments, mechanical behaviour and kinematics of polyminerally mylonites seem to be related to brittle-ductile deformation along the early-Tertiary steeply south dipping shear zone. The paper shows varying early-Alpine reactivation grades of pre-Alpine basement fragments (AA structural complexes) crosscut by early-Tertiary dextral exhumation shear zone. Polystage exhumation of reactivated basement fragments has been studied using microstructural and petrological methodological approaches.

2. Geological structure of the Kreuzeck Massif

2.1. Geological structure of the Kreuzeck Massif from the viewpoint of former investigations

Hoke (1990) published examples of the deformation styles of mesostructures and their relationship to metamorphic and mylonitic events from the northwestern part of the Kreuzeck Massif. Her's results point to Cretaceous

remetamorphism of the AA basement in the time interval around 100-90 Ma (a few K-Ar and Rb-Sr data). Oxburg et al. (1966) found a lot of 83-76 Ma (K-Ar ages on muscovite and biotite), or even younger 66 Ma (one age on muscovite and one on biotite) mineral ages at the boundary with the Tauern Window Pennine unit. An age of 61 Ma was found at the southern boundary with the main mylonite zone directly in the Kreuzeck Massif (MMZ, Hoke, 1990).

There are two different structural-metamorphic domains from the view-point of Alpine overprint (reactivation) in the Kreuzeck Massif built of AA structural complexes: the domain north of the MMZ with the Late Cretaceous K-Ar muscovite and biotite ages; and the domain south of the MMZ with the well preserved pre-Alpine (late-Variscan) K-Ar ages. Hoke (1990) included the northern domain into the Polinik unit and the southern one into the Strieden unit on the basis of the work in the area between the Möll valley and Strieden and Polinik Mt. peaks. She proposed amphibolite to eclogite facies Alpine reactivation in the Polinik, but only the lower greenschist-facies in the Strieden unit (Hoke, 1990, fig. 47).

The apatite FT ages (Staufenberg, 1987) of the Polinik AA complex are ranging from 6 to 23.4 Ma, likewise in the neighbouring Pennine Tauern Window. However the data from the southern „Altkristallin“ of the Kreuzeck Massif yield higher cooling ages up to 31.4 Ma, rarely approaching even 40 Ma, indicating the existence of separated blocks. This fact stresses the importance of the Möll, Drau and MMZ fault system (Fig. 2-4) during the Tertiary tectogenesis.

The lowest-T evolution period is also documented by zircon FT ages from the different structural complexes of the tectonostratigraphical nappe pile proposed by Putiš et al. (1997a) and described in the paragraph below. The zircon FT ages of the AA unit south of the Tauern Window yield a wide interval of 84-35 Ma (Frisch et al., 1999) reflecting different Mesozoic (Eoalpine, Cretaceous) and Tertiary tectonic blocks.

The strongly reactivated higher-grade metamorphic Variscan basement structural complexes („Altkristallin“) with the occurrences of Alpine amphibolites to eclogites were mapped also westwards of the Kreuzeck group – in the Schober group and mentioned in published short reports (Putiš et al., 1996, 1997a; Linner, 1997; Spaeth, 1997) on manuscripts to geological maps deposited in the Austrian Geological Survey in Vienna.

The new Metamorphic Map of the Eastern Alps (Hoinkes et al., 1999) does not yet contain all the newest findings of the eclogitic rocks and the picture of the metamorphism in the AA complexes can be precised in the area of question.

2.2. Geological structure of the Kreuzeck Massif based on the new investigations

The new compiled map of the Kreuzeck Massif (Fig. 3, after Putiš, 1998) and the published report (Putiš et al., 1997a) to this map yield a view on the whole Alpine tectonic structure of the Kreuzeck Massif S of the Tauern

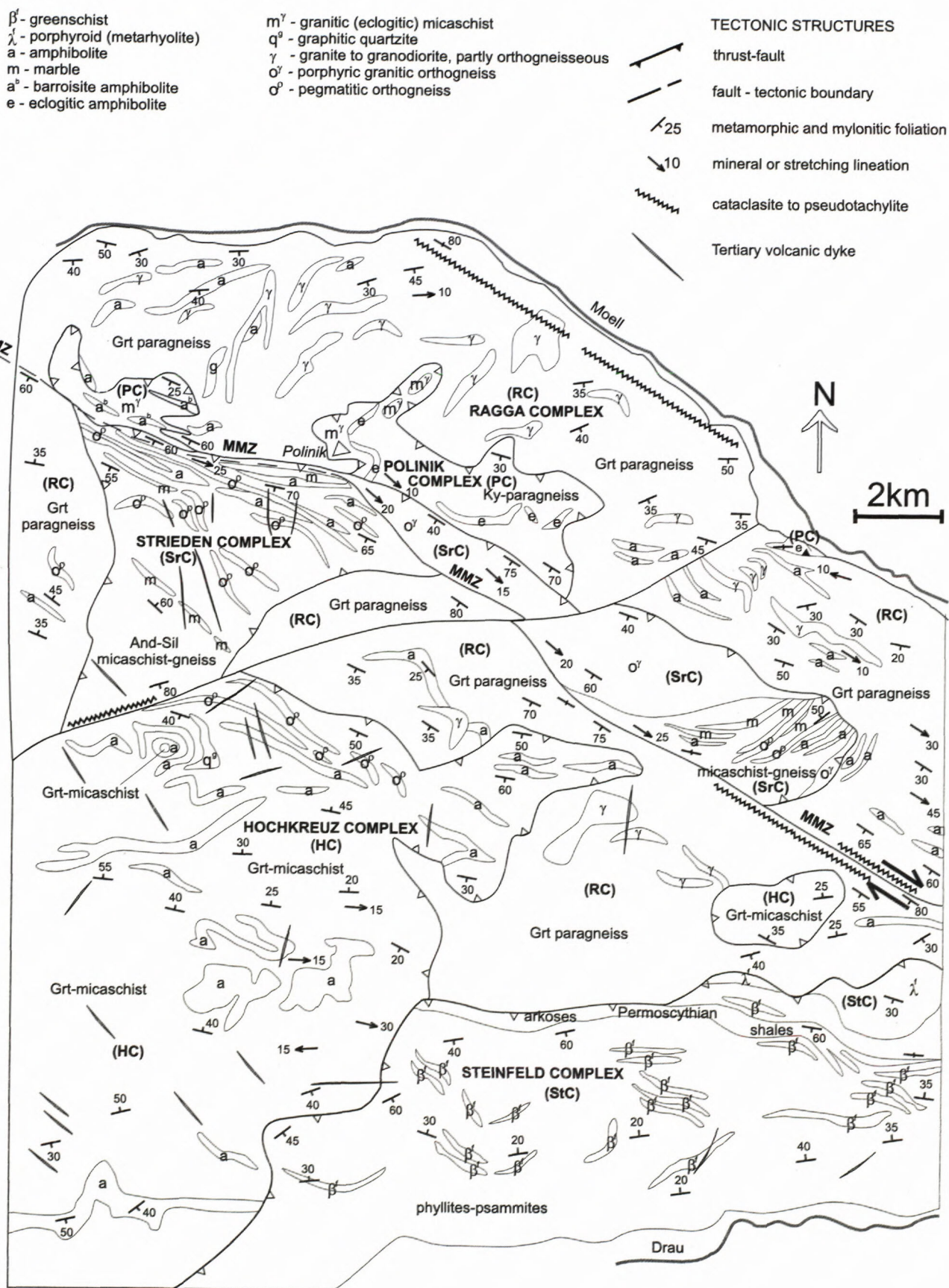


Fig. 3 Compiled geological-structural map of the central part of the Kreuzeck Massif (after Putiš et al., 1995-1997 and Putiš, 1997).

Window. The mapping work (Putiš et al., 1995, 1996, 1997b) revealed at least 5 stacked AA structural complexes (basement nappes) built of characteristic lithological members. They are (from north and tectonic bottom): the Ragga structural complex (gneisses, amphibolites, migmatites, partly orthogneissous granitoids), the Polinik structural complex (Ky-St-Grt gneisses, eclogitic high-Na augite amphibolites and Bar-bearing amphibolites, granitic feldspar-gneisses to micaschists, leucocratic granitic gneisses), the Strieden structural complex (Sil-And paragneisses and St-Grt micaschist gneisses, associated with Grt amphibolites, Cal-Dol-Tr marbles, small pegmatitic and large porphyric granitic gneisses), the Hochkreuz structural complex (micaschists, graphitic quartzites, large amphibolitic, gabbro-amphibolitic to layered amphibolitic bodies) and the Steinfeld structural complex (metapelites, metagreywackes, greenschists, porphyroids, Cld schists) covered by slightly (anchi-)metamorphosed Permo-Scythian sediments (arkoses, shales, quartzites).

According to our field work, the HP amphibolite facies (Cretaceous ?) metamorphism of the Polinik structural complex is restricted in the studied area along the MMZ and around the Polinik Mt. peak. Because of this reason, the rest of the former Polinik unit (defined by Hoke, 1990) further to north was included into the newly-defined Ragga structural complex showing only greenschist facies Alpine overprint (Putiš et al., 1997a, b).

The HP Polinik- and MP Strieden complexes are „rooted“ in dextral strike slip shear zone, which is considered to be their exhumation „suture„ (Putiš et al., 1998). It is located between the underlying gneiss-migmatite-granitic Ragga complex (present in the front of the AA nappe complex) and overlying Hochkreuz-Steinfeld complexes.

The types of mesostructures and their orientations are depicted in schematic structural-geological map (Fig. 3). Foliations and lineations outside the MMZ are mostly pre-Alpine metamorphic elements partly modified during the Alpine deformations. The MMZ, on the other hand, is characterized by subparallel mylonitic foliations, mineral and stretching lineations. In places, the older foliation is preserved in form of S-planes in S-C mylonites (Berthé et al., 1979) indicating top-to-WNW shear. Internal structure of this zone striking WNW-ESE is characterized by steeply dipping foliations and oblique to subhorizontal stretching lineations of strongly mylonitic rocks. The whole structure is cut by mostly NNW-SSE trending volcanic dykes dated 32-35 Ma (Deutsch, 1984). They are well fitting to dextral kinematics and the brittle-ductile stage of deformation.

The neighbouring Pennine Reisseck Massif is separated from the AA Kreuzeck Massif by a dextral strike slip fault zone (Ratschbacher et al., 1991), while an extensional normal fault boundary was found by Genser and Neubauer (1989) in the easternmost part of the Reisseck

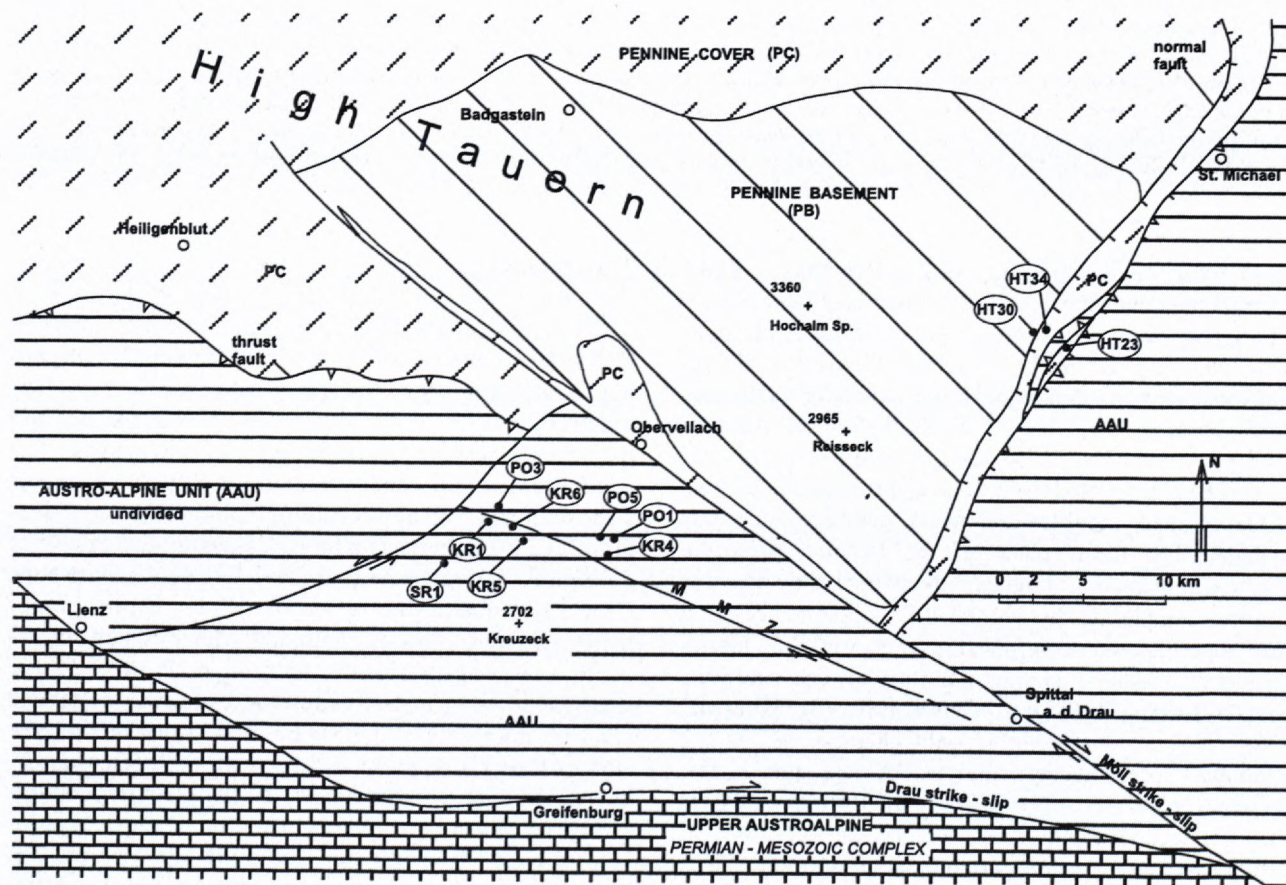


Fig. 4. Geological-tectonic sketch-map of the southeastern margin of the Tauern Window and Kreuzeck Massif in the Area 2, include the samples location. Austro-Alpine unit (AAU) is undivided. Pennine basement complex (PB). Pennine cover complex (PC).

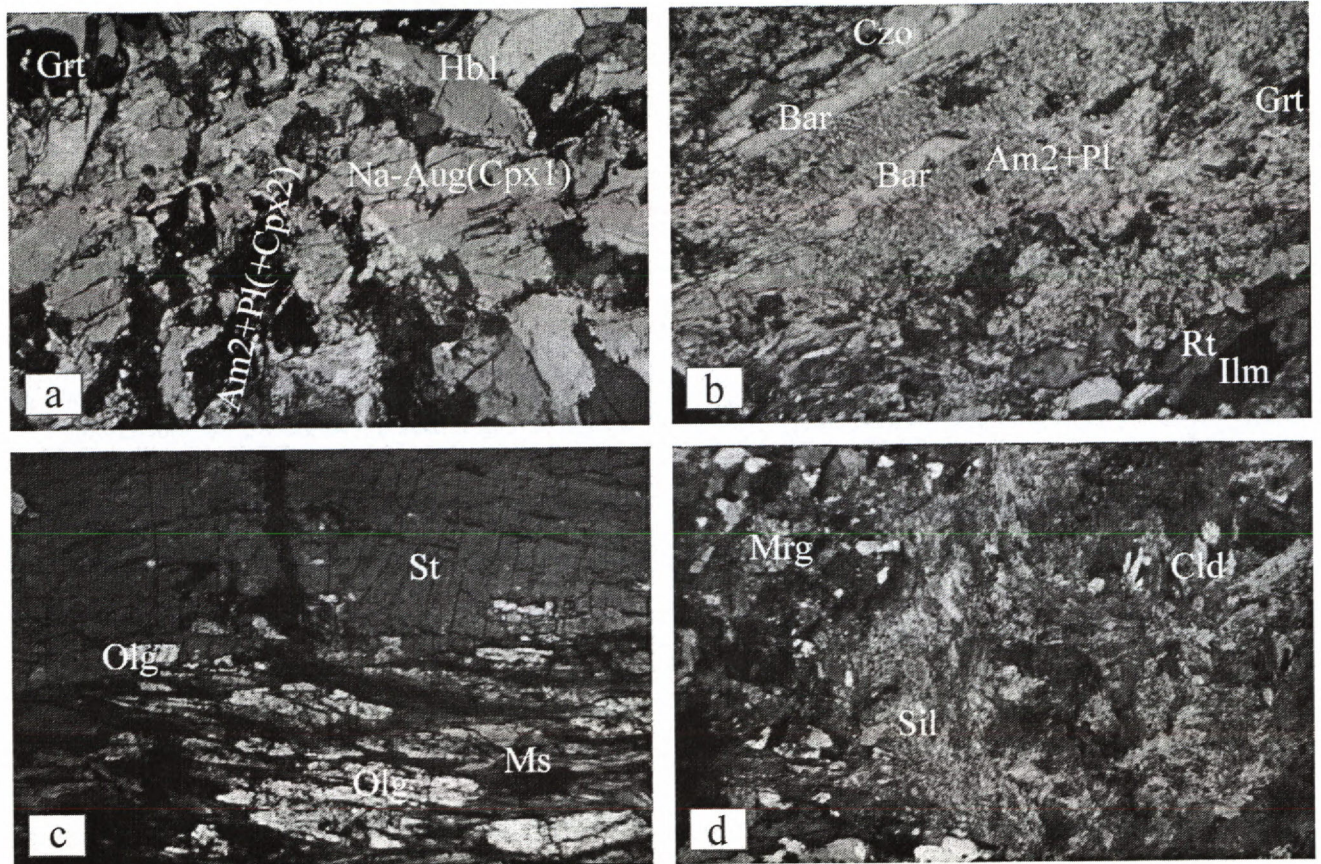
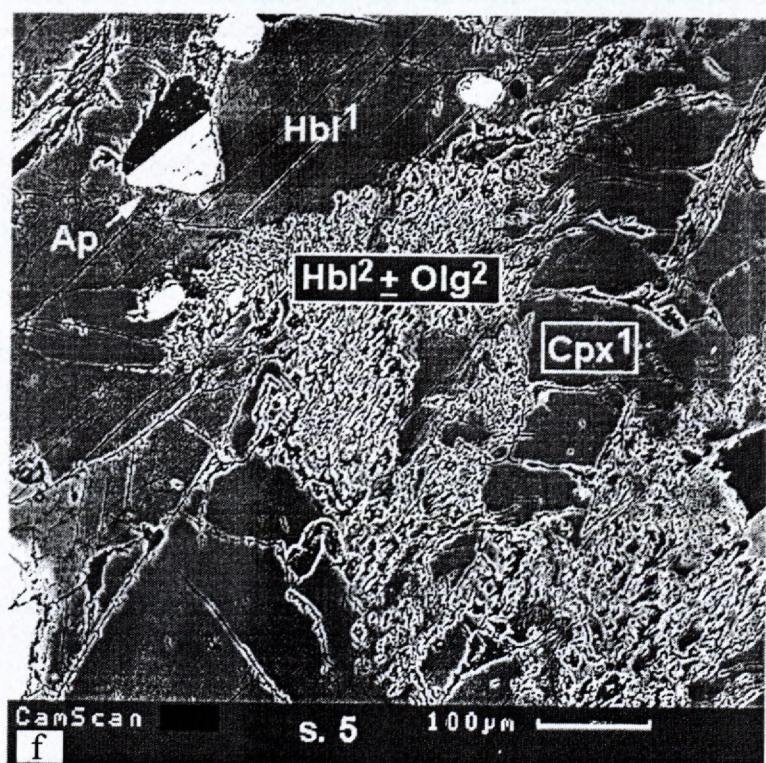
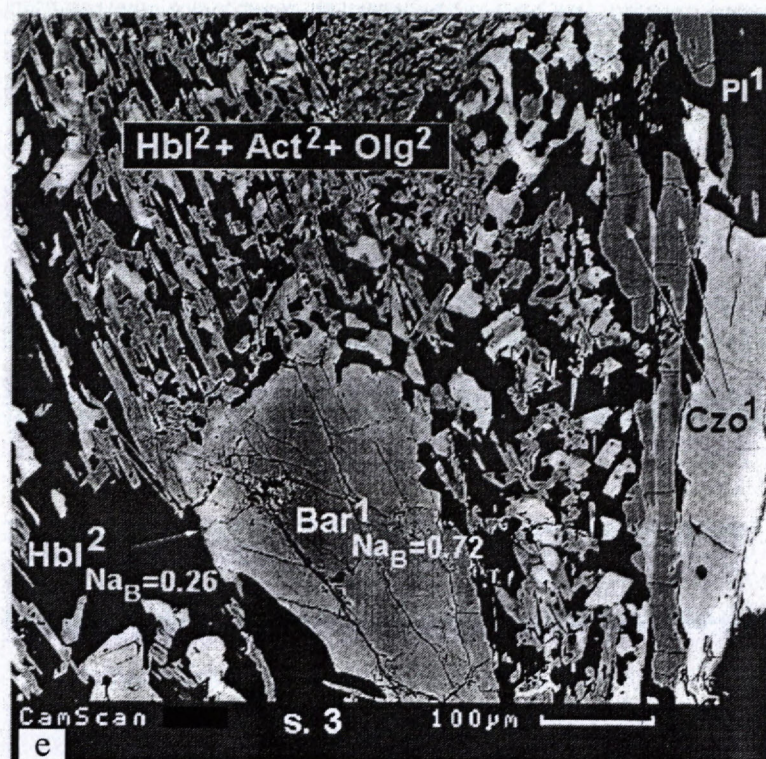


Fig. 5. Microstructures of metamorphic minerals of the Polinik (a, b) and Strieden (c, d) structural complexes. Sample-location according to Fig. 4. (a) High-Na Aug, Hbl (D1 Alpine); post-peak Am2, Pl, and rare Cpx2 symplectitic aggregates (D2 Alpine), HP amphibolite. (b) Bar (HP) amphibole prismatic crystals associated with Grt, Rut and Czo (D1 Alpine); symplectites of Am2 (Prg-, Ed-Prg-, or Ed-Act) and Olg associated with Ilm, Chl, Ep (D2 Alpine). (c) Late syntectonic St porphyroblast enclosing metamorphic schistosity with Olg, Ms, Bt and Qtz. (d) Snowball shaped Sil porphyroblasts associated with Bt (Variscan) and the superimposed (Alpine) recrystallization products: Cld, Ms and Mrg. (e) BSE image of symplectite from eclogitic amphibolite of the Polinik complex (s. PO5). (f) BSE image of symplectite from Bar HP amphibolite of the Polinik complex (s. PO3). Magnification: 18x (a, c), 25x (b), 30x (d).

Massif, where the Pennine unit merges below the overthrust Austro-Alpine one (Fig. 4). The Pennine basement is built of porphyritic „Zentralgneis“-type granitoids and less migmatitic gneisses. The overlying Pennine Mesozoic rocks are subdivided into two lithological and structural complexes (Bezák et al., 1995): the 1st one is the lower, volcano-sedimentary complex (Bt-Ep-Ab, Qtz-Ab-Phe-Chl, Ab-Ep-Chl-Hbl-Bt schists), and the 2nd one is the upper, calcschist-marble complex (marbles and marly marbles, calcareous phyllites). The thrust plane of the Pennine Mesozoic volcano-sedimentary complex overlying the Pennine basement complex is dipping 20-40° to the southeast. It bears superimposed extensional asymmetric S-C fabrics indicating a top-to-SE sliding along the distinct stretching lineation striking NW-SE to WNW-ESE (Bezák et al., 1995). Such tectonic style is only characteristic in the easternmost edge of the window, because just a few kilometres to the west, everywhere in the Pennine basement of the Risseck-Hochalm Massif the NW-SE to NNW-SSE striking stretching lineations are related to top-to-the NW(-NNW) nappe transport (Bezák et al., 1993, 1994) of the inferred older age (60 Ma?), comparing e.g. the results of Kurz et al. (1998) further to west.

3. Methodology

The newly-outlined geological-structural scheme (Fig. 3) was drawn on the basis of detailed field geological mapping (the Austrian Geological Survey mapping project 1995-1997, attended by M. Putiš et al.) and the complementary structural-petrological studies. The applied research methods embody the study of microstructures and mineral crystallographic preferred orientation (CPO) patterns (textures) of quartz and calcite or dolomite aggregates using the U-stage microscope (Univ. of Bratislava), reflection X-ray texture goniometer (Univ. of Graz), combined with electron microprobe analysing of rock-forming minerals of mylonitic rocks and some thermobarometric estimates. CamScan electron microscope in BSE mode was utilized for the study of very fine-grained deformed aggregates (Univ. of Aarhus), or for the study of symplectitic textures (Univ. of Moscow). EDS was used for identification or confirmation of calcitic and dolomitic layers in marble. Mineral abbreviations (see Appendix A) in text and figures are used after Kretz (1983) and end-members of Ca-amphiboles after Leake et al. (1997).



4. Petrography and P-T estimates of the Polinik and Strieden structural complexes

4.1. Polinik structural complex

The Polinik complex shows the strongest Alpine overprint of former structures among AA basement complexes. This is compatible with position of tectonic lenses

of the complex along the transpression exhumation shear zone („suture“).

Eclogitic amphibolites contain Alm (50-55%)-Prp (18-24%)-Grs(20-29%) garnet (Tab. 1) associated with high-Na Aug (=Cpx1, with the maximum 22 % of Jd, Tab. 2, Fig. 5a), Mg-Hbl1 (Tab. 3, Fig. 5a), and rare Bt1. The real eclogites (with the true Omp) have not yet been discovered. Black symplectitic rims around Cpx1 are composed of Mg-Hbl2+Olg, occasionally Cpx2(with ca. 5 to 3 % of Jd, Tab. 2, Fig. 5a). The symplectite replacement usually occupies only part of the Cpx1 boundary with Grt. Al-rich Prg to Ts amphiboles (Hbl2) (Tab. 3) form often the reaction rims around Grt; but Hbl2 from symplectites (Fig. 5e) around Cpx1 are represented by Al-poor Act-Hbl amphiboles. Garnet grains in eclogitic amphibolites have only a prograde zoning (Tab. 1) from core to rim, with increasing Prp content from 19 to 24 %, and decreasing Grs content from 28-29 to 19-21 %.

Grt-Hbl thermometry (Perchuk, 1989) using the Grt grains with Hbl(1) inclusions (Fig. 6 - s. PO5) revealed the prograde rise of T from 497 °C (cores of Grt) up to 533 °C (the outer zones). The maximum temperature of the burial stage has been obtained for contacts of Grt with adjoining Cpx1 and Hbl1: Grt (rim, with the maximum Prp content)+Na-Aug - 533 °C (Ai, 1994), and Grt (rim)+Hbl1 - 530 °C (Perchuk, 1989) (Fig. 6 - s. PO1). If the maximum Jd content in Cpx1 was 22 %, the minimum pressure at T ~ 530 °C deduced from the Jd isopleths in Cpx (Holland, 1980) was 11 kbar. Then the responding geothermal gradient during the D1 burial stage of the Cretaceous metamorphism of the Polinik complex was ca. 13 °C/km (Fig. 7). Decreasing T at the decreasing P is inferred for the D2 stage of the uplift, when the reactional Ts to Prg and Act-Hbl amphiboles have formed.

Some of metabasites contain Alm (48-50%)-Prp (25-28%)-Grs (20-23%) garnet (Tab. 4) associated with the Na-Ca amphibole (Am1) (Tab. 5, Fig. 5b), Czo, andesine-labradorite (Pl1) and single grains of Na-poor Kfs. Na-Ca amphibole is the Na-Ca barroisite (Leake et al., 1997) with NaB 0.60-0.73 per f.u., X Fe 0.31-0.34. Barroisite is replaced either by edenitic rims (NaB 0.09-0.33), or by the subparallel-oriented three-mineral symplectites (Fig. 5f) of edenite to pargasite (X Fe 0.37-0.48), actinolite (X Fe 0.23-0.29) (Tab. 5), and oligoclase (17-30% An). Ed to Prg and Act in these symplectites have often the sharp contacts, form the sepa-

Tab. 1. Microprobe analyses of zonal Grt containing inclusions of Hb. Grt-Cpx-Czo-Hb±Bt eclogitic amphibolite. Polinik structural complex. PO1 and PO5 samples location according to Fig. 4.

Sample	s. PO1 (Grt)					s. PO5 (Grt)						
						1-st grain				2nd grain		
	core		rim			core		rim		core		rim
SiO ₂	38.48	38.44	38.32	38.06	38.23	37.80	38.06	38.20	38.04	38.15	38.13	38.39
TiO ₂	0.06	0.09	-	-	-	0.14	0.07	0.06	-	0.14	0.08	0.05
Al ₂ O ₃	21.66	21.95	21.69	21.70	22.15	21.89	21.97	21.53	21.86	21.48	21.99	21.81
FeO	23.77	23.46	25.59	25.98	25.27	24.30	24.73	24.51	26.70	25.12	25.25	26.31
MnO	0.33	0.46	0.41	0.49	0.37	0.56	0.42	0.46	0.55	0.72	0.61	0.40
MgO	5.18	5.02	5.52	6.23	6.30	4.95	4.78	4.91	5.63	4.80	5.23	6.17
CaO	10.16	10.50	8.20	7.52	7.66	10.21	9.92	10.25	7.21	9.33	8.65	6.77
Total	99.64	99.92	99.73	99.98	99.98	99.85	99.95	99.92	99.99	99.74	99.94	99.90
Si	3.01	2.98	3.00	2.97	2.97	2.97	2.97	2.98	2.97	3.00	2.97	2.99
Ti	-	0.01	-	-	-	0.01	-	-	-	0.01	0.01	-
Al	1.99	2.01	2.00	1.99	2.03	2.02	2.02	1.98	2.01	1.99	2.02	2.00
Fe	1.55	1.52	1.66	1.69	1.64	1.59	1.61	1.60	1.74	1.64	1.65	1.71
Mn	0.02	0.03	0.03	0.03	0.02	0.04	0.03	0.03	0.04	0.05	0.04	0.03
Mg	0.60	0.58	0.64	0.72	0.73	0.58	0.56	0.57	0.66	0.56	0.61	0.71
Ca	0.85	0.87	0.69	0.63	0.64	0.85	0.83	0.86	0.60	0.78	0.72	0.56
X _{Fe}	0.72	0.72	0.72	0.70	0.69	0.73	0.74	0.74	0.73	0.74	0.73	0.70
Alm	51.3	50.6	55.2	55.1	54.2	51.9	53.3	52.3	57.4	54.2	54.5	56.7
Sps	0.7	1.0	0.9	1.0	0.8	1.2	0.9	1.0	1.2	1.6	1.3	0.9
Prp	19.9	19.3	21.2	23.5	24.0	18.9	18.4	18.7	21.6	18.4	20.2	23.7
Grs	28.1	29.0	22.7	20.4	21.0	28.0	27.4	28.0	19.8	25.8	24.0	18.7

rate prisms, and most probably their simultaneous crystallization reflect the miscibility gap between them (Spear, 1982). Garnets are without inclusions, and the inner part of grains have the weak prograde zoning (increasing Prp content to outward from 26 to 29 %, and decreasing Grs from 23 to 20 %), and the retrograde zoning in the rims (an inverse behaviour of Prp and Grs, Tab. 4, Fig. 6 – s. PO3). Garnet grains are also replaced by very fine-grained „black“ Al-pargasite (Tab. 5)-oligoclase/andesine-epidote kelyphitic rims. The strongly linear textures of symplectitic aggregates in Bar amphibolites are parallel to overall macroscopic subhorizontal stretching lineation of the Strieden complex within the transpression shear zone.

Owing to widespread formation of the reactional Hbl2-Ep2-Pl2 symplectites (Fig. 5b) always separating the Grt and Bar, the use of Grt-Hbl thermometry is problematic. Unfortunately, it is also impossible to use the Hbl-Grt-Pl-Qtz geobarometer because it is applicable (Kohn and Spear, 1990) only for associations containing the ordinary Ca-amphiboles, but not the Na-Ca barroisite.

The host rocks of metabasites are metapelites or Bt-Grt, St-Ky or Ky-Grt gneisses and migmatitic gneisses. The light-coloured mica-poor fine- to medium-grained orthogneiss bodies and medium- to coarse-grained orthogneisses represent original granitoid bodies within the metapelites. Some of them are feldspar-poor and resemble eclogitic mica-schists.

4.2. Strieden structural complex

The Strieden complex shows variable degree of Alpine overprint, depending on distance from the MMZ

(dextral strike slip shear zone). Deformation gradient culminates in fragments included into this deformation zone with predominating mineral assemblage of Alpine overprint. Such ductilely deformed rocks show subparallel fabrics and a unified kinematics with the exhumed HP rocks of the Polinik structural complex within the same shear zone. The latter fact speaks for common final exhumation of the HP Polinik and MP Strieden basement fragments.

In the Strieden complex Grt in all types of studied metapelitic/metapsammitic rocks (associated with normal amphibolites) have a prograde zoning along the whole profile (increasing Prp content from 5 % in the core to 10% in the rim); sometimes the prograde zoning is complicated by very narrow retrograde rims with an inverse - decreasing Prp content to 7-8 %. Grossular content is very low in garnets from Al-rich St-Grt schists (8 % in cores, and 3 % in the prograde rims), and it is high in Grt±Cal±Hbl-mica gneisses (about 22 % along the whole profile). Staurolite (Fig. 5c) is the Zn-poor (a maximum ZnO content is 0.12 wt. %), and it has the weak zoning (X_{Fe} 0.85 in the core, and 0.88 in the rim). However Hoke (1990) found the St grains with outer Zn-rich zone that might be recrystallized older grains. Plagioclase in all types of rocks is oligoclase (10-24% An). Large flakes of the prograde Na-rich muscovite1 (X_{Na} 0.24-0.25), and Bt (X_{Fe} 0.47-0.62), together with oligoclase and quartz are the major minerals of the matrix. Among common Bt and Ms1, large flakes of the prograde chlorite1 (X_{Fe} 0.52-0.57) are sometimes retained in matrix.

Grt-Bt geothermometry of St-Grt gneisses yields the maximum temperature of metamorphism at 614 °C

Tab. 2. Microprobe analyses of Cpx1 (large grains) and Cpx2 (from Hb2-Cpx2-Olg symplectites). Grt-Cpx-Czo-Hb±Bt eclogitic amphibolite. Polinik structural complex. PO1 and PO5 samples location according to Fig. 4.

Sample	s. PO5									s. PO1								
Type	Cpx ¹ large grains								Cpx ² from Hb ² ±Cpx ² ±Olg ² rims			Cpx ¹ large grains						
Name	sodic Aug								Aug			sodic Aug						
SiO ₂	54.52	54.38	54.12	54.70	54.24	54.63	54.43	54.76	53.20	53.08	54.05	54.65	54.20	54.16	54.45	54.06		
TiO ₂	0.05	-	0.06	0.10	0.16	0.09	0.03	0.17	0.08	-	-	0.09	0.15	0.07	0.09	0.12		
Al ₂ O ₃	5.14	5.18	4.10	4.97	5.26	4.86	4.99	4.61	1.27	3.04	1.22	3.97	3.68	3.98	3.14	2.63		
FeO	5.55	5.50	5.71	5.77	5.76	5.63	6.18	5.43	6.34	5.55	6.09	5.63	6.24	6.04	5.91	5.89		
MnO	-	0.04	0.04	-	0.03	0.12	-	-	0.04	0.09	0.08	0.05	0.01	-	0.07	-		
MgO	12.09	12.05	12.54	12.04	12.23	12.24	12.06	12.38	13.87	14.02	14.29	12.92	12.88	12.82	13.21	13.74		
CaO	19.43	19.49	20.39	19.31	19.10	19.09	18.92	19.56	24.79	23.58	23.46	20.30	20.78	20.53	21.16	21.97		
Na ₂ O	3.18	3.27	3.95	3.09	3.15	3.24	3.33	3.05	0.38	0.58	0.78	2.26	1.99	2.28	1.94	1.54		
K ₂ O	-	0.05	0.06	-	0.03	0.06	0.02	-	-	0.03	-	0.09	0.02	0.02	-	0.02		
Total	99.96	99.96	99.97	99.98	99.96	99.96	99.96	99.96	99.97	99.97	99.97	99.96	99.95	99.95	99.97	99.97		
Si	1.99	1.98	1.98	1.99	1.98	1.99	1.99	1.99	1.97	1.95	1.99	1.99	1.99	1.98	1.99	1.98		
Al _{IV}	0.01	0.02	0.02	0.01	0.02	0.01	0.01	0.01	0.03	0.05	0.01	0.01	0.01	0.02	0.01	0.02		
Al _{VI}	0.21	0.20	0.16	0.20	0.21	0.20	0.20	0.19	0.03	0.08	0.04	0.16	0.16	0.15	0.13	0.09		
Ti	-	-	-	-	0.01	-	-	0.01	-	-	-	-	-	-	-	-		
Fe ³⁺	0.01	0.01	0.04	0.01	-	0.02	0.02	0.02	-	-	0.01	-	-	-	0.01	-		
Fe ²⁺	0.16	0.16	0.14	0.17	0.18	0.15	0.17	0.15	0.20	0.17	0.18	0.17	0.19	0.19	0.17	0.18		
Mn	-	-	-	-	-	0.01	-	-	-	-	-	-	-	-	-	-		
Mg	0.66	0.66	0.68	0.65	0.66	0.66	0.66	0.67	0.77	0.77	0.79	0.70	0.70	0.70	0.72	0.75		
Ca	0.76	0.76	0.80	0.75	0.75	0.74	0.74	0.76	0.99	0.93	0.93	0.79	0.81	0.81	0.83	0.86		
Na	0.22	0.23	0.21	0.22	0.22	0.23	0.24	0.21	0.03	0.04	0.06	0.16	0.14	0.16	0.14	0.11		
K	-	-	-	-	-	-	-	-	-	-	-	-	-	-	-	-		
X _{Fe}	0.20	0.19	0.17	0.21	0.21	0.19	0.20	0.18	0.21	0.18	0.19	0.20	0.21	0.21	0.20	0.19		
Jd	21.7	21.9	17.3	21.2	22.0	20.6	21.1	19.6	2.7	4.2	5.3	16.4	14.1	16.1	13.5	10.9		
Acm	0.4	1.0	3.4	0.5	-	2.3	2.1	1.7	-	-	0.3	-	-	-	0.2	-		
Aug	77.9	77.1	79.3	78.3	78.0	77.1	76.8	78.7	97.3	95.8	94.4	83.6	85.9	83.9	86.3	89.1		

Tab. 3. Microprobe analyses of Hb1 (large grains, and inclusions in Grt), and Hb2 (rims around Grt, and from Hb2-Cpx2-Olg symplectites around Cpx1). Grt-Cpx-Czo-Hb±Bt eclogitic amphibolite. Polinik structural complex. PO1 and PO5 samples location according to Fig. 4.

TYPE	Hb ¹ in matrix				Inclusions of Hb ¹ in Grt				Hb ² around Grt				Hb ² from Hb ² ±Cpx ² ±Olg ² rims			
	PO5		PO1		PO5		PO1		PO5		PO1		PO5		PO1	
SiO ₂	49.03	50.81	49.69	49.94	48.57	50.23	48.83	50.44	43.02	39.84	40.90	39.17	50.12	52.79	52.62	49.90
TiO ₂	0.63	0.43	0.59	0.52	0.46	0.58	0.67	0.47	0.16	0.06	0.10	0.24	0.23	0.02	0.17	0.45
Al ₂ O ₃	9.18	7.91	8.64	7.83	10.73	8.79	10.07	8.83	16.71	21.02	18.67	19.87	7.42	4.77	5.56	7.49
FeO	10.20	9.44	9.84	10.77	10.60	10.19	10.61	9.49	15.50	16.80	17.83	15.40	10.41	9.68	9.37	11.79
MnO	0.20	0.08	0.10	-	-	-	0.04	0.04	0.05	0.17	0.29	0.07	0.14	0.14	0.08	0.25
MgO	15.68	16.39	16.02	16.10	14.56	15.22	15.07	16.27	9.25	6.35	7.20	8.30	15.24	16.60	16.58	14.82
CaO	10.03	10.50	10.74	10.32	10.38	10.40	10.69	10.51	10.66	10.56	10.98	11.14	12.71	13.10	12.52	12.14
Na ₂ O	2.51	1.70	1.97	1.57	2.07	2.12	1.74	1.77	2.37	2.43	2.16	3.05	1.05	0.42	0.37	0.80
K ₂ O	0.60	0.46	0.57	0.51	0.52	0.57	0.47	0.53	0.32	0.21	0.11	0.22	0.14	-	0.11	0.13
Total	98.06	97.72	98.16	97.56	97.89	98.10	98.19	98.35	98.04	97.44	98.24	97.46	97.46	97.52	97.38	97.77
Si	6.90	7.12	6.99	7.02	6.86	7.08	6.86	7.02	6.24	5.87	5.99	5.78	7.20	7.51	7.44	7.11
Al _{IV}	1.10	0.88	1.01	0.98	1.14	0.92	1.14	0.98	1.76	2.13	2.01	2.22	0.80	0.49	0.56	0.89
Al _{VI}	0.42	0.43	0.42	0.32	0.64	0.54	0.53	0.47	1.10	1.52	1.21	1.24	0.46	0.31	0.37	0.37
Ti	0.07	0.05	0.06	0.05	0.05	0.06	0.07	0.05	0.02	0.01	0.01	0.03	0.02	-	0.02	0.05
Fe ³⁺	0.73	0.68	0.60	0.94	0.61	0.43	0.70	0.71	0.58	0.54	0.71	0.49	0.08	0.06	0.23	0.47
Fe ²⁺	0.47	0.43	0.55	0.33	0.64	0.77	0.55	0.40	1.29	1.52	1.47	1.41	1.17	1.09	0.87	0.94
Mn	0.02	0.01	0.01	-	-	-	-	-	0.01	0.02	0.04	0.01	0.02	0.02	0.01	0.03
Mg	3.29	3.42	3.35	3.37	3.06	3.20	3.15	3.37	2.00	1.39	1.57	1.83	3.26	3.52	3.49	3.15
Ca	1.51	1.58	1.62	1.55	1.57	1.57	1.61	1.57	1.66	1.67	1.72	1.76	1.95	2.00	1.90	1.85
Na	0.68	0.46	0.54	0.43	0.57	0.58	0.47	0.48	0.67	0.69	0.61	0.87	0.29	0.12	0.10	0.22
K	0.11	0.08	0.10	0.09	0.09	0.10	0.08	0.09	0.06	0.04	0.02	0.04	0.03	-	0.02	0.02
X _{Fe}	0.27	0.25	0.26	0.27	0.29	0.27	0.28	0.25	0.49	0.60	0.59	0.51	0.28	0.25	0.24	0.31
(Na+K) _A	0.33	0.13	0.27	0.07	0.23	0.25	0.17	0.14	0.39	0.42	0.39	0.68	0.29	0.13	0.03	0.13
Na _B	0.46	0.42	0.37	0.45	0.43	0.43	0.39	0.43	0.34	0.31	0.24	0.23	0.03	-	0.09	0.12
Name	Hb	Hb	Hb	Hb	Hb	Hb	Hb	Hb	Ts	Ts	Ts	Prg	Hb	Act _{Al}	Hb	Hb

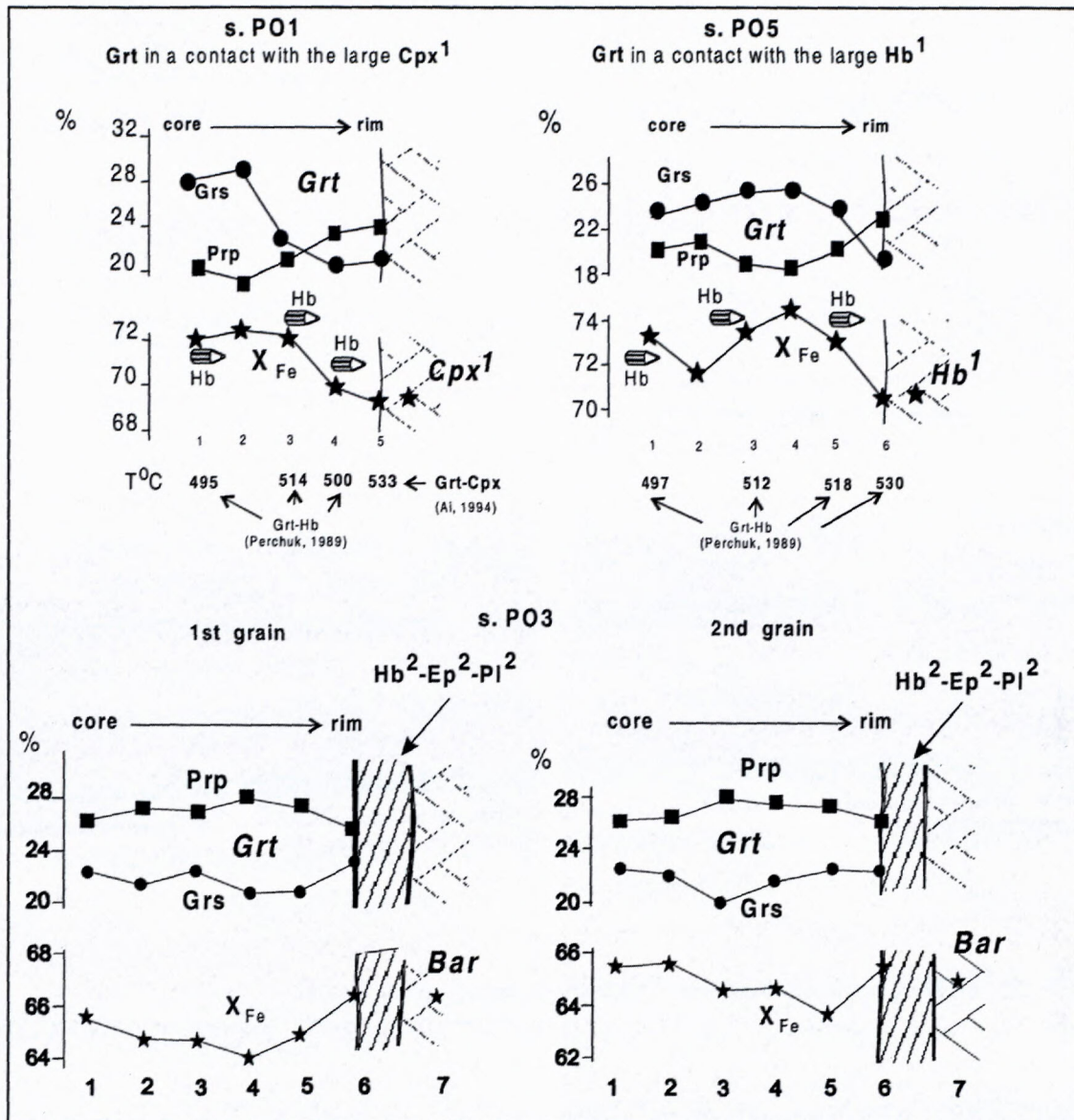


Fig. 6. (a) Compositional profile of Grt grains (s. PO1 and PO5) of HP Na-Aug-bearing eclogitic amphibolite and T estimates of prograde metamorphic stage using Grt-Cpx and Grt-Hb thermometry. The Hb „pencils“ indicate places of Hb inclusions along the Grt profile, used for Grt-Hb thermometry. (b) Compositional profile of Grt grains (s. PO3, with indicated Hb inclusions) of Bar amphibolite (a, b - the Polinik structural complex).

(Kleemann and Reinhardt, 1994). We consider the temperatures around 600 °C to be realistic for the pre-Alpine (Variscan) prograde burial stage.

And-Sil gneisses of the Strieden complex (Fig. 5d) also contain snowball-shaped Sil-Bt aggregates, pre-Alpine (Variscan) in age. The recrystallization of this aggregate led to formation of the rounded clusters of fine grains of Cld, Ms and Mgr probably due to reaction of Pl with Sil and Bt. Thus Cld, Ms and Mgr seem to be Alpine (D1, 2) recrystallization minerals of the originally Variscan gneisses. The same newly-formed minerals are observable in the Polinik Ky-Grt gneisses, where they belong to Alpine retrograde or exhumation D2 stage (Hoke, 1990). The temperatures around 500 °C are inferred for the Cretaceous (D1) collision stage of the AA Strieden complex, when the low-medium-T Cld-Mgr-Ms

association formed in metapelites of the complex. Such minerals are roughly corresponding to those of the D2 stage found in the Polinik eclogitic and barroisitic amphibolites (Hbl-bearing reactional rims and symplectites) and their host Ky-Grt gneisses, respectively. Because of these similarities and because such aggregates occur as accompanying mylonitic fabrics, the discussed newly-formed mineral assemblage of the Strieden complex is considered to be Alpine (Cretaceous) in age.

5. Microfabrics of quartz and calcite-dolomite mylonites

Thickening of the crust (include the mantle-lithosphere, after Stüwe and Sandiford, 1995) during Cretaceous deformation (e.g. Behrmann and Wallis, 1987; Laubscher, 1989;

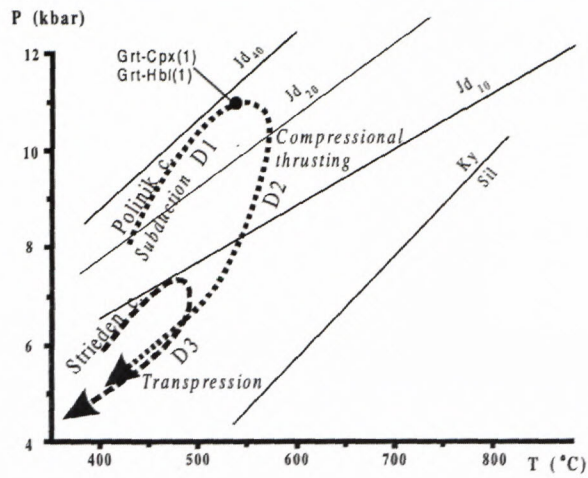


Fig. 7. Estimated P - T - t -paths of the Polinik and Strieden structural complexes in the Kreuzeck Massif (Area 2) based on thermo-barometric estimates (Fig. 6, Tab. 1-3).

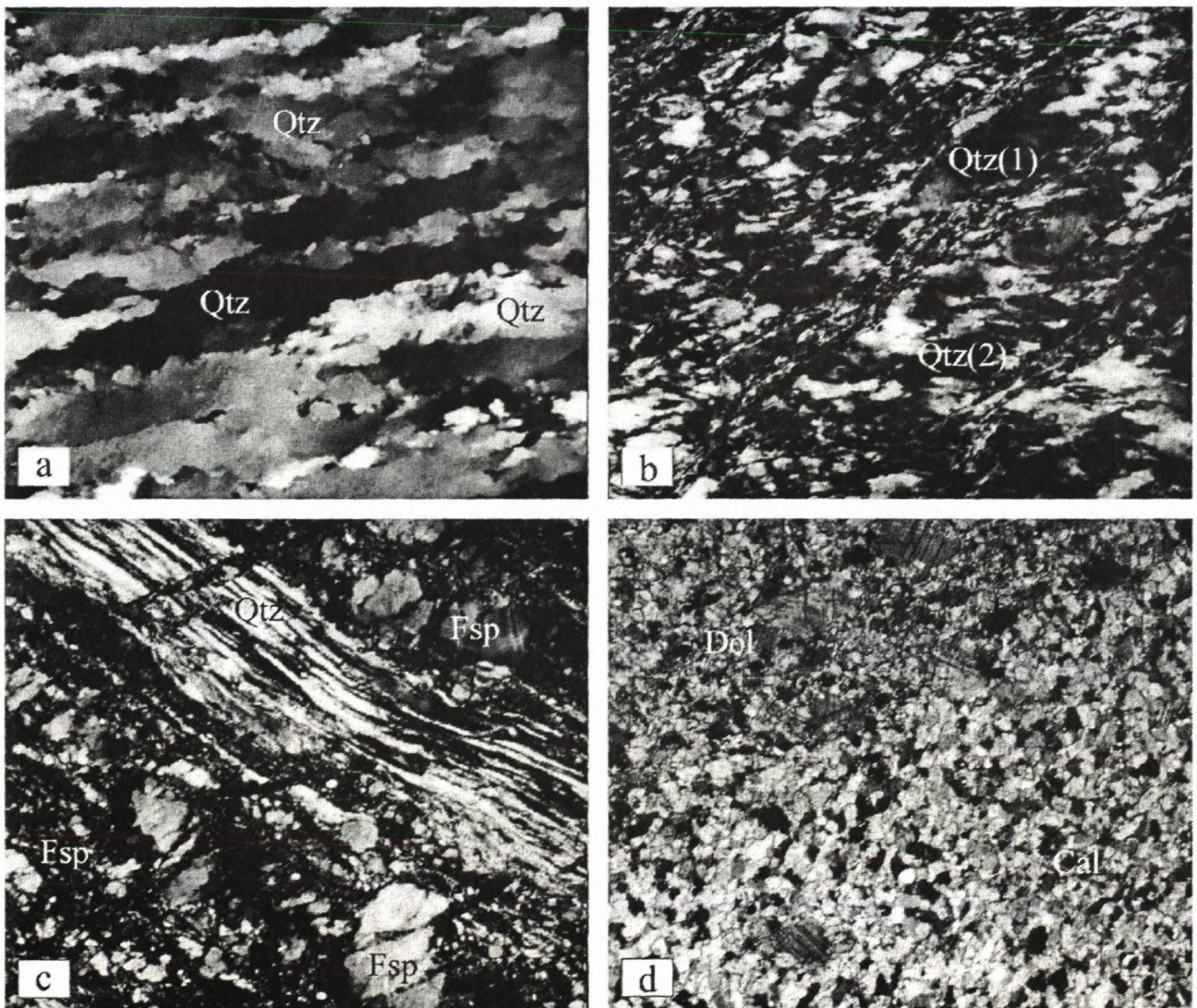


Fig. 8. Microstructures of mylonitic rocks of the Austro-Alpine structural complexes in the Area 2. Sample-location according to Fig. 4. (a) Qtz ribbons of a quartz-layer in gneiss mylonite (sample KR4). (b) Oblique Qtz recrystallized (new) grains indicating top-to-WNW shearing, quartzitic layer in micaschist-gneiss mylonite (s. KR5). (c) Plastic flow in thinned Qtz layer vs. cataclastic flow in Fsp layer, pegmatitic orthogneiss mylonite (s. KR6). (d) Alternation of calcite mylonitic and mylonitic/cataclastic dolomite layers in marble mylonite (s. KR1). (e) Alternation of Qtz and Fsp layers; deformation bands in plastically stretched Fsp layer (dark stripes). (f) Migrative deformation bands boundaries in Qtz. (g) A detail of (e) with two systems of bands: parallel and oblique to mylonitic foliation. (h) EBS image of dolomite porphyroclast with distinct deformation lamellae and core-mantle structure as the evidence of plastic deformation (s. KR1). Magnification: 18x (b, c), 27x (a), 67x (d).

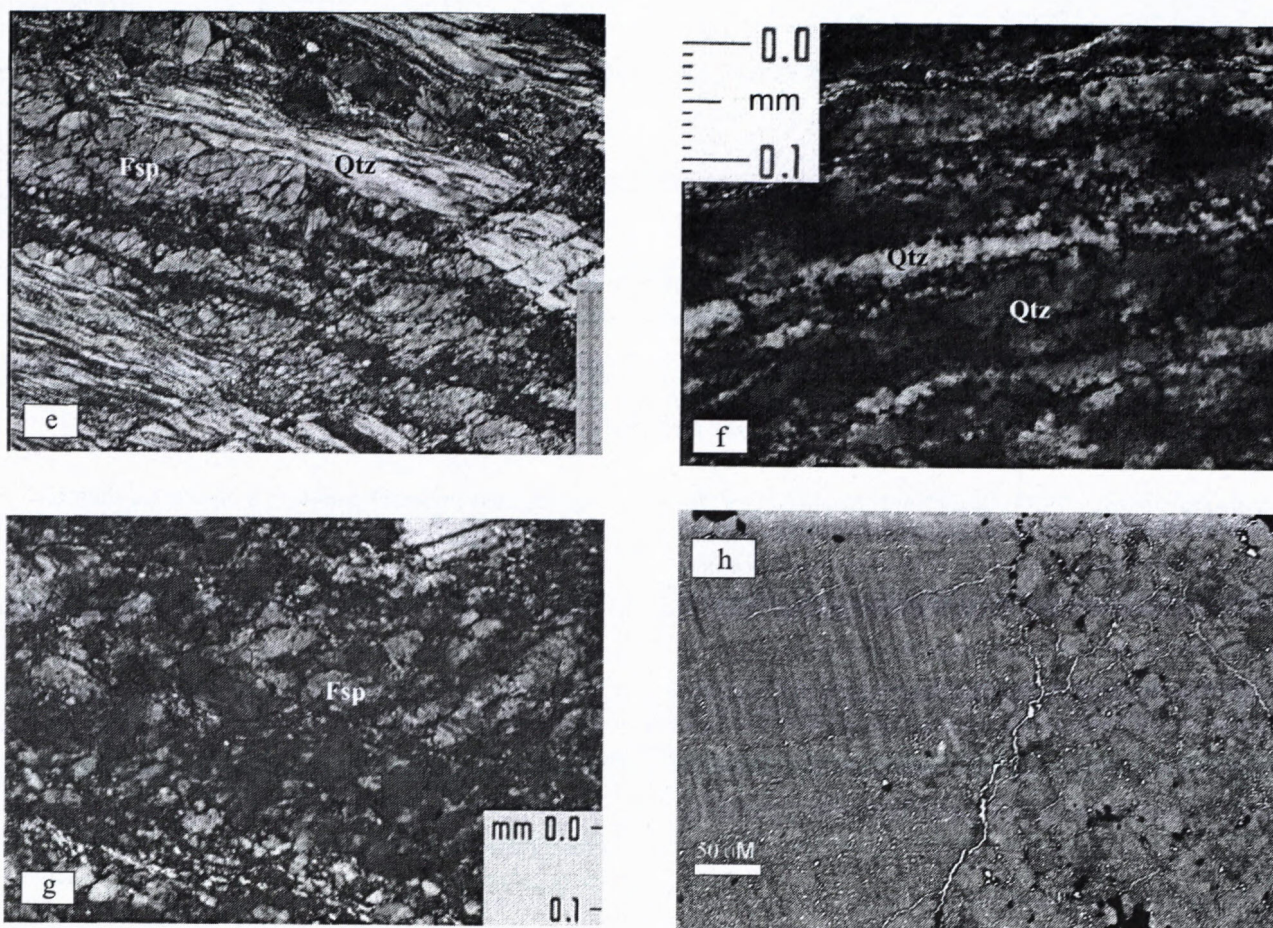


Fig. 8e-h

Tab. 4. Microprobe analyses of zonal Grt surrounded by the Hb2-Ep2-Pl2 rims. Grt-Bar amphibolite. Polinik structural complex. PO3 sample location according to Fig. 4.

	1st Grt grain						2nd Grt grain					
	core			rim			core			rim		
SiO ₂	38.83	38.55	38.96	38.59	38.80	38.78	38.47	38.46	38.07	38.50	38.08	38.76
TiO ₂	0.08	0.13	0.12	0.06	-	0.01	-	-	0.13	0.09	0.08	0.06
Al ₂ O ₃	22.12	22.26	22.11	22.22	21.95	22.07	22.15	22.12	22.02	22.10	21.81	22.02
FeO	23.23	23.41	23.62	23.38	22.91	23.30	23.63	23.64	23.45	23.67	24.25	23.54
MnO	0.61	0.69	0.60	0.50	0.57	0.64	0.60	0.50	0.63	0.49	0.60	0.47
MgO	6.85	6.86	7.29	7.17	7.31	6.81	6.96	7.29	7.14	7.48	7.34	6.61
CaO	8.18	8.03	7.23	7.91	8.34	8.09	8.12	7.87	8.16	7.42	7.70	8.46
Total	99.90	99.93	99.93	99.83	99.88	99.70	99.93	99.88	99.78	99.75	99.86	99.92
Si	3.00	2.97	3.00	2.99	2.99	3.00	2.98	2.98	2.96	2.99	2.96	2.99
Ti	-	0.01	0.01	-	-	-	-	-	0.01	-	-	-
Al	2.00	2.02	2.00	2.02	1.99	2.01	2.01	2.01	2.03	2.02	1.99	2.00
Fe	1.50	1.51	1.52	1.51	1.47	1.51	1.53	1.52	1.52	1.52	1.57	1.52
Mn	0.04	0.04	0.04	0.03	0.04	0.04	0.04	0.03	0.04	0.03	0.04	0.03
Mg	0.79	0.79	0.83	0.82	0.84	0.78	0.80	0.84	0.82	0.86	0.85	0.76
Ca	0.67	0.66	0.60	0.65	0.69	0.67	0.67	0.65	0.68	0.61	0.64	0.70
X _{Fe}	0.66	0.66	0.64	0.65	0.64	0.66	0.66	0.64	0.65	0.64	0.65	0.67
Alm	49.9	50.2	50.8	50.0	48.5	50.2	50.2	50.0	49.6	50.4	50.7	50.5
Sps	1.3	1.5	1.3	1.1	1.3	1.4	1.3	1.1	1.3	1.1	1.3	1.0
Prp	26.3	26.2	28.0	27.3	27.6	26.1	26.4	27.5	26.9	28.3	27.4	25.3
Grs	22.5	22.1	19.9	21.6	22.6	22.3	22.1	21.4	22.2	20.2	20.6	23.2

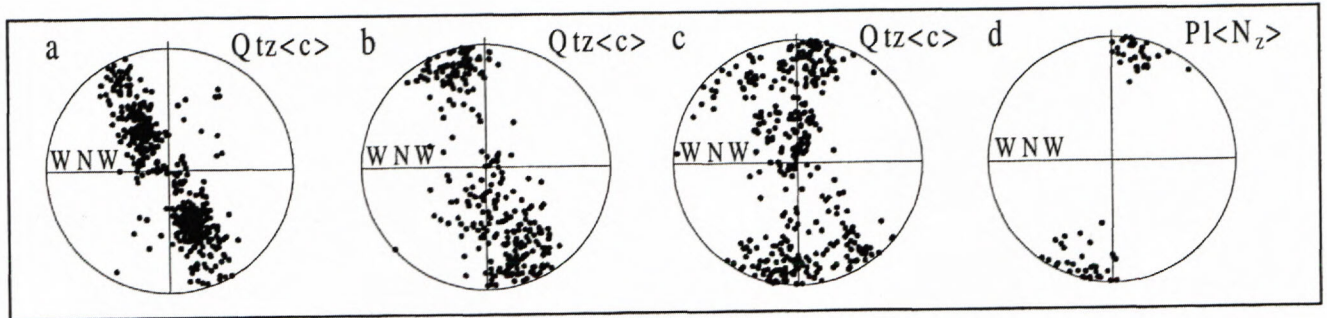


Fig. 9. The U-stage microscope patterns of Qtz and Cal of the Austro-Alpine structural complexes in the Area 2. The microstructures see in Fig. 8a-c. The asymmetric patterns indicate a top-to-W transpressional shear. (a) A rhomb slip in Qtz ribbons, mylonitic gneiss (s. KR4, measured only relic ribbon grains from parallel sections and not recrystallized grains, N=479). (b) Basal $\langle a \rangle$ slip in Qtz, quartzitic layer in mylonitic gneiss (s. KR5, N=287). (c) Prism $\langle a \rangle$ and basal $\langle a \rangle$ slip in Qtz, pegmatitic orthogneiss (s. KR6, N=305). (d) Relic preferred orientation of Pl(Nz) (s. KR6, N=66) indicates (010) [001] slip, pegmatitic orthogneiss.

Ratschbacher et al., 1989; Kurz and Neubauer, 1996; Wallis and Behrmann, 1996; Lammerer and Weger, 1998) resulted in Late Cretaceous to Early Tertiary emplacement of the AA structural complexes (the AA unit) onto the Pennine ones (Fig. 1-4). However, this event can be independent or postdating early-Alpine reactivation of the AA basement structural complexes. Although the radiometric ages are very rare, and most of them point to early Cretaceous exhumation of the AA basement rocks (Thöni and Jagoutz, 1992, 1993; Dallmeyer et al., 1992, 1998), the kinematics of the brittle-ductile exhumation shear zone in the Kreuzeck Massif seems to reflect early-Tertiary reactivation of the AA basement during the final exhumation of HP and MP rocks of the discussed AA Polinik and Strieden structural complexes.

The next part of the paper is devoted to microfabrics of the Polinik (sample KR4) and Strieden (samples KR1 - 6) AA structural complexes in the dextral strike slip shear zone dividing the whole Kreuzeck Massif in the WNW-ESE direction. The western part of this zone was termed by Hoke (1990) as the main mylonite zone (MMZ). This zone seems to be exhumation „suture“ of the Polinik and Strieden structural complexes. Moreover, we tried to find principal characteristics of evolution of textural patterns from the Kreuzeck Massif transpression shear zone comparing them to those from the normal-fault shear zone of eastern edge of the Pennine Tauern Window (samples HT 23, 30, 34) (Genser and Neubauer, 1989). The chosen samples represent characteristic diversity of a few tens of studied samples.

5.1. Microfabrics of quartz mylonites from the strike slip shear zone

The Qtz-rich layers in the light-coloured leucocrate granitic gneiss (s. KR4) of the Polinik Complex (Fig. 8a) are composed of large flattened Qtz ribbons (Wilson, 1975; Vauchez, 1980; Culshaw and Fyson, 1984; McLelland, 1984) with transitions into dynamically recrystallized grain aggregate.

The U-stage pole-figure (Fig. 9a) shows two maxima at the medium distance from the centre. This pattern is only characteristic for the large Qtz grains visible in form

of ribbons and indicates a higher-temperature rhomb slip system dominated during their plastic deformation.

The texture goniometer patterns (Fig. 10/1a,b) however reflect a bulk deformation of the same sample and represent the lower temperature basal $\langle a \rangle$ slip within the dynamically recrystallized aggregate replacing the ribbonous grains.

The straight Qtz-rich layers in paragneiss (s. KR5) of the Strieden Complex display a very pronounced preferred orientation of internal obliquely oriented new grains (Fig. 8b). Concentrations of muscovite flakes between the Qtz layers indicate original metamorphic foliation of paragneisses and quartzitic gneisses to muscovite quartzites. The newly-formed internal oblique grains of the Qtz layers exhibit unified extinction with the maximum optical (N_z/c) direction parallel to prismatic grain boundaries. Asymmetry of newly-formed grains is thus related to non-coaxial strain within the strike slip shear zone (Burg, 1986). The width of grains varies and depends on shape of almost equidimensional, through elongated up to fibrous grains which are sigmoidally rotated into direction parallel with the C-planes ($//$ to former metamorphic foliation). Fine-grained aggregate of Qtz along the C-planes represents narrow zones of high strain localization.

The U-stage pole figure pattern (Fig. 9b) confirms lower temperature non-coaxial deformation and the basal $\langle a \rangle$ slip system active within recrystallized Qtz layers.

The X-ray texture goniometer patterns (Fig. 10/2a,b) are compatible and also suggest basal $\langle a \rangle$ slip dominated in a simple shear regime.

Higher deformation rates at lower temperatures are indicated by the contemporary running dislocation creep in Qtz and cataclastic flow in Fsp layers (Fig. 8c) in mylonitic orthogneisses (originally pegmatitic veins, s. KR6) of the Strieden complex. The Qtz layers contain extremely stretched fibrous deformation bands. They have clearly migrative boundaries (Fig. 8f) showing dynamic bulging and formation of nearly equidimensional new grains probably due to dynamic rotation recrystallization mechanism (Poirier and Guillopé, 1978; Gleason and Tullis, 1993; Trimby et al., 1998).

Tab. 5. Microprobe analyses of amphiboles: large grains of Bar(=Am1), Ed-Prg and Act (=Am2) from Hb2-Act-Olg symplectites; Prg(=Am2) from Hb2-Ep-Olg rims around Grt. Grt-Bar amphibolite. Polinik structural complex. PO3 sample location according to Fig. 4.

Position	LARGE GRAINS IN MATRIX				Hb ² -Act ² -Olg ² symplectites									HB ² -EP ² -OLG ² RIMS around Grt		
	Bar ¹				Ed-Prg ²						ACT ²			Prg ²		
SiO ₂	47.43	45.81	47.16	47.87	44.10	43.90	44.49	43.81	41.24	45.10	53.73	52.76	55.21	40.19	40.42	37.78
TiO ₂	0.38	0.46	0.46	0.48	0.62	1.06	0.45	0.62	0.19	0.55	0.17	0.15	0.13	0.20	0.17	-
Al ₂ O ₃	13.62	13.35	13.56	14.09	12.40	11.86	13.80	12.66	15.47	11.14	2.59	5.25	1.39	16.87	16.96	20.83
FeO	11.13	12.40	12.16	10.38	14.08	13.46	13.34	13.02	16.39	13.36	11.51	9.32	9.48	15.42	15.72	17.24
MnO	0.21	0.14	0.18	-	0.09	0.01	0.19	0.14	0.13	0.15	0.39	0.13	0.27	0.25	0.17	0.36
MgO	13.19	13.45	13.10	13.22	12.00	12.59	12.07	12.51	10.09	12.85	16.02	16.47	17.90	9.66	9.68	7.54
CaO	8.92	9.19	9.22	8.49	11.73	11.97	10.70	12.04	11.48	12.08	12.73	12.94	12.87	11.66	11.62	10.82
Na ₂ O	2.94	2.63	2.12	3.25	1.77	1.84	2.28	1.75	2.02	1.76	0.21	0.32	0.17	2.51	2.57	2.93
K ₂ O	0.46	0.60	0.38	0.52	0.97	0.92	0.87	1.02	1.06	0.66	0.10	0.11	-	1.17	0.87	0.23
Total	98.28	98.03	98.34	98.30	97.76	97.61	98.19	97.57	98.07	97.65	97.45	97.45	97.42	97.93	98.18	97.73
Si	6.64	6.45	6.57	6.68	6.45	6.44	6.40	6.41	6.06	6.58	7.70	7.50	7.82	5.96	5.96	5.57
Al _{IV}	1.36	1.55	1.43	1.32	1.55	1.56	1.60	1.59	1.94	1.42	0.30	0.50	0.18	2.04	2.04	2.43
Al _{VI}	0.89	0.66	0.80	1.00	0.59	0.49	0.74	0.59	0.74	0.50	0.14	0.48	0.05	0.91	0.90	1.19
Ti	0.04	0.05	0.05	0.05	0.07	0.12	0.05	0.07	0.02	0.06	0.02	0.02	0.01	0.02	0.03	-
Fe ³⁺	0.84	1.20	1.14	0.72	0.47	0.39	0.67	0.39	0.77	0.40	0.14	0.05	0.14	0.45	0.54	0.96
Fe ²⁺	0.46	0.25	0.27	0.49	1.25	1.26	0.93	1.20	1.25	1.23	1.24	1.06	0.98	1.46	1.39	1.16
Mn	0.02	0.02	0.02	-	0.01	-	0.02	0.02	0.02	0.02	0.05	0.02	0.03	0.03	0.02	0.04
Mg	2.75	2.82	2.72	2.75	2.61	2.75	2.59	2.73	2.21	2.79	3.42	3.49	3.78	2.13	2.12	1.65
Ca	1.34	1.38	1.38	1.27	1.84	1.88	1.65	1.89	1.81	1.89	1.95	1.97	1.95	1.85	1.83	1.71
Na	0.80	0.72	0.57	0.88	0.50	0.52	0.64	0.50	0.58	0.50	0.06	0.09	0.05	0.72	0.73	0.84
K	0.08	0.11	0.07	0.09	0.18	0.17	0.16	0.19	0.20	0.12	0.02	0.02	-	0.22	0.16	0.04
X _{Fe}	0.33	0.34	0.35	0.31	0.40	0.37	0.39	0.37	0.48	0.37	0.29	0.24	0.23	0.48	0.48	0.57
(Na+K) _A	0.24	0.23	0.04	0.24	0.53	0.58	0.47	0.59	0.60	0.53	0.08	0.09	0.03	0.82	0.75	0.75
Na _B	0.64	0.60	0.60	0.73	0.15	0.12	0.33	0.10	0.18	0.09	-	0.02	0.01	0.12	0.14	0.14

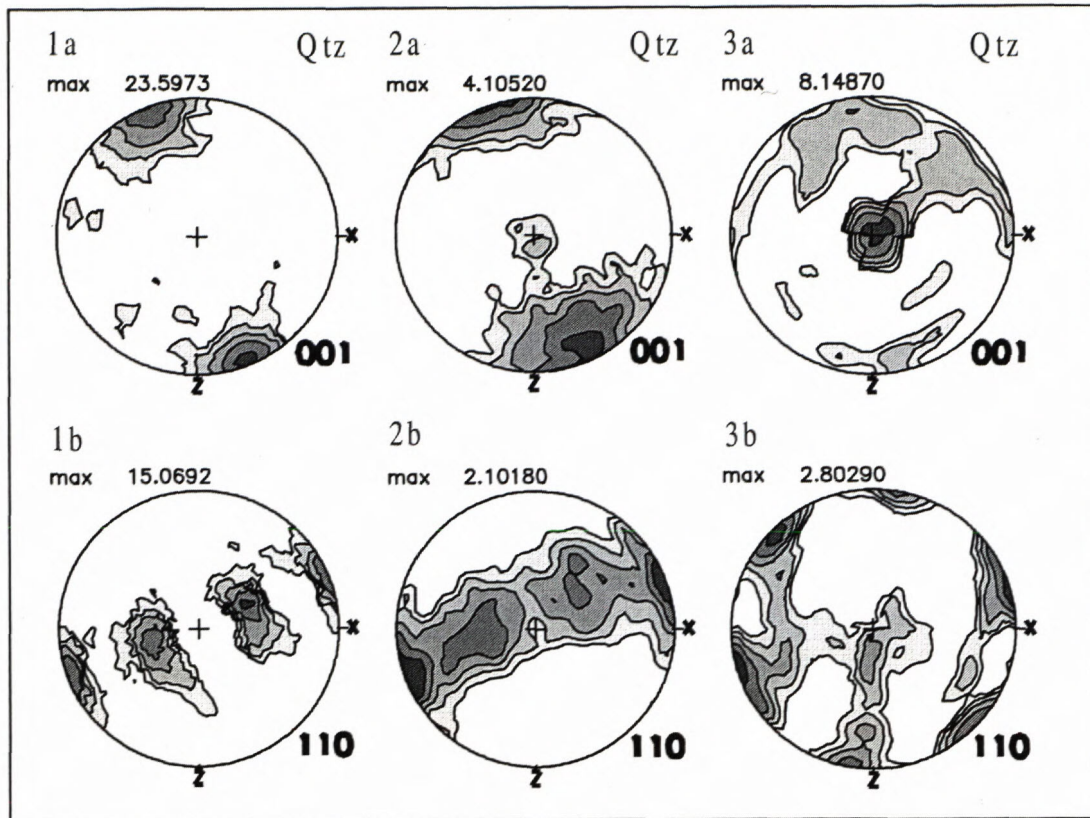


Fig. 10. X-ray texture goniometer patterns of Qtz of the Austro-Alpine structural complex in the Area 2. The microstructures see in Fig. 8a-c. The asymmetric patterns indicate a top-to-W transpressional shear. (1a, b) Basal $\langle a \rangle$ slip in Qtz of a gneiss mylonite (s. KR4, measured bulk deformation fabric with prevailing recrystallized grains). (2a, b) Basal $\langle a \rangle$ slip in Qtz, quartzitic layer in mylonitic gneiss (s. KR5). (3a, b) Dominated prism $\langle a \rangle$ slip in Qtz, pegmatitic orthogneiss (s. KR6).

The cataclastic gouge in Fsp layers seems to be the result of both, the higher strain rates and fluid pressures at the temperatures insufficient for the plastic flow. The Fsp layers and their porphyroclasts however preserve microfabrics of former plastic deformation (Jensen and Starkey, 1985). They are: deformation lamellae, narrow deformation bands with migrative boundaries parallel or oblique to mylonitic/cataclastic foliation (Fig. 8e, g).

The U-stage pole figure of Qtz (Fig. 9c) reflects prism $\langle a \rangle$ and basal $\langle a \rangle$ slips in a simple shear regime. The higher temperature stage (at about 500 °C) of plastic deformation of Fsp of some layers is indicated by preferred orientation of $PI N_z$ optical directions (Fig. 9d).

The X-ray texture goniometer patterns (Fig. 10/3a, b) confirm a dominated prism $\langle a \rangle$ slip in Qtz.

5.2. Microfabrics of calcite-dolomite marble mylonites from strike slip shear zone

Boudinaged lensoidal bodies of marbles represent original marble beds within a volcano-sedimentary probably Paleozoic (Strieden) complex. They comprise often undeformed coarse-grained (2-3 mm) Cal-Dol-Tr marbles, which transform to protomylonitic and ultramylonitic marbles towards the inner part of the strike slip shear zone. Dynamic recrystallization reflects active dis-

location creep micromechanism of plastic deformation (Fig. 8d). The relict rounded and flattened porphyroclasts exhibit dense deformation lamellae.

The microtexture of mylonitized marbles consists of two different and alternating types of bands or layers (Tab. 6, 7). One type is characteristic by almost homogeneous microtexture built of newly-formed dynamically

Tab. 6. EDS quantification results for dolomite in dolomite marble layer (s. KR1a).

Element	Gross	Net	%Wt	%At Wt	K-Ratio
Ca	928.98	902.39	43.23	26.26	0.71
Mg	357.37	339.92	24.95	24.98	0.21
C	31.10	28.12	0.71	1.44	0.00
O	95.00	91.65	31.11	47.32	0.08
Total			100.00	100.00	

Tab. 7. EDS quantification results for calcite in calcite marble layer (s. KR1b, c).

Element	Gross	Net	%Wt	%At Wt	K-Ratio
Ca	1705.41	1677.56	71.66	50.44	0.95
Mg	29.76	15.50	1.24	1.44	0.01
C	41.85	38.79	0.55	1.29	0.00
O	64.79	61.09	26.55	46.83	0.04
Total			100.00	100.00	

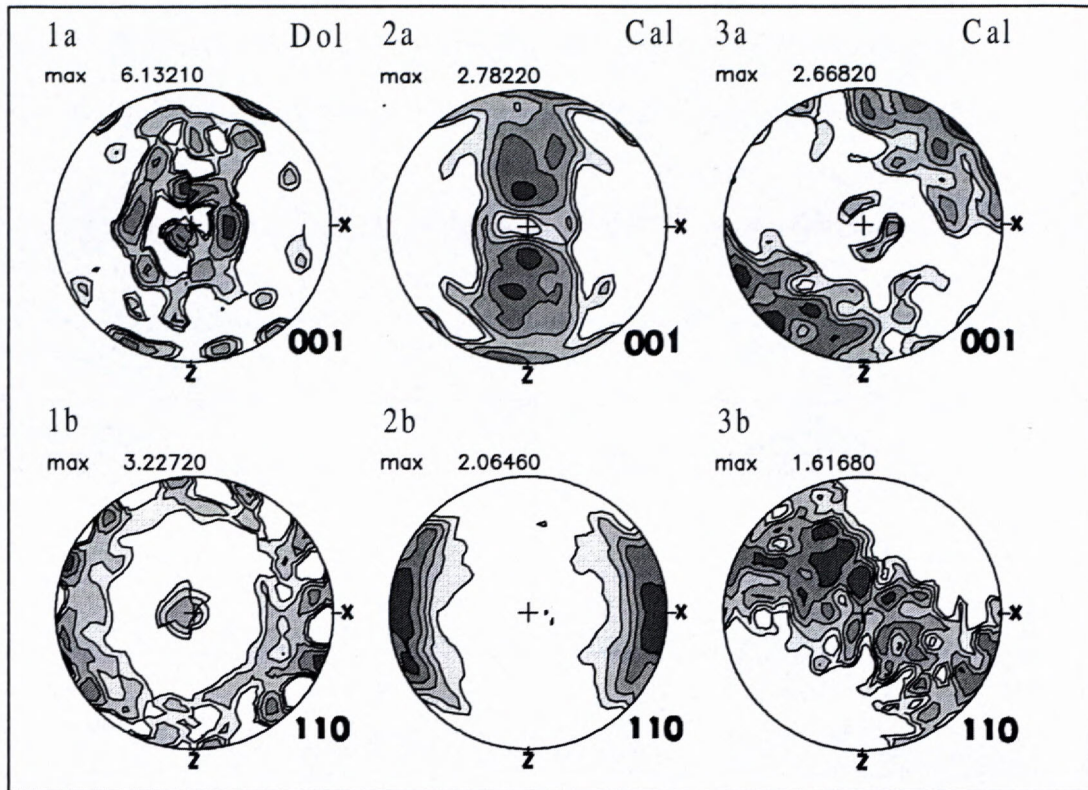


Fig. 11. X-ray texture goniometer patterns of Cal and Dol of the Austro-Alpine structural complex in the Area 2. The layered marble microstructure see in Fig. 8d. (1a,b) Dol pattern combining *f*-twinning and basal slip at *T* between 500 and 400 °C in marble layer rich in dolomite (s. KR1a). (2a,b) Almost symmetrical Cal *<c>* pattern of dynamically recrystallized marble mylonitic layer (s. KR1b). (3a,b) Asymmetrical Cal *<c>* pattern in dynamically recrystallized marble mylonitic layer (s. KR1c). The asymmetric Cal pattern indicates a top-to-W transpressional shear.

recrystallized equidimensional or polygonal grains with the straight boundaries usually meeting in the triple points. Such a mylonitic microtexture developed in Cal layers and is related to dislocation creep in marble (Nicolas and Poirier, 1976; Lafrance et al. 1994). On the other hand, neighbouring ultramylonitic/ultracataclastic layers are built of fine-grained dolomitic matrix with a lot of Dol porphyroclasts (Fig. 8d). The porphyroclasts show (*f*-) deformation lamellae and typical core-mantle structures (Fig. 8h) as the result of plastic deformation and dynamic recrystallization of their rims. Most of equidimensional (recrystallized) grains have straight boundaries meeting in the triple points, likewise in the Cal layers. They are often separated by fine-grained ultracataclastic matrix which is missing in the Cal layers. Transition from plastic to cataclastic flow (parallel to C-planes) indicates distinctive micromechanisms of flow applied due to strain partitioning between the Cal and Dol layers at the decreasing temperatures and increasing deformation rates during transpressional uplift.

The X-ray texture goniometer patterns of Dol and Cal (Fig. 11) are different, although representing the neighbouring layers (KR1a - KR1c) of the same sample (KR1). The dolomite layer (KR1a, Fig. 11/1a,b) shows a composite pattern, comprising combined *f*-twinning and a basal (001) slip. The maxima concentrated around

the middle are coeval with the angle relationship of the *c*-axes and *f*-twins (Nicolas and Poirier, 1976) subparallel with the horizontal reference line. Whereas the high-angle maxima close to the external part of the circle indicate basal slip active during the dynamic recrystallization of Dol. The neighbouring Cal mylonitic layers document either coaxial pure shear (KR1b, Fig. 11/2a,b), or non-coaxial simple shear (KR1c, Fig. 11/3a,b) in dynamically recrystallized aggregate (Wenk et al., 1987).

A remarkable change of grain size occurred in Cal layers: from 2-3(4) mm to 30-50 µm (Fig. 8d). Some rare Cal porphyroclasts are strongly (*e*-) twinned. Dol layers consist of distinctly (*f*-) twinned porphyroclasts (200-300 µm in size) surrounded by dynamically recrystallized (20-30 µm) newly-formed grains forming typical „core-mantle“ structures (Fig. 8h) within a cataclastic matrix. The width of twin lamellae varies from 5 to 10 µm.

Previously described mylonitic microstructures in Cal (and Dol) aggregates suggest higher differential stresses of plastic deformation (e.g. Schmid et al., 1980; Walker et al., 1990, fig. 18; Rowe and Rutter, 1990; Rutter, 1998, fig. 161.2). Supposing the strain rate between 10^{-12} - 10^{-6} s⁻¹ and the temperatures 300-200 °C, and taking into account twinned fabrics overprinted by the dynamically recrystallized aggregates, the estimated differential

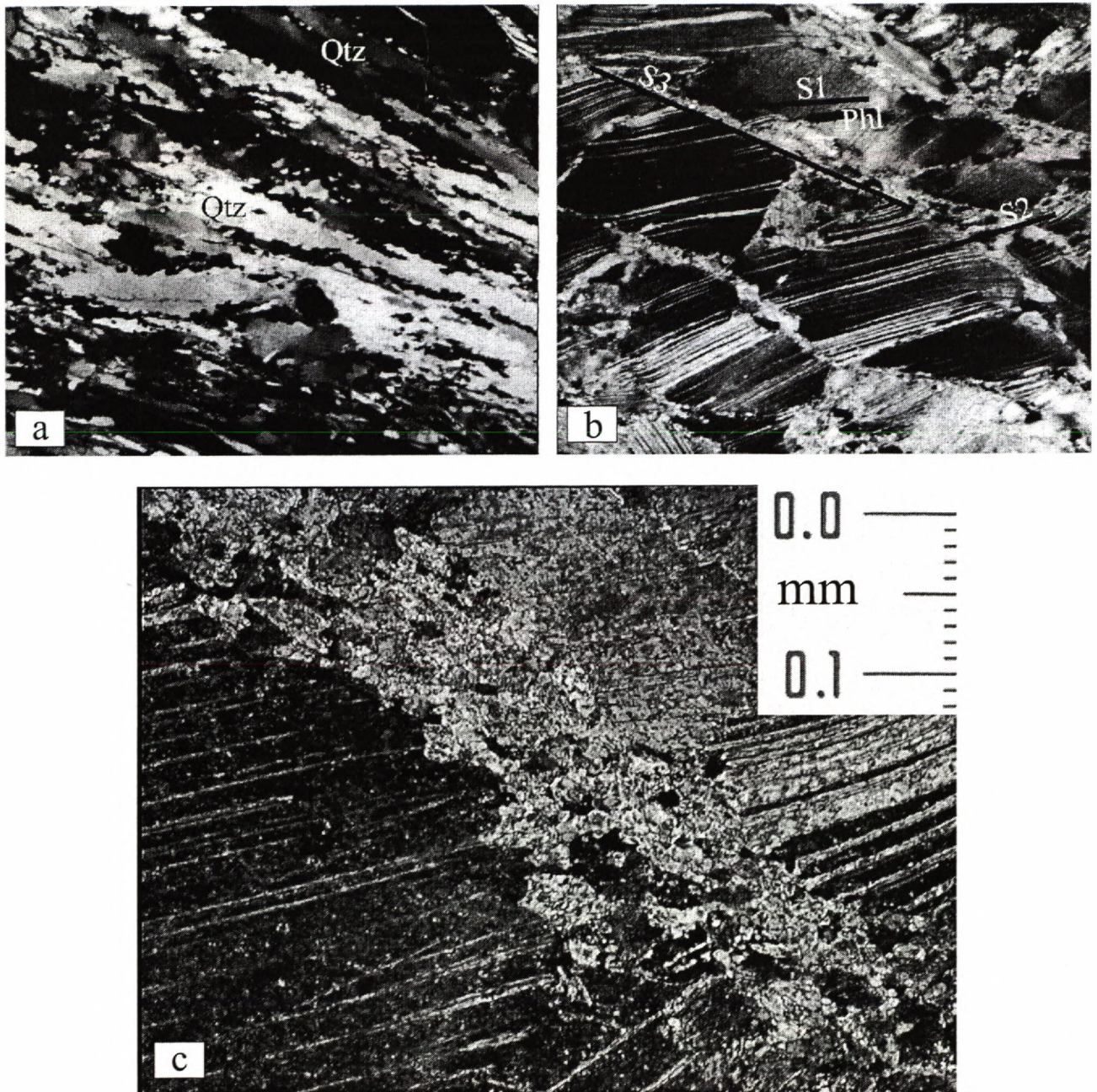


Fig. 12. Microstructures of mylonitic rocks of the Pennine structural complexes in the Area 2. Sample-location according to Fig. 4. (a) Recrystallized Qtz ribbons of „Zentralgneis“-type granitic orthogneiss mylonite (s. HT30). (b) Flattened Cal grains with distinct and parallel e-lamellae fabric cut by shear bands (s. HT23) marked by dynamically recrystallized grains. (c) A detail of ca. 100 μm wide shear band with dynamic aggregate of Cal grains (s. HT23). Magnification: 27x (a), 67x (b).

stresses (> 250 MPa) approach the boundary with high-stress exponential creep.

Thus we found characteristic evolution of microfabrics in high-strain (transpression-type) domains: it starts with deformation lamellae (in both Cal and Dol aggregates), which is easier in coarse-grained marbles. This is in agreement with simple shear experiments in the twinning regime if a single dominant twin orientation is observed, and the non-recrystallized original grains define a grain shape fabric which is oblique to the shear zone boundaries. The twinned grains preserve lobated grain

boundaries, which are assumed to represent the higher-temperature grain boundary migration that transforms at higher strains and differential stresses to mechanical twinning (regime 1, Schmid et al., 1980). Later on, minor subgrains and recrystallized grains form along the shear (C) foliation, indicating new strain localization, probably at lower temperatures and higher deformation rates. The latest stage is represented by almost entirely recrystallized twinned porphyroclasts, the relics of which flow within dynamically recrystallized matrix of new Cal grains, indicating an ultramylonitic stage. Mechanical twinning of

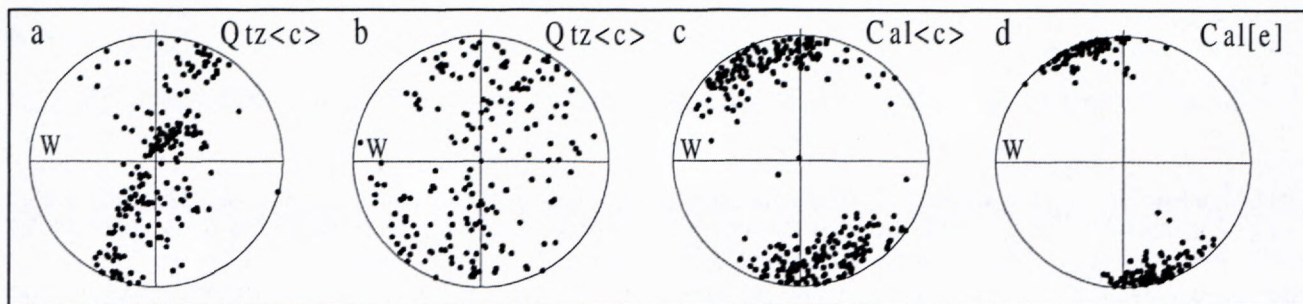


Fig. 13. The U-stage microscope patterns of Qtz and Cal of the Pennine structural complexes in the Area 2. The microstructures see in Fig. 12. The asymmetric patterns indicate a top-to-E extensional sliding. (a) Combined prism $\langle a \rangle$ and basal $\langle a \rangle$ slip in Qtz, Zentralgneis-type granitic mylonite (s. HT30, $N=223$). (b) Basal $\langle a \rangle$ slip in Qtz, quartzitic layer in marble-mylonite (s. HT23, $N=193$). (c) Cal $\langle c \rangle$ fabric of marble-mylonite due to e-twinning dominated (s. HT23, $N=300$). (d) Cal e-poles pattern, marble-mylonite (s. HT23, $N=195$).

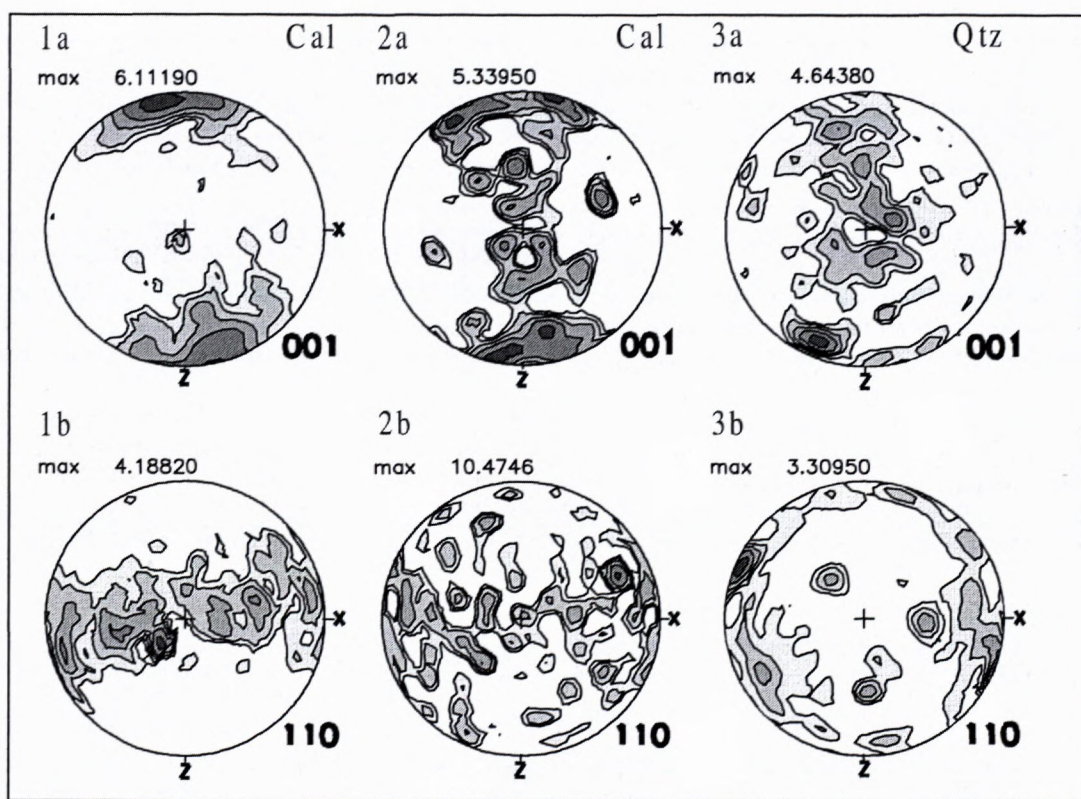


Fig. 14. X-ray texture goniometer patterns of Cal and Qtz of the Pennine structural complexes in the Area 2. The microstructures see in Fig. 12 b,c. The asymmetric patterns indicate a top-to-E extensional sliding. (1a,b-2a,b) Cal fabric of a twinned aggregate in marble-mylonite (1a,b - s. HT23, 2a,b - s. HT34). (3a,b) Combined prism $\langle a \rangle$, rhomb and basal slips in Qtz of Zentralgneis-type granitic mylonite (s. HT30).

Cal required higher differential stresses (usually between 180 and 270 MPa, e.g. Rowe and Rutter, 1990) that culminated during superposed dynamic (rotation) recrystallization, thus approaching the boundary of high-stress exponential creep (Walker et al., 1990; Rutter, 1998), providing at last distinct strain softening.

5.3. Microfabrics of quartz and calcite mylonites from normal-fault shear zone

At the eastern edge of the Tauern Window (Fig. 4), a top-to-E extensional transport has been documented by

Genser and Neubauer (1989) and dated by Cliff et al. (1985) in the time interval of 25-15 Ma.

The Qtz layers of „Zentralgneis“-type granite-gneisses (Fig. 12a) of the basement, or those of the cover marbles, exhibit distinct mylonitic fabrics. The U-stage (Fig. 13a, b) and X-ray texture goniometer (Fig. 14/3a,b) Qtz c-axes patterns of dynamically recrystallized aggregates are asymmetric. They reflect a basal $\langle a \rangle$ slip consistent with the top-to-the E extensional normal faulting (sliding).

Microtextures of the deformed marbles usually display 3 planar elements (Fig. 12b): 1. metamorphic (S) foliation defined by white micas and flattened Cal grains,

2. e-lamellae system oblique to S-planes at an acute angle,
3. high-angle shear bands (C-planes) cutting the previous fabrics and parallel to extensional normal fault.

Asymmetric U-stage pole figures of Cal <c> axes (Fig. 13c) and e-normals (Fig. 13d) suggest a top-to-the E simple shear (extensional sliding).

Asymmetric to almost symmetric X-ray texture goniometer patterns of Cal (Fig. 14/1a,b-2a,b) reflect deformation twinning in pure to simple shear regime and correspond to bulk flattening of marbles during the subvertical uplift and structural unroofing.

Textural patterns of Cal reflect only the first stage of the uplift deformation i.e. subvertical flattening of original metamorphic grains (400-800 μm of size, with predominating 500-600 μm) and the development of dense and narrow e-lamellae (15-30 μm) oriented at the acute angle to S(shape) foliation. The superimposed shear bands (C-planes) are related to newly-formed zones of strain localization due to an acceleration of deformation or top-to-E extensional sliding of the AA structural complexes from the Pennine ones at the eastern edge of the Tauern Window. Mechanical twinning changed to dynamic recrystallization, producing new grains 15-20 μm in size, excludingly within the about 100 μm narrow shear bands (Fig. 12c). Small grain size suggests high ductile flow stresses. Transition from ductile (dynamic recrystallization) to cataclastic flow, or power-law break up is locally observable in the C-planes of marbles accommodating an extreme exaggeration of deformation at the lowest temperatures of the uplift and exhumation.

6. Discussion on overprint evolution stages

The change of tectonic regime from compressional thrusting to strike slip is evident from the mapped geological structure of the Kreuzeck Massif, registered mesostructures as well as microstructures and related textural patterns of Qtz and Cal. It is inferred to be related to the closing of the Pennine ocean and following continental collision between the Apulia or Adria indenter (with the AA structural complexes) and the European plate. The age of the beginning of lateral strike slip movements (transpression?) is poorly constrained by one 61 Ma datum (K-Ar dating of fine-grained WhM from a mylonite, Waters ex Hoke, 1990). This event might roughly correspond to post-exhumation (from a subduction zone) collisional northward thrusting of the Pennine eclogite-bearing Grossglockner nappe that occurred around 60 Ma (Ar-Ar data on the phengitic WhM, Kurz et al., 1998).

An older, pre-Late-Cretaceous collisional compression and nappe thrusting of the AA structural complexes within the studied area can be inferred mainly from regional subhorizontal boundaries of the 5 crustal sheets or nappes (= structural complexes), thrust one over another, with the clear northern vergency (Putiš, 1998). This event appears to be compatible with practically the whole southern AA domain, and is considered to be Cretaceous (Frank et al., 1987; Thöni and Jagoutz, 1992, 1993;

Dallmeyer et al., 1992). The existing mineral K-Ar data from the Kreuzeck Massif indicate an older interval of cooling of the AA basement structural complexes around 90-80 Ma (Hoke, 1990; Oxburg et al., 1966). They are interpreted to reflect a mid-Cretaceous syncollisional exhumation event that changed to lateral strike slip newer basement exhumation period since ca. 70 Ma that is e.g. registered by the mentioned K-Ar data of 66 and 61 Ma in mylonites.

The Adria indenter initiated an extreme reduction of the width of the AA unit mainly due to subvertical transpressional (?) thinning, connected with inferred final exhumation of some early-Alpine HP-MP rocks in the time interval of ca 70 to 40 Ma. This event is constrained by the emplacement of 35-32 Ma old volcanic dykes (Deutsch, 1984) which are not metamorphosed or distinctly deformed. The dykes fill in brittle fractures of mylonitized AA basement structural complexes, being cut by ultracataclastic zones.

Although the ultracataclasites are partly superimposed on mylonites of the MMZ (defined by Hoke, 1990) in narrow newly localized deformation domains, the largest volume of these rocks (include the pseudotachylitic-like types) occurs independently along a megaflexure further to south, dividing the MMZ from subhorizontally stacked and piled basement nappes. This zone branches into shorter partial ultracataclastic domains of variable direction, although two conjugate (fault) systems are prevailing: WNW-ESE and NE-SW in the central part of the Kreuzeck Massif. A similar ultracataclastic zone occurs at the northern margin of the AA structural complexes and is located within the Ragga structural complex south of the Möll river (Putiš et al., 1997b). The zone striking WNW-ESE is subparallel to main Mölltal (in the N) and Oberdrautal (in the S) strike-slip fault zones, which are supposed to have been active since Oligocene, because they are not already cut by the volcanic dykes (ca. 32 Ma).

The HP Polinik and the MP Strieden structural complexes are the AA basement fragments showing the most conspicuous features of Cretaceous-Tertiary reactivation, because both complexes are located along the ductile-brittle strike-slip shear zone (MMZ).

The Polinik and Strieden structural complexes were tectonically emplaced onto the Ragga structural complex showing only greenschist facies LP/LT Alpine reactivation. Thus an inversed Alpine reactivation profile is observable in the Kreuzeck Massif. On the other hand, if one considers the Hochkreuz structural complex as the basis of higher AA nappes (so called the Upper Austro-Alpine, UAA), the discussed shear zone is directly developed at the boundary between the Ragga (LAA?) and Hochkreuz-Steinfeld (UAA) structural complexes. The exhumation „suture„ of the Polinik and Strieden structural complexes having a middle (MAA) position, indicates an extremely shortened domain of the AA basement that was probably subjected to Cretaceous continental subduction. Thus the earlier i.e. early-mid-Cretaceous tectonic evolution of the Kreuzeck Massif might have been connected with the evolution of the Meliata-Hallstatt ocean passive

continental margin. The Late Cretaceous-Tertiary strike slip shear zone and lateral thinning of the AA unit already suggests that the AA crust of the Kreuzeck Massif has become a part of the Pennine ocean active continental margin (Fig. 2).

7. Conclusions

The Austro-Alpine (AA) Polinik and Strieden basement structural complexes of the Kreuzeck Massif (south of the Pennine Tauern Window) bear features of polystage early-Cretaceous and early Tertiary overprint (reactivation) events. They were reconstructed from microstructures of the exhumed HP rocks and the associated mylonitoclastites within a Tertiary strike slip shear zone.

Petrological evolution culminated in HP amphibolite to eclogite facies during the subductional burial (D1, early-Cretaceous?) and changed to MP-LP/MT-LT amphibolite/greenschist-facies during the uplift (D2, mid-Cretaceous). Such a P-T path was estimated in the Polinik structural complex where no relics of pre-Alpine fabrics have been found and both (D1 and D2) stages are Alpine in age. The boundary amphibolite/greenschist-facies MP Alpine overprint was recognized in originally Variscan amphibolite facies assemblages of the Strieden structural complex.

Deformational evolution along the transpression shear zone is characteristic of higher strain rate and a competition between the dislocation creep and cataclastic flow during the (D3) exhumation of studied AA basement fragments. Ductile deformation of feldspar or dolomite aggregates changed to frictional cataclastic flow accompanied by a low temperature quartz and calcite crystal-plasticity. This seems to be a typical frictional-viscous flow (Handy et al., 1999) producing mylonitoclastites (resembling angular pseudotachylites, Curewitz and Karson, 1999) during decreasing temperatures and increasing deformation rates - the process observable in bimineralic or polymineralic high-strained rocks. Associated ultracataclastites fit well to this deformation trend, pointing to a rapid microstructural changes.

Measured textural patterns indicate:

a) Only quartz and calcite deformed ductilely, while feldspar and dolomite were at last subjected to cataclasis within the strike slip shear zone exposed in the Kreuzeck Massif. We found characteristic deformation sequence in calcite aggregate starting with deformation lamellae overprinted by dynamic (rotation) recrystallization. Such a mineral mechanics played an important role during the exhumation of AA basement fragments before an intrusion of volcanic dykes (dated 35-32 Ma) indicating transition to dominated brittle deformation regime, connected later with formation of ultracataclastite zones. Therefore frictional-viscous flow seems to be a transitional mechanism from a ductile to frictional (cataclastic) flow within the AA basement rocks located within or closely to strike slip shear zone (MMZ). Asymmetric patterns reflect a top-to-NW thrusting of steeply south-dipping tectonic fragments along the early-Tertiary dextral strike slip shear zone.

b) Miocene extension normal fault of the eastern edge of the Reisseck Massif yielded comparable quartz but different calcite textural patterns (to those from the Kreuzeck Massif) related to a top-to-east structural unroofing of the deeper Pennine unit at the southeastern margin of the Tauern Window. The calcite textural patterns show overprinted deformation lamellae by narrow (ca. 100 μm wide) extension shear bands accommodating newly-localized strain and reflecting a more rapid exhumation. The asymmetry of quartz and calcite textural patterns is in agreement with mesoscopically observable top-to-east sliding along the extensional deformation bands. They are good evidence that ductile deformation persisted until the latest exhumation period of the Pennine unit (before ca. 25-15 Ma, according to Cliff et al., 1985; Selverstone, 1988). In contrast, exclusively (ultra)cataclastites have been developed in the lateral strike slip fault zones of the Kreuzeck Massif AA unit at that time (25-15 Ma). Most of apatite FT ages obtained in both the AA and Pennine units (Staufenberg, 1987; Frisch et al., 1999) already indicate common AA-Pennine very low-temperature history during Oligocene-Miocene strike slip and normal fault tectonics connected with the postcollisional orogen-parallel extrusion of the Apulian (Adriatic) plate fragments (Frisch et al., 2000).

Acknowledgements

This paper was supported: by the Austrian Geological Survey mapping program, VEGA grant of Slovak Republic (No. 1/5228/98 and 1/8248/01, M.P.), Geological Institute of the K.F. University of Graz, Russian Foundation for Basic Research (project # 99-05-64058, S.P.K.). It benefited from research facilities at the Technical University of Denmark (Copenhagen-Lyngby), as well as Villum Kann Rasmussen Fonds for visiting researchers.

References

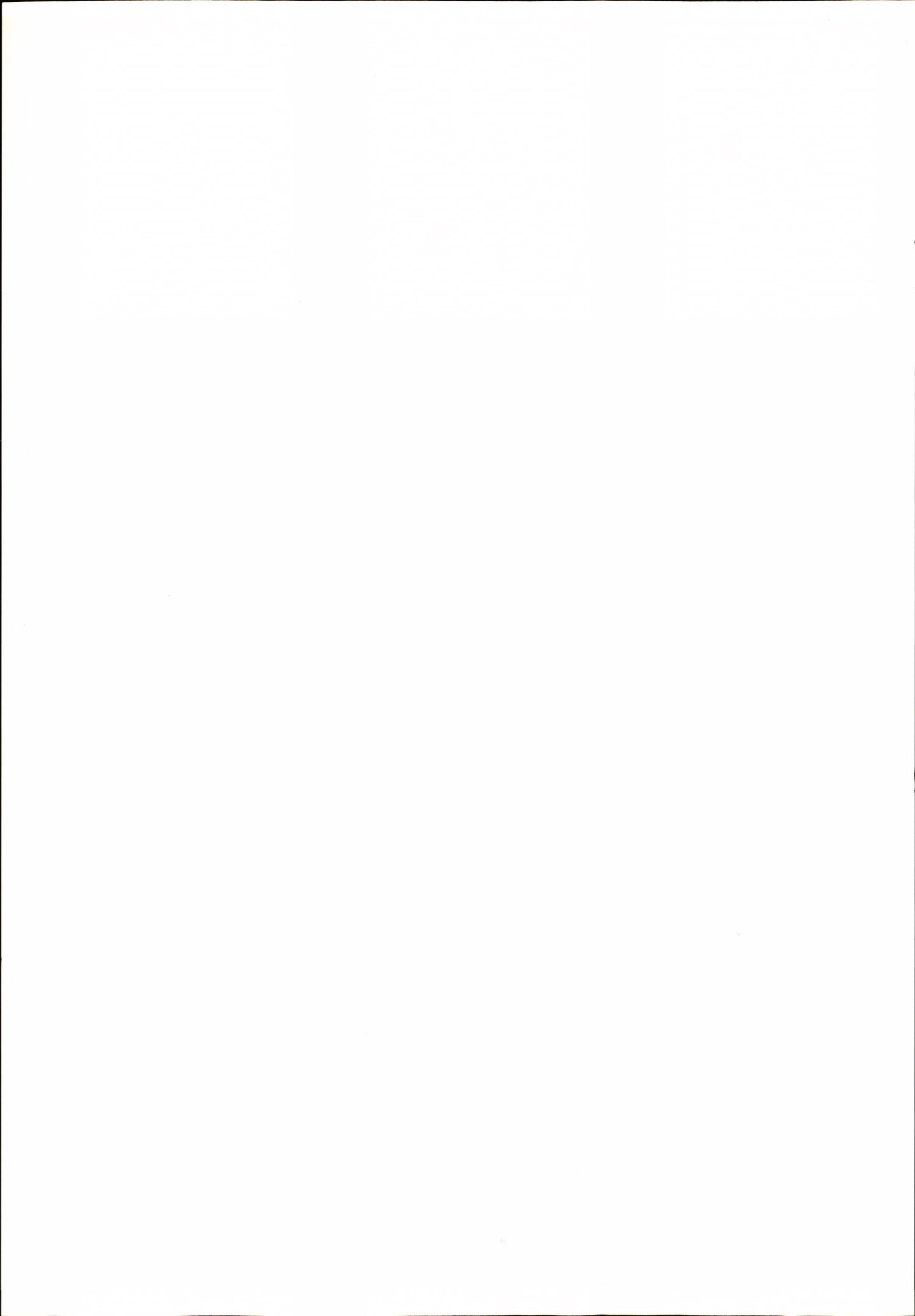
- Ai, Y., 1994: A revision of the garnet-clinopyroxene Fe^{2+} - Mg exchange geothermometer. *Contrib. Mineral. Petrol.* 115, 467-473.
- Barber, D.J., 1990. Regimes of plastic deformation - processes and microstructures: an overview. In: Barber, D.J., Meredith, P.G. (Eds.), *Deformation Processes in Minerals, Ceramics and Rocks*. Unwin Hyman, London, pp. 138-177.
- Behrmann, J.H., Wallis, S.R., 1987. Hangendverschuppung des Tauernfenster-Südrandes bei Kals (Osttirol) als Zeuge von coalpinem Underplating. *Jb. Geol. B.-A.* 130, 133-138.
- Berthé, D., Choukroune, P., Jegouzo, P., 1979: Orthogneiss, mylonite and non-coaxial deformation in granites: The example of the South Armorican shear zone. *J. Struct. Geol.* 1, 31-42.
- Bezák, V., Kohút, M., Kováčik, M., Madarás, J., Marko, M., Plašienka, D., Putiš, M., 1993. Bericht 1992 Über geologische Aufnahmen im Kristallin der Reisseck-Gruppe auf Blatt 182 Spittal an der Drau. *Jb. Geol. B.-A.* 136, 629-630.
- Bezák, V., Kohút, M., Kováčik, M., Madarás, J., Marko, M., Plašienka, D., Putiš, M., 1994. Bericht 1993 Über geologische Aufnahmen im kristallinen Grundgebirge auf Blatt 182 Spittal an der Drau. *Jb. Geol. B.-A.* 137, 523-524.
- Bezák, V., Broska, I., Kohút, M., Kováčik, M., Madarás, J., Marko, F., Plašienka, D., Putiš, M., Siman, P., 1995. Bericht 1994 Über geologische Aufnahmen im kristallinen Grundgebirge auf Blatt 182 Spittal an der Drau. *Jb. Geol. B.-A.* 138, 551-554.
- Blanckenburg, F. von, Davies, J.H., 1996. Feasibility of double slab breakoff (Cretaceous and Tertiary) during the Alpine convergence. *Eclogae Geol. Helv.* 89, 111-127.

- Burg, J.P., 1986. Quartz shape fabric variations and c-axis fabrics in a ribbon-mylonite: arguments for an oscillating foliation. *J. Struct. Geol.* 8, 123-131.
- Cliff, R.A., Droop, G.T.R., Rex, D.C., 1985. Alpine metamorphism in the south-east Tauern Window, Austria: II. heating, cooling and uplift rates. *J. Metam. Geol.* 3, 403-415.
- Culshaw, N.G., Fyson, W.K., 1984. Quartz ribbons in high grade granite gneiss: modifications of dynamically formed quartz c-axis preferred orientation by oriented grain growth. *J. Struct. Geol.* 6, 663-668.
- Curewitz, D., Karson, J.A., 1999. Ultracataclasis, sintering, and frictional melting in pseudotachylytes from East Greenland. *J. Struct. Geol.* 21, 1693-1713.
- Dallmeyer, R.D., Neubauer, F., Handler, R., Müller, W., Fritz, H., Antonitsch, W., Hermann, S., 1992. $^{40}\text{Ar}/^{39}\text{Ar}$ and Rb-Sr mineral age controls for the Pre-Alpine and Alpine tectonic evolution of the Austro-Alpine nappe complex, Eastern Alps. In: Neubauer, F. (Ed.), *ALCAPA - Field Guide*, Univ. of Graz, pp. 47-59.
- Dallmeyer, R.D., Neubauer, F., Handler, R., Fritz, H., Müller, W., Pana, D., Putiš, M., 1996. Tectonothermal evolution of the internal Alps and Carpathians: Evidence from $^{40}\text{Ar}/^{39}\text{Ar}$ mineral and whole-rock data. *Eclogae Geol. Helv.* 89, 203-227.
- Dallmeyer, R.D., Handler, R., Neubauer, F. and Fritz, H., 1998. Sequence of thrusting within a thick-skinned tectonic wedge: evidence from $^{40}\text{Ar}/^{39}\text{Ar}$ and Rb-Sr ages from the Austroalpine Nappe Complex of the Eastern Alps. *J. Geol.* 106, 71-86.
- Dal Piaz, G.V., 1999. The Austroalpine-Piedmont nappe stack and the puzzle of Alpine Tethys. In: Gosso, G., Jadoul, F., Sella, M., Spalla, M.I. (Eds.), *Mem. Sci. Geol.* (Padova), 51/1, 155-176.
- Deutsch, A., 1984. Young Alpine dykes south of the Tauern Window (Austria): A K-Ar and Sr isotope study. *Contrib. Mineral. Petrol.* 85, 45-57.
- Frank, W., Kralik, M., Scharbert, S., Thöni, M., 1987. Geochronological data from the Eastern Alps. In: Flügel, H.W., Faupl, P. (Eds.), *Geodynamics of the Eastern Alps*. Deuticke, Vienna, pp. 272-281.
- Frisch, W., Brügel, A., Dunkl, I., Kuhlemann, J., Satir, M., 1999. Post-collisional large-scale extension and mountain uplift in the Eastern Alps. In: Gosso, G., Jadoul, F., Sella, M., Spalla, M.I. (Eds.), *Mem. Sci. Geol.* (Padova), 51/1, 3-23.
- Frisch, W., Dunkl, I., Kuhlemann, J., 2000. Post-collisional orogen-parallel large-scale extension in the Eastern Alps. *Tectonophysics* 327, 239-265.
- Froitzheim, N., Schmid, S.M., Frey, M., 1996. Mesozoic paleogeography and the timing of eclogite-facies metamorphism in the Alps: A working hypothesis. *Eclogae Geol. Helv.* 89, 81-110.
- Genser, J., Neubauer F., 1989. Low angle normal faults at the eastern margin of the Tauern Window (Eastern Alps). *Mitt. Österr. Geol. Ges.* 81, 233-243.
- Gleason, G.C., Tullis, J., 1993. The role of dynamic recrystallization in the development of lattice preferred orientations in experimentally deformed quartz aggregates. *J. Struct. Geol.* 15, 1145-1168.
- Handy, M., Wissing, S.B., Streit, L.E., 1999: Frictional-viscous flow in mylonite with varied biminerale composition and its effect on lithospheric strength. *Tectonophysics* 303, 175-191.
- Hoinkes, G., Koller, F., Rantitsch, G., Dachs, E., Höck, V., Neubauer, F., Schuster, R., 1999. Alpine metamorphism in the Eastern Alps. *Schweizerische Mineralogische Petrographische Mitteilungen* 79, 155-181.
- Hoke, L., 1990. The Altkristallin of the Kreuzeck Mountains, SE Tauern Window, Eastern Alps - Basement crust in a convergent plate boundary zone. *Jb. Geol. B.-A.* 133, 5-87.
- Holland, T.J.B., 1980. The reaction albite=jadeite+quartz determined experimentally in the range 600-1200 grad. *C. Am. Mineralogist* 65, 129-134.
- Jensen, L.N., Starkey, J., 1985. Plagioclase microfabrics in a ductile shear zone from the Jotun Nappe, Norway. *J. Struct. Geol.* 7, 527-539.
- Kleemann, U., Reinhardt, J., 1994. Garnet-biotite thermometry revised: the effect of Al_{VI} and Ti in biotite. *Eur. J. Mineral.* 6, 925-941.
- Kohn, M.Y., Spear, F.S., 1990. Two new geobarometers for garnet amphibolites, with application to southeastern Vermont. *Am. Mineralogist* 75, 89-96.
- Kozur, H., 1991. The geological evolution at the western end of the Cimmerian ocean in the Western Carpathians and Eastern Alps. *Zbl. Geol. Pal.*, T. 1, H. 1, 99-121.
- Kretz, R., 1983. Symbols for rock-forming minerals. *Am. Mineralogist* 68, 277-279.
- Kurz, W., Neubauer, F., 1996. Deformation partitioning during up-doming of the Sonnblick area in the Tauern Window (Eastern Alps, Austria). *J. Struct. Geol.* 18, 1327-1343.
- Kurz, W., Neubauer, F., 1998. Eclogite meso- and microfabrics: implications for the burial and exhumation history of eclogites in the Tauern Window (Eastern Alps) from P-T-d paths. *Tectonophysics* 285, 183-209.
- Kurz, W., Neubauer, F., Unzog, W., Genser, J., Wang, X., 2000. Microstructural and textural development of calcite marbles during poly-phase deformation of Penninic units within the Tauern Window (Eastern Alps). *Tectonophysics* 316, 327-342.
- Lafrance, B., White, J.C., Williams, P.F., 1994. Natural calcite c-axis fabrics: an alternate interpretation. *Tectonophysics* 229, 1-18.
- Lammerer, B., Weger, M., 1998. Footwall uplift in an orogenic wedge: the Tauern Window in the Eastern Alps of Europe. *Tectonophysics* 285, 213-230.
- Laubscher, H., 1989. The tectonics of the Southern Alps and the Austro-Alpine nappes: a comparison. In: Coward, M.P., Dietrich, D., Park, R.G. (Eds.), *Alpine Tectonics*. Geological Society London, *Special Publications* 45, 229-241.
- Leake, B.E., Wooley, A.R., and 20 members of the Subcommittee on Amphibole, 1997. Nomenclature of amphiboles. Report of the Subcommittee on Amphiboles of the International Mineralogical Association Commission on New Minerals and Mineral Names. *Eur. J. Mineral.* 9, 623-651.
- Linner, M., 1997. Bericht 1996 über geologische Aufnahmen im Kristallin auf den Blättern 179 Lienz und 180 Winklern. *Jb. Geol. B.-A.* 140, 342-345.
- Mancktelow, N.S., Meier, A., Viola, G.A.M., Müller, W., Fügenschuh B., Seward, D., Villa, I.M., 1999. The Periadriatic and adjacent fault systems in the Eastern Alps south and west of the Tauern Window. Abstracts of the 4th Workshop on Alpine Geological Studies, Tübingen. *Tübinger Geowissenschaftliche Arbeiten, Series A*, 52, 7-9.
- McLelland, J.M., 1984. The origin of ribbon lineation within the southern Adirondacks, U.S.A. *J. Struct. Geol.* 6, 147-157.
- Neubauer, F., 1994. Kontinentkollision in den Ostalpen. *Geowissenschaften* 12, 136-140.
- Nicolas, A., Poirier, J.P., 1976. *Crystalline Plasticity and Solid State Flow in Metamorphic Rocks*. J. Wiley & Sons, London, New York, pp. 216-222.
- Oxburg, E.R., Lambert, R.St.J., Baardsgaard, H., Simons, J.G., 1966. Potassium Argon age studies across the southeast margin of the Tauern Window, the Eastern Alps. *Verh. Geol. B.-A.*, 17-33.
- Perchuk, L.L., 1989. Intercorrelation of Fe-Mg geothermometers using the Nernst law. *Geokhimiya* 5, 611-622 (in Russian).
- Plašienka, D., Grečula, P., Putiš, M., Hovorka, D., Kováč, M., 1997. Evolution and structure of the Western Carpathians: an overview. In: Grečula, P., Hovorka, D., Putiš, M. (Eds.), *Geological Evolution of the Western Carpathians. Mineralia Slovaca - Monograph*, Bratislava, pp. 1-24i.
- Platt, J.P., 1993. Exhumation of high-pressure rocks: a review of concepts and processes. *Terra Nova* 5, 119-133.
- Poirier, J.P., Guillopé, M., 1978. Deformation induced recrystallization of minerals. *Bull. Soc. fr. Minér. Cristallogr.* 102, 67-74.
- Powell, R., 1985. Regression diagnostics and robust regression in geothermometer/geobarometer calibration: the garnet-clinopyroxene geothermometer revised. *J. Metam. Geol.* 3, 231-243.
- Putiš, M., 1998. Compiled Geological map of the Kreuzeck Massif, Eastern Alps. Austrian Geological Survey, scale 1:25 000, Vienna.
- Putiš, M., Bezák, V., Janák, M., Kohút, M., Kováčik, M., Madarás, J., Marko, F., Plašienka, D., 1995. Geological map of the western part of the Kreuzeck Massif, Eastern Alps. Austrian Geological Survey, scale 1:25 000, Vienna.
- Putiš, M., Bezák, V., Janák, M., Kohút, M., Kováčik, M., Madarás, J., Marko, F., Plašienka, D. 1996. Geological map of the central part of the Kreuzeck Massif, Eastern Alps. Austrian Geological Survey, scale 1:25 000, Vienna.

- Putiš M., Bezák V., Kohút M., Kováčik M., Marko F., Plašienka D., 1997a. Bericht 1996 and 1997 über geologische Aufnahmen im Kristallin auf Blatt 181 Obervellach. *Jb. Geol. B.-A.* 140, 345-348.
- Putiš M., Bezák V., Kohút M., Kováčik M., Marko F., Plašienka D., 1997b. Geological map of the eastern part of the Kreuzeck Massif, Eastern Alps. Austrian Geological Survey, scale 1:25 000, Vienna.
- Putiš M., Fritz H., Unzog W., Wallbrecher E., Korikovsky, S.P., Pushkarev, Y.D., Kotov, A.B., 1998. Exhumation modes of austroalpine eclogite-bearing complexes in the vicinity of penninic windows, Eastern Alps. Abstracts of the XVI. Congress of the Carpathian-Balkan Geological Association, Vienna, Austria, 501.
- Putiš M., Korikovsky, S.P., Pushkarev, Yu.A., 2000. Petrotectonics of an Austroalpine eclogite-bearing complex (Sieggraben, Eastern Alps) and U-Pb dating of exhumation. *Jb. Geol. B.-A.* 142, 73-93.
- Putiš M., Korikovsky, S.P., Wallbrecher E., Unzog, W., Olesen, N.O., Fritz, H., 2002. Evolution of an eclogitized continental fragment in the Eastern Alps (Sieggraben, Austria). *J. Struct. Geol.* 24, 339-357.
- Ratschbacher, L., Neubauer, F., 1989. West-directed decollement of Austro-Alpine cover nappes in the eastern Alps: geometrical and rheological considerations. In: Coward, M.P., Dietrich, D., Park, R.G. (Eds.), *Alpine Tectonics. Geol. Soc. Spec. Publ.* 45, pp. 243-262.
- Ratschbacher, L., Wenk, H.-R., Sintubin, M., 1991. Calcite textures: examples from nappes with strain-path partitioning. *J. Struct. Geol.* 13, 369-384.
- Rowe, K.J., Rutter, E.H., 1990. Paleostress estimation using calcite twinning: experimental calibration and application to nature. *J. Struct. Geol.* 12, 1-17.
- Rutter, E.H., 1998. Experimental dynamic recrystallization of calcite rocks. In: Snoke, A.W., Tullis, J., Todd, V.R. (Eds.), *Fault-related Rocks A Photographic Atlas*. Princeton University Press, Princeton, New Jersey, pp. 542-543.
- Silverstone, J., 1988. Evidence for east-west crustal extension in the Eastern Alps: implications for the unroofing history of the Tauern window. *Tectonics* 7, 87-105.
- Schmid, S.M., Paterson, M.S., Boland, J.N., 1980. High temperature flow and dynamic recrystallization in Carrara marble. *Tectonophysics* 65, 245-280.
- Spaeth, G., 1997. Bericht 1995 über geologische Aufnahmen im Kristallin der Schobergruppe auf Blatt 179 Lienz. *Jb. Geol. B.-A.* 140, 387-389.
- Spear, F.S., 1982. Coexisting calcic amphiboles. Reviews in Mineralogy, v. 9B Amphiboles. In: Veblen D.B., Ribbe P.H. (Eds.), *Petrology and Experimental Phase Relations. Miner. Soc. Am.*, 69-76.
- Stampfli G.M. 1996. The Intra-Alpine terrain: A Paleotethyan remnant in the Alpine Variscides. *Eclogae Geol. Helv.* 89, 13-42.
- Stampfli G.M., Mosar, J., 1999. The making and becoming of Apulia. In: Gosso, G., Jadoul, F., Sella, M., Spalla, M.I. (Eds.), *Mem. Sci. Geol.* (Padova), 51/1, 141-154.
- Staufenberg, H., 1987. Apatite fission-track evidence for post-metamorphic uplift and cooling history of the eastern Tauern window and the surrounding Austroalpine (central Eastern Alps, Austria). *Jb. Geol. B.-A.* 130, 571-586.
- Stüwe, K., Sandiford, M., 1995. Mantle-lithospheric deformation and crustal metamorphism with some speculations on the thermal and mechanical significance of the Tauern Event, Eastern Alps. *Tectonophysics* 242, 115-132.
- Thöni, M., Jagoutz, E., 1992. Some new aspects of dating eclogites in orogenic belts: Sm-Nd, Rb-Sr, and Pb-Pb isotopic results from the Austroalpine Saualpe and Koralpe type-locality (Carinthia/Styria, southeastern Austria). *Geoch. Cosmoch. Acta* 56, 347-368.
- Thöni, M., Jagoutz, E., 1993. Isotopic constraints for eo-Alpine high-P metamorphism in the Austroalpine nappes of the Eastern Alps: bearing on Alpine orogenesis. *Schweiz. Mineral. Petrogr. Mitt.* 73, 177-189.
- Tollmann, A., 1977. *Geologie von Österreich. Band I: Die Zentralalpen*. Deuticke, Vienna.
- Trimby, P.W., Prior, D.J., Wheeler, J., 1998. Grain boundary hierarchy development in a quartz mylonite. *J. Struct. Geol.* 20, 917-935.
- Vauchez, A., 1980. Ribbon texture and deformation mechanisms of quartz in a mylonitized granite of Great Kabylia (Algeria). *Tectonophysics* 67, 1-12.
- Wallis, S.R., Behrmann, J.H., 1996. Crustal stacking and extension recorded by tectonic fabrics of the SE margin of the Tauern Window, Austria. *J. Struct. Geol.* 18, 1455-1470.
- Walker, A.N., Rutter, E.H., Brodie, K.H., 1990. Experimental study of grain-size sensitive flow of synthetic, hot-pressed calcite rocks. In: Knipe, R.J., Rutter, E.H. (Eds.), *Deformation Mechanisms, Rheology and Tectonics. Geol. Soc. Spec. Publ.* 54, pp. 259-284.
- Wenk, H.R., Takeshita, T., Bechler, E., Erskine, B., Mathies, S., 1987. Pure shear and simple shear calcite textures. Comparison of experimental, theoretical and natural data. *J. Struct. Geol.* 9, 731-745.
- Wilson, C.J.L., 1975. Preferred orientation in quartz ribbon mylonites. *Geol. Soc. Am. Bull.* 86, 968-974.

Appendix A

Mineral abbreviations in text and figures (after Kretz, 1983; end-members of Ca-amphiboles after Leake et al., 1997): Ab=albite, Acm=acmite, Act=actinolite, Ads=andesine, Alm=almandine, Am=amphibole, An=anortite, And=andalusite, Ath=anthophyllite, Aug=augite, Bar=barroisite, Bt=biotite, Cal=calcite, Chl=chlorite, Clid=chloritoid, Czo=clinozoisite, Cpx=clinopyroxene, Di=diopside, Dol=dolomite, Ed=edenite, Ep=epidote, Fsp=feldspars, Grs=grossular, Grt=garnet, Hb=horblende (as end member, sensu Leake et al., 1997), Hbl=hornblende, Ilm=ilmenite, Jd=jadeite, Kfs=kalifeldspar, Ky=kyanite, Mgr=margarite, Mnz=monazite, Ms=moscovite, Olg=oligoclase, Omp=omphacite, Phe=phengite, Pl=plagioclase, Prg=pargasite, Prp=pyrope, Px=pyroxene, Qtz=quartz, Rt=rutile, Ser=sericite, Sil=sillimanite, Sps=spessartite, St=staurolite, Tr=tremolite, Ts=tschermakite, Ttn=titanite, Tur=tourmaline, WhM=white mica, WR=whole-rock, Zo=zoisite, Zrn=zircon.



The Interactive Raw Material Information System ("IRIS") of Austria - the computer based Metallogenetic Map of Austria

LEOPOLD WEBER¹, FRITZ EBNER² & GÜNTHER HAUSBERGER³

¹ Federal Ministry of Economy and Labor, Mining Authority, Denisgasse 31, A 1200 Vienna

² University of Leoben, Institute of Geological Sciences, Peter-Tunner-Strasse 5, A 8700 Leoben

³ Geo- und Umweltinformatik, Roseggerstrasse 17, A 8700 Leoben

Abstract. During the past decades intensive programs were carried out to document the mineral occurrences and deposits, and the geochemical and geophysical distributions in Austria. These data were the base for the "Metallogenetic Map of Austria", which was designed and coordinated by L. WEBER. The map was drawn digitally and printed along with a voluminous explanation text book by the Austrian Geological Survey. As a further step an Interactive Raw material Information System (IRIS) was established.

Key words: Eastern Alps, Bohemian Massif, mineral deposits, metallogenetics, geochemistry, aeromagnetics

From the "Metallogenetic Map of Austria" to "IRIS"

Various geochemical and geophysical investigations have been initiated by the Austrian Ministry for Economy and the Ministry for Science during the past decades covering the areas of most of the Austrian states. More than 30000 stream sediment samples and more than 6000 heavy mineral samples from the Bohemian Massif and the crystalline complexes of the Eastern Alps were collected, analyzed, and published in the "Geochemical Atlas of the Republic of Austria 1:1 M" (Thalman et al., 1989).

An aeromagnetic survey program was carried out in 1977 to 1982. Different flight levels were used because of the rugged topography. The results were published in several scientific publications (see Blaumoser, 1992).

Since 1978 most of the Austrian mineral occurrences have been investigated and documented in detail. A brief overview is given by Haditsch (1979).

Weber, acting as chairman of the "Mineral Deposits Branch" of the Austrian Mining Association, suggested harmonizing the various data from modern geology, tectonics and mineralization into the "Metallogenetic Map of Austria." A project team with more than 40 representatives of science and industry was formed in 1991. The project was financed by the Austrian Academy of Science, the Geological Survey, the Austrian Science Foundation, the Technical Museum and the Austrian Mining Association. Support of software and hardware infrastructure was provided by the Joanneum Research Forschungsgesellschaft m.b.H. and the Kansas Geological Survey.

As a first step a data base containing information on more than 3000 mineral occurrences (mineral content, location, geological framework, tectonic unit, host rock, age of host rock, shape and size of mineralization, orien-

tation, literature and more) was established. This very important basis for the following steps of the project took several years to complete.

The next step was a first attempt to summarize mineral occurrences by their similarities such as host rocks, shape, and tectonic framework, in order to define specific metallogenetic districts. More than 150 districts were differentiated and discussed in detail which required several more workshops to conclude.

To distinguish between different mineralizations (stratiform-lenticular; veins-lodes; disseminated-stockwork; irregular shaped; or mineralizations in drill holes only) and mineral groups (Iron and steel alloying metals, base metals, special metals, precious metals, industrial minerals and mineral fuels) special shaped colored symbols were designed for the map. Each symbol reflects the location of the mineralization, its shape, mineral content, size and orientation.

As the existing geological map of Austria, published in 1935 (Vetters 1933) was no longer a suitable geological base, a new geological map of Austria had to be compiled by F. Ebner at a scale of 1:500.000. The digital map was created by using GIS software ARC-INFO by the Austrian Geological Survey.

After 6 years of intensive research work, the Metallogenetic map of Austria along with a very detailed "Handbook of Mineral Occurrences of Ores, Industrial Minerals and Mineral Fuels of Austria" (Weber, ed., 1997) was presented to the public at the International Symposium "Energievorräte und mineralische Rohstoffe: Wie lange noch?" (Weber, 1997). This was the first map of its kind in Austria. The legend of the Metallogenetic Map is in German and English. The textbook and the computer based system is in German only.

To avoid an "information overload" the visualization of features on the map had to be restricted (e.g., the num-

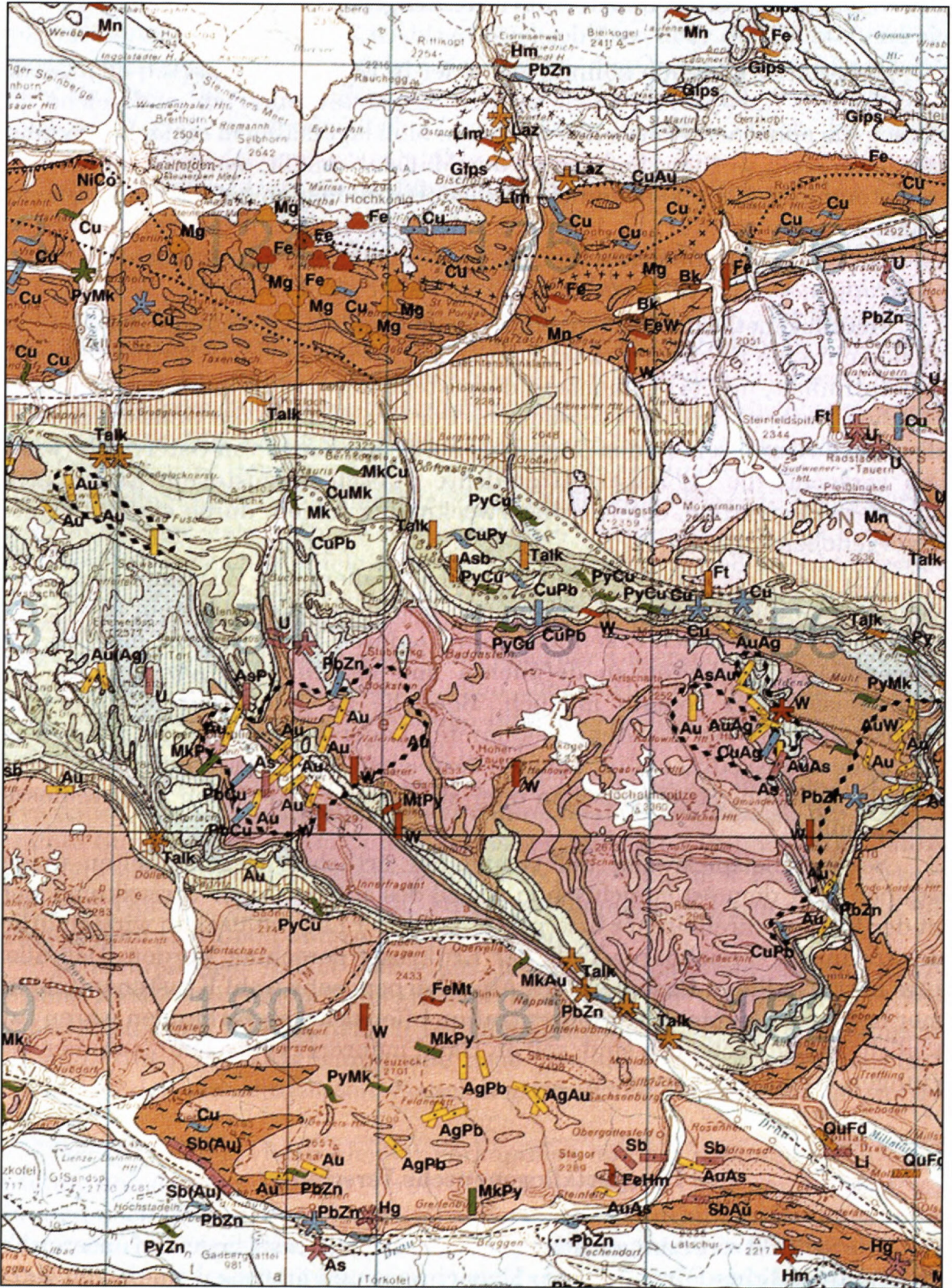


Fig. 1: Metallogenetic Map, detail (Central Alps, different gold districts).

ber of mineralization symbols displayed is related to the scale of the map). Therefore only the most important mineral occurrences had to be taken into consideration. On the other hand, it was impossible to visualize the results of the stream sediment geochemistry simultane-

ously. Each analyzed element (out of 35 elements) required a separate map.

Once a map is printed, corrections or changes are no longer possible. That, plus the fact that much information from geochemistry and geophysics could not be included

on the printed map, are reasons why the CD-ROM project has been launched. The aim of this project was to visualize geology, tectonics, geochemistry, airborne and terrestrial geophysics, and mineral occurrences simultaneously. The fact that all the data (geology, tectonics, mineralizations, geochemistry, and geophysics) had been stored digitally, made the project easier.

The first CD-ROM version of the "Metallogenetic Map of Austria" was presented mid 2000 to the public as "IRIS". IRIS is the abbreviation of Interactive Raw Materials Information System. The hardware requirement is described in detail below.

IRIS allows to visualize geology, tectonics, tectonics below surface, topography, drainage-system, analytical results of 35 elements of the geochemical survey, aeromagnetic survey, mineralization simultaneously, separate or in combinations. A zoom function allows the user to magnify areas of interest.

The IRIS data base provides the possibility of dynamically completing or correcting data as a main advantage of a computer based information system. It is in strict contrast to a printed map which exists only in a static and unchangeable form.

Basic data and scientific content of IRIS

IRIS is a simultaneous approach based on 5 layers containing the following maps:

- Geological map
- Metallogenetic map
- Geochemical map
- Aeromagnetic map
- Topography (situation), drainage system

Comprehensive information such as location of metallic raw materials, industrial minerals and mineral fuels in Austria can be generated by visualizing data for more than 3000 mineralizations (occurrences and deposits) in an interactive way.

Geology, tectonics

Austria comprises parts of the Variscan Bohemian massif, the Eastern and Southern Alps, Tertiary basins and Quaternary deposits. Magmatic intrusive bodies are situated at the Periadriatic lineament zone at the border of Eastern and Southern Alps. The geological base map shows the regional geological systems subdivided into two categories: major geological units and subunits. They also may be differentiated by lithology (Tab. 1).

The purpose for differentiation of subunits into lithologies is:

- to differentiate carbonate from siliciclastic rock
- to indicate basic (basaltic), acidic volcanic rock and ultrabasic rock
- to show the metamorphic facies.

Geological information is available through the layer "Geologie" and may be combined with the tectonic layer (activation of the menu field "Tektonik"). The layer offers an option to locate undifferentiated or differentiated tectonic lines. By activating the dynamic legend (left part

of screen) tectonic units are determined as faults or 1st and 2nd order thrust faults (both categories proved and assumed). The layer "Tektonik Basement" is related to the pattern of faults and thrust planes in the pre-Tertiary basement of the Molasse zone and other Neogene basins, based on oil and gas exploration work.

Topography (Situation), drainage system

By using the button "Situation" the topography will be displayed. This option available with larger magnification only, as in the general overview it is impossible to read the content. The same is with the drainage system ("Gewässernetz").

Geochemistry

The IRIS-System also contains geochemical background information of the Bohemian massif and the internal zones of the Eastern Alps (Austroalpine crystalline and Paleozoic zones), derived from stream sediment sampling and analyzing of 35 elements (published in the Geochemical Atlas of Austria (Thalman, et al., 1989).

Analyzed elements: Ag, Al, As, Ba, Be, Ca, Ce, Cr, Co, Cu, Fe, Ga, K, La, Mg, Mn, Mo, Na, Nb, Ni, P, Pb, Rb, Sb, Sc, Sn, Sr, Th, Ti, U, V, W, Y, Zn, Zr.

The mapping of geochemical data is one of the main advantages of this computer based information system and enables a practicable way to visualize the results of geochemistry, geology and mineralizations information simultaneously.

The concentration of each element (represented by categories in ppm or %) is visualized by colored dots. More detailed information is shown by activating the legend and clicking the sample location in the map.

Aeromagnetic

Aeromagnetic data is based on aeromagnetic survey work in 1977 - 1982 (Blaumoser, 1992). In a larger scale (general overview) positive anomalies of the total magnetic intensity are shown in areas as red shadings (light to dark according to percentage of intensity), negative anomalies as green shadings. In smaller scales (larger magnification) the total magnetic intensity is expressed by red and blue isolines, respectively indicating positive or negative anomalous magnetic domains. In both situations the active dynamic legend indicates the amount of the anomalies in nT and altitude of the flight levels in meters.

Mineralizations and metallogenetic districts

IRIS provides an extensive data base of 3029 Austrian mineral occurrences / deposits. Information on mineralization is given by choosing a particular deposit (mouse click in the map) of one of the metallogenetic layers described below, when the "i"-button is active. Detailed information is available by activating the list "all occurrences/deposits", shown in separate windows of the activated layer described below. The data base includes (e.g. Fig. 6):

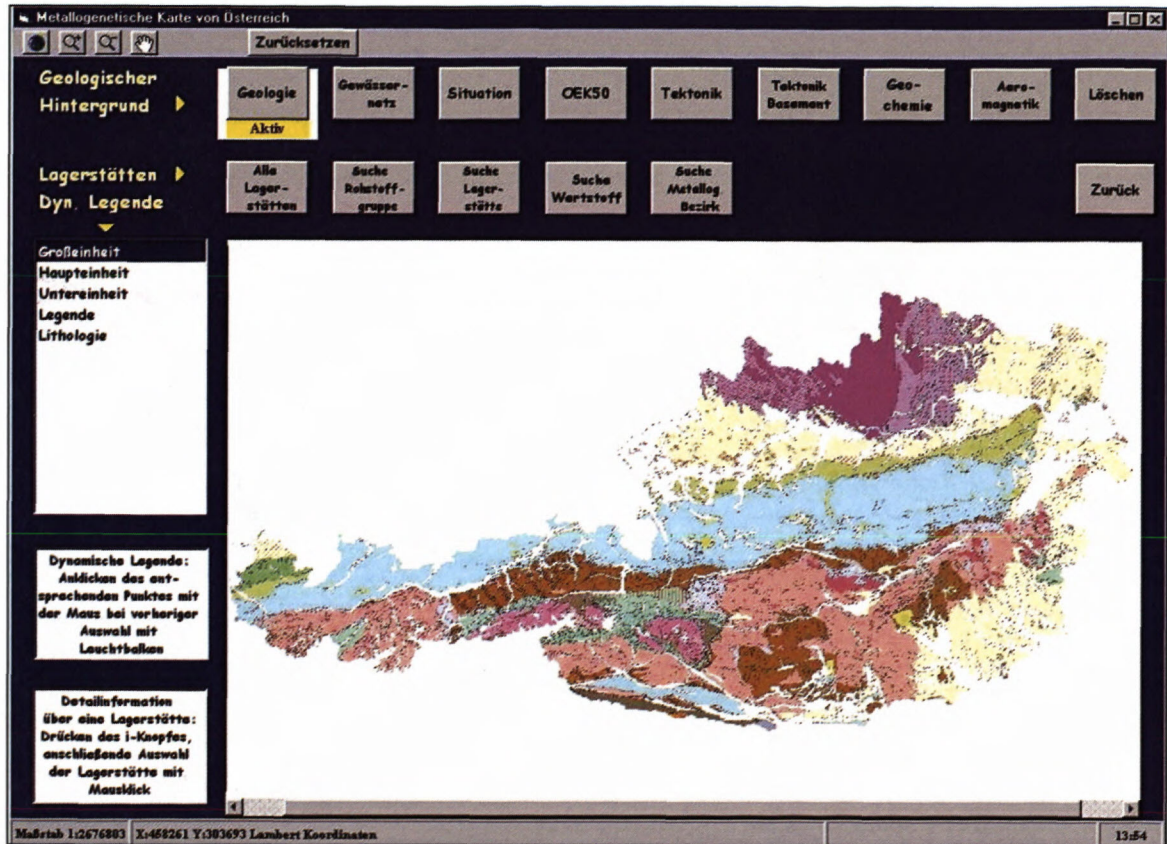


Fig. 2: Main menu of IRIS, general overview with layer „Geologie“.

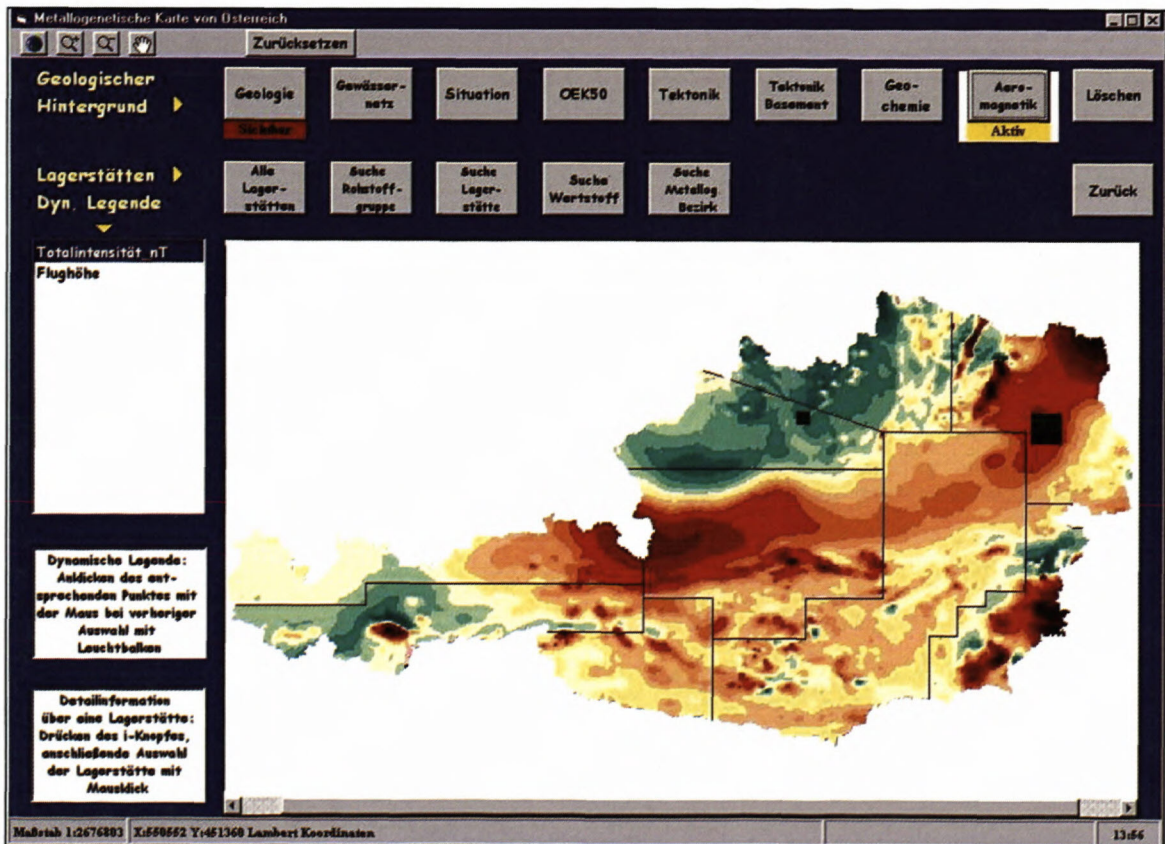


Fig. 3: Main menu of IRIS, general overview with layer „Aeromagnetik“: total magnetic intensity: red shadings: 20 - 375 nT; yellow shadings: 0 - 20 nT, green shadings: 0 - 50nT.

Tab. 1: Geological units of Austria. Boldfaced letters represent great regional geological systems. Differentiation into major units, subunits and lithologies. n.d. = no differentiation.

Major units	Subunits	Lithologies
n. d.	Quaternary n.d.	n.d.
n.d.	Tertiary Basins -Molasse zone, intramontane basins -Allochthonous molasse -Ernstbrunn "Klippen"	Tertiary sediments n.d., volcanic rocks n.d. n.d.
n.d.	Bohemian Massif -Permocarboniferous of Zöbing -Metamorphic of the Moldanubian and Moravian Complex -South Bohemian Pluton	n.d. differentiated n.d.
Helvetic Zone	Eastern Alps -Helvetic Zone -Liebenstein, Feuerstätter nappe	n.d. n.d.
Rhenodanubian Flysch Zone	-Flysch units -Ybbsitz-Zone	n.d. n.d.
Penninic Windows (Engadin, Hohe Tauern, Rechnitz) and Arosa-Zone)	-Permomesozoic units -Zentralgneiss unit -pre-granitoid formations -"Altkristallin"-Fm.	differentiated n.d. n.d. differentiated
Austroalpine Units	-Permomesozoic units of Calc-areous Alps and Drau Range -Gosau-Group -Central Alpine Permomesozoic -Marine Carboniferous units -Silbersberg nappe (Greywacke zone) -Continental Carboniferous molasse -Early Paleozoic units -Permocarboniferous granitoids -Austroalpine metamorphic units	differentiated n.d. differentiated n.d. n.d. n.d. differentiated n.d. differentiated
Periadriatic Intrusive Rocks	Periadriatic intrusive Rocks n.d.	differentiated
n.d.	Southern Alps -Triassic -Upper Carboniferous - Permian -Early Paleozoic - Lower Carboniferous	n.d. n.d. differentiated

- name of the occurrence/deposit
- mineral content
- geographic position and coordinates
- geological data (geological unit, metallogenetic district, lithology and age of host rock, orientation of deposit, shape of deposit)
- isotopic data (Pb, S, U if known)
- vitrinite reflectance of coals
- remarks

- references

Further information is given by figures (pictures of surface and underground outcrops, geological maps and cross-sections).

Metallogenetic information can be retrieved from the IRIS application by activating the legend, the "i"-button and the menu fields:

- "Alle Lagerstätten" (all deposits)
- "Suche Rohstoffe" (search for raw material groups)

- "Suche Lagerstätte" (search for occurrence/deposit)
- "Suche Wertstoff" (search for particular mineral commodity)
- "Suche Metallogenetischer Bezirk" (search for particular metallogenetic district).

All deposits/occurrences

In a larger scale (general overview) 3029 sites of occurrences/deposits are visualized by colored circles. The circles/symbols indicate individual groups of raw materials (specification of the groups see below):

- red: iron and ferro-alloy metals
- green: sulfides in general
- blue: non ferrous metals
- yellow: precious metals
- orange industrial minerals
- purple: special metals
- black: hard coal
- gray: graphite
- brown: lignites
- red/green: oil and gas.

In the general overview individual symbols characterize the shape of a deposit:

- stratiform, lenticular
- veins, lodes
- disseminated, stockwork
- irregular
- explored in drillholes.

Symbols are orientated (in relation to strike direction), wherever orientation of stratiform/lenticular and vein deposits are proved. Additional information is available by activating the dynamic legend:

- name of the occurrence/deposit
- state of the deposit (in operation or not)
- group of raw materials (see below)
- mineral commodity (see below)
- orientation (if known) of stratiform/lenticular and vein occurrences/deposits (see above)
- shape of the deposit (see above)
- importance of the deposit (minor and major importance).

Deposits of "major importance" are marked by larger symbols which indicate the specific groups of raw materials (general overview only). The category "major importance" includes all deposits still in operation or being exploited in the past decades. Deposits of economic importance in the future are also shown in large symbols. Other deposits were classified as deposits of "minor importance".

search for a group of raw material:

All mineral occurrences/deposits are arranged in specific groups (in brackets the number of occurrences/deposits):

- iron and steel alloying metals (463)
- base metals (468)
- non ferrous metals (167)

- precious metals (90)
- special metals (169)
- industrial minerals (1135)
- mineral fuels (537).

Deposits of each group can be visualized according to their position in the layer "search of mineral group". In a separate window all occurrences/deposits of the selected group is listed, including the major mineral paragenesis of the occurrences/deposits and position in the respected province of Austria.

search for mineral occurrence/deposit:

This layer includes a list of all occurrences/deposits within Austria (alphabetically) nominating the mineral commodities and geographical position (provinces).

By selecting one occurrence/deposit in the list the location is shown by a blinking dot (map "all occurrences/deposits") to select and zoom a more detailed area more easily. More information to the selected occurrence/deposit is displayed in a separate window immediately.

search for a mineral commodity:

All mineral commodities and the number of all known occurrences/deposits are listed alphabetically. A certain commodity may be selected from this list and all sites of the respected mineral commodity will be displayed on the screen. A list with all occurrences/deposits of this commodity appears in a separate window as well.

search for metallogenetic district:

Most of the mineral occurrences/deposits are grouped to districts. By knowing the sensitive problem in defining minerogenetic/metallogenetic units the term "metallogenetic district" is used for mineralizations with similar paragenesis, host rock lithology, shape and tectonic framework. mineralizations of a particular metallogenetic district are assumed to be of the same origin and age.

All districts are listed in alphabetical order. The district to be displayed can be selected by moving the light bar. After activating the enter-key only sites of this particular district will be shown on the screen. A detailed list with all occurrences/deposits within the district will occur in a separate window.

According to their similarities in paragenesis, host rocks, shape, and so forth, the following districts and their number in the major geological systems of Austria are processed.

Selected applications

1. Bohemian massif: Graphite district Variegated Series

The Austrian part of the Bohemian massif is part of the Middle European Variscan belt. The tectonic units are set up of medium to high grade metamorphic rock intruded by a huge mass of Variscan (Carboniferous) granitoids. Significantly there is an inverse metamorphic pattern with the highest (granulitic) metamorphic facies

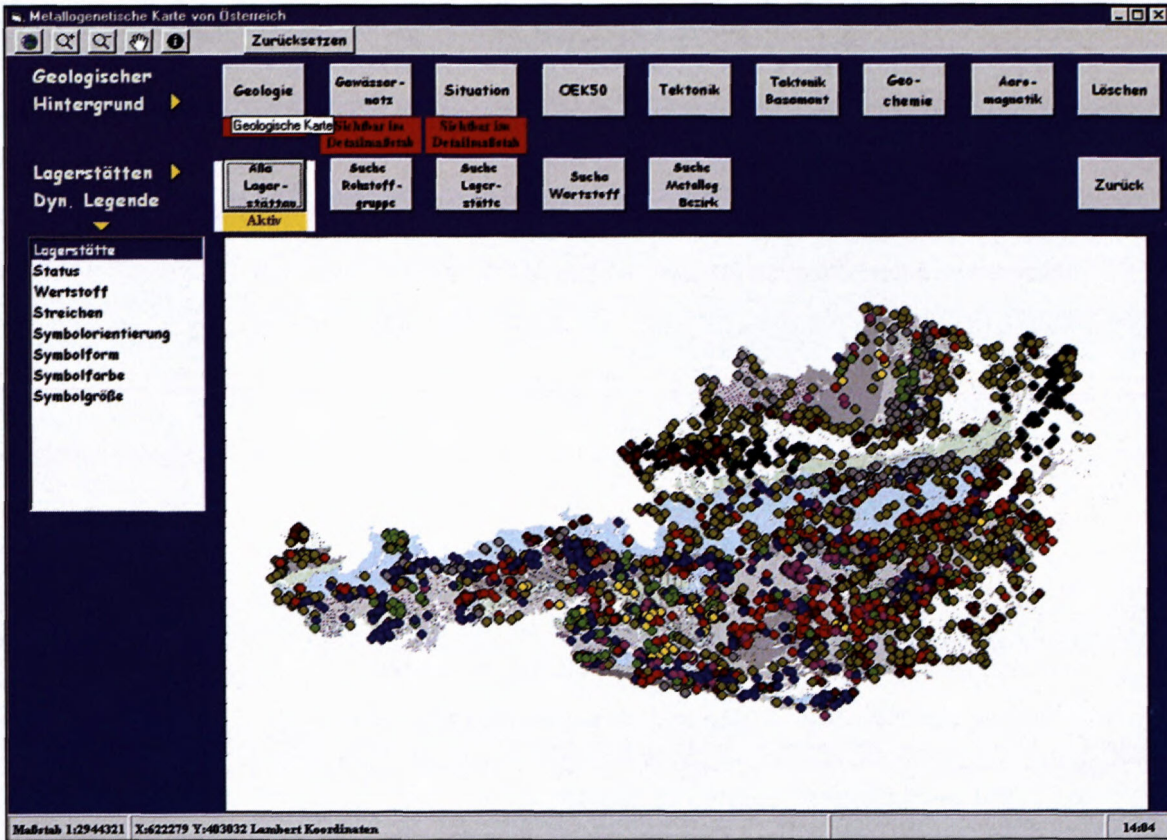


Fig. 4: Main menu of IRIS, general overview with layer „Alle Lagerstätten“ (all deposits/occurrences).

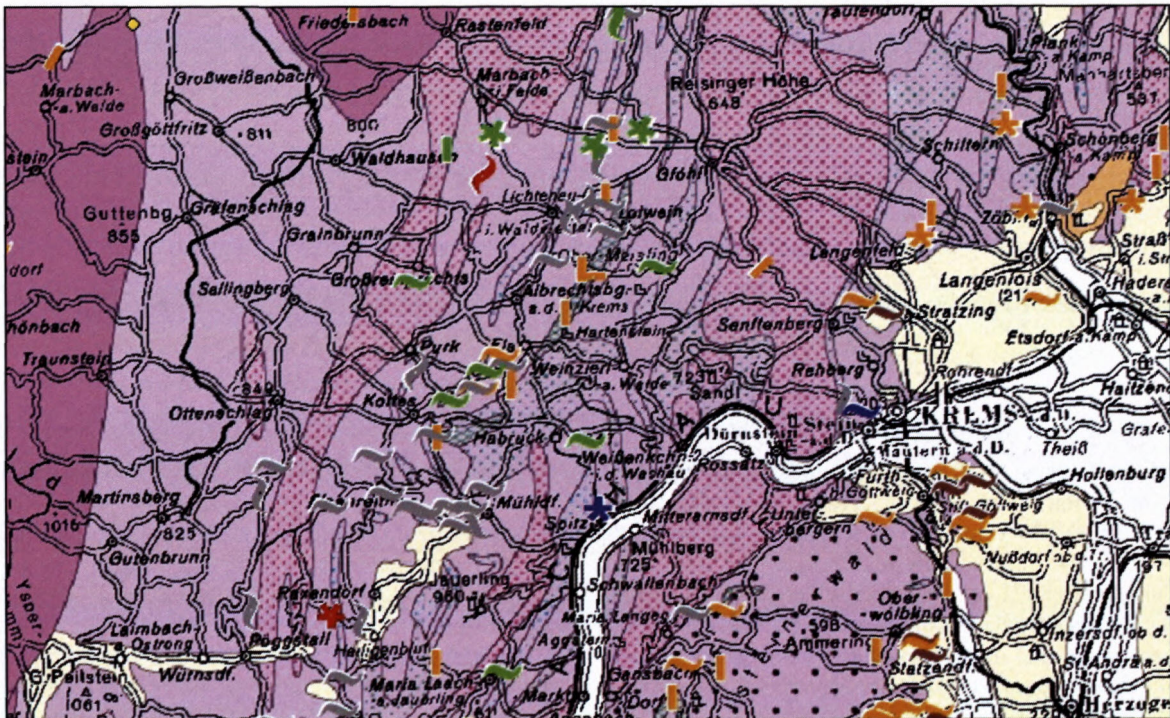


Fig. 5: Detail from the Bohemian Massif with graphite occurrences (grey symbols) of the „Graphite district Variegated Series“.

Detailinformation der Lagerstätte

Lagerstätte: Trandorf (Weinberg)
Bundesland: NOe

Wertstoff: Gra
Nebenprodukt:

Lage: zwischen Amstall und Elsenreith

ÖK50-Blatt: 36
Meridian: 34
BMN-Koord. Rechtswert: 67400
BMN-Koord. Hochwert: 360200
Gauß-Krüger-Koord. y= -76000
Gauß-Krüger-Koord. x= 5360200

Lagegenauigkeit: sichere Ortsangabe

Geologischer Rahmen

Großeinheit: Böhmisches Masse
Haupteinheit: Moldanubikum
Untereinheit: Moldanubisches Metamorphikum
Bezirk: Grafitbezirk Bunte Serie
Lithofazies: Saure Metasedimente
123
Nebengestein: Kalkmarmor, Paragneise, Amphibolite
Schichtbezeichnung: Bunte Serie
Alter des Nebengest. EC?
Form der Lagerstätte: lagenförmig (Orientierung bekannt)

Isotopenwerte Nebengestein

Blei:
Schwefel:
Uran:

Isotopenwerte Mineralisation:

Bemerkung:
mehrere Grafitlinsen, tektonisch steilgestellt; ehem. Grubenfelder Weinberg und Weinbergwald-Neu; Förderung 364931 t Rohgraphit. Restvermögen bis zu 25000 t Graphit bei Tieferlegung der Abbauschle.

Literatur:

WEBER, I. (1987 b):
Die geologischen Grundlagen des Grafitbergbaues in Niederösterreich.- In: Bergbau in Niederösterreich, Studien und Forschungen aus dem Niederösterr. Inst. f. Landeskunde, 10, 369–387, Wien.

Fig. 6: Detail information of the Trandorf graphite deposit (example).

overprint within the uppermost tectonic units. The Bohemian massif is eroded to deep crustal levels and therefore is devoid of any important ore mineralization.

A characteristic Late Proterozoic sequence of amphibolite, schists, gneisses and marbles (Bunte Serie; "variegated series") hosts numerous occurrences/deposits of flaky graphite deriving from sapropelitic protoliths, metamorphosed during Variscan orogeny.

In IRIS some 78 occurrences/deposits of graphite are archived, summarized within the "Grafitbezirk Bunte Serie" ("Graphite district Variegated Series"). In a map of small magnification this district can be well defined by the swarm of the respective symbols (Fig. 5). In a small

scale (great magnification) the symbols indicate the stratiform - lenticular character of the deposits and, if the orientation is known always a striking direction according to the general N-S strike of the "Bunte Serie" which is situated within the Moldanubian nappe complex east of the Gföhl gneiss and west of the Moravian nappe complex.

Today only the Weinberg deposit is in operation. This deposit is marked (in Fig. 5) by a larger symbol. Data of all deposits are archived in IRIS; Fig. 6 displays the base data for the Trandorf deposit (geographic position, geological situation, mineral commodity, byproducts, remarks and some references). There are available three figures as well (landscape with characteristic black col-

Tab. 2: Specification and number of metallogenetic districts in the great regional geologic system of Austria.

Districts related to mineral commodities	Bohemian Massif	Eastern Alps	Tertiary basins	Southera Alps
Iron and steel alloying metals				
iron ore i.g.		8		
iron/copper ore		1		
siderite		3		
hematite		3		
molybdenum	1			
manganese		2		
tungsten		2		
Non ferrous metals				
antimony		1		
lead/zinc		9		
lead/zinc (fahlore)		1		
lead/zinc baryte		1		
lead/zinc/iron		1		
copper		3		
polymetallic ores		19		
pyrrhotin/pyrite ("Kieserz")		7		
fahlore		3		
copper/iron ore		1		
copper (magnesite)		1		
copper/uranium ore		1		
polymetallic baryte-fluorite				1
Special metals				
bauxite		1		
Sb(As, Cu, Pb, Cu); Au, As-ore		1		
spodumene pegmatites		2		
uranium/fluor	1			
uranium ore		4		
Precious metals				
precious metal ore i.g.		2		
gold		7		
gold-tungsten		1		
silver		1		
Industrial minerals				
chromite-asbestos (magnesite)		1		
asbestos		1		
oil shale		2		
baryite		2		
bentonite		1		
bitumenous marls		1		
specularite		1		
evaporite		8		
graphite	1	1		
kaolin	1			
magnesite		2		
magnesite (siderite)		1		
magnesite (talc)		1		
magnesite (vermiculite)	1			
magnesite-scheelite		1		
phosphate-evaporite		1		
phosphate		1		
quartz-feldspar-pegmatite		2		
quartz sand - clay				1
talc-leucophyllite		2		
vermiculite	1			
Energy fuels				
anthrazite		1		
hard coal		4		
lignite/hard brown coal		2	22	
oil/gas			2	

ored soils covering the deposit; the open pit showing the generally heavily metamorphosed character of the deposits; graphitic gneisses with layered pyrite mineralization). In the stream sediment geochemistry, slightly enhanced V content indicates the sapropelite protolith character.

2. Schlaining antimony (stibnite) ore district

The Schlaining antimony (stibnite)-ore district (Cerny, et al. 1997) is situated in the Penninic Rechnitz Window in the southeastern margin of the Eastern Alps, close to Austrian/Hungarian border. The low grade volcanosedimentary metamorphic host rock (Cretaceous Rechnitz Group) is of oceanic origin (South Penninic ocean) and includes tectonic relicts of ophiolite complexes (Koller & Höck, 1992). During the Late Paleogene the Penninic oceanic units were overridden by the Lower Austroalpine Crystalline complex.

The oceanic and ophiolitic Penninic unit is bearing some small scale stratiform sulfide Fe/Cu-mineralizations and the vein type stibnite mineralizations of the Schlaining antimony district. The Schlaining mine was in operation until 1990. Some of these deposits contain remarkable Hg-mineralization. In some locations talc and asbestos were formed by hydrothermal alteration of the ultrabasic rocks.

Chromite mineralizations are not known in the Rechnitz window although the geochemical stream sediment information indicates some Cr anomalies. The geochemical anomaly fits perfect with an aeromagnetic anomaly. However, no chromite mineralizations are to be expected: The lack of chromium mineralization may be explained by the fact, that chromite mineralization occurs during the cooling of ultramafic melts. However chromium is likely a constituent of minerals like hornblendes, pyroxenites and so on. As a matter of fact, a careful interpretation of geology, geochemistry and geophysics is extremely necessary to distinguish between prospective areas and areas of minor interest.

Further Ni content of stream sediments partly reflects ultrabasic areas and their surroundings. Nevertheless such examples demonstrate how to use IRIS as a strategic instrument in the conception of mineral exploration projects. In the aeromagnetic information the pronounced magnetic anomaly is also related to the Penninic unit.

Outlook

The positive experience with IRIS is a big challenge to improve the data base and the interactive handling. The present release of IRIS allows to visualize only one element at once. In a next step the information supplied by the geochemical data base will be extended using multivariate geostatistical methods. By means of a Principal Component analysis areas of higher mineral potential may easily be separated from areas of minor interest. Geochemical anomalies in a favorable geologic framework, which fits with geophysical anomalies as well may indicate prospective zones. On the other side a careful interpretation of the data allow to distinguish between zones of potential mineralizations from zones of industrial pollution.

Other future steps will be the implementation of further geophysical data (gravity) and additional geochemistry (provinces of Niederösterreich and Oberösterreich) as well as a new layer displaying the metamorphic overprints of the Variscan and Alpine orogenic cycles.

GIS-Software and applied functions

IRIS was developed in Visual Basic 6.0 from Microsoft and MapObjects 2.0 from ESRI. MapObject is an ActiveX control (OCX) with more than 45 programmable ActiveX Automation objects that can be plugged in to many standard Windows development environments such as Visual Basic. The required GIS-functionality is supplied by MapObjects. The development was done under Windows NT 4.0.

The following functions have been used out of Map Objects integrated by Visual Basic:

- display, zooming, panning
- activate or erase maps by mouse click out of a given menu and overlay them using the transparency feature. The priority for the visibility of the maps is fixed.
- data support for ESRI shapefiles, TIFF- and JPEG Files
- 'map tip'-function to identify the detailed legend by clicking on a location.
- 'hot link'-function to show the mineral data base content including photo documents for a selected location
- display queried mineral deposit locations by using the 'blinking feature'
- maps using standard and specifically designed mineral location symbols in True Type Format.
- automatic change to the appropriate map display depending on the scale - e.g. change of symbols, change of visibility of geographic background map (topography, drainage system), change from raster to isolines for the aeromagnetic map.

Data supplier and used data formats

- Geological data base - digital version supplied by the Geologische Bundesanstalt (GBA), Vienna.
Formats: TIFF-file for the patterns, shapefiles for the polygon information - like geological units, line shapefile for the tectonic lines.
- Metallogenetic data base - supplied by L. Weber
Formats: point shapefile for the alphanumeric data and JPEG-Files for the photo documents.
- Geochemical data base - digital version supplied by G. Hausberger, copyright by GBA.
Format: point shapefile
- Aeromagnetic data base: digital version supplied by G. Hausberger, copyright by GBA.
Formats: Polygon shapefile for the overview map, line shapefile for the isolines, polygon shapefile for the flight levels.
- Topography (situation), drainage system - supplied by the Bundanstalt für Eich- und Vermessungswesen, Vienna.
Format: TIFF-Files.

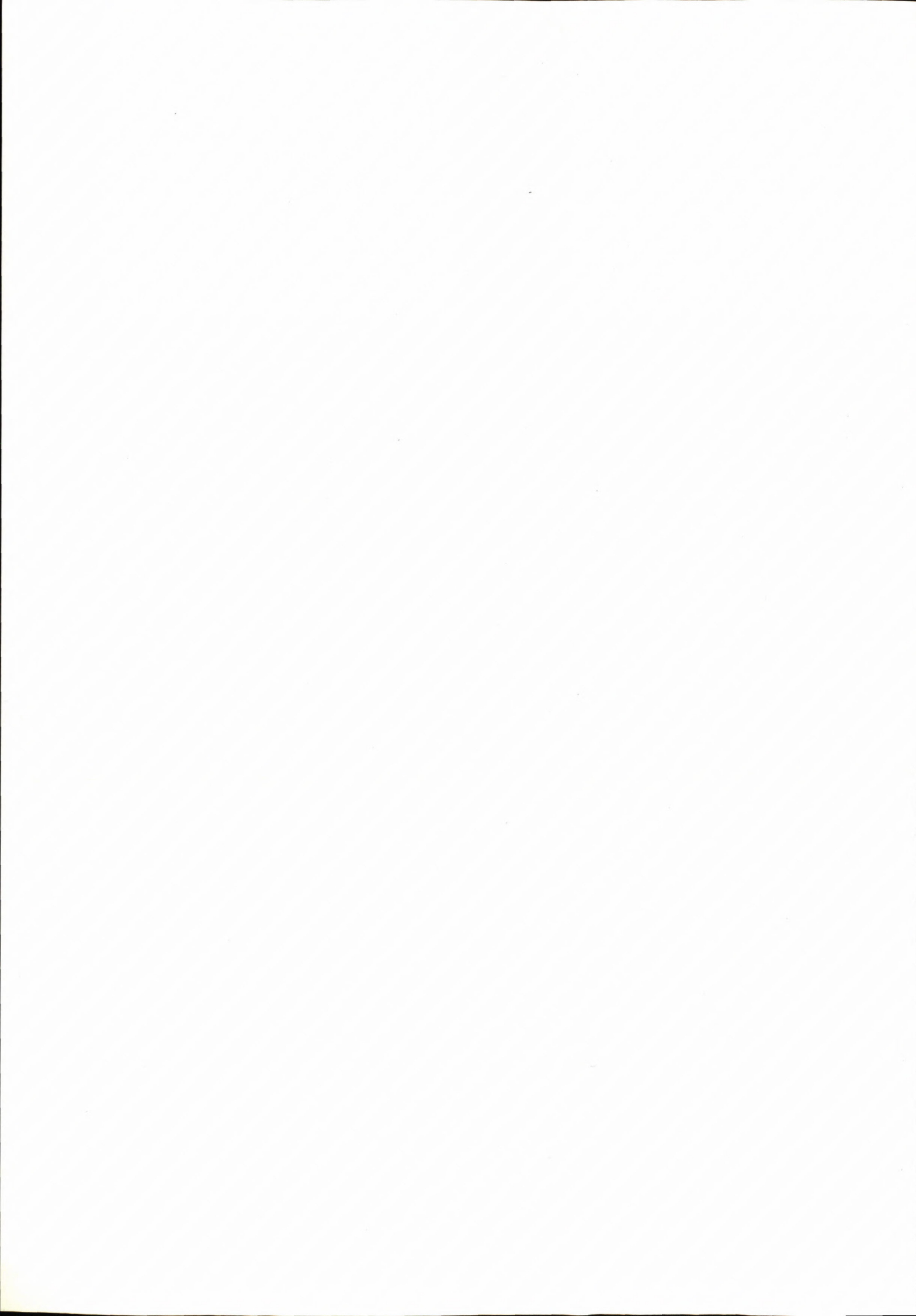
Technical requirements to run IRIS

Operating System: Windows 95, 98 or NT (version 4.0 and SP3 or higher),

Hardware: 64MB RAM, a minimum of 250MB free disk space. Pentium with 166 MHz or higher.

Selected Literature

- Blaumoser, N.H. 1992: Eine erste gesamte aeromagnetische Karte von Österreich und ihre Transformationen – A first complete aeromagnetic map of Austria and its transformations. *Mitt. Österr. Geol. Ges.*, 84, 185-203, Wien.
- Cerny, I., Schroll, E., Weber, L. 1997: Antimonerzbezirk Schlaining; in: Weber, L., ed. 1997: *Handbuch der Lagerstätten der Erze, Industriemineralien und Energierohstoffe Österreichs. Erläuterungen zur metallogenetischen Karte Österreichs 1:500.000.* Arch. f. Lagerst. forschung Geol. B.-A., 19, 607 p., Wien.
- Haditsch, J.G. 1979: Lagerstätten fester mineralischer Rohstoffe in Österreich und ihre Bedeutung. 53 p., 6 maps, Bundesministerium f. Handel, Gewerbe und Industrie, Wien.
- Koller, F. & Höck, V. 1992: The Mesozoic Ophiolites in the Eastern Alps – A review. *ALCAPA Field Guide*, 115-125, IGP/KFU, Graz.
- Thalman, F., Schermann, O., Schroll, E., Hausberger, G. 1989: *Geochemischer Atlas der Republik Österreich 1:1 Mio.*, Geol. B.-A., Wien.
- Vetters, H. 1933: *Geologische Karte der Republik Österreich 1:500.000 und der Nachbarländer.* Geologische Bundesanstalt, Vienna.
- Weber, L. (ed. 1997): *Handbuch der Lagerstätten der Erze, Industriemineralien und Energierohstoffe Österreichs. Erläuterungen zur metallogenetischen Karte Österreichs 1:500.000.* Arch. f. Lagerst. forschung Geol. B.-A., 19, 607 p., Wien.
- Weber, L. 1998: Die neue Metallogenetische Karte Österreichs – Das Rohstoffpotential Österreichs. *Österr. Akad. Wiss. Schriftenreihe Erdwiss. Komm.*, 12, 177-203.



New genus (*Superbirhyncha* gen. n.) for a rhynchonellid (Brachiopoda) from the Alpine Upper Triassic

MILOŠ SIBLÍK

Institute of Geology, Academy of Sciences of the Czech Republic, Rozvojová 135,
165 00 Praha 6 – Suchbátka < sibilik@gli.cas.cz >

Abstract: A new rhynchonellid genus *Superbirhyncha* was established for Upper Triassic *Rhynchonella superba* BITTNER, 1890

Key words: Northern Calcareous Alps, Triassic, Hallstatt Limestone, rhynchonellid, brachiopods

Introduction

During the preparations of the complement to the volume Brachiopoda triadica in the series Catalogus fossilium Austriae (Siblík, 1988) more numerous material of some species appeared making further study possible. In this paper the attention is focused on "*Rhynchonella superba* Bittner, the species known and described from the Upper Triassic Hallstatt Limestone. After the revision, a new genus *Superbirhyncha* gen. n. could be established, based on unusual features recognized in this species.

Descriptions

Superfamily: *Rhynchonellacea* GRAY, 1848

Family: *Praecyclothyrididae* MAKRIDIN, 1964

Subfamily: *Tetrarhynchiinae* AGER, 1965

Superbirhyncha gen. n.

Type species: *Rhynchonella superba* BITTNER, 1890 – Upper Triassic Hallstatt Limestone, Austria.

Diagnosis: Medium sized to large rhynchonellids, subtrigonal to rounded pentagonal in outline and strongly dorsibiconvex in profile. Width clearly surpassing length in most specimens. Some pedicle valves nearly flat. Fold and sulcus well developed anteriorly, not sharply separated from lateral slopes. Anterior commissure with strong uniplication. Pedicle beak erect and slightly swollen, pedicle opening submesothyridid. Low, blunt ribs visible anteriorly in the fold and sulcus, losing rapidly their distinctness towards umbos. Posteral and lateral parts of valves nearly smooth or with very poorly developed ribbing. Slight sulcation present posteriorly in brachial valve. Concentric lines visible near margins of shell.

Shell very thick. Lateral umbonal cavities largely filled with secondary shell material, hiding nearly completely dorsally divergent dental lamellae. Teeth strong, situated in large well-developed sockets, crenulated. Short and narrow but relatively deep septalium developed, more or

less hidden in the secondary material. Dorsal septum strong but short, reduced to a ridge. Inner socket ridges coalesced with thick hinge plates (Fig. 5). Crura radulifer. Muscle scars usually strongly impressed (esp. in the brachial valve) (Fig. 2).

Remarks: Semicostate valves and extensive development of secondary thickening are the most characteristic features of the new genus. *Superbirhyncha superba* is not very frequent species in the Alpine Triassic, and for the revision it was necessary to use mostly museum material. External resemblance of „*superba*“ and *Moisseievia moisseievi* Dagys from the Upper Triassic of Caucasus was mentioned by Dagys (1963, p. 48). However, the internal characters of *Moisseievia* as shown by Dagys (1963, Text-Fig. 14) differ substantially from those in *Superbirhyncha* gen. n. Dagys' species has fused hinge plates and neither septalium nor dorsal septum.

Distribution: Hallstatt Limestone, Upper Triassic.

Included species: For the present, the type species only.

Superbirhyncha superba (BITTNER, 1890) (Figs. 1 – 5)

1890 *Rhynchonella superba* nov. spec. – BITTNER, p. 228, Pl. 14, Figs. 1-5.

1895 *Rhynchonella superba* BITTNER. – BITTNER, p. 368.

1988 „*Rhynchonella superba* BITTNER – SIBLÍK, p.51.

Lectotype: Specimen figured by Bittner, 1890 in Pl. 14, Fig. 2 and deposited in the Institute of Palaeontology, University of Vienna (designated by Siblík, 1988). It derives from Mühlthal near Piesting, Lower Austria (Hallstatt Limestone, Norian).

Material: About 30 specimens coming mostly from the collections of the Natural History Museum in Vienna. They are up to 32.0 mm long, 32.5 mm wide and 20.7 mm thick.

Description: Quite exact description of the external characters was given already by Bittner (1890) who prop-

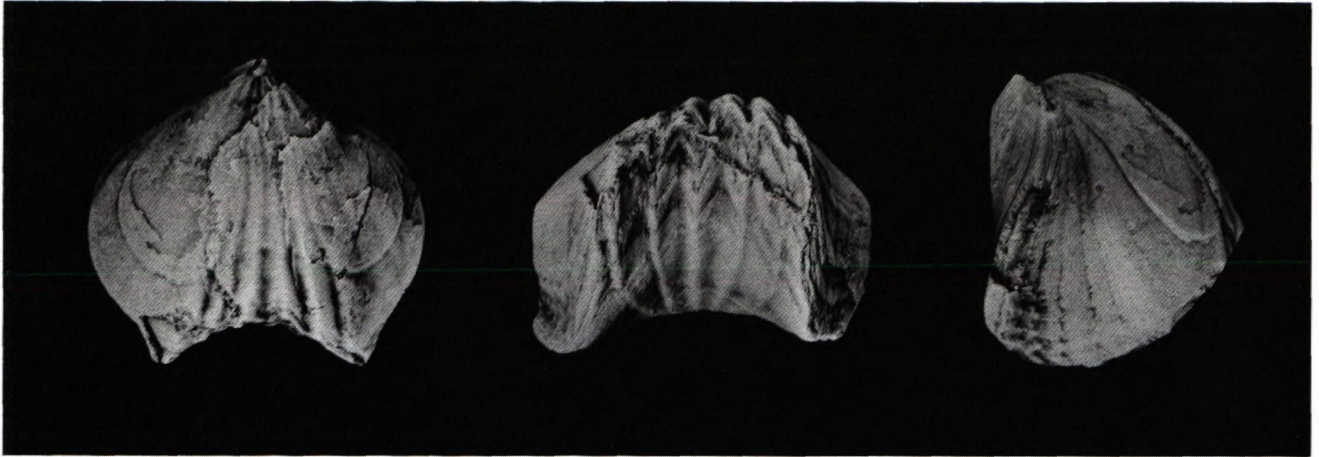


Fig. 1 *Superbirhyncha superba* (Bittner). Hütteneckalpe. NHM Wien. Photographs by Mr. J. Brožek, Prague. Magnified, x1.5

erly mentioned Palaeozoic habitus of „*superba*“. My comparative material showed 5 to 9 ribs on the fold (most frequently 7).

Remark: The most distinctive character of this species is the blunt ribs developed mostly in the fold and sulcus only.

Distribution: Norian (Mühlthal – Lower Austria; Leisling, Roßmoos, Siriuskogel, Hütteneckalpe – Upper Austria). A specimen collected by the present author on Feuerkogel near Aussee – Styria came from the scree and is thus without any stratigraphical value.

Acknowledgement:

This paper was made within the Research Project of the Institute of Geology, Academy of Sciences of the Czech Republic CEZ: Z3 013 912. I am indebted to Dr. H. Summesberger (Naturhistorisches Museum, Wien) who kindly provided access to the collections in his care and loaned some specimens as a comparative material for the study.

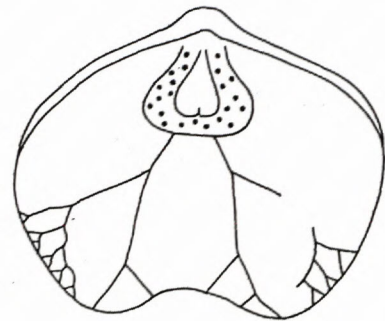


Fig. 2 *Superbirhyncha superba* (BITTNER). Hütteneckalpe. NHM Wien. Dorsal view of the specimen showing general muscle area and part of vascular markings. Enlarged, original width of the specimen 24.3 mm.

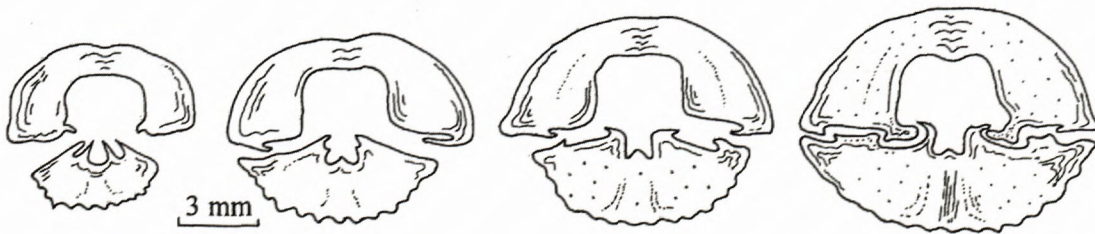


Fig. 4 *Superbirhyncha superba* (BITTNER). Feuerkogel near Bad Aussee. Four serial sections of another specimen through posterior part of shell. Original length of specimen 21.0 mm. Enlarged.

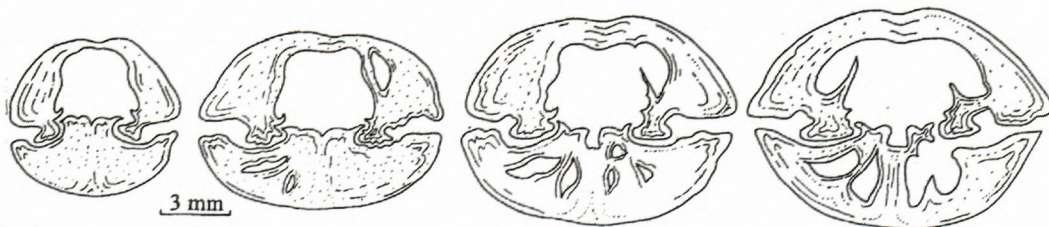


Fig. 5 *Superbirhyncha superba* (BITTNER). Hütteneckalpe. NHM Wien. Four serial sections through another specimen well showing coalesced hinge plates with inner socket ridges. Original length of specimen 23.1 mm. Enlarged.

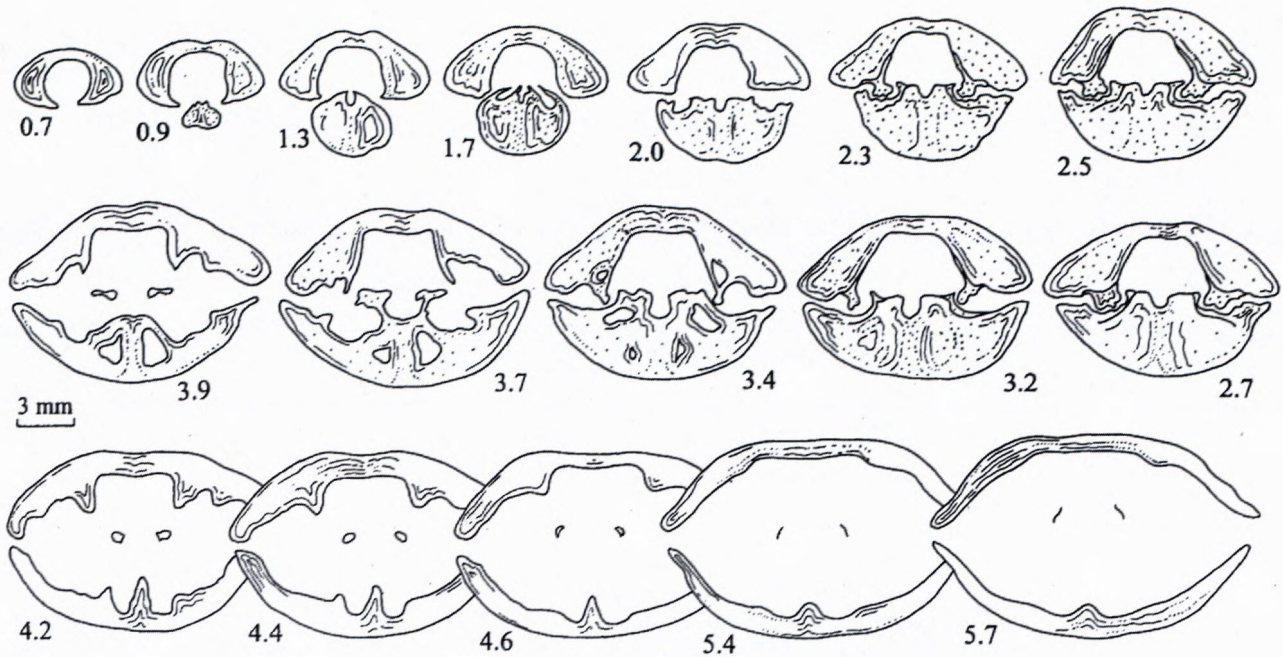


Fig. 3 *Superbirhyncha superba* (Bittner). Hütteneckalpe. NHM Wien. Serial sections through the posterior part of shell. Crura disappeared at 5.9 mm. Original length of specimen 23.6 mm. Enlarged.

References

Bittner A., 1890: Brachiopoden der alpiner Trias. – Abh. k. k. geol. Reichsanst. (Wien), 14, 1 – 320.
 Bittner A., 1895: Ein von Dr. Boese neuentdeckter Fundpunkt von Brachiopoden in den norischen Hallstätter Kalken des Salzkam-

mergutes, zwischen Rossmoos und Hütteneckalpe. – Verh. k. k. geol. Reichsanst. (Wien), 367 – 369.
 Dagens A. S., 1963: Upper Triassic brachiopods of the Southern USSR. – (Moscow), 1 – 238 (in Russian).
 Siblík M., 1988: Brachiopoda mesozoica, a) Brachiopoda triadica. – Catalogus fossilium Austriae Vc 2(a) (Wien), 1 – 145.





Instructions for authors

Slovak Geological Magazine – periodical of the Geological Survey of Slovak Republic is quarterly presenting the results of investigation and researches in wide range of topics: regional geology and geological maps, lithology and stratigraphy, petrology and mineralogy, paleontology, geochemistry and isotope geology, geophysics and deep structure, geology of deposits and metallogeny, tectonics and structural geology, hydrogeology and geothermal energy, environmental geochemistry, engineering geology and geotechnology, geological factors of the environment, petroarcheology.

The journal is focused on problems of the Alpine-Carpathian-Balkan region

General instructions

The Editorial Board of the Geological Survey of Slovak Republic – Dionýz Štúr Publishers accepts manuscripts in correct English. The papers that do not have sufficient accuracy in language level will be submitted back for language correction.

The manuscript should be addressed to the Chief Editor or the Managing Editor.

Contact address:

Geological Survey of Slovak Republic – Dionýz Štúr Publishers,
Mlynská dolina 1, 817 04 Bratislava, Slovak Republic

e-mail addresses: jvozar@gssr.sk
gabina@gssr.sk
http://www.gssr.sk

The Editorial Board accepts or refuses a manuscript with regard to the reviewer's opinion. The author is informed of the refusal within 14 days from the decision of the Editorial Board. Accepted manuscript is prepared for publication in an appropriate issue of the Magazine. The author(s) and the publishers enter a contract establishing the rights and duties of both parties during editorial preparation and printing, until the time of publishing of the paper.

Text layout

The manuscript should be arranged as follows: TITLE OF THE PAPER, FULL NAME OF THE AUTHOR(S); NUMBER OF SUPPLEMENTS (in brackets below the title, e.g. 5 figs., 4 tabs.), ABSTRACT (max. 30 lines presenting principal results) – KEY WORDS – INTRODUCTION – TEXT – CONCLUSION – ACKNOWLEDGEMENTS – APPENDIX – REFERENCES – TABLE AND FIGURE CAPTIONS – TABLES – FIGURES. The editorial board recommends to show a localisation scheme at the beginning of the article.

The title should be as short as possible, but informative, compendious and concise. In a footnote on the first page, name of the author(s), as well as his (their) professional or private address.

The text of the paper should be logically arranged. For the purpose of typography, the author may use a hierarchic division of chapters and sub-chapters, using numbers with their titles. The editorial board reserves the right to adjust the type according to generally accepted rules even if the author has not done this.

Names of cited authors in the text are written without first names or initials (e.g. Štúr, 1868), the names of co-authors are divided (e.g. Andrusov & Bystrický, 1973). The name(s) is followed by a comma before the publication year. If there are more authors, the first one, or the first two only are cited, adding et al. and publication year.

Mathematical and physical symbols of units, such as %, ‰, °C should be preceded by a space, e.g. 60 %, 105 °C etc. Abbreviations of the units such as second, litre etc. should be written with a gap. Only SI units are accepted. Points of the compass may be substituted by the abbreviations E, W, NW, SSE etc. Brackets (parentheses) are to be indicated as should be printed, i.e. square brackets, parentheses or compound. Dashes should be typed as double hyphens.

If a manuscript is typed, 2 copies are required, including figures. The author should mark those parts of a text that should be printed in different type with a vertical line on the left side of the manuscript. Paragraphs are marked with 1 tab space from the left margin, or by a typographic symbol. Words to be emphasized, physical symbols and Greek letters to be set in other type (e.g. *italics*) should be marked. Greek letters have to be written in the margin in full (e.g. *sigma*). Hyphens should be carefully distinguished from dashes.

Tables and figures

Tables will be accepted in a size of up to A4, numbered in the same way as in the text.

Tables should be typed on separate sheets of the same size as text, with normal type. The author is asked to mark in the text where the table should be inserted. Short explanations attached to a table should be included on the same sheet. If the text is longer, it should be typed on a separate sheet.

Figures should be presented in black-and-white, in exceptional cases also in colour which must be paid approx. 100 EUR per 1 side A 4. Figures should be presented by the author simultaneously with the text of the paper, in two copies, or on a diskette + one hard copy. Graphs, sketches, profiles and maps must be always drawn separately. High-quality copies are accepted as well. Captions should be typed outside the figure. The graphic supplements should be numbered on the reverse side, along with the orientation of the figures. Large-size supplements are accepted only exceptionally. Photographs intended for publishing should be sharp, contrast, on shiny paper. High quality colour photographs will only be accepted depending on the judgement of the technical editors.

If a picture is delivered in a digital form, the following formats will be accepted: *.cdr, *.dxf, *.bmp, *.tiff, *.wpg, *.fga, *.jpg *.gif, *.pcx. Other formats are to be consulted with the editors.

References

Should be listed in alphabetical and chronological order according to annotation in the text and consist of all references cited.

Standard form is as follows: 1. Family name and initials of author(s), 2. Publication year, 3. Title of paper, 4. Editor(s), 5. Title of proceedings, 6. Publishers or Publishing house and place of publishing, 7. Unpublished report – manuscript should be denoted MS. Unpublished paper can appear as personal communications only. 8. Page range.

Quotations of papers published in non-Latin alphabet or in languages other than English, French, Italian, Spain or German ought to be translated into English with an indication of the original language in parentheses, e.g.: (in Slovak).

Example:

Andrusov, D., Bystrický, J. & Fusán, O., 1973: *Outline of the Structure of the West Carpathians*. Guide-book for geol. exc. of Xth Congr. CBGA. Bratislava: Geol. Úst. D. Štúra, 44 p.

Beránek, B., Leško, B. & Mayerová, M., 1979: Interpretation of seismic measurements along the trans-Carpathian profile K III. In: Babuška, V. & Plančár, J. (Eds.): *Geodynamic investigations in Czecho-Slovakia*. Bratislava: VEDA, p. 201-205.

Lucido, O., 1993: A new theory of the Earth's continental crust: The colloidal origin. *Geol. Carpathica*, vol. 44, no. 2, p. 67-74.

Pitoňák, P. & Spišiak, J., 1989: Mineralogy, petrology and geochemistry of the main rock types of the crystalline complex of the Nízke Tatry Mts. MS – Archiv GS SR, Bratislava, 232 p. (in Slovak).

Proofs

The translator as well as the author(s) are obliged to correct the errors which are due to typing and technical arrangements. The first proofs are sent to author(s) as well as to the translator. The second proof is provided only to the editorial office. It will be sent to authors upon request.

The proofs must be marked clearly and intelligibly, to avoid further errors and doubts. Common typographic symbols are to be used, the list and meaning of which will be provided by the editorial office. Each used symbol must also appear on the margin of the text, if possible on the same line where the error occurred. The deadlines and conditions for proof-reading shall be stated in the contract.

Final remarks

These instructions are obligatory to all authors. Exceptions may be permitted by the Editorial Board or the managing editor. Manuscripts not complying with these instructions shall be returned to the authors.

1. Editorial Board reserves the right to publish preferentially invited manuscript and to assemble thematic volumes,

2. Sessions of Editorial Board – four times a year and closing dates for individual volumes will be on every 31th day of March, June, September and December.

3. To refer to one Magazine please use the following abbreviations: *Slovak Geol. Mag.*, vol. xx, no. xx. Bratislava: D. Štúr. Publ. ISSN 1335-096X.

